

PHYSICS OF STRINGS AND EXTRA DIMENSIONS

**PHYSICS OF STRINGS AND EXTRA DIMENSIONS:
FROM COSMOLOGY TO CONDENSED MATTER**

By

ALLAN I. BAYNTUN, M.Sc.

A Thesis

Submitted to the School of Graduate Studies
in Partial Fulfillment of the Requirements
for the Degree
Doctor of Philosophy

McMaster University

©Copyright by Allan I. Bayntun, 2012.

DOCTOR OF PHILOSOPHY (2012)
(Physics)

McMaster University
Hamilton, Ontario

TITLE: Physics of Strings and Extra Dimensions: From Cosmology to Condensed Matter

AUTHOR: Allan I. Bayntun, M.Sc.(McMaster University)

SUPERVISOR: Dr. C. Burgess

NUMBER OF PAGES: xiii, 165

Preface

The following is a summary of the work done over the past four years in my pursuit of a PhD. As one can see from the title and content, it is fairly apparent that my topics of interest are fairly separated in the high energy community. This can be understood from the fact that during my masters, I was primarily looking for classical solutions to higher dimensional supergravity theories, primarily motivated by low energy string theories. The tools I developed naturally lend themselves to the more active paradigm of large extra dimensions and brane dynamics as a potential solution to the cosmological constant problem. This is the basis for chapter 2.

My years at McMaster further piqued my interest into condensed matter systems and methods with its very strong and prevalent condensed matter group. Many of my peers have provided a great deal of insight and understanding into modern developments in the condensed matter field. Around the time I was starting my PhD, the field of holography from string theory applied to condensed matter was beginning to take off following strong physicists starting research programs into the topic such as Joseph Polchinski, Subir Sachdev, and Sean Hartnoll to name a few. Again the toolset I developed from my earlier years naturally led me to pursue research into condensed matter holography. A cursory introduction to holography in the context of condensed matter is presented in chapter 3, while the resulting papers from this research is presented in chapters 4 and 5. While these two topics are seemingly very different in that their applications differ significantly, they both stem from very fundamental developments in string theory during the 1990s and so actually demonstrate progress in which string theory could potentially make predictions outside of its initially intended predictions as a theory of quantum gravity.

This thesis is organized as a series of papers. As such, the chapters that are papers (Chapters 2, 4, and 5) have separate bibliographies at the end of their respective chapters. The remainder of the thesis has a single bibliography at the end of the entire text.

Contributed Works

Chapters 2, 4, and 5 in this thesis represent original works written at least in part by myself, Allan Ian Bayntun. The submission and publication status is as follows:

Chapter 2: New Journal of Physics 12 (2010) 075015 (arXiv:0912.3039)

Chapter 4: New Journal of Physics 13 (2011) 035012 (arXiv:1008.1917)

Chapter 5: Currently under submission in the Journal of High Energy Physics, and is available on the preprint server, arXiv at (arXiv:1112.3698).

All of these works have been produced with and co-authored my supervisor, Dr. C. P. Burgess. Dr. Leo van Nierop co-authored chapter 2 (New Journal of Physics 12 (2010) 075015), and both Dr. Sung-Sik Lee and Dr. Brian Dolan co-authored chapter 4.

Material from previously published works have been reformatted to conform to the required thesis guidelines. I grant an irrevocable, non-exclusive license to McMaster University and the National Library of Canada to reproduce this material as part of this thesis.

Abstract

The purpose of this thesis is twofold and motivated by recent developments in string theory and extra dimensional models. The first objective is to describe the development and progress in the codimension-2 brane paradigm as a potential cosmological scenario. Secondly, it presents the Anti-de Sitter/Conformal Field Theory (AdS/CFT) conjecture, also known as holography, as a tool for calculating physical quantities in condensed matter system and goes on to model the quantum Hall effect.

We first describe the initial development of treating back-reaction in codimension-2 branes systems with a scalar and gauge field. The purpose of this is to examine the low-energy effective dynamics on the brane. Furthermore, applications are then explored for D7-branes in F-theory as well as D3-branes in large extra dimensional scenarios explored as a model for the cosmological constant problem. The result of this work is that the higher and lower dimensional scenarios are consistent with each other once brane back-reaction is considered in these models. This work led to a number of future works one of which is in relation to the cosmological constant problem. While the subsequent work is beyond the scope of this thesis, we present a picture and further references for the reader.

The larger, later, portion of this thesis introduces the concept of holography, its origins, and the applicability to condensed matter systems. Furthermore, we discuss the applicability in particular to the quantum Hall effect (QHE) and present a model in the holographic language that correctly reproduces some of the physics of the QHE. This includes a paper in which we introduce the model, along with demonstration of symmetry properties and conductivity calculations, as well as a paper which examines the finite size scaling behaviour of the model. As a benefit to the reader, we present a ‘starter edition guide’ to the AdS/CFT dictionary preceding these papers for non-experts such that this thesis is self-contained.

The upshot is that these avenues of work, in particular quantum Hall-ography, have been very successful in modeling physics using tools originally developed by string theory. As such, it provides support for string theory as a model and framework, as well as providing more opportunities for future predictions of physical quantities.

Acknowledgements

First and foremost, I'd like to thank my supervisor Cliff Burgess, without which there wouldn't be a thesis to write! His patience and deep insight into the systems I was interested in and studied made it possible for me to truck ahead in this research and come to the results I have today. On a similar note, I would also like to thank my group-mates, in particular Leo van Nierop for showing me the ropes in my first paper and being an excellent collaborator. Also, in my last two papers, Sung-Sik Lee has been an invaluable help with his clear understanding and intuition of AdS/CFT and condensed matter systems in general. Also of utmost significance was Phillip Ashby, of which I've had a (barely) countably finite number of conversations on physics with. It was due to his almost random collection of vast physics knowledge that I've been able to become as knowledgeable and skilled in physics as I am today.

From a personal standpoint, I've had a vast array of support from my peers at McMaster, who have truly enriched my experience throughout my years in graduate school through thick and thin. It was through these experiences that a graduate student learns through much experimentation the proper beer/work ratio that maximizes productivity and inspiration! It is impossible to imagine what life in graduate school would be without them.

Saving the best for last, I truly appreciate my family for supporting me and giving me the opportunity to pursue a Ph.D. My parents in particular have given me the opportunity to explore and better understand this universe we live in with their constant encouragement. Finally, Sandy Hsu has given me the strength to continue pushing through my work by believing and supporting me more than a reasonable person should! Her constant support and tolerance of a husband in graduate school has given me the strength to carry on. Most importantly, her support in spite of having to also take care of our newborn, Satomi, is impossible to overstate.

Contents

0.1	Conventions	1
1	Introduction	3
1.1	Major Developments in String Theory	4
1.1.1	Strings, Supersymmetry, Branes, and Extra Dimensions	4
1.1.2	String Technology	5
1.2	Overview	10
2	Codimension-2 Brane-Bulk Matching: Examples from Six and Ten Dimensions	11
2.1	Introduction	13
2.2	The Bulk-Brane system	15
2.2.1	The bulk	15
2.2.2	Boundary conditions for codimension-2 branes	17
2.2.3	The brane constraint	19
2.2.4	The classical low-energy on-brane effective action	21
2.3	Examples	24
2.3.1	D7 branes in F-Theory	25
2.3.2	Brane-axion couplings in 6D	28
2.3.3	Warped and unwarped supersymmetric examples	32
2.4	Conclusions	40
	Chapter 2 Bibliography	41
3	Gravity-Gauge Duality and the Quantum Hall Effect	49
3.1	AdS/CFT: A simple picture	51
3.2	Temperature and Free Energy	52
3.3	Condensed Matter and the Quantum Hall Effect	53
3.3.1	The Quantum Hall Effect	54
4	Quantum Hall-ography	59
4.1	Introduction	61
4.2	Quantum Hall systems	63

4.2.1	Evidence for duality	63
4.2.2	The low-energy picture	69
4.3	Holographic Duality	72
4.3.1	Maxwell and the axio-dilaton	73
4.3.2	Duality relations	73
4.3.3	From $SL(2, R)$ to $SL(2, Z)$	74
4.3.4	Conductivities	75
4.4	Quantum Hall-ography	78
4.4.1	The setup	78
4.4.2	Duality relations	80
4.4.3	Holographic DC conductivities	81
4.4.4	Plateaux, semi-circles and the low-temperature limit	87
4.5	Discussion and conclusions	91
4.5.1	A model-building wish list	92
4.A	Some useful properties of $SL(2, R)$ and $SL(2, Z)$	95
4.B	DBI thermodynamics	98
4.C	Validity of the Probe-brane Approximation	101
4.D	DBI near-horizon extremal geometry	103
	Chapter 4 Bibliography	108
5	Holographic Finite Scaling	115
5.1	Introduction	117
5.1.1	The AdS/QHE system	119
5.1.2	Experimental finite-size effects	123
5.2	Finite-size effects in AdS/CFT systems	124
5.2.1	Finite size with no chemical potential	125
5.2.2	Finite size AdS/QHE black holes	127
5.3	The low-temperature phase: a charged star	137
5.3.1	Hydrostatic equilibrium for a charged star	138
5.3.2	Energetics of the transition	141
5.3.3	Shape of the transition curve	144
5.4	Conclusions	146
5.A	Conductivity for finite size	148
5.B	Free-energy calculations	150
	Chapter 5 Bibliography	151
6	Conclusion	159
6.1	Codimension-2 branes: Epilogue	159
6.2	Quantum Hall-ography: An Outlook	160

CONTENTS

ix

Thesis Bibliography

163

List of Figures

3.1	Cartoon of the various plateaux of the quantum Hall effect for varying magnetic field across the various Landau levels. Source: Glenton Jelbert licensed under the Creative Commons Attribution 3.0 Unported license	54
3.2	Cartoon of the density of states for strong magnetic fields at finite temperature. Increasing magnetic fields spreads the Landau levels apart, making it clear that for a wide range of magnetic fields the system is gapped. Source: Glenton Jelbert licensed under the Creative Commons Attribution 3.0 Unported license	57
4.1	Experimental traces of the Hall and ohmic resistances for a quantum Hall system, reproduced from ref. [14].	63
4.2	Evidence for the semi-circle law in the trace of the conductivities during a transition between two plateaux, reproduced from ref. [15].	64
4.3	Evidence for universality of critical resistivity, $\rho_{\star xx} = \rho_{xx}(B_c)$, from ref. [18].	65
4.4	Evidence for the duality, $\rho_{xx} \rightarrow 1/\rho_{xx}$, for resistivities equally spaced (in units of filling fraction, $\Delta\nu$) from the critical field, reproduced from ref. [19].	66
4.5	Evidence for the super-universality – the sharing of scaling exponents for transitions between different plateaux, reproduced from ref. [21].	67
4.6	The relation between RG flow and the action of the duality group, in the conductivity plane. If A flows to B, and D is B’s image under the group Γ , then the RG flow must take C to D if C is A’s image under Γ	68
4.7	A plot of some of the flow lines (for decreasing temperature) for the conductivities that are dictated by $\Gamma_0(2)$ invariance. The vertical axis represents σ^{xx} and the horizontal axis is σ^{xy} (in units of e^2/h). Flows are attracted to odd-denominator fractions at zero temperature, with bifurcations between different domains of attraction at specific magnetic fields. Notice that the semicircles that describe flow at constant magnetic field at the bifurcation between two basins of attraction are also lines along which the system moves when magnetic fields are varied at vanishingly small temperatures (colour online).	68

- 4.8 The conductivities (σ^{xx} plotted vs σ^{xy}), as computed using eqs. (4.71) and (4.72) with $\tau = 2 + i$. Each curve corresponds to a different choice for ν , stepping from $\nu = 1$ to $\nu = 10$ through integer values. σ_0 is the parameter along each curve, with $\sigma^{xy} \rightarrow \nu$ in the limit of large σ_0 . All lines are semi-circles centred on the real axis, and all pass through the point $\sigma = \tau$, for the reasons explained in the text (colour online). 87
- 4.9 Left panel: Curves of constant σ_0 and ν as computed semiclassically using the holographic model in the regime $\nu \gg \sigma_0^2$, $e^{-2\phi} \gg 1$. Horizontal lines represent loci of fixed σ_0 (and so also temperature), while the sloped lines describe those of fixed ν (and so also fixed magnetic field). Right panel: the same curves mapped to the strongly interacting near-plateau regime using an element of $SL(2, Z)$. The semi-circles radiating from the tip of the fan at the real axis represent lines of constant B , along which T varies. Those transverse to these are lines of constant T . These illustrate a plateau behaviour inasmuch as all curves converge to the same values of σ^{xx} and σ^{xy} for all values of magnetic field at low temperatures (colour online). 88
- 4.10 Left panel: Curves of constant magnetic field (or $\nu' = g(\nu)$) as computed semiclassically using the holographic model and mapped onto a plateau using an element $g \in PSL(2, Z)$. Right panel: the same curves for lines of constant T (or σ_0). Constant B lines are semicircles, while those along which B varies become semicircles at sufficiently low temperatures (colour online). 91
- 4.11 Experimental plots, reproduced from ref. [55], of the temperature dependence of the approach to various quantum Hall plateaux, showing an exponential form. 92
- 5.1 Hall resistance vs magnetic field for various temperatures, reproduced from [15]. B_c is the critical magnetic field where resistance doesn't change as temperature varies (colour online). 123
- 5.2 Top panel: $\partial R_{xy}/\partial B$ measured at $B = B_c$, as a function of temperature (reproduced from [15]), showing the transition from power-law temperature dependence to temperature-independence. Bottom panel: The transition temperature between these regimes vs system size (colour online). 124
- 5.3 Semi-log plot of the dilaton profile for $Q = 1000$ and $\hat{\mathcal{T}} = 10^{-5}$, for two asymptotic initial conditions (colour online). 130
- 5.4 Left panel: A plot of h_1 and ω as functions of r_h . Note that h_1 diverges and $\omega \rightarrow 0$ as $r_h \rightarrow 0$, a reflection of the minimum temperature discussed in the main text. Also note that $\omega \rightarrow 4$ and $h_1 \rightarrow r_h$ at large r_h , in agreement with the analytic large- r_h solution in the $z = 5$ region. Right panel: A plot of $T(r_h)$ and $dT/dr_h(r_h)$ against r_h showing that temperature has a minimum for the black hole solution. In both cases we choose the value $\hat{\mathcal{T}} = 1$ (colour online). 133
- 5.5 Plots, from top to bottom, of ω_{\star} , $h_{1\star}$ and $r_{h\star}$ vs $\hat{\mathcal{T}} = \kappa^2 L^2 \mathcal{T}$, where \star denotes evaluation at the r_h that minimizes the temperature $T(r_h)$. (colour online). 134

- 5.6 Here we plot the function $X(r)$ defined in (5.37) for two different values of Q with $\hat{\mathcal{T}} = 10$. (X_1 uses $Q = 200000$ and X_2 uses $Q = 800000$.) In the attractor region X is approximately constant, $X(\hat{\mathcal{T}})$, until r becomes sufficiently small that the large- r approximation fails. Even when $r \sim 1$ X remains Q -independent, and Q only determines where the crossover between the $z = 5$ and $z = 1$ regions occurs. 136
- 5.7 Two cartoons of r_h/L and r_c/L as a function of system size for fixed temperature and charge density. The upper (lower) r_h curve uses a temperature corresponding to the $z = 1$ ($z = 5$) region. The shaded area marked $1/L$ shows where finite-size effects become important. The curves for $r_h(L)$ stop for small L due to the existence of a minimum temperature. The left panel chooses \mathcal{T} small enough that $\hat{\mathcal{T}} \ll 1$ throughout, while in the right panel \mathcal{T} is larger so $\hat{\mathcal{T}}$ is negligible only to the far left. The curves assume $n = 0$ (*i.e.* $\mathcal{T} \propto L^2$). 137
- 5.8 A plot of the properties of the interior of an incompressible star for $Q = 1.25$, $\hat{\mathcal{T}} = 1/1000$. The assumption of constant mass and charge density is used as an illustrative example, since we are not interested in the exact values of stellar masses or radii (colour online). 140
- 5.9 Left panel: A comparison of the black-hole horizon radius, r_h , and stellar size, r_s , for a shared choice of asymptotic boundary conditions in the special case that the external geometry just outside the star or black hole has the $z = 5$ asymptotic form (see text for discussion). Right panel: The integrands for the two terms in (5.75) for the free-energy difference between stellar and black-hole geometries. The red curves labeled I_1, I_2 , and I_3 give the contribution of the stellar interior, for the following values of central pressure: $\kappa^2 L^2 p(0) = 10^5, 10$, and 1 for which $r_s = 1.56, 1.42$, and 0.74 respectively. The remaining three (green) curves show the contribution from the exterior geometry. These curves rise sharply at r_h , which can be seen to occur at $r_h = 1.39, 1.25$, and 0.66 respectively. All curves stop at the value $r = r_s$ appropriate to the solution in question. The free energy difference evaluates to $\Delta F_1 = -.21$, $\Delta F_2 = -.01$, and $\Delta F_3 = .045$. Left panel uses $\hat{\mathcal{T}} = 10^{-5}$, and right panel uses $\hat{\mathcal{T}} = 10^2$ (colour online). 142
- 5.10 Derivative of the free energy in the black hole phase as a function of horizon position (in units of $4\pi L/\kappa^2$). Notice its singular behaviour as the temperature approaches the minimum of the black hole phase. 146

0.1 Conventions

High energy physics seems to be a particularly privileged field in physics where in addition to the expected battleground between scientists on the fronts of various models, conventions in which to approach a calculation invoke heated debate. As the purpose of this thesis is to in fact explicitly show calculations for various physical quantities, we must inevitably pick a side to many of these conventional debates. We start with a fairly innocuous and universally accepted convention. That is, we take the charge of the electron to be negative. Now that we have lulled the reader into a false sense of security, we move onto the more important and useful conventions that will be heavily used throughout the remainder of this text.

Units

We work in natural units. Both \hbar and c are set to unity, in addition to the less standard Boltzmann constant, $k_B = 1$, which will be important when calculating temperatures in the AdS/CFT formalism in chapter 3. The consequence of this is that all dimensional quantities will be expressed in terms of powers of mass (we could similarly use length instead, but standard convention dictates that we count powers of mass.) If we use Newton's constant, $8\pi G_N = \kappa^2$, as an example, we conclude that in 4 dimensions, it has dimensions $[\text{mass}]^{-2}$. As such, the Planck mass in d dimensions is given by

$$M_P^{2-d} = 16\pi G_N = 2\kappa^2.$$

While throughout the text, we will be primarily focusing on the gravitational constant κ^2 instead of the Planck mass, the Planck mass is an important scale to keep in mind as a reminder for the validity of any calculation that uses classical (super-)gravity as its effective theory.

Geometrical conventions

These conventions are the more hotly debated and far from agreed upon in the literature. For space-time distances, we choose to use the mostly plus metric,

$$\eta_{\mu\nu} = \begin{pmatrix} - & & & & \\ & + & & & \\ & & + & & \\ & & & + & \\ & & & & \ddots \\ & & & & & + \end{pmatrix}.$$

The benefits of this metric are quite numerous¹. The primary advantage for this work is since there are more spatial dimensions than temporal ones, any calculation involving geometrical quantities (which amount to most in this text) would do well to have the number of minus signs minimized to avoid propagation of errors. A secondary advantage is when performing a Wick rotation to calculate physical quantities of the CFT in AdS/CFT, the metric becomes entirely positive and much more intuitive.

Furthermore, we follow the less standard definition of curvature in general relativity and therefore the subsequent curvature tensors and scalar, as per Weinberg [2]. These are

$$\begin{aligned}R_{\beta\gamma\delta}^{\alpha} &= \partial_{\delta}\Gamma_{\gamma\beta}^{\alpha} - \partial_{\gamma}\Gamma_{\beta\delta}^{\alpha} + \Gamma_{\delta\sigma}^{\alpha}\Gamma_{\beta\gamma}^{\sigma} - \Gamma_{\gamma\sigma}^{\alpha}\Gamma_{\beta\delta}^{\sigma} \\R_{\alpha\beta} &= R_{\alpha\gamma\beta}^{\gamma} \\R &= R^{\alpha}_{\alpha}.\end{aligned}\tag{1}$$

With regards to indices, when mentioning arbitrary dimensions, time will be labeled as x^0 . Furthermore, capital Latin indices, $MN \dots$ denote all dimensions (when the total number of dimensions are greater than 4). Greek indices, $\alpha\beta \dots$, denote either 4 dimensions or simply a subspace of a larger dimensional theory, and lowercase Latin indices, $ij \dots$ denote 3 dimensions and less.

¹For a number of very good reasons as to why this is the ‘right’ metric to use, an excellent exposition is given in appendix E of [1]

Chapter 1

Introduction

For centuries, the foundation of science and its progress has benefited largely from large scale differences and their decoupling. As an everyday example that perhaps lends itself to one's intuition, take the population of humans on Earth. One can study the sociology and economics of the populous¹ without needing to know a lot of the more complicated details of the subjects themselves. For instance one persons purchasing decision will likely not have an impact on the general growth trajectory of the world as a whole.

Similarly, as we move further and further to smaller scales in which complicated behaviour is either unimportant or simplified, we see the same effect in the more 'hard' sciences such as biology, chemistry, and physics. The detailed chemical properties of hydrocarbons are not necessarily important in the behaviour of biological systems, for instance the simplification of hydrophobic or hydrophilic strings are commonly employed in biophysics. The precise structure of a nucleus in an atom is similarly abstracted from chemical reactions and potential chemical compounds possible. At shorter distance scales, physics takes over as the field of study, from analyzing crystal structures down to the Planck scale, or the motion of planets to objects on the size of the Hubble scale. Again, due to the power of scale separation, many fields of physics exist as useful fields of study in their own right without the need to study all areas of physics to get a good understanding of the system in question. Indeed, the reason the Standard Model is a good description of particle physics at higher energies (as opposed to atomic energies) is because the relevant degrees of freedom significantly change from the weak scale instead to the atomic scale.

Of course this view of physics and science in general becomes a double edged sword. If someone were to be given the final theory in which all of physics and science is based, there would be no way of predicting the world we see around us for the same reasons². Just as it is impossible to uniquely predict the atom from the standard model, and DNA from chemistry, the laws of physics we see at

¹While neither of these fields are strictly scientific due to their imprecise nature and large unpredictability, the fact that they are collective behaviour of the scientific discipline of psychology still stands.

²For a particularly good exposition on this argument of "reductionism does not imply constructionism" see [3]

lower energies will unlikely be a unique solution to this ‘final theory’.

One of the goals of current particle physics is the understanding of particles and scales beyond those of the standard model. At the very least, there must be at least one ‘more fundamental’ theory that includes a consistent quantum mechanical description of gravity at very high energies³. Superstring theory, over many years of research by the high energy community, has been shown to be a perturbatively consistent quantum theory of gravity. The idea that string theory will ultimately be the appropriate description of physics at the Planck scale has led to a large amount of models at lower energies that incorporate the principles and mathematics of string theory to describe the world around us. This ‘phenomenological’ approach has the benefit of having real-world observables to compare results against for validation as a model, while still retaining distinct features one would see in string theory at lower energies. Of course the downside is that this approach ultimately requires a description of how to obtain these models from a more fundamental string theory. This work consists of models that take this phenomenological approach with the view that one should be able to reproduce real-world experiments as priority over obtaining our models from a string theory.

1.1 Major Developments in String Theory

In order to fully understand the work presented in this thesis, some context should be introduced to properly motivate the models presented here. To that end, we give a brief overview of some of the major developments in string theory from a qualitative standpoint. This exposition is by no means exhaustive, and is largely based on the reviews of [4, 5, 6] and the introductory chapter of Polchinski’s string theory text [7].

1.1.1 Strings, Supersymmetry, Branes, and Extra Dimensions

String theory, originally a potential model for the strong interactions [8], became a potential theory for quantum gravity when it was realized that the lowest lying non-tachyonic mode of the closed string spectrum was a massless spin-2 particle. However, for bosonic string theory, a tachyonic (negative mass-squared) mode existed, indicating an inconsistent theory. This led to the immediate conclusion that if we insist that string theory must be a theory of quantum gravity, then these strings must be supersymmetric at the Planck scale. Moreover, one of the conditions for a Lorentz-invariant vacuum to exist as a solution requires the strings live in 10 dimensions (9 of space and 1 of time) [7].

Unfortunately, we are acutely aware that at the energies we experience in our everyday lives that supersymmetry doesn’t manifest itself as particles in the standard model. Even more importantly, as of this writing, the only dimensions we can currently access are of 3 spatial and 1 temporal. Clearly the lack of supersymmetry and extra dimensions up to and including the scale of the standard model suggest that if string theory is to remain a viable theory at higher energies, some mechanism must

³Typically in modern proposals, many models include more in between the weak scale and the Planck scale

exist such that at lower energies we see the world around us and not a bunch of supersymmetric particles free to move in a 10 dimensional space-time!

In addition to the required existence of strings and supersymmetry, it was realized much later that for open strings⁴, their endpoints behave in a collective way such that at low energies it is more appropriate to describe them as surfaces spanned by the endpoints of the strings (see chapter 8 of [7]). These surfaces have been since denoted as ‘branes’ and have been the subject of much extra-dimensional phenomenology.

The important point here, from a phenomenological perspective, is that there are now two methods of ‘hiding’ these extra dimensions from modern experiments. The first approach would be to make any extra dimensions periodic and small such that no current experiment could probe the small dimensions. This is referred to as ‘compactification’. The second approach is using the observation that string endpoints (which are interpreted as particles at lower energies) are restricted to living on these branes. It then becomes a reasonable possibility to suggest that our observable universe is a 3-brane⁵ of which all particles we observe (aside from gravity which is much less constrained) are restricted to the dimensions we’re familiar with, being 3 of space and 1 of time.

In fact, combinations of the above are also possible, where for instance compactifications occur over some dimensions, leaving a number of extra dimensions large, but utilizing branes as a way of trapping the standard model in 4 space-time dimensions. Motivated by these many possible realizations of low energy string theory, the phenomenological approach typically assumes a lower dimensional theory with a number of ingredients motivated by string theory. These possible ingredients include branes, supersymmetry, extra scalar fields, extra gauge fields, and of course extra dimensions. As we have stated already, we take the phenomenological position, and while we expect our models to be a low energy description of a string theory, as of this writing it is not known explicitly how these models will manifest themselves as a low energy string theory.

At this point, we have made some very qualitative arguments in favour of the phenomenological approach. To further motivate and quantify this approach, we give a brief overview of extra-dimensional compactification and brane physics.

1.1.2 String Technology

Up until this point, we have given many arguments as to how to take a phenomenological approach to model building and why this is a more feasible approach. While the approach we take is a bottom-up one - where a model is constructed with the intention of embedding it in a string theory if the model is viable - there also exists the top-down approach where one starts with a string theory and makes a number of assumptions and compactifications to produce a lower-dimensional model. Here we

⁴In a string theory, there are generally two possible configurations for a string. Either a string is open, like a spaghetti noodle, or it is closed, like a hula-hoop

⁵A p-brane is conventionally referred to as a p-spatial dimensional surface that also propagates through time, or a p+1 space-time surface.

sketch the technology used in the top-down approach, as to give a good understanding towards the motivation of the bottom-up approach, where one simply ‘writes down a theory,’ and the justification of the content of such a theory.

Compactification

Typically in extra-dimensional theories, one has to explain why we physically do not see extra dimensions at energies that we currently can access. The simplest method of hiding any extra dimensions is through toroidal compactification. That is, if we have an extra dimension x^d , where $d + 1$ is the total number of dimensions, we make the identification

$$x^d \simeq x^d + 2\pi a \tag{1.1}$$

such that the extra dimension is wrapped up like a cylinder. Clearly, as we take $a \rightarrow 0$ the extra dimension essentially vanishes and the only dynamics one would expect to see are in the remaining dimensions. From a geometric point of view, this is essentially singling out one dimension in the metric. If we rewrite the metric as

$$ds^2 = g_{MN} dx^M dx^N = g_{\mu\nu} dx^\mu dx^\nu + e^{2\phi} (dx^d + A_\mu dx^\mu)^2, \tag{1.2}$$

then we have essentially separated the extra, to be compactified, dimension from the rest of the metric. When we take the remaining dimensions indices to be raised and lowered by the metric $g_{\mu\nu}$, there are a few advantages to this parameterization. First we can see that the inverse metric takes the simple form,

$$g^{MN} = \delta_\mu^M \delta_\nu^N g^{\mu\nu} - \delta_d^M \delta_\mu^N e^{-2\phi} A^\mu - \delta_\mu^M \delta_d^N e^{-2\phi} A^\mu + \delta_d^M \delta_d^N e^{-2\phi} (1 + A_\mu A^\mu). \tag{1.3}$$

Furthermore, we see the determinant of g_{MN} separates nicely into⁶

$$\det(g_{MN}) = e^{2\phi} \det(g_{\mu\nu}). \tag{1.4}$$

Finally, a diffeomorphism of the form

$$x^d \rightarrow x^d + \Lambda(x^\mu), \tag{1.5}$$

is equivalent to the gauge transformation

$$A_\mu \rightarrow A_\mu + \partial_\mu \Lambda, \tag{1.6}$$

⁶To see this, note how the metric must be the inverse of the inverse metric. From the method of cofactors, we know that $g_{dd} = \det g^{\mu\nu} / \det(g^{MN})$. Since the inverse of the determinant is the determinant of the inverse, this completes the proof.

when we assume the metric functions are independent of the extra dimension. To see how the Ricci scalar must decompose, consider the scaling

$$x^d \rightarrow x^d \lambda. \quad (1.7)$$

To leave the metric invariant, we must impose both $A_\mu \rightarrow A_\mu \lambda$ and $\phi \rightarrow \phi - \ln \lambda$. Since we know the Ricci scalar is diffeomorphic invariant, it is therefore gauge invariant in the extra dimensional vector, A_μ . The only quantity consistent with gauge invariance and two derivatives is F^2 , and from the previous scaling argument, we see that it must appear as

$$R^{d+1} = R^d + H(\partial\phi) + B e^{2\phi} F_{\mu\nu} F^{\mu\nu}, \quad (1.8)$$

where H is some function of derivatives of the scalar field, and B is a constant from the decomposition, and R^d is built from $g_{\mu\nu}$. Furthermore, since the kinetic term of the dilaton can not be coupled to the gauge field⁷ the kinetic term of the dilaton must possess a shift symmetry. Writing the action then becomes

$$S = - \int d^d x e^\phi \sqrt{-g} \frac{1}{2\kappa'^2} (R^d + C(\partial\phi)^2 + B e^{2\phi} F_{\mu\nu} F^{\mu\nu}), \quad (1.9)$$

where $\kappa'^2 = \kappa^2/(2\pi a)$ is the lower dimensional gravitational constant and we have dropped boundary terms. We can rescale A_μ to put B in standard form, but to determine C , we must keep track of two-derivative terms on the scalar field in R^d . Due to gauge invariance, we ignore terms with the gauge field, A_μ as a multiplicative factor, as it must be canceled in the final result. The relevant parts of the connections are then

$$\delta\Gamma_{dd}^\mu = - e^{2\phi} \partial^\mu \phi \quad (1.10)$$

$$\delta\Gamma_{\mu d}^d = \partial_\mu \phi, \quad (1.11)$$

where the δ 's signify these are not the full connection coefficients. When inserting these into the definition of the Ricci scalar, (1), the compactified action becomes

$$S = - \int d^d x e^\phi \sqrt{-g} \left[\frac{1}{2\kappa'^2} (R^d + 2(\partial\phi)^2) + \frac{1}{4} e^{2\phi} F_{\mu\nu} F^{\mu\nu} \right]. \quad (1.12)$$

The upshot is we see how extra scalar and gauge fields naturally arise from dimensional compactification, as well as the fact that the extra scalar field now plays a role of a dynamical coupling constant for the gauge field. To see the behaviour on compactified fields, we look at the action of a

⁷If the kinetic term of the dilaton was coupled to the gauge field, it must be only through the field strength, $F_{\mu\nu}$. However, to preserve general covariance, the indices must be contracted in such a way that the only allowed term would be $(\partial\phi)^2 F$, but this has more than two derivatives, which could not descend from the Ricci scalar.

massless free scalar,

$$S_\psi = - \int d^{d+1}x \sqrt{-g^{d+1}} g^{MN} \partial_M \psi^d \partial_N \psi^{d*}. \quad (1.13)$$

Since ψ must be periodic in the extra dimension, it must take on the form $\psi^d = e^{inx^d/a} \psi(x^\mu)$ where n is an integer. Expanding the action gives us

$$S_\psi = - \int d^d x \sqrt{-g} e^\phi \left[g^{\mu\nu} \left(\partial_\mu \psi + \frac{in}{a} e^{-\phi} A_\mu \psi \right) \left(\partial_\nu \psi^* - \frac{in}{a} e^{-\phi} A_\nu \psi^* \right) + e^{-\phi} \frac{n^2}{a^2} \right]. \quad (1.14)$$

Here we see not only does a massless field gain a number of different mass modes associated with the extra dimensions, but that the charge with respect to the new gauge field is proportional to its mass. This is known as a Kaluza-Klien (KK) tower of modes as each mass and charge are equally spaced for all possible modes. As one would expect, if one makes this extra dimension small enough, these additional modes become hidden by the large energy gap required to excite the particle, and the particle looks entirely like a neutral d dimensional particle.

T-duality

Here we motivate the existence of branes. For a much more technical introduction, see [7]. Our approach here is to motivate them from a heuristic standpoint. That is, using some very basic string technology we hope to give some plausibility arguments as to the requirement of their existence as degrees of freedom in a string theory.

If we take (1.14), and write down the zero-momentum energy states for this massless extra-dimensional particle, the spectrum would have the form

$$E_\psi \sim \frac{n}{a}. \quad (1.15)$$

However, if instead of a scalar particle, we allowed for an extended closed string to propagate in all of these dimensions, we would have an additional winding mode. The string itself, being closed, could possibly wind around the extra dimensions an integer number of times. Remembering that the energy contained in a string is proportional to the product of its tension times its length, it is quite intuitive to say the contribution from these winding modes would be of the form $\delta E \sim nR$. Therefore the total contribution from the extra dimensions to the energetics of a closed string is

$$E_{\text{string}} \sim \frac{n}{a} + ma. \quad (1.16)$$

Here we see an important feature of closed strings compared to a scalar field. In the case of the scalar field, we can simply hide the extra dimensional energetics by making the extra dimension small enough. In the case of closed strings, however, taking $a \rightarrow 0$ yields a continuous spectrum of winding modes as the KK modes disappear. This property of $R \sim 1/R$ for the degrees of freedom

of strings is known as T-duality. The important point is that there is no way of hiding this extra dimension from the point of view of strings.

However, if we were to consider an open string, it would still have the KK-modes associated with a compactified extra dimension, but not have the winding modes a closed string has. This is simply because there is nothing preventing an open string from unwinding itself around the compactified direction. From the point of view of degrees of freedom, as we take $R \rightarrow 0$, it naively seems that closed strings preserve their degrees of freedom while open strings do not. This is inconsistent since both types of strings interact with each other, and therefore one could lose or gain degrees of freedom in a scattering process. The technical resolution to this apparent paradox is beyond the scope of this thesis, but the sketch is as follows. As we take $a \rightarrow 0$, the open string is further restricted along this periodically identified hyperplane. However, just as open strings pick up a new massless degree of freedom to propagate into, these closed strings must also be free to roam in this T-dual dimension. An additional ‘stringy’ technicality is that the Neumann boundary condition of the open string becomes a Dirichlet boundary condition in the dual co-ordinate.

This boundary condition suggests that the effective degrees of freedom at low energies would be the collective behaviour of these string endpoints. Since these endpoints lay on a hypersurface of the full dimensionality of the theory, we describe the collective behaviour of them as surfaces, or ‘branes’. If these branes do not interact with any gauge fields of interest, their action is simply proportional to their world-volume,

$$S_{\text{brane}} = -T_p \int d^p x e^{-\phi} \sqrt{-\star g} \quad (1.17)$$

where \star denotes the pullback of the metric. Simply put, the pullback is the action of evaluating the metric along the hypersurface of the brane direction. If we oriented a p – brane such that it was normal to the other $d + 1 - p$ dimensions, the pullback would be the block of the metric in the p directions evaluated at the position of the brane in the $d + 1 - p$ directions. The additional scalar field is a stringy feature that we take as a given from a phenomenological approach which will end up being scaled out by putting the metric in the Einstein frame. In chapter 2, we assume the brane action takes this form with the scalar field associated with this brane a constant. Furthermore, we assume it has $d - 1$ dimensions and perpendicular to the extra 2 dimensions, giving it the form of simply an integral over the 4 dimensional metric.

We can further write down a brane action that interacts with a U(1) charge. This action takes the form

$$S_{\text{brane}} = -T_p \int d^p x e^{-\phi} \sqrt{|\star g + \ell^2 F|}, \quad (1.18)$$

where we have introduced a length scale for the gauge field, that is left arbitrary from a phenomenological standpoint and F only carries indices in the brane directions. Again, the derivation of this action is beyond the scope of this work, but the form for this action can be motivated by requiring

that the action only transform in the directions corresponding to the brane directions. This is the brane action we use when considering the holographic quantum Hall model.

The upshot of these expressions is that they provide very real motivation for the extra dimensional and holographic models as string theory provides a wealth of theoretical objects and tools in which to construct these phenomenological models.

1.2 Overview

We're now ready to give a summary of the work in this thesis given the motivation for the phenomenological approach. Chapter 2 is work on the brane-world large extra dimensions paradigm. The exact purpose of this chapter is setting up a formalism for brane back-reaction in the large extra dimensions paradigm. In addition to this, solutions will be explored as the acid test to the reliability of this framework.

From then on, this thesis concentrates on the gauge-gravity paradigm as applied to condensed matter systems. This is also known as the Anti-de Sitter/Conformal Field Theory (AdS/CFT) correspondence or holography. Chapter 3 gives an overview of this conjecture and outlines various properties and relations to condensed matter systems. In this chapter, we also fill in the appropriate calculations not included in the following papers for the benefit of the reader not familiar with the AdS/CFT paradigm. Furthermore, we also introduce the quantum Hall effect as well as its current theoretical and experimental understanding. Chapter 4 is a paper which introduces a particular holographic model for quantum Hall systems and goes on to calculate a number of observables present in real quantum Hall systems. Chapter 5 further refines this model by comparing another physical observable, the dynamical critical exponent, to experiments and further constrains the parameter space of this 'Hall-ography' model such that it reproduces experimental data.

Finally, chapter 6 summarizes all of the material contained in this thesis. We both provide a brief recap of the reasoning of these particular research programs, as well as an overview of the importance of this research taken as a whole in this research field in physics. Furthermore, we provide some further motivation for potential future endeavors, as well as the current status of these paradigms in the community.

Chapter 2

Codimension-2 Brane-Bulk

Matching: Examples from Six and Ten Dimensions

Preface

This work borrows from the ideas outlined earlier in string theory in section 1.1.2. In particular it focuses on the concept of branes and their roles on the exterior geometry and their own particular space spanned from a low energy perspective. The thrust of this paper is to extend the methods introduced in [9] to include gauge fields and apply it to known examples of effective theories. That is, we develop a formalism that directly provides a low energy, lower-dimensional theory from the standpoint of brane-world phenomenology provides a step towards connecting extra-dimensional models to current observables and therefore a testing ground for extra-dimensional phenomenology.

Indeed, recent research based off this formalism has been extremely fruitful. In addition for providing an inflationary model from the large extra dimensions paradigm [10], it has provided a perfectly ‘natural’ explanation to the cosmological constant problem [11]. This will be further explored in the conclusion to this thesis, but the important takeaway is that this has become an important tool and the start of a theme towards quantifying observables using models motivated by stringy techniques.

Abstract

Experience with Randall-Sundrum models teaches the importance of following how branes back-react onto the bulk geometry, since this can dramatically affect the system's low-energy properties. Yet the practical use of this observation for model building is so far mostly restricted to branes having only one transverse dimension (codimension-1) in the bulk space, since this is where tools for following back-reaction are well-developed. This is likely a serious limitation since experience also tells us that one dimension is rarely representative of what happens in higher dimensions. We here summarize recent progress on developing the matching conditions that describe how codimension-2 branes couple to bulk metric, gauge and scalar fields. These matching conditions are then applied to three situations: $D7$ -branes in F-theory compactifications of 10D Type IIB string vacua; 3-branes coupled to bulk axions in unwarped and non-supersymmetric 6D systems; and 3-branes coupled to chiral, gauged 6D supergravity. For each it is shown how the resulting brane-bulk dynamics is reproduced by the scalar potential for the low-energy moduli in the dimensionally reduced, on-brane effective theory. For 6D supergravity we show that the only 4D-maximally symmetric bulk geometries supported by positive-tension branes are flat.

2.1 Introduction

Space-filling branes, situated around extra dimensions, provide a remarkable framework for approaching phenomenological problems. Besides being well-motivated — for instance arising very naturally within string theory — branes lead to novel kinds of low-energy physics that can cut to the core of many of the naturalness issues that currently plague particle physics and cosmology.

The realization that not all particles need ‘see’ the same number of dimensions (because brane-bound particles are trapped to move only along the branes) is the first type of brane-related insight to have made a major impact on physics, leading to the recognition that the scale of gravity can be much smaller than the Planck scale [1]. A second major revelation came with the realization that the back-reaction of branes on their environment can strongly influence their low-energy properties, such as by providing deep gravitational potential wells within the extra dimensions that redshift the energy of those branes that live within them [2].

Although branes can in principle have a great variety of dimensions, almost all of the detailed exploration of brane-bulk back-reaction is specialized to the case of codimension-1 branes: *i.e.* those branes that span just one dimension less than the dimension of the full spacetime. This is partially because tools for describing how branes back-react on their surroundings are only well-developed for codimension-1 surfaces, since in this case the problem can be expressed in terms of the Israel junction conditions [3]. This restriction to codimension-1 objects is potentially very limiting because the special nature of kinematics in one dimension makes it unlikely that back-reaction for codimension-1 branes is representative of back-reaction for branes with higher codimension.

The main obstacle to understanding how properties of higher-codimension branes are related to the bulk geometries they source is the fact that these bulk geometries typically diverge at the position of their sources. (The most familiar example of this for a codimension-3 object is the divergence of the Coulomb potential of a nucleus evaluated at the nuclear position.) It is one of the special features of codimension-1 objects that the bulk fields they source typically do not diverge at their positions. They instead cause discontinuities of derivatives across their surfaces, whose properties are captured by the Israel junction conditions.

The next-simplest case consists of codimension-2 objects, whose back-reaction is complicated enough to allow the possibility of bulk fields diverging at the positions of the sources. Although bulk fields *can* diverge for codimension-2 sources, they *needn't* do so in time-independent situations. (For instance, they can instead give rise to conical singularities, such as for cosmic strings in 4D spacetime [4]. When bulk fields do not diverge the relation between bulk and brane properties is easier to formulate, and so better studied [5].) The potential for divergent bulk configurations makes codimension-2 branes more representative of systems with more generic codimension than are codimension-1 branes. But dynamics in two dimensions is still simple enough to allow explicit closed-form solutions to be known for the bulk configurations sourced by codimension-2 branes, allowing a detailed study of their properties.

Tools for describing how bulk fields respond to the properties of source branes were recently developed in the general case, including where the bulk fields diverge [6, 7, 8], opening up the properties of codimension-2 branes for phenomenological exploration. These tools — summarized (and slightly generalized) in §2 below for a fairly general class of scalar-tensor-Maxwell theories in n extra dimensions — boil down to a set of matching conditions that relate the near-brane limit of the radial derivatives of the bulk fields to the action for the brane in question.

In §3 we apply these tools to three kinds of examples: compact geometries sourced by D7 branes in F-theory compactifications of 10D Type IIB supergravity; 3-branes coupled to a bulk axion within unwarped, non-supersymmetric 6D scalar/Maxwell/Einstein theory; and 3-branes coupled to 6D chiral gauged supergravity. We draw the following lessons from these comparisons:

- F-theory compactifications [10] of 10D Type IIB supergravity sourced by D7-branes serve as a reality check, since string theory tells us the detailed form of both the brane and bulk actions [9], and explicit solutions are known for the transverse spacetimes that are sourced by these branes [21]. We verify the codimension-2 brane/bulk matching conditions by checking that the asymptotic forms for the solutions are related to the known brane actions in the prescribed way.
- In 6D axion-Maxwell-Einstein theory, flux-compactified solutions are known for the bulk that interpolates between two 3-branes, and these are simple enough to allow the explicit calculation of how branes contribute to the low-energy axion potential [11]. From the perspective of six dimensions the resulting axion stabilization arises through the requirement that both branes be consistent in their demands on the bulk. We show that the stabilized value agrees precisely with the result of minimizing the low-energy axion potential as seen by an observer who has integrated out the extra dimensions below the Kaluza-Klein (KK) scale. We also show how this potential gives the same value for the curvature of the maximally symmetric on-brane geometry as is calculated from the higher-dimensional field equations.
- Stable flux compactifications are also known for 6D chiral gauged supergravity [12], having up to two singularities that represent the positions of two source branes [13]. These solutions are known in explicit closed form for the most general solutions having a flat on-brane geometry and axial symmetry in the bulk; and in a slightly more implicit form for solutions with de Sitter or anti-de Sitter on-brane geometry. In this case we use the matching conditions to show that the only bulk configurations that can be supported by positive-tension branes have flat induced on-brane geometries, with (possibly warped) bulk geometries with nonsingular limits as the source branes are approached. We also show how geometries that diverge at the brane positions can arise from specific kinds of negative-tension branes, while no maximally symmetric solutions exist at all for many kinds of brane sources (presumably corresponding to time-dependent runaway bulk geometries, such as those considered in [14]).

§4 briefly summarizes some of the implications of these results.

2.2 The Bulk-Brane system

We start by describing the brane-bulk framework within which we work. This starts with a statement of the scalar-metric-Maxwell system whose equations we use, followed by a statement of how the near-brane boundary conditions of the bulk fields are related to the action of the branes which are their source. Finally we describe the contribution of each brane to the low-energy scalar potential that is valid over distances much longer than the size of the extra dimensions, and identify a constraint which allows a simple description of this contribution given the properties of the brane tension.

2.2.1 The bulk

The starting point is the statement of the equations of motion that govern the bulk.

General formulation

We assume the following action for the n -dimensional bulk physics, describing a general scalar-tensor theory coupled to a Maxwell field,¹

$$S = \int_{\mathcal{M}} d^n x \mathcal{L}_B + \int_{\partial\mathcal{M}} d^{n-1} x \mathcal{L}_{GH} \quad (2.1)$$

where

$$\mathcal{L}_B = -\sqrt{-g} \left\{ \frac{1}{2\kappa^2} g^{MN} \left[\mathcal{R}_{MN} + \mathcal{G}_{AB}(\phi) \partial_M \phi^A \partial_N \phi^B \right] + \frac{1}{4} f(\phi) F_{MN} F^{MN} + V(\phi) \right\}, \quad (2.2)$$

and the Gibbons-Hawking lagrangian [17] is

$$\mathcal{L}_{GH} = \frac{1}{\kappa^2} \sqrt{-\hat{\gamma}} K, \quad (2.3)$$

and is required in the presence of boundaries in order to make the Einstein action well posed. Here $F = dA$ is the field strength of the Maxwell field, \mathcal{R} is the Ricci scalar for the 6D spacetime metric, g_{MN} , and \mathcal{G}_{AB} is the metric of the target space within which the scalar fields, ϕ^A , $A = 1, \dots, N$, take values. $\hat{\gamma}_{ij} = g_{MN} \partial_i x^M \partial_j x^N$ is the induced metric, and K is the trace, $\hat{\gamma}^{ij} K_{ij}$, of the extrinsic curvature, of the boundary surface, $\partial\mathcal{M}$.

This bulk action is chosen to be general enough to include the bosonic part of the supersymmetric

¹Our metric is mostly plus, with Weinberg's curvature conventions [15], which differ from those of MTW [16] only by an overall sign in the definition of the Riemann tensor.

theories of interest. Its field equations are

$$\frac{1}{2\kappa^2} (\mathcal{R}_{MN} + \mathcal{G}_{AB} \partial_M \phi^A \partial_N \phi^B) + \frac{f}{2} F_M{}^P F_{NP} + \frac{1}{n-2} \left[V - \frac{f}{4} F_{PQ} F^{PQ} \right] g_{MN} = 0, \quad (2.4)$$

$$\mathcal{G}_{AB} \square \phi^B - \kappa^2 \left[\frac{\partial V}{\partial \phi^A} + \frac{1}{4} \frac{\partial f}{\partial \phi^A} F_{MN} F^{MN} \right] = 0, \quad (2.5)$$

and

$$\nabla_M (f F^{MN}) = 0, \quad (2.6)$$

where

$$\square \phi^A := g^{MN} \left[\nabla_M \partial_N \phi^A + \Gamma_{BC}^A(\phi) \partial_M \phi^B \partial_N \phi^C \right], \quad (2.7)$$

with $\Gamma_{BC}^A(\phi)$ being the Christoffel connection built from the metric \mathcal{G}_{AB} .

Metric *ansätze*

Our interest is in configurations whose geometries are maximally symmetric in the brane directions, for which it is convenient to specialize to the metric

$$\begin{aligned} ds^2 = g_{MN} dx^M dx^N &= e^{2W} \hat{g}_{\mu\nu} dx^\mu dx^\nu + g_{mn} dx^m dx^n \\ &= e^{2W} \hat{g}_{\mu\nu} dx^\mu dx^\nu + e^{2C} dz d\bar{z}, \end{aligned} \quad (2.8)$$

where $\hat{g}_{\mu\nu}(x)$ denotes a maximally symmetric $(n-2)$ -dimensional metric. The coordinates are $x^M = \{x^\mu, x^m\}$, with x^μ , $\mu = 0, \dots, n-3$ labelling the brane directions, and $m = n-2, n-1$ (or $z = x^{n-2} + ix^{n-1}$) being coordinates for the two dimensions transverse to the branes. The functions W and C are generally singular at the positions of any source branes. For instance, if $e^C = (\ell/r)^a$ for $r^2 = |z|^2$, then the proper distance becomes $\rho = [\ell/(1-a)](\ell/r)^{a-1}$ and $e^B = \ell(\ell/r)^{a-1} = (1-a)\rho$, showing that the metric in this case has a conical singularity at $r = \rho = 0$, with defect angle $\delta = 2\pi a$.

For some applications, particularly very near a brane, it is useful to further specialize to the most general *ansatz* consistent with cylindrical symmetry in the two transverse dimensions, $\{x^m, m = n-2, n-1\}$. This leads to the following metric:

$$\begin{aligned} ds^2 &= d\rho^2 + e^{2B} d\theta^2 + e^{2W} \hat{g}_{\mu\nu} dx^\mu dx^\nu \\ &= e^{2C} \left(dr^2 + r^2 d\theta^2 \right) + e^{2W} \hat{g}_{\mu\nu} dx^\mu dx^\nu \end{aligned} \quad (2.9)$$

where θ labels the direction of cylindrical symmetry, and the functions $B = B(\rho)$ and $W = W(\rho)$ depend on the proper distance, ρ , only — or $C = C(r)$ is a function only of r .

The bulk scalars are similarly just functions of ρ , $\phi^A = \phi^A(\rho)$, and a gauge can be chosen to that

the only nonzero component for the Maxwell field is $A_M = A_\theta(\rho) \delta_M^\theta$, and so

$$F_{\rho\theta} = -F_{\theta\rho} = A'_\theta, \quad (2.10)$$

where the prime denotes differentiation with respect to ρ .

The Einstein equations subject to this *ansatz* reduce to

$$\frac{1}{n-2} e^{-2W} \hat{R} + W'' + (n-2)(W')^2 + W'B' - \frac{1}{n-2} \kappa^2 e^{-2B} f(A'_\theta)^2 + \frac{2\kappa^2 V}{n-2} = 0 \quad (\mu\nu) \quad (2.11)$$

$$B'' + (B')^2 + (n-2)W'B' + \frac{n-3}{n-2} \kappa^2 e^{-2B} f(A'_\theta)^2 + \frac{2\kappa^2 V}{n-2} = 0 \quad (\theta\theta) \quad (2.12)$$

$$(n-2) [W'' + (W')^2] + B'' + (B')^2 + \mathcal{G}_{AB} \phi^{A'} \phi^{B'} + \frac{n-3}{n-2} \kappa^2 e^{-2B} f(A'_\theta)^2 + \frac{2\kappa^2 V}{n-2} = 0 \quad (\rho\rho), \quad (2.13)$$

while the dilaton and Maxwell equations become

$$e^{-B-4W} \left(e^{B+4W} \mathcal{G}_{AB} \phi^{B'} \right)' + \mathcal{G}_{AB} \Gamma_{CD}^B \phi^{C'} \phi^{D'} - \kappa^2 \left[\frac{\partial V}{\partial \phi^A} + \frac{1}{4} \frac{\partial f}{\partial \phi^A} e^{-2B} (A'_\theta)^2 \right] = 0, \quad (2.14)$$

and

$$\left(e^{-B+4W} f A'_\theta \right)' = 0. \quad (2.15)$$

2.2.2 Boundary conditions for codimension-2 branes

General formulation

Suppose an $(n-2)$ -dimensional, space-filling, codimension-2 brane is located at a position, $x^m = x_b^m$, within the 2 extra dimensions, with brane action

$$S_b = - \int_{x_b} d^{n-2}x \sqrt{-\gamma} \left[L_b(\phi^A, A_\theta, g_{\theta\theta}) + \dots \right], \quad (2.16)$$

where L_b denotes the brane lagrangian, which is potentially a function of the bulk scalars, ϕ^A , and the tangential components of the bulk Maxwell field and metric, A_M and g_{MN} , but not their derivatives. (Ellipses denote the possible subdominant, higher-derivative effective interactions that can also be present.) We imagine the geometry surrounding the brane to be given by the axisymmetric *ansatz* of eq. (2.9), with the brane located at $\rho = 0$, so θ denotes the angular direction about its position. Because our interest is in maximally symmetric solutions along the brane directions we do not entertain a dependence of T_b on any components of A_M and g_{MN} apart from A_θ and $g_{\theta\theta}$.

The induced metric on the brane is $\gamma_{\mu\nu} = g_{MN} \partial_\mu x^M \partial_\nu x^N = e^{2W} \hat{g}_{\mu\nu}$. Because of the warp factor appearing in this metric, for later purposes it is convenient to define the ‘warped’ tension, T_b , by

$T_b = e^{(n-2)W} L_b$, so that the brane action becomes

$$S_b = - \int_{x_b} d^{n-2}x \sqrt{-\hat{g}} \left[T_b(\phi, A_\theta, g_{\theta\theta}, W) + \dots \right]. \quad (2.17)$$

The back-reaction of such a brane onto the bulk geometry dictates the asymptotic near-brane behaviour of the bulk fields nearby,² through codimension-2 matching conditions that generalize [6, 7, 8] the more familiar ones that are encountered for codimension-1 branes. For the bulk scalars these state

$$\lim_{\rho \rightarrow 0} \oint_{x_b} d\theta \left[\frac{1}{\kappa^2} \sqrt{-g} \mathcal{G}_{AB} \partial_\rho \phi^B \right] = - \frac{\delta S_b}{\delta \phi^A}, \quad (2.18)$$

where the integration is about a small circle of proper radius ρ encircling the brane position, x_b , which is taken to be situated at $\rho = 0$. Similarly, the Maxwell matching condition is

$$\lim_{\rho \rightarrow 0} \oint_{x_b} d\theta \left[\sqrt{-g} f F^{\rho M} \right] = - \frac{\delta S_b}{\delta A_M}, \quad (2.19)$$

Finally, the metric matching condition is

$$\lim_{\rho \rightarrow 0} \oint_{x_b} d\theta \left[\frac{1}{2\kappa^2} \sqrt{-g} (K^{ij} - K g^{ij}) - (\text{flat}) \right] = - \frac{\delta S_b}{\delta g_{ij}}, \quad (2.20)$$

where K_{ij} is the extrinsic curvature of the fixed- ρ surface, for which the local coordinates are those appropriate for surfaces of constant ρ : $\{x^i, i = 0, 1, \dots, n-2\}$. Here ‘flat’ denotes the same result evaluated near the origin of a space for which the brane location $\rho = 0$ is nonsingular.

Axially symmetric ansatz

Specialized to the *ansatz* of eq. (2.9) the scalar-field matching condition becomes

$$\left[\frac{2\pi}{\kappa^2} e^{B+(n-2)W} \sqrt{-\hat{g}} \mathcal{G}_{AB} \phi^{B'} \right]_{x_b} = \frac{\partial}{\partial \phi^A} \left[\sqrt{-\hat{g}} T_b \right]. \quad (2.21)$$

With the same *ansatz*, the corresponding result for the Maxwell field reduces to

$$\left[2\pi \sqrt{-\hat{g}} e^{-B+(n-2)W} f A'_\theta \right]_{x_b} = \frac{\partial}{\partial A_\theta} \left[\sqrt{-\hat{g}} T_b \right] := \sqrt{-\hat{g}} J_b(\phi), \quad (2.22)$$

where the last equality defines the quantity J_b .

Finally, for fixed- ρ surfaces in this *ansatz*, $K_{ij} = \frac{1}{2} \partial_\rho g_{ij}$, and the comparison ‘flat’ metric is $ds_{\text{flat}}^2 = d\rho^2 + \rho^2 d\theta^2 + e^{2W_{\text{nat}}} \hat{g}_{\mu\nu} dx^\mu dx^\nu$, with $W'_{\text{nat}} \rightarrow 0$ as $\rho \rightarrow 0$. Since $K_{\theta\theta} = B' e^{2B}$ and $K_{\mu\nu} = W' e^{2W} \hat{g}_{\mu\nu}$, we have $K = g^{ij} K_{ij} = B' + (n-2)W'$, and so the $(\mu\nu)$ components of the metric

²A familiar example of this from electrostatics is the $1/\rho$ dependence of the Coulomb potential that occurs in the immediate vicinity of a point charge situated at $\rho = 0$.

matching conditions give

$$\left[-\frac{2\pi}{\kappa^2} \sqrt{-\hat{g}} e^{(n-2)W} [e^B ((n-3)W' + B') - 1] \right]_{x_b} = \sqrt{-\hat{g}} T_b(\phi), \quad (2.23)$$

while the $(\theta\theta)$ components are,

$$\begin{aligned} \left[\frac{2\pi}{\kappa^2} \sqrt{-\hat{g}} e^{B+(n-2)W} ((n-2)W') \right]_{x_b} &= -2 \frac{\partial}{\partial g_{\theta\theta}} \left[\sqrt{-\hat{g}} T_b \right] \\ &:= (n-2) \sqrt{-\hat{g}} U_b(\phi), \end{aligned} \quad (2.24)$$

where the last equality defines U_b . Just as T_b physically represents the brane tension, J_b can be interpreted as describing microscopic axial currents within the brane, or equivalently any microscopic magnetic flux these currents enclose within the brane. Once the dimensions transverse to the brane are dimensionally reduced, U_b turns out [6, 7] to be related to the brane contribution to the scalar potential within the low-energy 4D effective theory defined below the KK scale (as is seen in more detail later).

2.2.3 The brane constraint

These matching conditions, when combined with the bulk equations of motion, imply an important constraint relating the quantities T_b , J_b and U_b [18, 6, 7]. This constraint comes from eliminating second derivatives, ∂_ρ^2 , of the fields from the field equations, and so can be regarded as the ‘Hamiltonian’ constraint on the initial data when integrating the field equations in the ρ direction. When written in the form given above, the relevant combination of Einstein equations is $(n-2)(\mu\nu) + (\theta\theta) - (\rho\rho)$, which imply

$$\begin{aligned} (n-3)(n-2)(W')^2 + 2(n-2)W'B' - \mathcal{G}_{AB} \phi^{A'} \phi^{B'} \\ - \kappa^2 e^{-2B} f(A'_\theta)^2 + e^{-2W} \hat{R} + 2\kappa^2 V = 0. \end{aligned} \quad (2.25)$$

To turn this into a constraint on brane properties, multiply it through by $e^{2B+2(n-2)W}$ and take the limit $x \rightarrow x_b$, using the above matching conditions to eliminate the derivatives $\phi^{A'}$, B' , W' and A'_θ in favour of the brane functions T_b , J_b and U_b . The required matching conditions are

$$\begin{aligned} \left[e^B \phi^{A'} \right]_{x_b} &= e^{-(n-2)W} \mathcal{G}^{AB} \frac{\partial \mathcal{T}_b}{\partial \phi^B} \quad \text{with} \quad \mathcal{T}_b := \frac{\kappa^2 T_b}{2\pi} \\ \left[\kappa A'_\theta \right]_{x_b} &= e^{-(n-2)W} \frac{\mathcal{J}_b}{f} \quad \text{with} \quad \mathcal{J}_b := \frac{\kappa e^B J_b}{2\pi} \\ \left[e^B W' \right]_{x_b} &= e^{-(n-2)W} \mathcal{U}_b \quad \text{with} \quad \mathcal{U}_b := \frac{\kappa^2 U_b}{2\pi} \\ \text{and} \quad \left[e^B B' - 1 \right]_{x_b} &= -e^{-(n-2)W} \left[\mathcal{T}_b + (n-3) \mathcal{U}_b \right], \end{aligned} \quad (2.26)$$

where each of \mathcal{U}_b , \mathcal{T}_b and \mathcal{J}_b is dimensionless (keeping in mind e^B has dimensions of length). Using eqs. (2.26) in eq. (2.25) we find the desired constraint:

$$(n-3)(n-2)(\mathcal{U}_b)^2 + 2(n-2)\mathcal{U}_b \left[e^{(n-2)W} - \mathcal{T}_b - (n-3)\mathcal{U}_b \right] - \mathcal{G}^{AB} \frac{\partial \mathcal{T}_b}{\partial \phi^A} \frac{\partial \mathcal{T}_b}{\partial \phi^B} - \frac{(\mathcal{J}_b)^2}{f} + e^{2B+2(n-2)W} \left[e^{-2W} \hat{R} + 2\kappa^2 V \right]_{x_b} = 0. \quad (2.27)$$

This crucially simplifies once we use the fact that near the brane $e^B \rightarrow 0$ as $\rho \rightarrow 0$. (This states that the circumference of small circles about the brane must vanish as the radius of the circles vanishes. If not true, the object at $\rho = 0$ would not be interpreted as a codimension-2 brane.) The key observation [6, 7] is that the quantities $\kappa e^{2B} J_b$, $e^{2B-2W} \hat{R}$ and $\kappa^2 e^{2B} V$ also tend to vanish in this limit (as would be true, for instance, if $e^{-2W} \hat{R}$, V and J_b were bounded at the brane positions), implying that the constraint becomes

$$(n-2)\mathcal{U}_b \left[2e^{(n-2)W} - 2\mathcal{T}_b - (n-3)\mathcal{U}_b \right] - (\mathcal{T}'_b)^2 \simeq 0, \quad (2.28)$$

where $(\mathcal{T}'_b)^2 = \mathcal{G}^{AB} \partial_A \mathcal{T}_b \partial_B \mathcal{T}_b$.

What is important about this last form of the constraint is that the on-brane curvature drops out in this limit, meaning that eq. (2.28) cannot be read as being solved for \hat{R} . Instead, this constraint expresses a consistency condition for the brane action and junction conditions, imposed by the bulk equations of motion. In practice it provides a very simple method for computing the quantity $\mathcal{U}_b(\phi)$ once expressions for $\mathcal{T}_b(\phi)$ are given, since solving eq. (2.28) implies

$$\mathcal{U}_b = \frac{1}{n-3} \left[\left(e^{(n-2)W} - \mathcal{T}_b \right) \pm \sqrt{\left(e^{(n-2)W} - \mathcal{T}_b \right)^2 - \left(\frac{n-3}{n-2} \right) (\mathcal{T}'_b)^2} \right]. \quad (2.29)$$

Here the root is chosen for which $\mathcal{U}_b \rightarrow 0$ when $(\mathcal{T}'_b)^2 \rightarrow 0$, and so is \pm according to whether sign $(e^{(n-2)W} - \mathcal{T}_b)$ is \mp . This means that \mathcal{U}_b has the same sign as does $(e^{(n-2)W} - \mathcal{T}_b)$. Notice also that requiring the square root never be complex requires

$$\frac{n-3}{n-2} (\mathcal{T}'_b)^2 \leq \left(e^{(n-2)W} - \mathcal{T}_b \right)^2. \quad (2.30)$$

This last condition can be nontrivial, even though control over the semiclassical approximation requires $|\mathcal{T}_b| \ll 1$ and $(\mathcal{T}'_b)^2 \ll 1$. This is because it can happen that $e^W \rightarrow 0$ at the brane, in which case eq. (2.30) becomes a constraint on the size of $(\mathcal{T}'_b)^2 / \mathcal{T}_b^2$.

For $(\mathcal{T}'_b)^2 \ll (e^{(n-2)W} - \mathcal{T}_b)^2$ eq. (2.29) becomes

$$\mathcal{U}_b \simeq \frac{(\mathcal{T}'_b)^2}{2(n-2)(e^{(n-2)W} - \mathcal{T}_b)} + \frac{(n-3)(\mathcal{T}'_b)^4}{8(n-2)^2(e^{(n-2)W} - \mathcal{T}_b)^3} + \dots \quad (2.31)$$

2.2.4 The classical low-energy on-brane effective action

Over distances much longer than the size of the two compact dimensions transverse to the brane the classical bulk dynamics is governed by the motion of the massless Kaluza-Klein states. The dynamics are effectively d -dimensional, with $d = n - 2$. To understand the dynamics from this d -dimensional perspective, it is useful to integrate out the extra dimensions to obtain the low-energy lower-dimensional effective theory. At the classical level this amounts to eliminating all of the massive KK states as functions of their massless counterparts, using the bulk classical equations of motion.

In the present instance the massless KK states consist of the on-brane metric and Maxwell fields, $\hat{g}_{\mu\nu}$ and A_μ , as well as any d -dimensional scalars, φ^a , descending from ϕ^A and/or from moduli in the metric components, g_{mn} , in the extra dimensions. To obtain the low-energy potential, $V_{\text{eff}}(\varphi)$, for the various d -dimensional scalars, φ^a , we eliminate the massive Kaluza-Klein modes in the action, as functions of $\hat{g}_{\mu\nu}$ and φ^a . The transverse metric, g_{mn} , is eliminated by using the trace reversed (mn) Einstein equations, which single out the kinetic terms for g_{mn} :

$$\frac{1}{2\kappa^2} (\mathcal{R}_{mn} + \mathcal{G}_{AB} \partial_m \phi^A \partial_n \phi^B) + \frac{f}{2} F_m{}^P F_{nP} + \frac{1}{n-2} \left[V - \frac{f}{4} F_{PQ} F^{PQ} \right] g_{mn} = 0, \quad (2.32)$$

These comprise two independent equations, which we take to be the sum and difference of the $(\rho\rho)$ and $(\theta\theta)$ components. The difference gives

$$(n-2) \left(W'' + (W')^2 - W' B' \right) + \mathcal{G}_{AB} \phi^{A'} \phi^{B'} = 0, \quad (2.33)$$

while the sum is equivalent to contracting eq. (2.32) with g^{mn} , to give

$$\frac{1}{2\kappa^2} (\mathcal{R}_{(2)} + \mathcal{G}_{AB} \partial_m \phi^A \partial^m \phi^B) = -\frac{n-3}{2(n-2)} f F_{mn} F^{mn} - \frac{2}{n-2} V, \quad (2.34)$$

where we write the higher-dimensional curvature scalar as

$$\begin{aligned} \mathcal{R} = g^{MN} \mathcal{R}^P{}_{MPN} &= \mathcal{R}_{(n-2)} + \mathcal{R}_{(2)} \\ \text{where } \mathcal{R}_{(2)} = g^{mn} \mathcal{R}^P{}_{mPn} &= R_{(2)} + (n-2)(\square W + \nabla W \cdot \nabla W) \\ &= R_{(2)} + (n-2) \left[W'' + (W')^2 + B' W' \right] \\ \text{and } \mathcal{R}_{(n-2)} = g^{\mu\nu} \mathcal{R}^P{}_{\mu P\nu} &= e^{-2W} \hat{g}^{\mu\nu} \hat{R}_{\mu\nu} + (n-2) [\square W + (n-4) \nabla W \cdot \nabla W] \\ &= e^{-2W} \hat{g}^{\mu\nu} \hat{R}_{\mu\nu} + (n-2) \left[W'' + (n-4)(W')^2 + B' W' \right]. \end{aligned} \quad (2.35)$$

Here $R_{(2)} = g^{mn} R^p{}_{mpn}$ and $\hat{g}^{\mu\nu} \hat{R}_{\mu\nu}$ respectively denote the curvature scalars built from the 2D metric, g_{mn} , and the 4D metric, $\hat{g}_{\mu\nu}$.

Using eq. (2.34) to eliminate $\mathcal{R}_{(2)}$ from the bulk action then yields the bulk contribution to the

lower-dimensional lagrangian density.³ Using $\sqrt{-g} = \sqrt{-\hat{g}} \sqrt{g_2} e^{(n-2)W}$, we find

$$\begin{aligned}
\mathcal{L}_{\text{eff}}(\varphi) &= - \int d^2x \sqrt{g_2} e^{(n-2)W} \left[\frac{1}{2\kappa^2} \mathcal{R}_{(n-2)} + \frac{4-n}{4(n-2)} f F_{mn} F^{mn} + \frac{n-4}{n-2} V \right] \\
&= - \int d^2x \sqrt{g_2} e^{(n-2)W} \left\{ \frac{1}{2\kappa^2} \left[e^{-2W} \hat{g}^{\mu\nu} \hat{R}_{\mu\nu} + (n-2) \left(W'' + (n-4)(W')^2 + B'W' \right) \right] \right. \\
&\quad \left. + \frac{4-n}{4(n-2)} f F_{mn} F^{mn} + \frac{n-4}{n-2} V \right\} \\
&= - \int d^2x \sqrt{g_2} e^{(n-2)W} \left\{ \frac{1}{2\kappa^2} \left[e^{-2W} \hat{g}^{\mu\nu} \hat{R}_{\mu\nu} + (n-2) \left((n-5)(W')^2 + 2W'B' \right) \right. \right. \\
&\quad \left. \left. - \mathcal{G}_{AB} \phi^{A'} \phi^{B'} \right] + \frac{4-n}{4(n-2)} f F_{mn} F^{mn} + \frac{n-4}{n-2} V \right\} . \\
&= - \int d^{n-2}x \sqrt{-\hat{g}} \left[\frac{1}{2\kappa_N^2} \hat{g}^{\mu\nu} \hat{R}_{\mu\nu} + V_B \right], \tag{2.36}
\end{aligned}$$

where the second to last equality uses the second independent bulk field equation, eq. (2.33), the last equality defines the bulk potential, V_B , and the lower-dimensional Newton's constant, $\kappa_N^2 = 8\pi G_N$, is given by

$$\frac{1}{\kappa_N^2(\varphi)} := \frac{1}{\kappa^2} \int d^2x \sqrt{g_2} e^{(n-4)W}. \tag{2.37}$$

In general this depends on the low-energy scalar fields, a dependence that can be removed by performing a Weyl rescaling to reach the lower-dimension Einstein frame.

To obtain the complete low-energy scalar potential, V_{eff} , the bulk contribution, V_B , must be combined with two other contributions, both associated with the source branes. The first of these comes from the boundary terms of the bulk action [6, 7], such as the Gibbons-Hawking term for the metric, evaluated at a small surface, Σ_b , situated a short proper distance, $\rho = \epsilon$, from the position of each of the source branes:

$$\begin{aligned}
S_{GH} &= \sum_{b=0}^1 \lim_{\epsilon \rightarrow 0} \oint_{\Sigma_b} d\theta d^{n-2}x \frac{1}{\kappa^2} \sqrt{-\hat{\gamma}} K \\
&= \frac{2\pi}{\kappa^2} \sum_{b=0}^1 (-)^b \int_{\rho=\rho_b} d^{n-2}x \sqrt{-\hat{g}} e^{B+(n-2)W} \left[B' + (n-2)W' \right] \\
&= - \sum_{b=0}^1 \int_{\rho=\rho_b} d^{n-2}x \sqrt{-\hat{g}} \left\{ \left[-T_b - (n-3)U_b \right] + (n-2)U_b \right\} \\
&= - \sum_{b=0}^1 \int_{\rho=\rho_b} d^{n-2}x \sqrt{-\hat{g}} \left(U_b - T_b \right). \tag{2.38}
\end{aligned}$$

Here we use the axisymmetric *ansatz*, as is appropriate very near the source branes. The relative sign,

³Although in principle the extra-dimensional part of the trace reversed $(\mu\nu)$ Einstein equation, $ER_{\mu\nu}(x, y) = 0$ could also be used to eliminate massive KK modes, this *cannot* be used to eliminate $R_{(n-2)}$ from V_B because the integration in eq. (2.36) projects onto the zero-mode component of $E_{\mu\nu} = 0$.

$(-)^b$, and the overall sign in the second line arise because primes denote $d/d\rho$ while the derivatives appearing in the Gibbons-Hawking action and matching conditions are outward directed, and this is in the $d\rho$ direction for one brane and $-d\rho$ for the other. The last line uses the matching conditions described earlier to exchange W' and B' for terms involving the brane action, using the fact that the contribution of $[e^B K]_{\text{flat}}$ cancels between the two branes.

The second contribution to the 4D scalar potential comes from the contribution of the brane action itself, eq. (2.16). Combining these with V_{4B} above gives the full 4D scalar potential in the classical limit as in [7],

$$\begin{aligned} - \int d^{n-2}x \sqrt{-\hat{g}} V_{\text{eff}} &= - \int d^{n-2}x \sqrt{-\hat{g}} V_B + \sum_{b=0}^1 \left[S_b + \lim_{\epsilon \rightarrow 0} S_{\text{GH}} \right] \\ &= - \int d^{n-2}x \sqrt{-\hat{g}} V_B - \sum_{b=0}^1 \int d^{n-2}x \sqrt{-\hat{g}} \left[T_b + (U_b - T_b) \right], \end{aligned} \quad (2.39)$$

where the notation W_b is a reminder that W is evaluated at the brane position. This shows that (within the classical approximation) the effect of the Gibbons-Hawking terms is to ensure that the net contribution of each brane to the low-energy scalar potential is given by the quantity U_b , appropriately warped. The complete low-energy scalar potential is therefore,

$$\begin{aligned} V_{\text{eff}} &= V_B + \sum_b U_b \\ &= \sum_b U_b + \int d^2x \sqrt{g_2} e^{(n-2)W} \left\{ \frac{1}{2\kappa^2} \left[(n-2) \left\{ (n-5)(W')^2 + 2W'B' - \mathcal{G}_{AB} \phi^{A'} \phi^{B'} \right\} \right] \right. \\ &\quad \left. + \frac{4-n}{4(n-2)} f F_{mn} F^{mn} + \frac{n-4}{n-2} V \right\}. \end{aligned}$$

Stationary points

For some purposes it is sufficient to obtain the value of the potential, $V_{\text{eff}}(\phi_0)$, evaluated at its stationary point, where $V'_{\text{eff}}(\phi_0) = 0$. This can be obtained from the higher-dimensional action by eliminating fields using *all* of the equations of motion, and not just those of the massive KK modes. In this case we may directly use the equation of motion,

$$\frac{1}{2\kappa^2} \left(\mathcal{R} + \mathcal{G}_{AB} \partial_M \phi^A \partial^M \phi^B \right) = - \frac{(n-4)}{4(n-2)} f F_{MN} F^{MN} - \frac{nV}{n-2}, \quad (2.40)$$

rather than eq. (2.34) for $R_{(2)}$. Using this to eliminate \mathcal{R} from the bulk action yields

$$\begin{aligned} S_{\text{ext}} &= - \int d^n x \sqrt{-g} \left[\frac{1}{2\kappa^2} \left(\mathcal{R} + \mathcal{G}_{AB} \partial_M \phi^A \partial^M \phi^B \right) + \frac{1}{4} f F_{MN} F^{MN} + V \right]_{\text{cl}} \\ &= - \frac{2}{n-2} \int d^n x \sqrt{-g} \left[\frac{1}{4} f F^{mn} F_{mn} - V \right]. \end{aligned} \quad (2.41)$$

When comparing with the low-energy theory we must also evaluate the low energy action at its stationary point. That is, we evaluate the action

$$S_{\text{eff}} = - \int d^{n-2}x \sqrt{-\hat{g}} \left[\frac{1}{2\kappa_N^2} \hat{R}_{(n-2)} + V_{\text{eff}} \right], \quad (2.42)$$

at the solution to the low-energy field equations,

$$\frac{1}{2\kappa_N^2} \hat{R}_{(n-2)} = - \frac{(n-2)}{n-4} V_{\text{eff}}, \quad (2.43)$$

leading to

$$S_{\text{ext}} = \frac{2}{n-4} \int d^{n-2}x \sqrt{-\hat{g}} V_{\text{eff}}(\varphi_0). \quad (2.44)$$

Using the previous results for V_{ext} and the brane contribution then gives

$$\frac{2}{n-4} V_{\text{eff}}(\varphi_0) = - \sum_b e^{(n-2)W_b} U_b - \frac{2}{n-2} \int d^2x \sqrt{g_2} e^{(n-2)W} \left[\frac{1}{4} f F^{mn} F_{mn} - V \right]. \quad (2.45)$$

In many cases of interest the bulk contribution to this expression can itself also be written as a sum of contributions localized at the position of each brane. This is true, in particular, whenever the bulk action, $S_B = \int d^n x \mathcal{L}_B$, enjoys a classical scaling symmetry, under which $\mathcal{L}_B[\lambda^{p_i} \psi_i] \equiv \lambda \mathcal{L}_B[\psi_i]$, for arbitrary real, constant λ . (This type of scale symmetry generically holds for higher-dimensional supergravity theories in particular.) When this is true the lagrange density satisfies the identity

$$\begin{aligned} \mathcal{L}_B &\equiv \sum_i p_i \left[\psi_i \frac{\partial \mathcal{L}_B}{\partial \psi_i} + \partial_\mu \psi_i \frac{\partial \mathcal{L}_B}{\partial (\partial_\mu \psi_i)} \right] \\ &= \sum_i \left\{ \partial_\mu \left[p_i \frac{\partial \mathcal{L}_B}{\partial \partial_\mu \psi_i} \right] + p_i \psi_i \left[\frac{\partial \mathcal{L}_B}{\partial \psi_i} - \partial_\mu \left(\frac{\partial \mathcal{L}_B}{\partial (\partial_\mu \psi_i)} \right) \right] \right\}, \end{aligned} \quad (2.46)$$

which shows [20] that the action becomes a total derivative whenever it is evaluated at an arbitrary classical solution. Whenever this is true the entire low-energy potential can be interpreted as the sum over brane contributions, much as was done for the Gibbons-Hawking term above.

2.3 Examples

It is instructive to test the above construction by applying it to situations for which explicit solutions are known for the higher-dimensional theory. We do so in this section using F-theory compactifications of 10D Type IIB supergravity to 8 dimensions in the presence of space-filling D7 branes, and using compactifications to 4 dimensions of supersymmetric and nonsupersymmetric six-dimensional theories.

2.3.1 D7 branes in F-Theory

We start with F-theory [10] compactifications of Type IIB supergravity to 8 dimensions, which serves as an example where explicit forms for the bulk and brane actions are known, as are closed-form expressions for the bulk sourced by various space-filling brane configurations [21]. This provides a check on the validity of the matching conditions, and on the low-energy on-brane scalar potential.

The bulk fields to be followed in this case are the metric, g_{MN} , and the axio-dilaton,

$$\tau = C_0 + i e^{-\phi}, \quad (2.47)$$

where C_0 is the Ramond-Ramond scalar and ϕ is the 10D dilaton, for which the string coupling is $g_s = e^\phi$. The bulk action for these fields in the 10D Einstein frame is

$$S_B = -\frac{1}{2\kappa^2} \int d^{10}x \sqrt{-g} g^{MN} \left[\mathcal{R}_{MN} + \frac{\partial_M \bar{\tau} \partial_N \tau}{2(\text{Im } \tau)^2} \right], \quad (2.48)$$

which is invariant under $\text{PSL}(2, R)$ transformations

$$\tau \rightarrow \frac{a\tau + b}{c\tau + d}, \quad (2.49)$$

with the real parameters a through d satisfying $ad - bc = 1$. Quantum effects are expected to break this to $\text{PSL}(2, Z)$, for which the parameters are restricted to be integers. Since $e^\phi \geq 0$ the field τ lives in the upper-half τ plane, but because of the symmetry it suffices to consider τ to live within the fundamental domain, \mathcal{F} , defined by modding out the upper half plane by a $\text{PSL}(2, Z)$.

Bulk solutions

The scalar field equation for this action is

$$\partial \bar{\partial} \tau + \frac{2 \partial \tau \bar{\partial} \tau}{\bar{\tau} - \tau} = 0, \quad (2.50)$$

which is satisfied by any holomorphic function, $\tau = \tau(z)$, for which $\bar{\partial} \tau = 0$.

Explicit solutions to the field equations to this model are known [21], for which two of the dimensions are compactified. Using complex coordinates, $z = x^8 + ix^9$, for the compact dimensions, the solutions are given by

$$j(\tau(z)) = P(z) \quad \text{and} \quad ds^2 = \eta_{\mu\nu} dx^\mu dx^\nu + e^{2C(z, \bar{z})} d\bar{z} dz, \quad (2.51)$$

where the properties of the functions $j(\tau)$, $P(z)$ and $C(z, \bar{z})$ are now described.

The function $j(\tau)$, is the standard bijection from the fundamental domain, \mathcal{F} , to the complex

sphere, given in terms of Jacobi ϑ -functions by

$$j(\tau) = \frac{1728 [E_4(\tau)]^3}{[E_4(\tau)]^3 - [E_6(\tau)]^2}, \quad (2.52)$$

where $E_k(\tau)$ are the Eisenstein modular forms [22]. For large $\text{Im } \tau$, $j(\tau)$ diverges zero exponentially quickly, and the factor of 1728 is chosen so that it asymptotes to $j(\tau) \simeq e^{-2\pi i \tau} + \dots$.

$P(z)$ is a holomorphic function, whose singularities occur at the locations of the source branes, $z = z_i$ for $i = 1, \dots, N$. Since the singularities of the metric turn out to be conical when $P(z)$ has isolated poles as $z \rightarrow z_i$, it is convenient to choose $P(z)$ to be a ratio of polynomials. The simplest case could be taken as $P = 1/z$, describing a source at $z = 0$, but it turns out that the metric obtained from the Einstein equations is not compact in this case. The metric is compact when $P(z)$ has 24 zeroes, such as for the choice

$$P(z) = \frac{4(24f)^3}{27g^2 + 4f^3}, \quad (2.53)$$

with $f(z)$ a polynomial of degree 8 and $g(z)$ a polynomial of degree 12. This gives a compactification of Type IIB supergravity on CP^1 , corresponding to an F-theory reduction on $K3$ [10].

Finally, the metric function $C(z, \bar{z})$ is chosen by solving the Einstein equation. Using $\mathcal{R}_{z\bar{z}} = 2\partial\bar{\partial}C$ and $\bar{\partial}\tau = 0$, this equation of motion is

$$2\partial\bar{\partial}C = \frac{\partial\tau\bar{\partial}\bar{\tau}}{(\tau - \bar{\tau})^2} = \partial\bar{\partial} \ln(\text{Im } \tau). \quad (2.54)$$

The required solution is

$$e^{2C(z, \bar{z})} = (\text{Im } \tau) \left| \eta^2(\tau) \prod_{i=1}^N (z - z_i)^{-1/12} \right|^2, \quad (2.55)$$

where $\eta(\tau) = q^{1/24} \prod_k (1 - q^k)$, for $q = e^{2\pi i \tau}$, denotes the Dedekind η -function, and the product runs over the singularities of $P(z)$. The first factor of this expression is chosen to satisfy eq. (2.54), and the holomorphic factors are chosen to ensure invariance under $\text{PSL}(2, Z)$, and by the requirement that the result does not vanish anywhere.

Brane sources

The presence of branes in these solutions is signaled by singularities where $P(z) \simeq c_i/(z - z_i)$, for which $q = e^{2\pi i \tau} \simeq (z - z_i)/c_i$, and so the above solution implies

$$\begin{aligned} \tau(z) &\simeq \frac{1}{2\pi i} \ln(z - z_i) + \dots \\ \text{and } e^{2C(z, \bar{z})} &\simeq k \text{Im } \tau, \end{aligned} \quad (2.56)$$

for constant k . As $z \rightarrow \infty$, on the other hand, $P(z)$ remains bounded and so τ approaches some finite value. In this case the metric function becomes

$$e^{2C(z, \bar{z})} \propto (z\bar{z})^{-N/12}, \quad (2.57)$$

and so if we change coordinates to $z = 1/w$ we have $e^{2C} dz d\bar{z} \simeq |w|^{(N-24)/6} dw d\bar{w}$, which is nonsingular because $N = 24$. But each individual brane contributed to this an amount $e^{2C} \simeq |w|^{1/6} dw d\bar{w} \propto r^{1/6} (dr^2 + r^2 d\theta^2)$, which we saw below eq. (2.9) corresponds to a deficit angle of $\delta = \pi/6$.

Matching conditions

We are now in a situation to use these solutions to test the matching conditions found in earlier sections. We can do so even though the geometry involved is not axisymmetric, because it becomes effectively axisymmetric in the near-brane limit.

To this end we assume a brane action of the form

$$S_b = - \int d^8x \sqrt{-\gamma} T_b(\tau, \bar{\tau}), \quad (2.58)$$

where for a D7-brane in the Einstein frame we expect

$$T_b = T_* e^\phi = \frac{T_*}{\text{Im } \tau} = \frac{2i T_*}{\tau - \bar{\tau}}, \quad (2.59)$$

for constant T_* .

Keeping in mind that $W = 0$ for the bulk solutions given above, the matching condition for the bulk scalar, eq. (2.21), becomes

$$\frac{2\pi}{\kappa^2} \left[\frac{e^B}{4(\text{Im } \tau)^2} \partial_\rho \tau \right]_{x_b} = \frac{2\pi}{\kappa^2} \left[\frac{r}{4(\text{Im } \tau)^2} \partial_r \tau \right]_{x_b} = \frac{\partial T_b}{\partial \bar{\tau}} = \frac{T_*}{2i(\text{Im } \tau)^2}. \quad (2.60)$$

This uses the change of variables $d\rho = e^C dr$ and $e^B = r e^C$ to convert from proper distance to conformally-flat coordinates near the brane. Using the near-brane limit $\tau \simeq \ln r / 2\pi i$ to evaluate $[r \partial \tau / \partial r]_{x_b} \simeq 1 / (2\pi i)$, we find the matching condition becomes $T_* = 1 / (2\kappa^2)$.

Notice that since e^ϕ is the string coupling constant, this semiclassical reasoning presupposes $\text{Im } \tau = e^{-\phi}$ is large near the brane, so that $\kappa^2 T_b = \kappa^2 T_* / \text{Im } \tau = 1 / (2 \text{Im } \tau) \ll 1$. This is automatically satisfied as $r \rightarrow 0$ because $\text{Im } \tau \simeq -(\ln r) / 2\pi$.

The metric matching conditions can be understood in a similar way. First, matching the on-brane components of the metric gives, from eq. (2.23)

$$-\frac{2\pi}{\kappa^2} \left[e^B \partial_\rho B - 1 \right]_{x_b} = -\frac{2\pi}{\kappa^2} \left[r \partial_r B - 1 \right]_{x_b} = -\frac{2\pi}{\kappa^2} \left[r \partial_r C \right]_{x_b} = T_b(\tau, \bar{\tau}) = \frac{T_*}{\text{Im } \tau}, \quad (2.61)$$

which again uses $e^B \partial_\rho = r \partial_r$ as well as $B = C + \ln r$. Using eq. (2.55) gives $e^{2C} \simeq \text{Im } \tau$ near the brane, and so $r \partial_r C \simeq \frac{1}{2} (r \partial_r \text{Im } \tau) / \text{Im } \tau$ to get $[r \partial_r C]_{x_b} = -1/(4\pi \text{Im } \tau)$. Once again the dependence on $\text{Im } \tau$ is consistent on both sides and so the matching condition boils down to the statement $2\kappa^2 T_* = 1$, as above.

A further check comes from using the values for κ^2 and T_* for a D7-brane predicted in string theory [9]. Using $T_* = 2\pi/\ell_s^8$ and $\kappa^2 = \ell_s^8/4\pi$, where $\ell_s = 2\pi\sqrt{\alpha'}$ is the string length, we have

$$2\kappa^2 T_* = 2 \left(\frac{\ell_s^8}{4\pi} \right) \left(\frac{2\pi}{\ell_s^8} \right) = 1, \quad (2.62)$$

as required.

Finally, the absence of warping in the bulk solution — $W = 0$ — implies that the remaining metric matching condition, eq. (2.24), degenerates to $U_b = 0$. To compute U_b in the present instance we use the constraint, eq. (2.29), specialized to $n = 10$ dimensions

$$\mathcal{U}_b = \frac{1}{7} \left[(1 - \mathcal{T}_b) - \sqrt{(1 - \mathcal{T}_b)^2 - \frac{7}{8} (\mathcal{T}'_b)^2} \right], \quad (2.63)$$

where $\mathcal{T}_b = \kappa^2 T_b / 2\pi = \kappa^2 T_* / (2\pi \text{Im } \tau)$, and use

$$(\mathcal{T}'_b)^2 = 2 (\text{Im } \tau)^2 \frac{\partial \mathcal{T}_b}{\partial \tau} \frac{\partial \mathcal{T}_b}{\partial \bar{\tau}} = \frac{1}{2 (\text{Im } \tau)^2} \left(\frac{\kappa^2 T_*}{2\pi} \right)^2 = \frac{1}{8\pi^2 (\text{Im } \tau)^2}. \quad (2.64)$$

Clearly $(\mathcal{T}'_b)^2 = 0$ because $\text{Im } \tau \rightarrow \infty$ as one approaches the brane, and this in turn ensures $U_b = 0$, as desired.

As a final check we compute the effective scalar potential, V_{eff} , for the KK scalar zero mode in the 8D theory on the brane, after dimensional reduction. Because $U_b = 0$ this simply amounts to evaluating the action, eq. (2.48), at the classical solution to the extra-dimensional Einstein equations, which state

$$\mathcal{R}_{mn} + \frac{1}{4 (\text{Im } \tau)^2} \left[\partial_m \tau \partial_n \bar{\tau} + \partial_n \tau \partial_m \bar{\tau} \right] = 0. \quad (2.65)$$

We see that $V_{\text{eff}} = 0$ in the effective theory, which is consistent with the maximally symmetric on-brane geometry being flat.

2.3.2 Brane-axion couplings in 6D

We next apply the above matching conditions to the example of two branes coupled to a bulk Goldstone mode (axion), ϕ , in six dimensions. Since 6D examples with flat on-brane geometries are already discussed in some detail in refs. [7], we concentrate here on solutions to the higher-dimensional equations for which the on-brane geometry is known to be curved. Our purposes is to provide a nontrivial example for which the shape of the full low-energy potential, $V_{\text{eff}}(\varphi)$, and

its value at its stationary point, $V_{\text{eff}}(\varphi_0)$, can be computed explicitly directly from the higher-dimensional theory. Because this allows a check on how V_{eff} varies from its minimum, it allows us to verify that the extremal point is actually a local minimum of the low-energy potential.

The simplest such a system starts with gravity coupled to a single bulk scalar and Maxwell field, with the bulk lagrangian density given by,

$$\mathcal{L}_B = -\sqrt{-g} \left\{ \frac{1}{2\kappa^2} g^{MN} [\mathcal{R}_{MN} + \partial_M \phi \partial_N \phi] + \frac{1}{4} F_{MN} F^{MN} + \Lambda \right\}, \quad (2.66)$$

where Λ is a bulk cosmological constant whose value can be chosen to obtain any desired curvature on the brane. Notice that the choices $f(\phi) = 1$ and $V(\phi) = \Lambda$ ensure the action has a shift symmetry, $\phi \rightarrow \phi + \xi$, that guarantees the existence of a scalar KK zero mode having a constant profile across the bulk. This is the only such classically massless scalar KK mode, because the presence of the bulk cosmological term, Λ , breaks the rigid scaling symmetry that the Einstein action normally has. This breaking ensures that the presence of Λ removes the ‘breathing’ mode corresponding to rigid expansions of the extra dimensional geometry, that would otherwise have been a low-energy scalar zero mode.

Bulk solutions

The field equations in this case admit explicit solutions for which the 4D on-brane geometry is maximally symmetric and the extra dimensions are axially symmetric [5, 11]. Using the *ansatz* of eq. (2.9), a simple solution is

$$ds^2 = \hat{g}_{\mu\nu} dx^\mu dx^\nu + d\rho^2 + \alpha^2 L^2 \sin^2 \left(\frac{\rho}{L} \right) d\theta^2 \quad (2.67)$$

$$F_{\rho\theta} = \alpha \mathcal{B}_0 L \sin \left(\frac{\rho}{L} \right), \quad (2.68)$$

with $\phi = \phi_0$ constant. The bulk field equations imply the following relation amongst the constants \mathcal{B}_0 , L and Λ :

$$\mathcal{R}_{(2)} = -\frac{2}{L^2} = -\kappa^2 \left(\frac{3\mathcal{B}_0^2}{2} + \Lambda \right), \quad (2.69)$$

and the curvature of the on-brane metric is given by

$$\hat{R} = 2\kappa^2 \left(\frac{\mathcal{B}_0^2}{2} - \Lambda \right). \quad (2.70)$$

When $\alpha = 1$ the extra-dimensional metric describes a sphere of radius L . When $\alpha \neq 1$ the geometry would still look like a sphere if we redefine $\theta \rightarrow \alpha\vartheta$, although ϑ is then not periodic with period 2π . This indicates there are conical singularities at both $\rho = 0$ and $\rho = \pi L$, with defect angle given by $\delta = 2\pi(1 - \alpha)$.

Brane properties

We now ask for a pair of brane sources located at these two singularities that can support this geometry. We again take codimension-2 brane actions of the form

$$S_b = - \int d^4x \sqrt{-\gamma} T_b(\phi). \quad (2.71)$$

Because the bulk solution has constant scalar, $\phi = \phi_0$, its derivative, $\partial_\rho \phi$, vanishes at both branes. This is only consistent with the scalar matching condition if $T'_b(\phi)$ also vanishes for both branes when evaluated at the same place: $\phi = \phi_0$. The vanishing of $T'_b(\phi)$ at $\phi = \phi_0$ also ensures $U_b(\phi)$ vanishes there, and this is consistent with the $(\theta\theta)$ matching condition, eq. (2.24), because $W = 0$ throughout the bulk in the classical solution ensures $\partial_\rho W = 0$ at the brane positions.

Finally, the $(\mu\nu)$ matching condition, eq. (2.23), reads

$$-\frac{2\pi}{\kappa^2} \left[e^B B' - 1 \right]_{x_b} = T_b(\phi_0). \quad (2.72)$$

Using $e^B = \alpha L \sin(\rho/L)$ gives $e^B B' \rightarrow \alpha$ as $\rho \rightarrow 0$, and so this matching condition gives the usual expression for the defect angle in terms of the brane tension,

$$\delta = 2\pi(1 - \alpha) = \kappa^2 T_b(\phi_0), \quad (2.73)$$

and so $\mathcal{T}_b = \kappa^2 T_b / 2\pi = 1 - \alpha$.

The 4D perspective

We now show how the above picture is reproduced in the low-energy 4D effective theory below the Kaluza-Klein scale. Although we cannot ask in the low-energy theory about the profiles of bulk fields within the extra dimensions, we can use it to understand the curvature, \hat{R} , of the 4D on-brane geometry and the value, ϕ_0 , to which the low-energy scalar field is fixed.

To this end we explore the scalar potential, V_{eff} , for the KK zero mode of the scalar, ϕ , as it is moved away from ϕ_0 . To do so requires more information about the shape of $T_b(\phi)$, so we choose for simplicity,

$$T_b(\phi) = M_b^4 + \frac{\mu_b^4}{2} (\phi - \phi_0)^2, \quad (2.74)$$

although any choice for $T_b(\phi)$ would do, so long as both tensions share a common zero for $\partial T_b / \partial \phi$.

With this choice we have

$$\mathcal{T}_b = \frac{\kappa^2 M_b^4}{2\pi} + \frac{\kappa^2 \mu_b^4}{4\pi} (\phi - \phi_0)^2, \quad \mathcal{T}_b' = \frac{\kappa^2 \mu_b^4}{2\pi} (\phi - \phi_0), \quad (2.75)$$

and so to lowest nontrivial order in κ^2

$$\begin{aligned} \mathcal{U}_b &= \frac{1}{3} \left[(1 - \mathcal{T}_b) - \sqrt{(1 - \mathcal{T}_b)^2 - \frac{3}{4} (\mathcal{T}_b')^2} \right] \\ &\simeq \frac{(\mathcal{T}_b')^2}{8(1 - \mathcal{T}_b)} + \frac{3(\mathcal{T}_b')^4}{128(1 - \mathcal{T}_b)^3} + \dots \end{aligned} \quad (2.76)$$

Specialized to the above tension this becomes

$$U_b \simeq \frac{\kappa^2 \mu_b^8}{16\pi} (\phi - \phi_0)^2 + \dots \quad (2.77)$$

Notice [26] that because \mathcal{U}_b is quadratic in \mathcal{T}_b' , both it and its derivative \mathcal{U}'_b naturally vanish at zeroes of \mathcal{T}_b' . Furthermore, the coefficient of $(\phi - \phi_0)^2$ in U_b is suppressed relative to the same term in T_b by an additional power of the small dimensionless factor $\kappa^2 \mu_b^4 / 8\pi \ll 1$. The full expression for the effective potential (2.40) in this case reduces to

$$\begin{aligned} V_{\text{eff}} &= \sum_b U_b + V_B(\phi_0) + \frac{1}{2} V_B''(\phi_0) (\phi - \phi_0)^2 + \dots \\ &= \sum_b U_b + \int d^2x \sqrt{g_2} e^{4W} \left\{ -\frac{1}{8} F_{mn} F^{mn} + \frac{1}{2} \Lambda \right\} + \frac{1}{2} V_B''(\phi_0) (\phi - \phi_0)^2 + \dots \\ &= \sum_b U_b + \frac{\pi}{2} \left(\Lambda - \frac{\mathcal{B}_0^2}{2} \right) \int_0^{\pi L} d\rho e^B + \frac{1}{2} V_B''(\phi_0) (\phi - \phi_0)^2 + \dots \\ &= \left(\Lambda - \frac{\mathcal{B}_0^2}{2} \right) 2\pi\alpha L^2 + \frac{1}{2} \left[V_B''(\phi_0) + \sum_b \frac{\kappa^2 \mu_b^8}{8\pi} \right] (\phi - \phi_0)^2 + \dots \end{aligned}$$

using that both W' and ϕ' vanish when $\phi = \phi_0$. More explicit progress requires the calculation of $V_B''(\phi_0)$, although this can be expected to be non-negative due if the bulk solution is stable. This shows that $V_{\text{eff}}(\phi)$ is minimized at $\phi = \phi_0$, and this is how the 4D theory understands the value at which ϕ is stabilized.

The value of the potential at this minimum has a direct physical interpretation, since it sets the value of the 4D curvature through the 4D Einstein equations. These read, as usual

$$\hat{R}_{\mu\nu} - \frac{1}{2} \hat{R} \hat{g}_{\mu\nu} - \kappa_N^2 V_{\text{eff}} \hat{g}_{\mu\nu} = 0, \quad (2.78)$$

where the 4D Newton coupling is

$$\frac{1}{\kappa_N^2} = \frac{2\pi}{\kappa^2} \int_0^{\pi L} d\rho e^B = \frac{4\pi\alpha L^2}{\kappa^2}, \quad (2.79)$$

and so

$$\hat{R} = -4\kappa_N^2 V_{\text{eff}}(\phi_0) = 2\kappa^2 \left(\frac{\mathcal{B}_0^2}{2} - \Lambda \right), \quad (2.80)$$

in agreement with the higher-dimensional result, eq. (2.70). Notice that this agreement requires, in particular, that the brane tensions $T_b(\phi_0) = M_b^4$ drop out of the low-energy potential.

Finally, notice that evaluating the potential, eq. (2.78), at its minimum by evaluating the action at the classical solution gives a result that agrees with the general expression (2.45), which in the present instance evaluates to

$$\begin{aligned} V_{\text{eff}}(\varphi_0) &= -\sum_b e^{4W_b} U_b - \frac{1}{2} \int d^2x \sqrt{g_2} e^{4W} \left[\frac{1}{4} f F^{mn} F_{mn} - V \right] \\ &= \frac{1}{2} (4\pi\alpha L^2) \left(\Lambda - \frac{\mathcal{B}_0^2}{2} \right). \end{aligned} \quad (2.81)$$

2.3.3 Warped and unwarped supersymmetric examples

A large class of examples of explicit flux compactifications with nontrivial warping and scalar profiles in the extra dimensions is provided by solutions [19, 20, 23, 24, 25, 13, 14] to chiral 6D supergravity [12]. Our goal with this example is to identify the properties of the branes that are required to source the known solutions. In general the existence of solutions hinges on the consistency of these brane properties with the form of the intervening bulk, but these solutions are not known in closed form in the case where the on-brane dimensions are curved. In this situation it is much easier to investigate the existence of solutions using the equivalent formulation in terms of minima of the low-energy scalar potential, since it is much easier to determine when such solutions exist.

The solutions of interest take as their starting point the following bosonic part of the supersymmetric action

$$\mathcal{L}_B = -\sqrt{-g} \left\{ \frac{1}{2\kappa^2} g^{MN} \left[\mathcal{R}_{MN} + \partial_M \phi \partial_N \phi \right] + \frac{1}{4} e^{-\phi} F_{MN} F^{MN} + \frac{2g^2}{\kappa^4} e^\phi \right\}, \quad (2.82)$$

where the constant g denotes the 6D gauge coupling for the Maxwell field. Because this lagrangian enjoys the property $\mathcal{L}_B \rightarrow \lambda^2 \mathcal{L}_B$ when $e^\phi \rightarrow \lambda^{-1} e^\phi$ and $g_{MN} \rightarrow \lambda g_{MN}$, the arguments of section 2.2.4 imply it becomes a total derivative once evaluated at an arbitrary classical solution [20]:

$$\mathcal{L}_B(g_{MN}^c, A_M^c, \phi^c) = \frac{1}{2\kappa^2} \sqrt{-g^c} \square \phi^c. \quad (2.83)$$

Bulk solutions

For this system it is useful to choose a slightly different metric *ansatz* [23],

$$ds^2 = \mathcal{W}^2 \hat{g}_{\mu\nu} dx^\mu dx^\nu + a^2 \left(\mathcal{W}^8 d\eta^2 + d\theta^2 \right), \quad (2.84)$$

where $a = a(\eta)$, $\mathcal{W} = \mathcal{W}(\eta)$ and $\hat{g}_{\mu\nu}$ is, a maximally symmetric 4D de Sitter metric, with $\hat{R} = -12H^2$. With these choices the proper circumference of a circle along which θ varies from zero to 2π at fixed η is $2\pi a(\eta)$, and $d\rho = a\mathcal{W}^4 d\eta$. The dilaton is similarly taken to depend only on η , $\phi = \phi(\eta)$, and

the Maxwell field is given by $A_\theta = A_\theta(\eta)$, so that

$$F_{\eta\theta} = Q a^2 e^\phi. \quad (2.85)$$

In this case the content of Maxwell's equations is that Q must be a constant, while the dilaton and the trace-reversed Einstein equations become

$$\phi'' = \frac{2g^2}{\kappa^2} a^2 \mathcal{W}^8 e^\phi - \frac{\kappa^2 Q^2}{2} a^2 e^\phi, \quad (2.86)$$

and

$$(\mu\nu): \quad \frac{\mathcal{W}''}{\mathcal{W}} - \frac{(\mathcal{W}')^2}{\mathcal{W}^2} + \frac{1}{2} \phi'' = \left(\frac{\mathcal{W}'}{\mathcal{W}} + \frac{1}{2} \phi' \right)' = 3 H^2 a^2 \mathcal{W}^6 \quad (2.87)$$

$$(\theta\theta): \quad \frac{a''}{a} - \frac{(a')^2}{a^2} + \frac{1}{2} \phi'' = \left(\frac{a'}{a} + \frac{1}{2} \phi' \right)' = -\kappa^2 Q^2 a^2 e^\phi. \quad (2.88)$$

In all of these equations primes denote $d/d\eta$. The 'Hamiltonian constraint' — *i.e.* the $(\eta\eta)$ Einstein equation — in these variables is similarly

$$\frac{1}{2} (\phi')^2 - \frac{4 a' \mathcal{W}'}{a \mathcal{W}} - \frac{6 (\mathcal{W}')^2}{\mathcal{W}^2} = \frac{2g^2}{\kappa^2} a^2 \mathcal{W}^8 e^\phi - 6 H^2 a^2 \mathcal{W}^6 - \frac{\kappa^2}{2} Q^2 a^2 e^\phi. \quad (2.89)$$

The scale invariance of the full 6D field equations under $e^\phi \rightarrow e^\phi/\lambda$ and $g_{MN} \rightarrow \lambda g_{MN}$ can be seen from the invariance of the above equations under

$$\left\{ \phi, a, \mathcal{W}, H \right\} \rightarrow \left\{ \phi + \phi_0, a e^{-\phi_0/2}, \mathcal{W}, H e^{\phi_0/2} \right\}, \quad (2.90)$$

for ϕ_0 an arbitrary real constant. In the case $H = 0$ this symmetry implies the existence of a one-parameter family of classical solutions, and a corresponding flat direction (labelled by ϕ_0) that represents a classically massless KK zero mode coming from a combination of the metric and ϕ fields.

The above field equations are written so that their right-hand-sides tend to zero in the near-brane regions, for which $a \rightarrow 0$. For regions where these right-hand-sides are negligible the equations simplify to

$$\phi'' \simeq \left(\frac{\mathcal{W}'}{\mathcal{W}} \right)' \simeq \left(\frac{a'}{a} \right)' \simeq 0, \quad (2.91)$$

and so, letting $b = \{0, 1\}$ for the branes at $\eta = \{-\infty, +\infty\}$ respectively,

$$\phi \simeq (-)^b q_b \eta, \quad \mathcal{W} \simeq \mathcal{W}_b e^{(-)^b \omega_b \eta} \quad \text{and} \quad a \simeq a_b e^{(-)^b \alpha_b \eta}, \quad (2.92)$$

with different choices for the constants α_b , ω_b and q_b applying for the two limits, $\eta \rightarrow \pm\infty$. For both

asymptotic regions these are related by the constraint, eq. (2.89), so that

$$q_b^2 = 4\omega_b(2\alpha_b + 3\omega_b). \quad (2.93)$$

Notice that it is only consistent in the near-brane limit to ignore the quantities $a^2\mathcal{W}^6$, a^2e^ϕ and $a^2\mathcal{W}^8e^\phi$ on the right-hand sides of eqs. (2.87) through (2.89) if

$$2\alpha_b + 6\omega_b > 0, \quad 2\alpha_b + q_b > 0 \quad \text{and} \quad 2\alpha_b + 8\omega_b + q_b > 0. \quad (2.94)$$

The first of these also guarantees the convergence of the 4D gravitational constant, which is given by (*c.f.* eq. (2.37))

$$\frac{1}{\kappa_N^2} = \frac{2\pi}{\kappa^2} \int_{-\infty}^{\infty} d\eta a^2 \mathcal{W}^6. \quad (2.95)$$

Furthermore, since our interest is in solutions where $a \rightarrow 0$ at the positions of the brane sources, we demand $\alpha_b > 0$. This ensures that the circumference of small circles encircling the branes vanishes in the limit that the branes are approached. But if $\alpha_b > 0$, then ω_b must also be non-negative. To see this, suppose ω_b were negative. Then eq. (2.93) would imply $-2\alpha_b - 3\omega_b > 0$, and so adding this to the first of eqs. (2.94) would give $\omega_b > 0$, in contradiction with the assumption that it is negative. By contrast, the constant q_b can take either sign.

Solutions to these equations are known to exist for nonzero H [25], although not yet in an explicit closed form. Closed-form solutions are known, however, in the special case where H vanishes, given by [23, 20]

$$\begin{aligned} e^\phi &= \mathcal{W}^{-2} e^{\phi_0 - \lambda_3 \eta} \\ \mathcal{W}^4 &= \left(\frac{\kappa^2 Q \lambda_2}{2g \lambda_1} \right) \frac{\cosh[\lambda_1(\eta - \eta_1)]}{\cosh[\lambda_2(\eta - \eta_2)]} \\ \text{and} \quad a^{-4} &= \left(\frac{2g \kappa^2 Q^3}{\lambda_1^3 \lambda_2} \right) e^{2(\phi_0 - \lambda_3 \eta)} \cosh^3[\lambda_1(\eta - \eta_1)] \cosh[\lambda_2(\eta - \eta_2)]. \end{aligned} \quad (2.96)$$

Here η_i and λ_j are integration constants, and there is no loss of generality in choosing, say, $\lambda_2 \geq 0$. The equations of motion require the constants to satisfy $\lambda_2^2 = \lambda_1^2 + \lambda_3^2$ — and so, in particular, $\lambda_2 \geq |\lambda_1|$ (with equality if and only if $\lambda_3 = 0$). ϕ_0 is an arbitrary constant corresponding to the scale invariance associated with the flat direction.

Because the terms involving H in the equations of motion become negligible in the near-brane limit, the $H = 0$ solutions also provide a more detailed picture of the asymptotic regions at $\eta \rightarrow \pm\infty$. The corresponding metric singularities are generically curvature singularities, except when $\lambda_3 = 0$, in which case they turn out to be conical [24]. The $\lambda_3 = 0$ solutions include the unwarped, constant-dilaton ‘rugby ball’ configurations of ref. [19] as the special case where $\eta_1 = \eta_2$. Notice also that the

limiting behaviour is as given in eq. (2.92), with

$$\alpha_b = \frac{1}{4} [3\lambda_1 + \lambda_2 + 2(-)^b \lambda_3] \geq 0, \quad \omega_b = \frac{1}{4} (\lambda_2 - \lambda_1) \geq 0, \quad (2.97)$$

and

$$q_b = (-)^{b+1} \lambda_3 - \frac{1}{2} (\lambda_2 - \lambda_1). \quad (2.98)$$

Notice that the condition $\omega_b \geq 0$ follows from $\lambda_2 \geq |\lambda_1|$, while $\alpha_b \geq 0$ is a consequence of

$$3(\lambda_2 + \lambda_1) - 2\lambda_3 = \sqrt{\lambda_2 + \lambda_1} \left(3\sqrt{\lambda_2 + \lambda_1} - 2\sqrt{\lambda_2 - \lambda_1} \right) \geq 0. \quad (2.99)$$

A special role is played by the combination

$$\omega_b + \frac{q_b}{2} = (-)^{b+1} \frac{\lambda_3}{2}, \quad (2.100)$$

since this dictates the size of the Hubble constant, H . This can be seen by integrating eq. (2.87), and using eq. (2.95) to obtain [25],

$$3H^2 \int_{-\infty}^{\infty} d\eta a^2 \mathcal{W}^6 = \frac{3\kappa^2 H^2}{2\pi\kappa_4^2} = \left[\left(\ln \mathcal{W} + \frac{\phi}{2} \right)' \right]_{\eta=-\infty}^{\eta=+\infty} = - \sum_b \left(\frac{q_b}{2} + \omega_b \right). \quad (2.101)$$

When evaluated for the solutions of eq. (2.96), this reduces to the Friedmann equation

$$H^2 = - \frac{2\pi\kappa_4^2}{3\kappa^2} \sum_b \left[\frac{q_b}{2} + \omega_b \right] = \frac{\kappa_4^2}{3} \left[\frac{2\pi}{\kappa^2} \sum_b (-)^b \frac{\lambda_3}{2} \right] = 0 \quad (2.102)$$

as required. For more general solutions eqs. (2.96) hold only approximately in the near-brane region, so the constant λ_3 could differ for the asymptotic region near each brane.

Notice, in particular, that eq. (2.101) shows that $H^2 > 0$ (4D de Sitter space) requires at least one of the q_b to be negative. Furthermore, choosing $q_b < 0$ is sufficient to ensure that the contribution to H^2 of the corresponding brane is positive, because

$$- \left(\frac{q_b}{2} + \omega_b \right) = \frac{|q_b|}{2} - \omega_b = \sqrt{3\omega_b^2 + 2\alpha_b\omega_b} - \omega_b = \omega_b \left(\sqrt{3 + \frac{\alpha_b}{\omega_b}} - 1 \right) \geq 0. \quad (2.103)$$

This uses both eq. (2.93) and the property that α_b and ω_b are both non-negative.

Brane properties

As usual, the matching conditions relate the asymptotic bulk solutions to the properties of the source branes. Using $\mathcal{W} = e^W$, $a = e^B$ and $a\mathcal{W}^4 d\eta = d\rho$, and taking the brane action to be

$S_b = - \int d^4x \sqrt{-\gamma} L_b = - \int d^4x \sqrt{-\hat{g}} T_b$, the scalar matching condition, eq. (2.21), becomes

$$\frac{2\pi}{\kappa^2} \left[e^{B+4W} \partial_\rho \phi \right]_{x_b} = \frac{\partial}{\partial \phi} \left[e^{4W} L_b \right] \implies \left[(-)^b \partial_\eta \phi \right]_{x_b} = q_b = \frac{\kappa^2}{2\pi} \left(\frac{\partial T_b}{\partial \phi} \right), \quad (2.104)$$

where the sign arises because the direction away from the brane is $(-)^b d\eta$ in the two asymptotic regions. The $(\theta\theta)$ metric matching condition, eq. (2.24), similarly becomes

$$\frac{2\pi}{\kappa^2} \left[e^{B+4W} \partial_\rho W \right]_{x_b} = U_b(\phi) \implies \left[(-)^b \left(\frac{\partial_\eta \mathcal{W}}{\mathcal{W}} \right) \right]_{x_b} = \omega_b = \frac{\kappa^2 U_b}{2\pi}. \quad (2.105)$$

Finally, the $(\mu\nu)$ components of the metric matching conditions are

$$-\frac{2\pi}{\kappa^2} \left[e^{4W} [e^B (3\partial_\rho W + \partial_\rho B) - 1] \right]_{x_b} = T_b(\phi), \quad (2.106)$$

and so

$$\left\{ (-)^b \left[3 \left(\frac{\partial_\eta \mathcal{W}}{\mathcal{W}} \right) + \left(\frac{\partial_\eta a}{a} \right) \right] - \mathcal{W}^4 \right\}_{x_b} = 3\omega_b + \alpha_b - \mathcal{W}^4(x_b) = -\frac{\kappa^2 T_b}{2\pi}. \quad (2.107)$$

There are now two qualitatively different cases that are worth considering separately, depending on whether or not $\omega_b = 0$ or $\omega_b > 0$.

Solutions with only conical singularities:

If $\omega_b = 0$, then eq. (2.93) implies $q_b = 0$ as well, and so both ϕ and \mathcal{W} asymptote to constants near the brane. Because $\omega_b = 0$ implies $\mathcal{W} \simeq \mathcal{W}_b$ is constant in the near-brane regime, the behaviour $a \sim e^{\alpha_b \eta}$ implies the extra-dimensional metric is proportional to

$$e^{2\alpha_b \eta} (\mathcal{W}_b^8 d\eta^2 + d\theta^2) = d\rho^2 + \left(\frac{\alpha_b \rho}{\mathcal{W}_b^4} \right)^2 d\theta^2, \quad (2.108)$$

showing that it has only a conical singularity at the brane position, with defect angle $\delta_b = 2\pi(1 - \alpha_b/\mathcal{W}_b^4)$.

When $\omega_b = q_b = 0$, the matching conditions boil down to

$$\frac{\kappa^2 T'_b}{2\pi} = \frac{\kappa^2 U_b}{2\pi} = 0 \quad \text{and} \quad \delta_b = \frac{\kappa^2 T_b}{\mathcal{W}_b^4} = \kappa^2 L_b. \quad (2.109)$$

The last of these relates the tension to the size of the conical defect angle in the usual way, while the first states that the value taken by ϕ near each brane must be at a stationary point of the tension on that brane. (Since this is also automatically a zero of U_b , the second condition is redundant.) In order for solutions to exist the two tensions must be related to one another by the known asymptotic limits of the given bulk solution. That is, if $\phi_b = \lim \phi(\eta)$ as $\eta \rightarrow -(-)^b \infty$, then T_b must satisfy

$T'_b(\phi_b) = 0$ at both ends.

Since its right-hand-side is non-negative, eq. (2.87) shows that it is only possible to have $\omega_b = q_b = 0$ at *both* branes if $H = 0$. If $H = 0$ the solutions given in eqs. (2.96) have this property (for both branes) when $\lambda_3 = 0$ (and so also $\lambda_1 = \lambda_2 := \lambda$). Notice that \mathcal{W} and $e^\phi = \mathcal{W}^{-2}$ need not be identically constant in this case unless $\eta_1 = \eta_2$.

From the point of view of the 4D theory the result $H = 0$ is understood for these solutions in terms of the vanishing of the classical low-energy 4D effective potential,

$$V_{\text{eff}} = V_B + \sum_b U_b = 0. \quad (2.110)$$

This vanishes because eq. (2.83) (when $\phi' = 0$ near the branes) shows that the bulk contribution to the low energy potential vanishes, $V_B = 0$, and eq. (2.109) implies $U_b = 0$ for both branes.

If T'_b should vanish identically, then so must also U_b and V_{eff} . In this case the vanishing of V_{eff} shows that the flat direction, corresponding to the scaling $\phi \rightarrow \phi + \phi_0$ and $g_{MN} \rightarrow e^{-\phi_0} g_{MN}$, is not lifted by the classical couplings to the branes. But if T_b depends nontrivially on ϕ , then U_b becomes nonzero as soon as ϕ differs from its asymptotic value ϕ_b , implying that V_{eff} depends nontrivially on ϕ_0 . Since $U_b(\phi_0)$ is given by

$$\mathcal{U}_b = \frac{1}{3} \left[(\mathcal{W}^4 - \mathcal{T}_b) - \sqrt{(\mathcal{W}^4 - \mathcal{T}_b)^2 - \frac{3}{4} (\mathcal{T}_b')^2} \right], \quad (2.111)$$

where $\mathcal{T}_b = \mathcal{T}_b(\phi_b + \phi_0)$, it is non-negative (provided $\mathcal{T}_b < \mathcal{W}^4$). Because the bulk action is known to be stable against small fluctuations about the bulk solutions [27], it follows that $V_{\text{eff}}(\phi_0)$ must be minimized by any configuration for which it vanishes, such as $\phi_0 = 0$ (which corresponds to $\lim \phi = \phi_b$). This shows how the 4D theory sees that the flat direction, ϕ_0 , of the bulk equations becomes fixed at the same value as is chosen by the matching conditions when viewed from the higher-dimensional perspective.

Solutions with $\omega_b > 0$

On the other hand, if $\omega_b > 0$ then $e^W = \mathcal{W} \rightarrow 0$ as the brane is approached. In this case the scalar and $(\mu\nu)$ matching conditions are

$$q_b = \frac{\kappa^2 T'_b}{2\pi} = \mathcal{T}_b' \quad \text{and} \quad 3\omega_b + \alpha_b = -\frac{\kappa^2 T_b}{2\pi} = -\mathcal{T}_b. \quad (2.112)$$

Since α_b and ω_b are both positive, the last of these conditions implies $T_b < 0$. The third matching condition in this case is

$$\omega_b = \frac{\kappa^2 U_b}{2\pi} = \mathcal{U}_b = \frac{1}{3} \left[-\mathcal{T}_b - \sqrt{\mathcal{T}_b^2 - \frac{3}{4} (\mathcal{T}_b')^2} \right], \quad (2.113)$$

which also requires $\mathcal{T}_b < 0$ if \mathcal{U}_b and ω_b are to be positive.

Because we use coordinates for which the branes are situated at $\eta \rightarrow \pm\infty$, we demand that these matching conditions be satisfied as identities in η in the asymptotic regimes. Use of the asymptotic forms for the bulk solutions in this regime corresponds to expanding the brane tension about the value taken by ϕ at the brane.

This determines the functional form for the brane action, $T_b(\phi, a, W) = e^{4W} L_b(\phi, a)$, required to source the given bulk solution. Because e^ϕ and all metric functions behave as exponentials near the branes — *c.f.* eq. (2.92) — the brane action must have the form $L_b = -\Lambda_b e^{\xi_b \phi} \mathcal{F}(a e^{\zeta_b \phi})$, where $\mathcal{F}(x)$ is an arbitrary function and the powers ξ_b and ζ_b are chosen to ensure the η -independence in the near-brane regime of

$$T_b = -\Lambda_b \mathcal{W}^4 e^{\xi_b \phi} \mathcal{F}(a e^{\zeta_b \phi}) , \quad (2.114)$$

for constant Λ_b . The parameters ξ_b and ζ_b therefore satisfy

$$4\omega_b + \xi_b q_b = \alpha_b + \zeta_b q_b = 0 . \quad (2.115)$$

In terms of $\mathcal{F}(x)$, the scalar matching condition becomes

$$q_b = \frac{\kappa^2}{2\pi} \left(\frac{\partial T_b}{\partial \phi} \right) = -\frac{\kappa^2 \Lambda_b}{2\pi} \mathcal{W}^4 e^{\xi_b \phi} \left[\xi_b \mathcal{F}(x) + \zeta_b x \mathcal{F}'(x) \right]_{x=ae^{\zeta_b \phi}} , \quad (2.116)$$

while the metric matching conditions similarly give

$$3\omega_b + \alpha_b = -\frac{\kappa^2 T_b}{2\pi} = \frac{\kappa^2 \Lambda_b}{2\pi} \mathcal{W}^4 e^{\xi_b \phi} \mathcal{F}(a e^{\zeta_b \phi}) , \quad (2.117)$$

and so on.

To go further requires making choices for the function $\mathcal{F}(x)$. We discuss for simplicity a power-law, $\mathcal{F}(x) = x^{\sigma_b}$, which to concretely illustrate the brane-bulk interaction.

Power-law tension: $\mathcal{F}(x) = x^{\sigma_b}$

Perhaps the simplest choice for the function $\mathcal{F}(x)$ appearing above is a power: $\mathcal{F}(x) = x^{\sigma_b}$, for σ_b a constant. In this case

$$T_b = -\Lambda_b \mathcal{W}^4 a^{\sigma_b} e^{\lambda_b \phi} , \quad (2.118)$$

where $\lambda_b = \xi_b + \zeta_b \sigma_b$, and so

$$4\omega_b + \sigma_b \alpha_b + \lambda_b q_b = 0 , \quad (2.119)$$

is required to ensure that the η -dependence cancels in T_b within the near-brane regime. This last equation is to be regarded as being solved for σ_b .

The scalar matching condition, eq. (2.104), then boils down to

$$q_b = -\lambda_b \mathcal{W}_b^4 a_b^{\sigma_b} \left(\frac{\kappa^2 \Lambda_b}{2\pi} \right). \quad (2.120)$$

The $(\mu\nu)$ metric matching condition, eq. (2.107), similarly gives

$$3\omega_b + \alpha_b = \mathcal{W}_b^4 a_b^{\sigma_b} \left(\frac{\kappa^2 \Lambda_b}{2\pi} \right). \quad (2.121)$$

Combining (2.120) and (2.121), gives the parameter λ_b as

$$\lambda_b = -\frac{q_b}{3\omega_b + \alpha_b}. \quad (2.122)$$

Clearly $q_b < 0$ implies $\lambda_b > 0$ and vice versa, because α_b and ω_b are both positive. Notice that $\lambda_b > 0$ implies $T_b \rightarrow 0$ in the ‘weak-coupling’ limit $e^\phi \rightarrow 0$.

Given α_b and ω_b , solving the above conditions gives $q_b = \pm 2\sqrt{\omega_b(2\alpha_b + 3\omega_b)}$ (from eq. (2.93)), λ_b (from eq. (2.122)), and the combination $\mathcal{W}_b^4 a_b^{\sigma_b} (\kappa^2 \Lambda_b / 2\pi)$ (from eq. (2.121)). The power of a appearing in T_b works out to be

$$\sigma_b = \frac{4\omega_b}{3\omega_b + \alpha_b} > 0. \quad (2.123)$$

One might think that the last matching condition, involving U_b , gives an independent equation that can be used to relate ω_b to α_b , but this turns out not to be independent due to the relation between U_b and T_b and the constraint, eq. (2.93).

The 4D perspective

In this section, we evaluate the full action at its classical solution to determine the value of V_{eff} at its minimum. For supergravity the full bulk action evaluates to a total derivative at any classical solution, giving

$$S_{B,\text{ext}} = \frac{1}{2\kappa^2} \int d^6x \sqrt{-g} \square\phi = \frac{\pi}{\kappa^2} \int d^4x \sqrt{-\hat{g}} \left[\partial_\eta \phi \right]_{-\infty}^{\infty} = -\sum_b \frac{T'_b}{2}. \quad (2.124)$$

Adding to this the brane action and Gibbons-Hawking term, which combine to

$$\sum_b \left(S_{GH} + S_b \right) = -\int d^4x \sqrt{\hat{g}} U_b \quad (2.125)$$

gives the total action evaluated at the classical solution

$$S_{\text{ext}} = -\int d^4x \sqrt{-\hat{g}} \sum_b \left(U_b + \frac{T'_b}{2} \right). \quad (2.126)$$

Comparing this with eq. (2.44) (for $n = 6$) gives

$$V_{\text{eff}}(\phi_0) = - \sum_b \left(U_b + \frac{T'_b}{2} \right). \quad (2.127)$$

Using this in the four-dimensional Einstein equations gives the 4D curvature

$$\hat{R} = -12H^2 = -4\kappa_N^2 V_{\text{eff}}(\phi_0), \quad (2.128)$$

and so

$$H^2 = \frac{\kappa_N^2}{3} V_{\text{eff}} = -\frac{\kappa_N^2}{3} \sum_b \left(U_b + \frac{T'_b}{2} \right) = -\frac{2\pi\kappa_N^2}{3\kappa^2} \sum_b \left(\omega_b + \frac{q_b}{2} \right), \quad (2.129)$$

where the last equality uses the matching conditions to rewrite U_b and T'_b in terms of the bulk solution. This agrees with the bulk field equations, eq.(2.101), and so shows that the 4D and 6D pictures agree. In order to identify the value of ϕ_0 itself requires calculating V_{eff} away from its minimum, which requires a full dimensional reduction of the supergravity action.

2.4 Conclusions

This paper summarizes the bulk-brane matching conditions for codimension-2 objects (following the presentation given for scalar-tensor theories in [7], with generalizations to include a general coupling to the Maxwell field [6]), and describes several applications to higher-dimensional brane systems: F-theory compactifications involving space-filling codimension-2 D7-branes situated within 10 dimensions; unwarped 3-brane flux compactifications in 6 dimensional scalar-Maxwell-Einstein theory; and warped and unwarped 3-brane flux compactifications of 6D chiral gauged supergravity. The latter two cases involve geometries that are maximally symmetric — but possibly curved — in the directions parallel to the branes.

The comparison with the F-theory compactifications provides a sanity check on the junction conditions, since both the brane and bulk actions are explicitly known for Type IIB string vacua [9], as are explicit solutions for the surrounding bulk geometry [21]. We show that the near-brane asymptotic form of the bulk configurations in this case precisely agrees with what the matching conditions would predict, given the explicit D7-brane action. Furthermore, this comparison lies within the weak-coupling regime since the bulk solution implies the string coupling becomes weak in the near-brane limit.

When applied to six-dimensional systems, the bulk-brane matching conditions can provide a stabilization mechanism for the bulk scalars (like a bulk axion, or the dilaton) provided the brane couplings break the appropriate symmetry that protects the scalar's mass. When this is so, the value to which the scalar stabilizes can be understood from the higher-dimensional point of view as being due to the consistency of the matching conditions at the two branes. Alternatively it can

be regarded as the value which minimizes the effective potential in the low-energy, on-brane action below the KK scale, although this requires a calculation of the potential away from its minimum.

Although many of the bulk solutions considered in six dimensions (supersymmetric or not) have de Sitter curvature along the four brane directions [5, 14], we show that for 6D gauged chiral supergravity only 4D-flat branes can be sourced by positive-tension branes. To establish this we first show that for any 6D theory a codimension-2 brane tension must be negative whenever the warp factor tends to zero near the brane. We then prove that the supergravity field equations imply the warping vanishes near the brane unless the near-brane geometry has a conical singularity. Finally, the desired result follows once the field equations are used to see that any geometry having only conical singularities necessarily is flat in the 4 brane directions.

This necessity for negative tension in order to obtain de Sitter and anti-de Sitter branes echoes the various no-go theorems for finding 4D-de Sitter solutions from extra-dimensional gravity [28], even though the curvatures of the bulk geometries considered make these theorems not directly apply. This suggests that the curvature assumptions made in these theorems may be somewhat stronger than is necessary.

The relation to 4D de Sitter geometries has potential applications to searches for cosmic inflation within an extra-dimensional context. This is because inflationary configurations often lay nearby pure de Sitter solutions. In particular, a broad class of time-dependent solutions are known [14] for the bulk field equations in 6D supergravity, and for some of these the on-brane 4D geometry is likely to undergo an accelerated expansion. The extension of the arguments of this paper to these time-dependent situations would be most worthwhile, since they could provide instances of explicit inflationary models for which there is both a higher- and lower-dimensional understanding of why the universe accelerates. (By contrast, current inflationary models typically rely on the low-energy 4D effective theory to conclude that the universe inflates.) Work along these lines is in progress [29].

Acknowledgements

We wish to thank Hyun-Min Lee and A. Papazoglou for discussions about codimension-2 branes and inflation, as well as Anshuman Maharana and Fernando Quevedo for advice about F-theory. Our research has been supported in part by funds from the Natural Sciences and Engineering Research Council (NSERC) of Canada, McMaster University and Perimeter Institute. Research at the Perimeter Institute is supported in part by the Government of Canada through NSERC and by the Province of Ontario through the Ministry of Research and Information (MRI).

Bibliography

- [1] N. Arkani-Hamed, S. Dimopoulos and G. Dvali, *Phys. Lett.* **B429** (1998) 263 [hep-ph/9803315]; *Phys. Rev.* **D59** (1999) 086004 [hep-ph/9807344];
I. Antoniadis, N. Arkani-Hamed, S. Dimopoulos and G. Dvali, *Phys. Lett.* **B436** (1998) 257 [hep-ph/9804398];
K. Benakli, *Phys. Rev.* **D60**, 104002 (1999) [hep-ph/9809582]; C. P. Burgess, L. E. Ibáñez and F. Quevedo, *Phys. Lett.* **B447**, 257 (1999) [hep-ph/9810535];
P. Horava and E. Witten, *Nucl. Phys.* **B475** (1996) 94 [hep-th/9603142]; *Nucl. Phys.* **B460** (1996) 506 [hep-th/9510209];
E. Witten, *Nucl. Phys.* **B471** (1996) 135 [hep-th/9602070];
J. Lykken, *Phys. Rev.* **D54** (1996) 3693 [hep-th/9603133].
- [2] L. Randall, R. Sundrum, *Phys. Rev. Lett.* **83** (1999) 3370 [hep-ph/9905221]; *Phys. Rev. Lett.* **83** (1999) 4690 [hep-th/9906064].
- [3] K. Lanczos, *Phys. Z.* **23** (1922) 239–543; *Ann. Phys.* **74** (1924) 518–540;
C.W. Misner and D.H. Sharp, *Phys. Rev.* **136** (1964) 571–576;
W. Israel, *Nuov. Cim.* **44B** (1966) 1–14; *errata Nuov. Cim.* **48B** 463.
- [4] A. Vilenkin, *Phys. Rev.* **D23** (1981) 852;
R. Gregory, *Phys. Rev. Lett.* **59** (1987) 740;
A. G. Cohen and D. B. Kaplan, “The Exact Metric About Global Cosmic Strings,” *Phys. Lett.* **B215**, 67 (1988);
A. Vilenkin and P. Shellard, *Cosmic Strings and other Topological Defects*, Cambridge University Press (1994);
R. Gregory and C. Santos, “Cosmic strings in dilaton gravity,” *Phys. Rev. D* **56**, 1194 (1997) [gr-qc/9701014].

- [5] F. Leblond, R. C. Myers and D. J. Winters, “Consistency conditions for brane worlds in arbitrary dimensions,” *JHEP* **0107** (2001) 031 [arXiv:hep-th/0106140];
S. M. Carroll and M. M. Guica, “Sidestepping the cosmological constant with football-shaped extra dimensions,” [hep-th/0302067];
I. Navarro, “Codimension two compactifications and the cosmological constant problem,” *JCAP* **0309** (2003) 004 [hep-th/0302129];
E. Papantonopoulos and A. Papazoglou, “Brane-bulk matter relation for a purely conical codimension-2 brane world,” *JCAP* **0507** (2005) 004 [arXiv:hep-th/0501112].
- [6] C. P. Burgess, D. Hoover and G. Tasinato, “UV Caps and Modulus Stabilization for 6D Gauged Chiral Supergravity,” *JHEP* **0709** (2007) 124 [arXiv:0705.3212 [hep-th]].
- [7] C. P. Burgess, D. Hoover, C. de Rham and G. Tasinato, “Effective Field Theories and Matching for Codimension-2 Branes,” *JHEP* **0903** (2009) 124 [arXiv:0812.3820 [hep-th]].
- [8] P. Bostock, R. Gregory, I. Navarro and J. Santiago, “Einstein gravity on the codimension 2 brane?,” *Phys. Rev. Lett.* **92** (2004) 221601 [arXiv:hep-th/0311074];
J. Vinet and J. M. Cline, *Phys. Rev. D* **71** (2005) 064011 [hep-th/0501098];
M. Peloso, L. Sorbo and G. Tasinato, “Standard 4d gravity on a brane in six dimensional flux compactifications,” *Phys. Rev. D* **73** (2006) 104025 [arXiv:hep-th/0603026];
B. Himmetoglu and M. Peloso, *Nucl. Phys. B* **773** (2007) 84 [hep-th/0612140];
B. Himmetoglu and M. Peloso, “Isolated Minkowski vacua, and stability analysis for an extended brane in the rugby ball,” *Nucl. Phys. B* **773** (2007) 84 [hep-th/0612140];
C. de Rham, “The Effective Field Theory of Codimension-two Branes,” *JHEP* **0801** (2008) 060 [arXiv:0707.0884 [hep-th]];
E. Papantonopoulos, A. Papazoglou and V. Zamarias, “Regularization of conical singularities in warped six-dimensional compactifications,” *JHEP* **0703** (2007) 002 [arXiv:hep-th/0611311];
“Induced cosmology on a regularized brane in six-dimensional flux compactification,” *Nucl. Phys. B* **797** (2008) 520 [arXiv:0707.1396 [hep-th]];
D. Yamauchi and M. Sasaki, “Brane World in Arbitrary Dimensions Without Z_2 Symmetry,” *Prog. Theor. Phys.* **118** (2007) 245 [arXiv:0705.2443 [gr-qc]];
N. Kaloper and D. Kiley, “Charting the Landscape of Modified Gravity,” *JHEP* **0705** (2007) 045 [hep-th/0703190];
M. Minamitsuji and D. Langlois, “Cosmological evolution of regularized branes in 6D warped flux compactifications,” *Phys. Rev. D* **76** (2007) 084031 [arXiv:0707.1426 [hep-th]];

- S. A. Appleby and R. A. Battye, “Regularized braneworlds of arbitrary codimension,” *Phys. Rev. D* **76** (2007) 124009 [arXiv:0707.4238 [hep-ph]];
- C. Bogdanos, A. Kehagias and K. Tamvakis, “Pseudo-3-Branes in a Curved 6D Bulk,” *Phys. Lett. B* **656** (2007) 112 [arXiv:0709.0873 [hep-th]];
- O. Corradini, K. Koyama and G. Tasinato, “Induced gravity on intersecting brane-worlds Part I: Maximally symmetric solutions,” *Phys. Rev. D* **77** (2008) 084006 [arXiv:0712.0385 [hep-th]];
- F. Arroja, T. Kobayashi, K. Koyama and T. Shiromizu, “Low energy effective theory on a regularized brane in 6D gauged chiral supergravity,” *JCAP* **0712** (2007) 006 [arXiv:0710.2539 [hep-th]];
- O. Corradini, K. Koyama and G. Tasinato, “Induced gravity on intersecting brane-worlds Part II: Cosmology,” *Phys. Rev. D* **78** (2008) 124002 [arXiv:0803.1850 [hep-th]];
- V. Dzhunushaliev, V. Folomeev and M. Minamitsuji, “Thick brane solutions,” arXiv:0904.1775 [gr-qc].
- [9] For a review with references see J. Polchinski, *TASI Lectures on D-Branes* [hep-th/9611050].
- [10] C. Vafa, “Evidence for F-Theory,” *Nucl. Phys. B* **469** (1996) 403 [arXiv:hep-th/9602022];
- D. R. Morrison and C. Vafa, “Compactifications of F-Theory on Calabi–Yau Threefolds – I,” *Nucl. Phys. B* **473** (1996) 74 [arXiv:hep-th/9602114]; “Compactifications of F-Theory on Calabi–Yau Threefolds – II,” *Nucl. Phys. B* **476** (1996) 437 [arXiv:hep-th/9603161]. Sen, Ashoke, “F-theory and Orientifolds” *Nucl. Phys. B* **475** (1996) 562 [arXiv:hep-th/9605150].
- [11] A. Kehagias, “A conical tear drop as a vacuum-energy drain for the solution of the cosmological constant problem,” *Phys. Lett. B* **600** (2004) 133 [arXiv:hep-th/0406025];
- T. Kobayashi and M. Minamitsuji, “Brane cosmological solutions in six-dimensional warped flux compactifications,” *JCAP* **0707** (2007) 016 [arXiv:0705.3500 [hep-th]];
- D. Kiley, “Rotating Black Holes on Codimension-2 Branes,” *Phys. Rev. D* **76** (2007) 126002 [arXiv:0708.1016 [hep-th]];
- [12] H. Nishino and E. Sezgin, *Phys. Lett.* **144B** (1984) 187; “The Complete N=2, D = 6 Supergravity With Matter And Yang-Mills Couplings,” *Nucl. Phys.* **B278** (1986) 353; S. Randjbar-Daemi, A. Salam, E. Sezgin and J. Strathdee, *Phys. Lett.* **B151** (1985) 351.
- [13] A. Salam and E. Sezgin, “Chiral Compactification On Minkowski X S**2 Of N=2 Einstein-Maxwell Supergravity In Six-Dimensions,” *Phys. Lett. B* **147** (1984) 47;
- S. L. Parameswaran, G. Tasinato and I. Zavala, “The 6D SuperSwirl,” *Nucl. Phys. B* **737** (2006) 49 [arXiv:hep-th/0509061];

- H. M. Lee and C. Ludeling, “The general warped solution with conical branes in six-dimensional supergravity,” *JHEP* **0601** (2006) 062 [arXiv:hep-th/0510026];
- H. M. Lee and A. Papazoglou, “Supersymmetric codimension-two branes in six-dimensional gauged supergravity,” *JHEP* **0801** (2008) 008 [arXiv:0710.4319 [hep-th]];
- C. P. Burgess, S. L. Parameswaran and I. Zavala, “The Fate of Unstable Gauge Flux Compactifications,” arXiv:0812.3902 [hep-th];
- [14] A. J. Tolley, C. P. Burgess, C. de Rham and D. Hoover, “Scaling solutions to 6D gauged chiral supergravity,” *New J. Phys* **8** (2006) 324 [arXiv:0608.083 [hep-th]];
- A. J. Tolley, C. P. Burgess, C. de Rham and D. Hoover, “Exact Wave Solutions to 6D Gauged Chiral Supergravity,” *JHEP* **0807** (2008) 075 [arXiv:0710.3769 [hep-th]];
- M. Minamitsuji, “Instability of brane cosmological solutions with flux compactifications,” *Class. Quant. Grav.* **25** (2008) 075019 [arXiv:0801.3080 [hep-th]].
- H. M. Lee and A. Papazoglou, “Codimension-2 brane inflation,” *Phys. Rev. D* **80** (2009) 043506 [arXiv:0901.4962 [hep-th]].
- [15] S. Weinberg, *Gravitation and Cosmology*, Wiley 1973.
- [16] C. W. Misner, J. A. Wheeler and K. S. Thorne, *Gravitation*, W. H. Freeman & Company 1973.
- [17] G.W. Gibbons and S.W. Hawking, *Phys. Rev.* **D15** (1977) 2752.
- [18] I. Navarro and J. Santiago, “Gravity on codimension 2 brane worlds,” *JHEP* **0502** (2005) 007 [arXiv:hep-th/0411250].
- [19] Y. Aghababaie, C.P. Burgess, S. Parameswaran and F. Quevedo, *Nucl. Phys.* **B680** (2004) 389–414, [hep-th/0304256];
- C. P. Burgess, *Annals Phys.* **313** (2004) 283 [arXiv:hep-th/0402200]; *AIP Conf. Proc.* **743** (2005) 417 [arXiv:hep-th/0411140].
- [20] Y. Aghababaie *et al.*, “Warped brane worlds in six dimensional supergravity,” *JHEP* **0309** (2003) 037 [hep-th/0308064];
- [21] B. R. Greene, A. D. Shapere, C. Vafa and S. T. Yau, “Stringy Cosmic Strings And Noncompact Calabi-Yau Manifolds,” *Nucl. Phys. B* **337** (1990) 1.
- [22] N. Koblitz, *Introduction to Elliptic Curves and Modular Forms*, Springer Verlag (1984).
- [23] G. W. Gibbons, R. Guven and C. N. Pope, “3-branes and uniqueness of the Salam-Sezgin vacuum,” *Phys. Lett. B* **595** (2004) 498 [hep-th/0307238];

- [24] C. P. Burgess, F. Quevedo, G. Tasinato and I. Zavala, “General axisymmetric solutions and self-tuning in 6D chiral gauged supergravity,” *JHEP* **0411** (2004) 069 [hep-th/0408109];
- [25] A. J. Tolley, C. P. Burgess, D. Hoover and Y. Aghababaie, “Bulk singularities and the effective cosmological constant for higher co-dimension branes,” *JHEP* **0603** (2006) 091 [arXiv:hep-th/0512218].
- [26] C. P. Burgess, D. Hoover and G. Tasinato, “Technical Naturalness on a Codimension-2 Brane,” *JHEP* **0906** (2009) 014 [arXiv:0903.0402 [hep-th]].
- [27] H. M. Lee and A. Papazoglou, “Scalar mode analysis of the warped Salam-Sezgin model,” [hep-th/0602208];
C. P. Burgess, C. de Rham, D. Hoover, D. Mason and A. J. Tolley, “Kicking the rugby ball: Perturbations of 6D gauged chiral supergravity,” *JCAP* **0702** (2007) 009 [arXiv:hep-th/0610078].
S. L. Parameswaran, S. Randjbar-Daemi and A. Salvio, “Gauge fields, fermions and mass gaps in 6D brane worlds,” *Nucl. Phys. B* **767** (2007) 54 [arXiv:hep-th/0608074]; “Stability and Negative Tensions in 6D Brane Worlds,” *JHEP* **0801** (2008) 051 [arXiv:0706.1893 [hep-th]]; “General Perturbations for Braneworld Compactifications and the Six Dimensional Case,” *JHEP* **0903** (2009) 136 [arXiv:0902.0375 [hep-th]].
- [28] J. M. Maldacena and C. Nunez, “Supergravity description of field theories on curved manifolds and a no go theorem,” *Int. J. Mod. Phys. A* **16** (2001) 822 [hep-th/0007018]; G. W. Gibbons, R. Kallosh and A. D. Linde, “Brane world sum rules,” *JHEP* **0101** (2001) 022 [hep-th/0011225]; E. Teo, “A no-go theorem for accelerating cosmologies from M-theory compactifications,” *Phys. Lett. B* **609** (2005) 181 [hep-th/0412164]; M. P. Hertzberg, S. Kachru, W. Taylor and M. Tegmark, “Inflationary Constraints on Type IIA String Theory,” *JHEP* **0712**, 095 (2007) [arXiv:0711.2512 [hep-th]]; D. H. Wesley, “New no-go theorems for cosmic acceleration with extra dimensions,” [arXiv:0802.2106 [hep-th]]; “Oxidised cosmic acceleration,” [arXiv:0802.3214 [hep-th]];
P. J. Steinhardt and D. Wesley, “Dark Energy, Inflation and Extra Dimensions,” *Phys. Rev. D* **79** (2009) 104026 [arXiv:0811.1614 [hep-th]].
- [29] A. Bayntun, C.P. Burgess and L. van Nierop, to appear.

Chapter 3

Gravity-Gauge Duality and the Quantum Hall Effect

In this section, we present the basic concepts of the holographic principle as well as its motivation in the application of this framework to the quantum Hall effect. While it is far from a comprehensive review, the purpose of this chapter is to make the reader familiar with the calculations to be done in the later sections while introducing some ideas that are not made explicit in the following papers. For an introduction of AdS/CFT to non-specialists, see [12]. See [13] for reviews from a high energy physics perspective, and [14] for a condensed matter perspective.

The holographic principle was originally proposed by Maldacena [15] and further explored by Witten [16] in the context of Yang-Mills theory and in particular QCD and phase transitions [17]. While at the time of writing, the AdS/CFT conjecture is only shown to be exact for the case of Type IIB string theory and the dual being $\mathcal{N} = 4$ Super-Yang Mills, there is more and more evidence piling up in favour of this correspondence.

We first briefly review the original conjecture, as presented in [18], and provide further evidence for this correspondence as well as some sample calculations that are typically done from a phenomenological standpoint. Typically one starts off with a stack of N D3 branes in type IIB supergravity. In this theory, there are simply two parameters, the string coupling g_s and the string length l_s . The other parameters in this theory, such as the brane tension and gravitational coupling, are related to these parameters through $T_{D3} \sim 1/g_s$ and $\kappa^2 \sim g_s^2$ with their engineering dimensions provided by the string length scale. Each of these branes carry an independent $U(1)$ charge. Remembering that the theory of D-branes is the T-dual version to a theory of open strings, the effective theory of these string endpoints can be thought of as particles in a QFT transforming under an $SU(N)$ symmetry from this stack of branes.

The solutions to these D3 branes in type IIB supergravity correspond to black p-brane solutions. In the limit where $N \rightarrow \infty$ and $g_s \rightarrow 0$ such that the 't Hooft coupling, $NT_{D3}\kappa^2 = Ng_s = \lambda$ remains

fixed, the near-horizon region of these black p-branes correspond to an $\text{AdS}_5 \times \text{S}_5$ space described by the metric

$$ds^2 = \frac{r^2}{L^2} (-dt^2 + dx^i dx^i) + \frac{L^2 dr^2}{r^2} + L^2 d\Omega_5^2. \quad (3.1)$$

The AdS subspace of this metric has its AdS scale, L , related to the 't Hooft coupling by $L^2 \sim \sqrt{\lambda}$ and again its dimensions given by the string scale. On the CFT side, the large N limit corresponds to the planar limit with the 't Hooft coupling, λ , now the gauge coupling of the CFT when we relate the string coupling to the CFT gauge coupling by $g_s = g_{YM}^2$. We can now see the importance of the 't Hooft coupling. When $\lambda \ll 1$, then the CFT is perturbative, but the AdS scale on the gravity side is smaller than the string length, and so supergravity is no longer a consistent description of the geometry. Similarly, at large 't Hooft coupling, the CFT is no longer perturbative, but the AdS scale is much larger than the string scale, so supergravity is now an appropriate description of our system. This particular system has a number of specific features that also have a correspondence in the CFT as well as its gravity dual, however we focus on the main result with regards to the 't Hooft coupling of these two systems.

The upshot is as follows. A strongly interacting non-perturbative CFT can be seen as a weakly interacting gravitational theory in an extra dimension. It is this particular aspect of the correspondence this thesis will concentrate on. Calculations of a strongly interacting CFT can be done using gravity in an AdS geometry in one extra dimension.

Possibly one of the most convincing arguments in general is that the calculation of entropy using the holographic principle is identical to that of Hawking's original proposal of black hole entropy [19], and provides an alternate method of calculating the entropy of the system. From a theoretical standpoint, the holographic correspondence is a step towards understanding why a black hole, which has the maximum entropy configuration of an object of that size, has an entropy proportional to its surface area. Naively one would expect the entropy of a system to be proportional to the volume, as available states increase with volume. However, the gauge-gravity duality tells us the relevant degrees of freedom exist entirely on the AdS boundary for a black hole, which is proportional to the black hole surface area.

Aside from these more philosophical questions on the nature of entropy in black holes, the AdS/CFT correspondence provides us a very real way of doing calculations in a CFT that would otherwise be intractable. The basic AdS/CFT proposal is

$$\mathcal{Z}_{\text{CFT}} = \mathcal{Z}_{\text{gravity-string}}. \quad (3.2)$$

At this level, the correspondence isn't very useful, since typically it is hard to calculate anything on either side of this equation. As was shown above, the large- N limit and large 't Hooft coupling allow us to make calculations in a CFT using classical gravity. The correspondence that we're interested

in investigating is then along the lines

$$\mathcal{Z}(J)_{\text{CFT}} = e^{-iS_{\text{AdS-on-shell}}(\phi_{\text{boundary}})}. \quad (3.3)$$

This is a statement that operator expectation values (coupled to some source J) in the CFT correspond to boundary values of fields in the AdS space. In general, the operator expectation value is related to the functional derivative of the CFT, and therefore AdS action, given by

$$\langle \mathcal{O} \rangle = \left. \frac{\delta S_{\text{AdS-on-shell}}}{\delta \phi} \right|_{\text{boundary}}. \quad (3.4)$$

At this point we can introduce the AdS/CFT dictionary. For scalar operators such as order parameters or mass gaps, the corresponding bulk field is a scalar. Similarly fermionic fields correspond to fermionic operators in the CFT. Conserved vector operators, such as the current, correspond to gauge fields in the bulk. In fact, the conservation of the current in the CFT directly corresponds to gauge invariance in the bulk. This can be similarly expressed as conservation of local symmetries in the bulk correspond to global symmetries on the boundary CFT.

3.1 AdS/CFT: A simple picture

We further illustrate some intuition that can be gained from this correspondence. Consider the action of a CFT unbroken by quantum effects,

$$S_{\text{CFT}} = \int d^{d-1}x \mathcal{L}_{\text{CFT}}. \quad (3.5)$$

Because this action is truly conformal, a rescaling of co-ordinates can be absorbed by the rescaling of the fields since there are no other scales in the theory. These fields will carry dimensions such that the total action of rescaling the co-ordinates and fields cancel at the level of the action. If we were instead to understand the dimensions of these fields as an energy scale, then rescaling the co-ordinates corresponds to rescaling the energy scale. If we wanted to recast this statement as a gravitational theory with the understanding that the gravity theory lives in an extra dimension corresponding to the energy scale, the metric would be

$$ds^2 = \frac{L^2}{z^2} (\eta^{\mu\nu} d^\mu x d^\nu x + dz^2), \quad (3.6)$$

where we can see a rescaling of $x \rightarrow \lambda x$ is canceled by a rescaling of $z \rightarrow \lambda z$. From dimensional analysis, we conclude that z is the inverse energy scale, and $z \rightarrow 0$ is the UV of the CFT.

3.2 Temperature and Free Energy

In the interest of giving the reader a better understanding of the calculations involved in the gauge-gravity framework, we present some calculations of quantities not explicitly computed in chapters 4 and 5. We start by introducing the temperature for a metric of the form

$$ds^2 = -e^{\xi(r)}h(r)dt^2 + \frac{dr^2}{h(r)} + \frac{r^2}{L^2}ds_{\text{boundary}}^2, \quad (3.7)$$

with the assumption that at some radius, $h(r_h) = 0$ as well as the assumption that this metric asymptotes as $r \rightarrow \infty$ to

$$ds^2 = -\frac{r^2}{L^2}dt^2 + \frac{L^2}{r^2}dr^2 + \frac{r^2}{L^2}ds_{\text{boundary}}^2. \quad (3.8)$$

We can see that this is simply the metric of (3.6) with the identification $z = L^2/r$. The reason for this asymptotic assumption is that the CFT metric is given as

$$ds_{\text{CFT}}^2 = \frac{L^2}{r^2}ds_{\text{AdS}}^2 \Big|_{r \rightarrow \infty}, \quad (3.9)$$

with the truncation of the r direction in the CFT metric. This allows us to obtain a finite CFT metric under the assumption that the metric is asymptotically AdS. The temperature of the CFT is defined as the inverse periodicity in $\beta = it$. The way to see this periodicity is by expanding the metric near the horizon, $h(r_h) = 0$. If we assume $h(r) \approx h'(r_h)(r - r_h)$, the metric then becomes

$$ds^s = e^{\xi(r_h)}h'(r_h)(r - r_h)d\beta^2 + \frac{dr^2}{h'(r_h)(r - r_h)}, \quad (3.10)$$

where we have ignored the CFT spatial directions. If we change to polar co-ordinates with $A\rho^2 = (r - r_h)$ for some arbitrary constant A the metric is then

$$ds^s = e^{\xi(r_h)}h'(r_h)Ad\beta^2 + \frac{4Ad\rho^2}{h'(r_h)}. \quad (3.11)$$

For this metric to be in standard polar form, $A = h'(r_h)/4$. Now we see that in order for there not to be a conical singularity (or a deficit angle), β must have periodicity $4\pi e^{-\xi(r_h)}/h'(r_h)$. Because the periodicity, β is identified with temperature as $T = \beta^{-1}$, the temperature of the CFT is

$$4\pi T = e^{\xi(r_h)}h'(r_h). \quad (3.12)$$

The free energy of the CFT is defined by

$$F(T) = -T \ln(\mathcal{Z}_{\text{CFT}}), \quad (3.13)$$

and by the correspondence this becomes

$$\begin{aligned} F(T) &= -T \ln \left(e^{iS_{\text{AdS-on-shell}}} \right) \\ &= -iT S_{\text{AdS-on-shell}}. \end{aligned} \tag{3.14}$$

Finally, since we work at finite temperature defined by the Euclidean time, the free energy takes on the form

$$F(T) = -T S_{\text{AdS-on-shell}}. \tag{3.15}$$

Here we have seen not only the reasoning and intuition behind the AdS/CFT correspondence, but also a number of calculations that have potential to make contact with physical observables for the particular system we're interested in. These ideas will be important in understanding the entire motivation behind the motivation for the application of this technique to condensed matter systems. Furthermore, these quantities calculated complete the calculations of interest in the quantum Hallography proposal, which include further observables such as the conductivity, system size, and explicit calculations of the free energy.

3.3 Condensed Matter and the Quantum Hall Effect

Up until this point, we have motivated why AdS/CFT is an excellent calculational tool. Methods and techniques theorists have been using for years in gravity can now be applied to strongly coupled systems of which have resisted other more conventional tools. Implicit in the AdS/CFT correspondence is that the field theory is conformal, and any deviations from this are done by introducing operators that deform this conformal symmetry. To understand how this relates to condensed matter systems, consider a typical correlation function in condensed matter,

$$\Delta(x, y) \sim \frac{e^{-|x-y|/\xi}}{|x-y|^{d-2+\eta}}. \tag{3.16}$$

where ξ is the correlation length, d is the number of dimensions of the system, and η is the anomalous dimension of the correlator. As the temperature of the system reaches a critical temperature for a phase transition, the correlation length diverges. That is, each particle effectively sees each other particle in the system, without any screening effects. As the critical temperature is reached, the divergence of the correlation length tells us there is no longer a scale in the system, and so all physical functions must be self-similar in $|T - T_c|$, or power laws. This can be explicitly seen in (3.16) as we take $\xi \rightarrow \infty$ and the correlator is a pure power law in the separation of the operators. This lack of a scale is precisely what a conformal theory is, and this tells us that the theory of critical phenomena can be understood as a conformal field theory. That is, near a transition, observables become power laws and can be described by a conformal field theory. Indeed, this is the exact

motivation as to why we wish to apply AdS/CFT methods to condensed matter systems. The one extra condition we require is for the system to be strongly interacting, as was stated above to be able to use this correspondence to do calculations on the gravity side. In the next section we explore the quantum Hall effect to justify the use of AdS/CMT on this system.

3.3.1 The Quantum Hall Effect

The integer quantum Hall effect was initially discovered by [20], and in a triumph of theory, immediately described by Laughlin in [21]. Initially, a strong magnetic field was applied to a semi-conducting material, and the Hall voltage (and thus conductivity) was measured. Doing a simple calculation using standard electrodynamics, we can calculate what the hall conductivity would be. If we define a resistivity tensor as

$$E_i = \rho_{ij} J_j, \quad (3.17)$$

and then assume the Ohmic resistivity (ρ_{ii}) approaches zero as we lower the temperature of the system, we can calculate the Hall resistivity from the Lorentz force law. That is

$$F_i = q(E_i - \epsilon_{ijk} v_j B_k) \quad (3.18)$$

$$0 = E_i - \epsilon_{ijz} J_j \frac{B_z}{\rho_q}, \quad (3.19)$$

where ρ_q is the charge density of the system. Comparing (3.19) with (3.17) gives us the expression for the Hall resistivity,

$$\rho_{xy} = \frac{B_z}{\rho_q}. \quad (3.20)$$

And so we see that the Hall resistivity¹ should linearly increase with the magnetic field at sufficiently low temperatures. However, experiments have shown this not to be the case, and instead observe resistance curves such as figure 3.1. That is the Hall resistivity (and therefore conductivity) take on plateaux for large values of magnetic field, and quickly jump to another plateau at some critical magnetic field. This clear quantization stems from the fact that the system is quantum mechanical and to preserve gauge invariance. To understand this effect, we borrow the arguments made originally by Laughlin. To understand this effect, consider the Hamiltonian for a charged

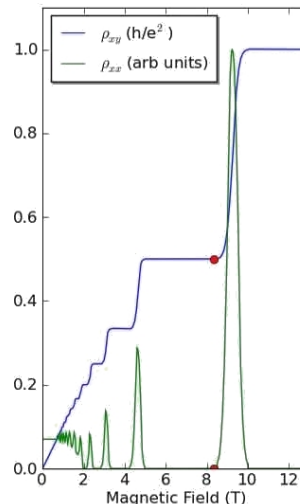


Figure 3.1. Cartoon of the various plateaux of the quantum Hall effect for varying magnetic field across the various Landau levels. Source: Glenton Jelbert licensed under the Creative Commons Attribution 3.0 Unported license

¹It should be noted that throughout the remainder of the thesis, aside from this introduction, we will be focusing on the conductivity matrix, which is defined as $\sigma_{ij} = (\rho_{ij})^{-1}$. Note from this definition, for non-zero Hall resistivity, vanishing Ohmic resistivity implies vanishing Ohmic conductivity.

particle in the $x - y$ plane with the y direction periodically identified and in a constant magnetic field in the z direction,

$$H = \frac{1}{2m}p_x^2 + \frac{1}{2m}(p_y - eBx)^2 + eEx, \quad (3.21)$$

where we have specifically made a gauge choice for the vector potential, A_μ , to be entirely in the y direction, and the periodicity of y is b such that $y + b \sim y$. Since there is no potential in the y direction, we can treat p_y as a constant of the Hamiltonian in the x direction. Pulling out a factor of the magnetic field gives us

$$H = \frac{1}{2m}p_x^2 + \frac{1}{2}m \left(\frac{eB}{m} \right)^2 \left(\frac{p_y}{eB} - x \right)^2 + eEx, \quad (3.22)$$

which is simply the harmonic oscillator with energy levels separated by eB/m - known as ‘Landau levels’. How does this explain the clear quantization of resistivity conductivity levels? Consider the fact that each particle has access to each of these Landau levels. We also know that fermions have a Fermi energy in which they fill up all the available states below that energy level as in figure 3.2. Now consider the fact that the Fermi energy is fixed, and due to finite temperature effects, these Landau levels are broadened (but not enough such that they overlap.) Clearly as we sweep through values of the magnetic field, the Fermi energy will not cross a Landau level for a range of magnetic fields. In this region, the system is gapped and the conductivity becomes fixed at a specific value. Only when the Fermi energy reaches a Landau level may the conductivity vary, and this is the point where the Hall conductivity varies to a new plateau.

To determine the value of the conductivity at a plateau, we vary the Hamiltonian with respect to the vector potential, with the response being the current. Clearly since there is no A_x , the only current is in the y direction, in response to an electric field in the x direction. This tells us immediately in the gapped region the ohmic conductivity vanishes, and the Hall conductivity is non-zero. To see the value of the Hall conductivity, we use the relation

$$\frac{\partial \langle H \rangle}{\partial A_y} = j_y. \quad (3.23)$$

We now assume that any variation of A_y takes the form $\delta A_y = \delta\Phi/b$. For this particular variation our Hamiltonian takes the form

$$\delta \langle H \rangle = \frac{\delta\Phi}{b} \int dx \int dy j_y = \frac{\delta\Phi}{I_y}, \quad (3.24)$$

which can similarly be rewritten as $\partial \langle H \rangle / \partial \Phi = I_y$. We have re-expressed the variation in terms of Φ due to the constraint coming from the periodicity of the gauge transformation. In particular, when $\delta\Phi = nh/e = n\Phi_0$, this simply changes the periodicity of the wavefunction in the y direction

and is a gauge transformation. If we now assume that the system is varied by Φ_0 we get the response

$$I_y = \frac{\Delta\langle H \rangle}{\Phi_0}. \quad (3.25)$$

Finally to understand how the Hamiltonian responds to this variation, we realize that the addition of a quanta of flux Φ_0 is equivalent to shifting the periodicity of the wavefunction in the y -direction. To see this, we can see that adding a Φ_0 flux is equivalent to taking $p_y \rightarrow p_y - e\Phi_0/b$ in (3.21). This tells us that an integer number of electrons can change their contribution to the conductivity. The change in the Hamiltonian then must be

$$\Delta\langle H \rangle = \nu e \Delta V \quad (3.26)$$

from dimensional considerations if we assume any energy shift comes from the electrons. The prefactor ν is restricted to be an integer if we require an integer number of electrons contributing to the energy shift. Finally, from this relationship, (3.25) and $\Phi_0 = h/e$ we get the conductivity

$$\sigma_{xy} = \nu \frac{e^2}{h}. \quad (3.27)$$

The physical picture that emerges is as follows. As one adjusts the magnetic field at a plateau, for each quanta of flux that is added, an integer number of additional electrons contribute to the conductivity such that the conductivity is constant as a function of magnetic field. It is in this sense in which we attach flux quanta to electrons in the quantum Hall effect.

In fact, this quantization can also be seen from an effective field theory approach, in addition to topological considerations, which will be further outlined in 4.2.2. For now, we briefly mention the fractional quantum Hall effect.

Aside from the integer quantum Hall effect mentioned above, it was noticed in [22] that for lower temperatures and stronger magnetic fields that n was no longer an integer, but a fraction, p/q (for most known fractions, q is odd). While it is specifically this effect that is the thrust of the remainder of this thesis, it should be noted why this effect is so interesting. The fact that the coefficient, n , is a fraction suggests that the charge carriers of the system are now fractionally charged. This implies that the degrees of freedom of the system has drastically changed from the non-interacting state. It is for these reasons that the fractional system is generally believed to be a strongly interacting one. Because of this, AdS/CFT provides an excellent tool for beginning to understand the dynamics of the quantum Hall effect and its low energy degrees of freedom. To further apply AdS/CFT, it is clear that the inter-plateaux transitions are perfect candidates for a conformal field theory since the degrees of freedom become ungapped in these regions. For these reasons we can consider the effective theory in between plateaux as a phase transition and therefore a perfect candidate for AdS/CMT. In this chapter, we have motivated AdS/CFT in general and how it was originally

used and implemented, as well as some basic calculations in this framework. Furthermore, we have motivated the application of holography to condensed matter systems using the theory of phase transitions as a particular motivation. Finally, we have introduced the quantum Hall effect, some basic features, as well as the way in which AdS/CFT can be a useful tool in explaining some of its strongly interacting features. In the following chapters, we introduce a particular model for the quantum Hall effect in AdS/CMT, in addition to calculating many observables, their ramifications and comparison to modern experiments in these quantum Hall systems.

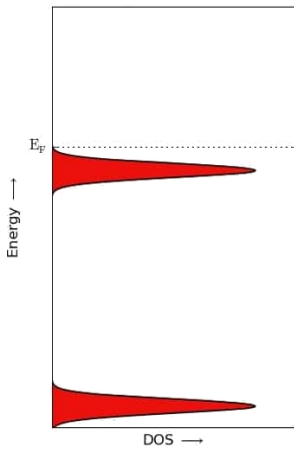


Figure 3.2. Cartoon of the density of states for strong magnetic fields at finite temperature. Increasing magnetic fields spreads the Landau levels apart, making it clear that for a wide range of magnetic fields the system is gapped. Source: Glenton Jelbert licensed under the Creative Commons Attribution 3.0 Unported license

Chapter 4

Quantum Hall-ography

Preface

After having previously introduced the ideas of gauge-gravity duality in chapter 3, we can go on to present a model in which uses this framework to account for the observables in the fractional quantum Hall effect (FQHE). The particular benefit of this model is that it inherently has the symmetries and dualities of the quantum Hall effect built into the model. Furthermore, it also has the benefit of allowing us to model and predict other measurable quantities based on the holographic dictionary. The overall purpose of this paper is to introduce the quantum Hall-ography model, and calculate the conductivity. It is then shown that the theoretical conductivity has some remarkable similarities to those of experiment, as well as agreeing with a particular scaling exponent.

Abstract

Transitions among quantum Hall plateaux share a suite of remarkable experimental features, such as semi-circle laws and duality relations, whose accuracy and robustness are difficult to explain directly in terms of the detailed dynamics of the microscopic electrons. They would naturally follow if the low-energy transport properties were governed by an emergent discrete duality group relating the different plateaux, but no explicit examples of interacting systems having such a group are known. Recent progress using the AdS/CFT correspondence has identified examples with similar duality groups, but without the DC ohmic conductivity characteristic of quantum Hall experiments. We use this to propose a simple holographic model for low-energy quantum Hall systems, with a nonzero DC conductivity that automatically exhibits all of the observed consequences of duality, including the existence of the plateaux and the semi-circle transitions between them. The model can be regarded as a strongly coupled analog of the old ‘composite boson’ picture of quantum Hall systems. Non-universal features of the model can be used to test whether it describes actual materials, and we comment on some of these in our proposed model. In particular, the model indicates the value $\frac{2}{5}$ for low-temperature scaling exponents for transitions among quantum Hall plateaux, in agreement with the measured value 0.42 ± 0.04 .

4.1 Introduction

Applications of AdS/CFT duality [1, 2, 3] to condensed matter physics [4] carry a whiff of a fishing expedition. The goal is to explore the properties of strongly interacting conformal field theories (CFTs) using their calculable gravity duals in anti-de Sitter space (AdS). The jackpot would be to find a model that describes a strongly correlated system of real electrons; systems that have resisted approaches using other theoretical tools. Without a systematic way to derive the magic CFT directly from underlying electron dynamics one throws theoretical darts into field space, hoping to find that right ‘hyperbolic cow.’

Like any fishing expedition, it always helps to have some local guidance towards the good fishing holes. What would be useful are a set of simple properties, like symmetries, that are known to be prerequisites for a successful description of a particular system. Knowledge of these properties could help guide the search for theories that are relevant to life in the lab.

In this paper we argue that quantum Hall systems [5] are likely to be profitable places to fish, for two reasons. First, they involve strongly correlated electrons, and for decades have been a source of new experimental phenomena requiring theoretical explanation. But their phenomenology also points to symmetry properties that seem relatively easy to find in an AdS framework, and these symmetries can help narrow down the search for the killer model. Our purpose is threefold: to briefly summarize the relevant phenomenology and the symmetries to which we believe they point; to propose a particular class of AdS/CFT models that captures these symmetries; and to identify a class of tests for such models that go beyond the implications of the symmetries, to be used to home in on an experimentally successful model.

The symmetries of interest are not symmetries in the usual sense. Rather they are a large group of duality transformations that appear to map the various quantum Hall states into one another, and which commute with the RG flow of these systems at very low temperatures as one approaches the many quantum Hall plateaux. In particular, we summarize in §2 the evidence for the existence of discrete duality transformations of this type, acting on the ohmic (σ_{xx}) and Hall (σ_{xy}) conductivities according to the rule

$$\sigma := \sigma_{xy} + i\sigma_{xx} \rightarrow \frac{a\sigma + b}{c\sigma + d}, \quad (4.1)$$

where a, b, c and d are integers satisfying the $SL(2, Z)$ condition $ad - bc = 1$, but with c restricted to be even. The consequences of this symmetry include a number of well-measured effects for quantum Hall systems, including the kinds of fractional states that can arise as attractors in the low-energy limit; which states can be obtained from which others by varying magnetic fields; detailed predictions for some of the trajectories through the conductivity plane as the temperature, T , and magnetic field, B , are varied; as well as others.

§2 describes the qualitative picture: at low energies the flow in coupling-constant space appears to be onto a two-dimensional surface that governs the final approach to the various quantum Hall

ground states. The flow in this two-dimensional surface is constrained by the emergent symmetry, eq. (4.1), and can be traced experimentally by varying both B and T . What is missing is a simple class of candidate models to describe this two-dimensional flow, including the emergent duality. Besides providing an existence proof, having such a model in hand would allow this picture to be sharpened considerably by allowing its implications to be explored in more detail.

What is encouraging is that there is good evidence that transformations like eq. (4.1) arise quite generically in CFTs having conserved currents in two spatial dimensions [6, 7]. Furthermore, the development of the AdS/CFT correspondence has opened up new tools for exploring strongly interacting 2+1 dimensional CFTs, with the conserved current being dual on the gravity side to an electromagnetic gauge potential. In this language the dual version of the CFT's discrete dualities are rooted in electric-magnetic duality. Applications of these tools to condensed matter remain very promising [4], and studies of the simplest holographic charge-carrying systems do reveal a number of duality-related features [8, 9].

The most striking examples to emerge to date of explicit systems with symmetries like eq. (4.1) are those based on dilatonic black branes [10, 11] — briefly described in §3 — for which the electric-magnetic duality is also accompanied by an action on the dilaton and axion fields (as in Type IIB supergravity in 10 dimensions). If the duality symmetries provide a good guide, it is among this type of AdS/CFT system that a description of low-energy quantum Hall systems is likely to reside. (See also [12] for other discussions of quantum Hall systems within an AdS/CFT context.) The main drawback of the simplest dilaton black brane models is their prediction of vanishing DC ohmic conductivity at nonzero temperature. This clearly cannot describe real quantum Hall systems, for which the evidence for eq. (4.1) relies almost exclusively on DC charge-transport properties.

For this reason we propose, in §4, a slight modification of this model, following a recent proposal [13] for strange metal holography. In this proposal the field content of the AdS dual is the same as for ref. [11] — *i.e.* gravity, Maxwell field, dilaton and axion — but with the Maxwell kinetic term described by the (dilaton) Dirac-Born-Infeld (DBI) action rather than the dilaton-Maxwell action. The DBI action shares the desired duality of the dilaton-Maxwell action, but also allows nonzero DC conductivities with which to probe its implications. Following [13] we treat the charge carriers in the probe-brane approximation, coupled to an uncharged black brane. (The brane geometry can also be chosen to have Lifshitz form if it is desired to introduce different powers, z , for temporal and spatial scalings.) Physically, this corresponds to regarding the charge carriers as perturbations to the CFT described by the black hole.

Finally, §5 describes a number of the model's predictions that go beyond its basic duality properties. These are tests whose comparison with experiment ultimately provide the scorecard of how successful this, or any other, model is. A hopeful feature of the model explored here is that it provides a simple calculation of the scaling exponents that are measured in transitions between Hall plateaux and between plateaux and the Hall insulator (see §2 for details), that agrees with

observations. Yet the most important message is probably not whether this model succeeds or fails; rather what is important is that there is now a good class of AdS/CFT models having duality properties that closely resemble those of real quantum Hall systems. Hopefully the fishing will be good.

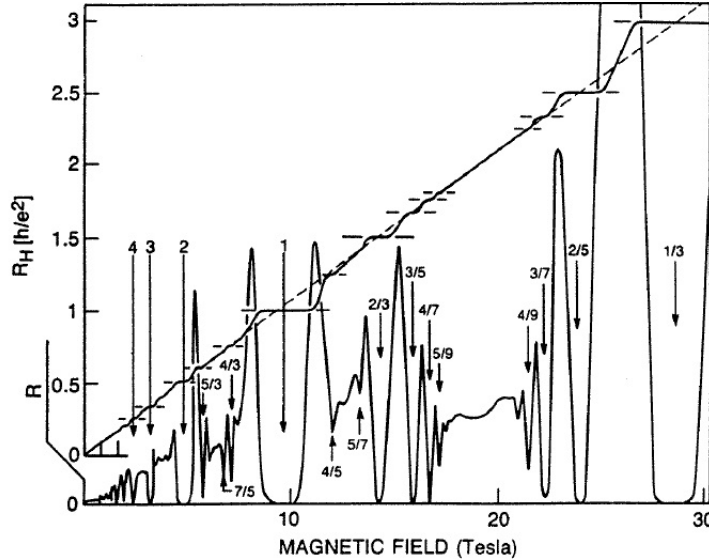


Figure 4.1. Experimental traces of the Hall and ohmic resistances for a quantum Hall system, reproduced from ref. [14].

4.2 Quantum Hall systems

This section has a two-fold purpose. First, it is meant to summarize briefly the experimental evidence for duality in quantum Hall systems, since this motivates using duality to guide the search for theoretical descriptions. This is followed by a description of the low-energy effective theory, including a discussion of the ‘composite boson’ model that allows some intuition for the potential origin of the underlying duality transformations, and are the precursors for the effective theories described in the remainder of the paper.

4.2.1 Evidence for duality

Quantum Hall systems are remarkable in a number of ways, not least of which is the very existence, stability and precision of the various plateaux — see Fig. 4.1 — for which the ohmic DC conductivity, σ_{xx} , vanishes¹ and the DC Hall conductivity, σ_{xy} , is quantized (in units of e^2/h , or $e^2/2\pi$ when

¹Notice that the vanishing of the conductivity, σ_{xx} , also ensures the same for the resistivity, ρ_{xx} , when the Hall conductivity is nonzero, $\sigma_{xy} \neq 0$.

$\hbar = 1$). The quantized value for σ_{xy} at a plateau is always consistent with a fraction, p/q , and (with a very few exceptions, to do with other kinds of physics) q is odd.

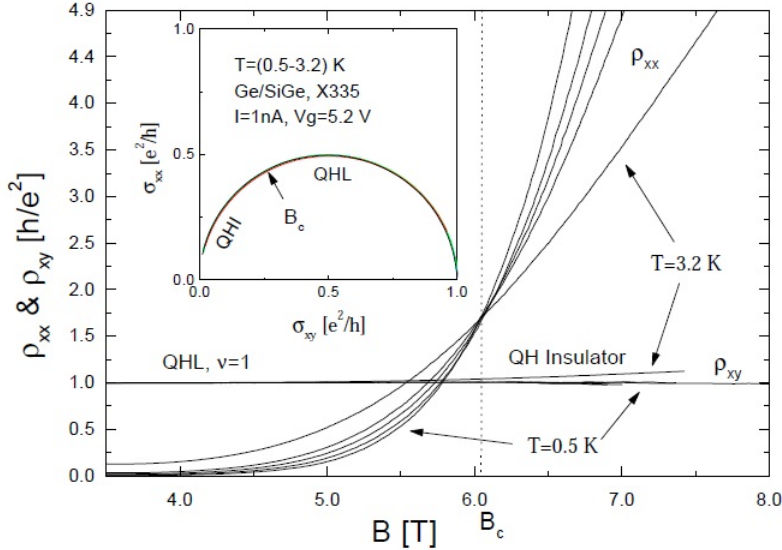


Figure 4.2. Evidence for the semi-circle law in the trace of the conductivities during a transition between two plateaux, reproduced from ref. [15].

Some relevant experiments

The evidence for duality lies in the nature of the transitions that are observed to occur between these plateaux as B is changed, as well as in the details of how they are approached at low temperatures. For example:

Selection Rule: As Fig. 4.1 shows, for clean samples a large number of plateaux can be accessed with changing magnetic field, but there is a pattern to the plateaux that are found adjacent to one another. Whenever two plateaux, labeled by the fractions p/q and r/s are clearly adjacent, they satisfy $|ps - qr| = 1$. There are only two exceptions to this rule in Fig. 4.1 — $\frac{5}{3} \rightarrow \frac{7}{5}$ and $\frac{4}{5} \rightarrow \frac{5}{7}$ — but in both cases these two plateaux are not cleanly adjacent to one another.

Semi-circle Law: The precise shape of the resistance curves between two well-defined adjacent plateaux becomes striking once it is drawn as a curve in the $\sigma_{xx} - \sigma_{xy}$ plane. A sample experimental trace of this appears in the inset of Fig. 4.2, which shows that the trajectory sweeps out a precise semi-circle, with centre midway between the two plateaux.

Critical points: The remainder of Fig. 4.2 shows the dependence of the resistivities on magnetic field, for several choices of temperature. These show that at fixed B , the resistivity ρ_{xx} (and so

also, for nonzero B , σ_{xx}) fall to zero with decreasing temperature near a plateau. But for very large magnetic fields, eventually the ohmic resistivity *grows* as the temperature falls, defining a regime called the *quantum Hall insulator* [16]. The crossover between these two regimes defines a critical magnetic field, B_c , for which ρ_{xx} is temperature-independent (also visible in Fig. 4.2). The value, $\rho_{*xx} = \rho_{xx}(B_c)$, of the resistivity at the critical field appears to be universal inasmuch as it is largely sample-independent. For the transition from the $\sigma_{xy} = 1$ state to the Hall insulator the critical resistivity takes on a value consistent with $\rho_{*xx} = h/e^2$ — see Fig. 4.3. (As both Figs. 4.2 and 4.3 show, the universality of this critical value is not completely clear in all experiments. The interpretation of this is examined more carefully in [17], where it is found that this implication of duality symmetries can be more sensitive to perturbations (like Landau-level mixing) than are some of the others (like the semicircle law).)

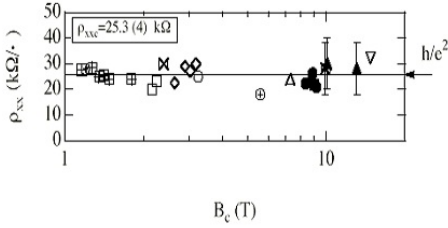


Figure 4.3. Evidence for universality of critical resistivity, $\rho_{*xx} = \rho_{xx}(B_c)$, from ref. [18].

below which deviations from a power are seen [22]. In particular, if the ohmic resistivity is compared at equidistant points on opposite sides of the critical magnetic field, with distance measured by filling fraction, ν , then eq. (4.2) implies

$$\rho_{xx}(\nu_c - \Delta\nu) = \frac{\rho_{*xx}^2}{\rho_{xx}(\nu_c + \Delta\nu)}. \quad (4.4)$$

More remarkably, this duality also appears to hold beyond the linear-response regime. This is shown in Fig. 4.4, whose left panel plots the entire current-voltage relation for the corresponding points on either side of the critical point. Curves equidistant from the critical point (measured using filling fraction) are mirror images of one another, reflected through the line $V = I$. This is shown in the right panel, in which the upper curves are reflected and superimposed on the lower curves. This reflection invariance implies the relation $\rho_{xx} \rightarrow 1/\rho_{xx}$ when restricted to the slope of the approximately straight lines near zero voltage, which is the linear-response regime. But the Figure shows it also applies in the regime for which $I(V)$ is noticeably curved. The full nonlinear reflection symmetry is equivalent to the condition $\rho_{xx}(V) \rightarrow 1/\rho_{xx}(V)$, where $\rho_{xx}(V) := dI/dV$ is

Duality: The dependence on temperature and magnetic field of ρ_{xx} in a transition from a plateau to the Hall insulator is measured to be consistent with

$$\rho_{xx} = \rho_{*xx} \exp \left[-\frac{(\nu - \nu_c)}{\nu_0(T)} \right], \quad (4.2)$$

where

$$\nu := \left| \frac{\rho}{B} \right| \quad (4.3)$$

is the filling fraction and ν_c is the filling fraction at the critical field. The phenomenological function $\nu_0(T)$ is consistent with a power law down to very small temperatures,

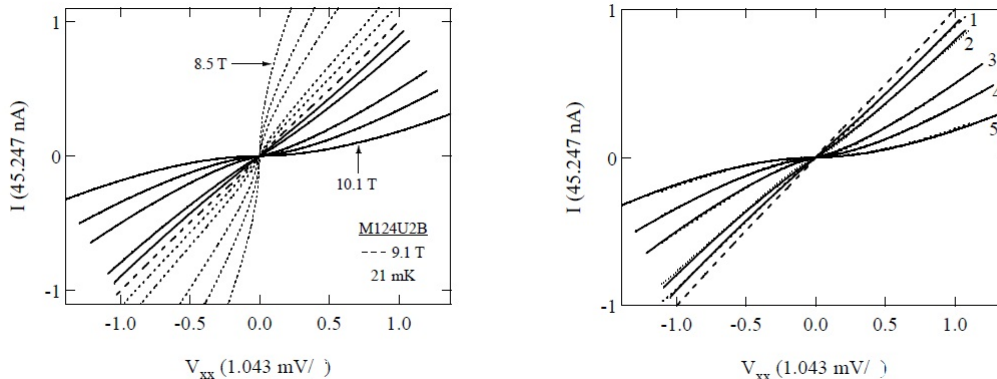


Figure 4.4. Evidence for the duality, $\rho_{xx} \rightarrow 1/\rho_{xx}$, for resistivities equally spaced (in units of filling fraction, $\Delta\nu$) from the critical field, reproduced from ref. [19].

the nonlinear, potential-dependent, resistivity.

Super-universality: Historically, the first evidence for duality came from the study of scaling behaviour as the temperature is lowered for magnetic fields chosen to lie at the transition between two plateaux (for a review, see *e.g.* [20]). The scaling occurs in the slope of the inter-plateau step in the Hall resistivity, which diverges in the zero-temperature limit. The width, ΔB , of the region of nonzero ohmic resistivity between the two plateaux also scales, in that it vanishes like a power of temperature:

$$\frac{d\rho_{xy}}{dB} \propto T^{-\alpha} \quad \text{and} \quad \Delta B \propto T^{\beta}. \quad (4.5)$$

Remarkably, measurements not only show $\alpha = \beta = 0.42 \pm 0.04$ for the transition between two specific plateaux; they also show that the values of α and β are the same for the transitions between different pairs of plateaux [21]. This equivalence of scaling exponents for different transitions is called ‘super-universality’, and is seen in Fig. 4.5. A nontrivial check on the AdS/CFT picture described below is its ability to account for this kind of scaling and these observed values for α and β .

Connection to duality

What is not yet clear is why these striking observational features are evidence for duality.

Historically, early indications for duality in interacting systems [23] combined with the observed equivalence of scaling behaviour at the transitions between different critical points, together with the shape (in the conductivity plane) of the flow to low temperature to motivate the guess that a duality group might be relevant to quantum Hall systems. Early observations about duality [23] in field theory, and the similarity between the phase structure seen in the temperature flows and properties of $SL(2, Z)$ led the authors of ref. [24] to propose the existence of a group of symmetries

acting on the complex conductivity $\sigma = \sigma_{xy} + i\sigma_{xx}$ (in units of e^2/h) according to

$$\sigma \rightarrow \frac{a\sigma + b}{c\sigma + d}, \quad (4.6)$$

where the integers a through d satisfy the constraint $ad - bc = 1$. It was subsequently noticed [25, 26] that odd-denominator plateaux are singled out as endpoints to the temperature flow if the group is restricted to the subgroup $\Gamma_0(2)$ defined by the condition that the integer c must be even,² leading to predictions for the universal values for the conductivities, like ρ_{*xx} , at the critical points.

Similar conclusions were reached at much the same time in the condensed-matter community [27], where more detailed thinking about the microscopic dynamics led to the Law of Corresponding States, whose action on filling fractions implies an action on conductivities of the $\Gamma_0(2)$ form. Once restricted to zero temperature these can be regarded as a set of transformations relating the ground state wavefunctions for the various quantum Hall plateaux, as was implicit in the work of Jain and collaborators [28]. Although the concrete connection of the experiments to what the electrons are doing was a step forward, a downside was the necessity to resort to mean-field reasoning (see however [29]).

The precise relation between the above observations and a duality group came with the observation that *all* of the above experiments — including the semi-circle law [30], universal critical points for transitions between general plateaux [31]³ and the validity of $\rho_{xx} \rightarrow 1/\rho_{xx}$ duality, even beyond linear response [33] — follow as exact consequences of particle-hole invariance together with the assumption that the $\Gamma_0(2)$ action commutes with the RG flow of the conductivities in the low-energy theory. (Fig. 4.6 illustrates what it means for the action of the group to commute with the RG flow, and Fig. 4.7 shows a pattern of flow lines that is consistent with commuting with the duality group $\Gamma_0(2)$.)

Furthermore, there are good reasons to believe that such duality transformations, acting on the conductivities as in eq. (4.6), should actually arise in low-energy systems in two spatial dimensions. This was first argued [6] as a general consequence of the similar kinematics of weakly interacting pseudo-particles and vortices, in a picture (like the ‘composite boson’ framework, described below) where these were the dominant charge carriers in the low-energy effective theory.⁴ In this language

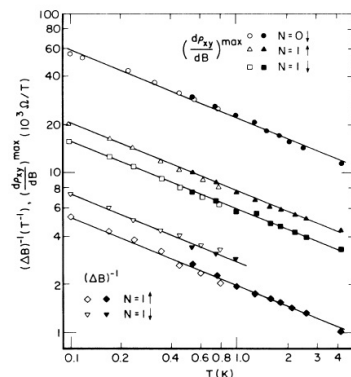


Figure 4.5. Evidence for the super-universality – the sharing of scaling exponents for transitions between different plateaux, reproduced from ref. [21].

²In terms of the generators S and T of $SL(2, Z)$, defined below, $\Gamma_0(2)$ can be regarded as that subgroup generated by ST^2S and T .

³Spin effects can also modify the precise position of the critical points [17, 32].

⁴Because this argument only relies on using duality to relate the conductivity produced by a vortex with that produced by a quasi-particle — as opposed to trying to explicitly compute either result separately, as done in [27] — it can apply equally well at zero- and finite-temperature and so side-steps the objection of [8] based on the subtleties

the two independent generators of $\Gamma_0(2)$ turn out to be particle-vortex duality [35], and the freedom to add 2π statistics flux to any quasi-particles.

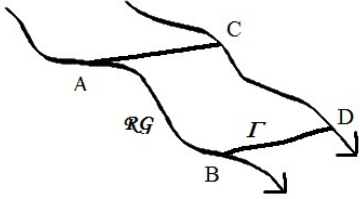


Figure 4.6. The relation between RG flow and the action of the duality group, in the conductivity plane. If A flows to B, and D is B’s image under the group Γ , then the RG flow must take C to D if C is A’s image under Γ .

Similar arguments showed that it would be a slightly different subgroup of $SL(2, Z)$ — the subgroup⁵ $\Gamma_\theta(2)$ — that would be relevant to quantum Hall systems built from microscopic bosons rather than fermions [6]. Because this group differs in detail from $\Gamma_0(2)$, it leads to the prediction of a suite of experimental results for bosonic quantum Hall systems that are similar to those described above (such as by including a semi-circle law), but which differ in detail (such as by predicting different plateaux)⁶ [6]. In particular, the bosonic subgroup $\Gamma_\theta(2)$ contains the weak-strong duality transformation, $\sigma \rightarrow -1/\sigma$, that is not present for the observed quantum Hall systems, but which was observed early on to be a symmetry of scalar electrodynamics in 2+1 dimensions [36].

It has since been argued [7] that eq. (4.6) should emerge on very general grounds for *any* 2+1 dimensional CFT having a conserved $U(1)$ symmetry, making its emergence at low energies essentially automatic for any system having such a CFT governing its far-infrared behaviour. In particular, ref. [7] shows that it is the full $SL(2, Z)$ group that generically emerges in this way for theories

of the ordering of the $T \rightarrow 0$ and $\omega \rightarrow 0$ limits.

⁵This subgroup is generated by the elements S and T^2 of $SL(2, Z)$.

⁶ $\Gamma_\theta(2)$ can also have implications for quantum Hall effects in more complicated systems, like graphene, where there is more than one species of conduction electron [34].

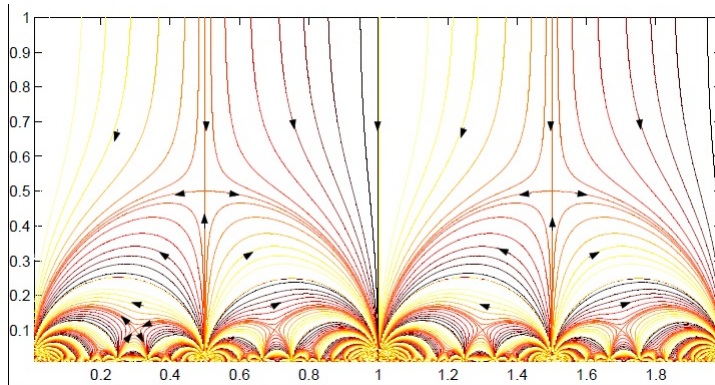


Figure 4.7. A plot of some of the flow lines (for decreasing temperature) for the conductivities that are dictated by $\Gamma_0(2)$ invariance. The vertical axis represents σ^{xx} and the horizontal axis is σ^{xy} (in units of e^2/h). Flows are attracted to odd-denominator fractions at zero temperature, with bifurcations between different domains of attraction at specific magnetic fields. Notice that the semicircles that describe flow at constant magnetic field at the bifurcation between two basins of attraction are also lines along which the system moves when magnetic fields are varied at vanishingly small temperatures (colour online).

defined in geometries that admit a spin structure, while only the subgroup $\Gamma_\theta(2)$ emerges if a spin structure is absent.

4.2.2 The low-energy picture

The overall picture that emerges from the convergence of theory and experiments for quantum Hall systems is as follows. In two spatial dimensions the huge degeneracy of Landau levels in a magnetic field leads to ground states that can be very sensitive to electron interactions, allowing the possibility of the strongly correlated Laughlin ground states describing the various quantum Hall plateaux. Transport properties near these plateaux at the low temperatures relevant to the conductivity measurements is governed by a low-energy effective theory obtained by integrating out the short-distance electron modes.

Far infrared: Integer quantum Hall systems

In the very far infrared the effective zero-temperature theory obtained by integrating out all of the high-energy excitations is a function of the electromagnetic probe field, A_μ , used to explore the electromagnetic transport:

$$\Gamma_{\text{IR}} = -\frac{k}{2\pi} e^2 \int_X d^3x \epsilon^{\mu\nu\lambda} A_\mu \partial_\nu A_\lambda, \quad (4.7)$$

where the electron charge, e , is temporarily restored, and X denotes the region containing the quantum Hall fluid. Topological considerations [7] imply the coefficient k is in general quantized to be an integer.⁷ The current arising from the probe field A_μ inferred from eq. (4.7) is

$$J^\mu = \frac{\delta\Gamma_{\text{IR}}}{\delta A_\mu} = -\frac{ke^2}{2\pi} \epsilon^{\mu\nu\lambda} F_{\nu\lambda}, \quad (4.8)$$

which when evaluated with only $E_x = F_{tx}$ nonzero and compared with $J_i = \sigma_{ij} E_j$ implies the conductivities

$$\sigma_{xx} = 0 \quad \text{and} \quad \sigma_{xy} = -\sigma_{yx} = k, \quad (4.9)$$

in units of $e^2/h = e^2/2\pi$ (using $\hbar = 1$). Thus is captured the integer quantum Hall plateaux.

A potential puzzle about the low-energy action Γ_{IR} is that it is not gauge invariant when X has a boundary, as real quantum Hall systems do. In this case the failure of gauge invariance in eq. (4.7) is canceled by a related failure coming from degrees of freedom that live exclusively on the boundary, ∂X . These degrees of freedom are the ones that actually transport the charge in the low-energy theory, which moves along the boundaries of the quantum Hall domains. Because these are restricted to the boundaries they are described by a chiral 1+1 dimensional CFT, whose $U(1)$

⁷Given a spin structure k could be half-integer, however we take the case of no spin structure because for the quantum Hall experiments of most interest the Zeeman splitting is larger than the Landau level spacing. See however [5] for a review of more complicated cases where electron spins can be important, and [17, 37] for preliminary discussions of how duality arguments change in this case.

anomaly provides the required cancelation.

Far infrared: fractional quantum Hall systems

Another puzzle about eq. (4.7) is that the quantization of k seems to preclude on general grounds the possibility of having fractional quantum Hall plateaux. A resolution to this puzzle is suggested by the ‘composite boson’ picture of quantum Hall systems, as is now described [38].⁸

The composite boson model starts with the observation that statistics is a supple concept in 2+1 dimensions where fractional statistics are allowed, and in particular can be explicitly implemented through the artifice of having particles carry with them flux tubes of a fictitious electromagnetic field, a_μ [41]. Specifically, if $S[\psi, A]$ is the action for point particles, ψ , having charge e coupled to an electromagnetic field, A_μ , then the deformation

$$S_\vartheta[\psi, A, a] := S[\psi, A + a] - \frac{e^2}{2\vartheta} \int d^3x \epsilon^{\mu\nu\lambda} a_\mu \partial_\nu a_\lambda, \quad (4.10)$$

describes the same theory where the statistics of the ψ particles is shifted by the angle ϑ . For instance, if a two-particle state described by the action $S[\psi, A]$ originally acquired a phase η when the two particles are interchanged, then when described by $S_\vartheta[\psi, A, a]$ they instead acquire the phase $\eta e^{i\vartheta}$ on interchange. They do so because the gaussian integral over a_μ produces a saddle point that sets its magnetic field, $b = \partial_x a_y - \partial_y a_x$, proportional to the charge density, and so which is nonzero where the particles are but vanishes where they are not. For point particles this is equivalent to attaching a flux quantum to each particle, and it is the Aharonov-Bohm phase of this flux that produces the change in statistics.

With this in mind, the electrodynamics of 2+1 dimensional fermions can instead be regarded as that of bosons coupled to a statistics field with angle

$$\vartheta = (2n + 1)\pi. \quad (4.11)$$

In this picture the quantum Hall plateaux with fractions $1/(2n + 1)$ can be qualitatively understood using the following mean-field picture. For a macroscopic number of bosons, the accumulated statistical flux can be thought of as a constant background field, b . But because the charge carriers couple only to the sum $A_\mu + a_\mu$, special things can happen when the real magnetic field cancels this background statistics field. For these special values where $B + b = 0$ the bosons see no net field, and so are free to Bose-Einstein condense — producing a superconducting phase. This condensation is how the strongly correlated fractional quantum Hall state is understood in this picture. Due to the choice, eq. (4.11), the cancelation happens when the filling fraction is $\nu = 1/(2n + 1)$, corresponding to the principle series of fractional states described by the Laughlin wave-function.

⁸The related ‘composite fermion’ model [39] is widely used in theoretical studies of quantum Hall systems, and has also been discussed within an AdS/CFT framework [40].

In this picture there is also a qualitative understanding of the stability of these plateaux to small changes of B . The ‘superconductor’ then sees a net magnetic field, but the idea is that the superconductor is a Type II superconductor for which this field penetrates as a vortex without destroying the condensation. These vortices have fractional statistics, and correspond to the quasi-particles of the Laughlin fluid. The plateau ends for fields, B , large enough that there are so many vortices that the superconductivity is ruined. The picture then is that the vortices themselves condense, producing a quantum Hall state, p/q with $p \neq 1$. This process continues generating the many plateaux observed in a hierarchical way [28]. Although the mean-field arguments are suspect, this is a conceptually attractive framework for understanding quantum Hall dynamics, for which notions of particle-vortex duality are likely to be useful [6].

Coming back to the far-infrared effective action, the above picture suggests that eq. (4.7) should be generalized to

$$\exp\{i\Gamma_{\text{IR}}[A]\} := \int \mathcal{D}a_\mu \exp\left\{-\frac{ke^2}{2\pi} \int_X d^3x \epsilon^{\mu\nu\lambda} (A_\mu + a_\mu) \partial_\nu (A_\lambda + a_\lambda) - \frac{e^2}{2\vartheta} \int d^3x \epsilon^{\mu\nu\lambda} a_\mu \partial_\nu a_\lambda\right\}. \quad (4.12)$$

If the first term is the result that would be obtained, as above, from a system of electrons, then electrons could also give eq. (4.12) for $\vartheta = 2n\pi$, since any shift of statistics by an integer multiple of 2π has no effect. Integrating out a_μ , leads to the Hall conductivity

$$\sigma_{xy} = \frac{k}{2nk + 1}, \quad (4.13)$$

which is a fraction (in units of $e^2/h = e^2/2\pi$), though always with an odd denominator.

For future reference, notice that a quantum Hall system built from bosons would instead correspond to the choice $\vartheta = (2n + 1)\pi$, leading to

$$\sigma_{xy}(\text{bosons}) = \frac{k}{(2n + 1)k + 1}. \quad (4.14)$$

In units of $e^2/h = e^2/2\pi$ this is a fraction p/q , with q odd if p is even, and vice versa. Note in particular that if all else is equal, then shifting statistics angle by $\vartheta \rightarrow \vartheta + \pi$ shifts the complex conductivity by⁹

$$\frac{1}{\sigma} \rightarrow \frac{1}{\sigma} + 1. \quad (4.15)$$

Not quite so deep in the infrared

The interest in this paper is in the approach to the quantum Hall plateaux for small temperatures, rather than in the ground states themselves, and so the goal is to obtain an effective low-energy

⁹In terms of the generators $S(\sigma) = -1/\sigma$ and $T(\sigma) = \sigma + 1$, this corresponds to $\sigma \rightarrow ST^{-1}S(\sigma)$.

description that is not quite so far in the infrared as the Chern-Simons action just described. It is for this effective theory that any emergent duality group should be found if it is to be relevant for the experiments that probe the approach to, and transitions between, different quantum Hall plateaux.

The observational evidence is that this regime is described by some system with a $\Gamma_0(2)$ duality group that commutes with its RG flow, but real progress in constructing candidate effective field theories has been blocked by the lack of examples of strongly correlated systems explicitly displaying the emergent duality. Once such a model is in hand its implications that go beyond implications of duality can be tested, to see if it describes the experimental systems.

The remainder of this paper identifies a first candidate using recently developed tools from the AdS/CFT correspondence. As discussed in the introduction, for the present purposes, the great virtue of this correspondence is twofold: it provides a calculable laboratory of strongly interacting 2+1 dimensional systems; and it naturally produces systems having emergent duality groups.

4.3 Holographic Duality

AdS/CFT formulations of 2+1 dimensional CFTs involve electromagnetic gauge fields in 3+1 dimensional asymptotically AdS backgrounds. Particle-vortex interchange in the CFT corresponds to the interchange of electric and magnetic fields on the AdS side, so part of the ease of having an emergent duality in the CFT is the propensity on the AdS side for the electromagnetic theory to be invariant under electric-magnetic interchange. Since this transformation takes the electromagnetic coupling from weak to strong (and vice versa), on the AdS side it is useful to have a scalar field, ϕ , whose value tracks the size of this coupling.

Another generator is needed to obtain a group like $SL(2, Z)$ — or one of the level-two subgroups, like $\Gamma_0(2)$ or $\Gamma_\theta(2)$ — and given the above discussion it is natural to seek this as the freedom to change particle statistics by 2π . Since particle statistics are described by a Chern-Simons term in the CFT, on the AdS side it is natural to seek a symmetry that shifts the coefficient of $F \wedge F$. For this reason it is also useful to have a scalar field, χ , whose value tracks this interaction.

The minimal set of fields to follow in the AdS formulation should then be gravity, the electromagnetic field plus the two scalars: the dilaton, ϕ , and axion, χ . These fields naturally appear in the low-energy limit of string theory, so the kinds of theories entertained here are likely to arise generically in more explicit string constructions. (In this paper we take a phenomenological point of view, and do not try to embed the 3+1 dimensional field theory into an explicit stringy framework. Although this would be instructive, most of the additional bells and whistles live at very high energies and so are likely to decouple from the low-energy limit that is always of interest for the applications we have in mind.)

The holographic interpretation of black holes with this field content has recently been worked out [10, 11]. Although these models cannot themselves directly provide descriptions of quantum Hall

systems, since for nonzero magnetic fields their DC ohmic conductivity vanishes at finite temperature, they are interesting in their own right. This section briefly recaps some of their features, with the goal of describing the duality transformations of interest for the model of real interest in the next section.

4.3.1 Maxwell and the axio-dilaton

The starting point is the Einstein-Maxwell action coupled to the axio-dilaton in 3+1 dimensions:¹⁰

$$S = - \int d^4x \sqrt{-g} \left\{ \frac{1}{2\kappa^2} \left[R - 2\Lambda + \frac{1}{2} (\partial_\mu \phi \partial^\mu \phi + e^{2\phi} \partial_\mu \chi \partial^\mu \chi) \right] + \frac{1}{4} e^{-\phi} F_{\mu\nu} F^{\mu\nu} + \frac{1}{4} \chi F_{\mu\nu} \tilde{F}^{\mu\nu} \right\}, \quad (4.16)$$

where $\tilde{F}_{\mu\nu} := \frac{1}{2} \epsilon_{\mu\nu\lambda\rho} F^{\lambda\rho}$, and $\epsilon_{\mu\nu\lambda\rho}$ has a factor of $\sqrt{-g}$ extracted so that it transforms as a tensor (rather than a tensor density). The constant $\Lambda = 3/L^2$ is the AdS cosmological constant and $\kappa^2 = 8\pi G$ is Newton's constant, so weak curvature requires $\kappa^2/L^2 \ll 1$. Similarly, the Maxwell coupling is $g^2 \propto e^\phi$ so weak coupling corresponds to $e^\phi \ll 1$.

4.3.2 Duality relations

The couplings of this action are chosen to ensure the existence of a duality group, and at the classical level there is an embarrassment of riches since the equations of motion are invariant under the group $SL(2, R)$. To see the action of this group define the axio-dilaton by

$$\tau := \chi + ie^{-\phi}, \quad (4.17)$$

for which weak coupling corresponds to large $\text{Im } \tau$. Then the χ and ϕ kinetic terms become

$$\partial_\mu \phi \partial^\mu \phi + e^{2\phi} \partial_\mu \chi \partial^\mu \chi = \frac{\partial_\mu \tau \partial^\mu \bar{\tau}}{(\text{Im } \tau)^2}, \quad (4.18)$$

which is invariant under the transformations

$$\tau \rightarrow \frac{a\tau + b}{c\tau + d} \quad \text{and} \quad g_{\mu\nu} \rightarrow g_{\mu\nu}, \quad (4.19)$$

where a, b, c and d are arbitrary real numbers that satisfy the $SL(2, R)$ condition $ad - bc = 1$.

To define the action on the Maxwell field, following [44] define

$$G^{\mu\nu} := -\frac{2}{\sqrt{-g}} \left(\frac{\delta S}{\delta F_{\mu\nu}} \right) = e^{-\phi} F^{\mu\nu} + \chi \tilde{F}^{\mu\nu}, \quad (4.20)$$

¹⁰We use a 'mostly plus' metric signature and Weinberg's curvature conventions [42], which differ from those of MTW [43] only by an overall sign in the Riemann tensor.

which takes the simple form

$$\mathcal{G}^{\mu\nu} = \bar{\tau} \mathcal{F}^{\mu\nu}, \quad (4.21)$$

when written in terms of the complex quantities

$$\mathcal{F}_{\mu\nu} := F_{\mu\nu} - i\tilde{F}_{\mu\nu} \quad \text{and} \quad \mathcal{G}_{\mu\nu} := -\tilde{G}_{\mu\nu} - iG_{\mu\nu}. \quad (4.22)$$

Eq. (4.21) is invariant under the transformation, eq. (4.19), provided the Maxwell field transforms as

$$\begin{pmatrix} \mathcal{G}_{\mu\nu} \\ \mathcal{F}_{\mu\nu} \end{pmatrix} \rightarrow \begin{pmatrix} a & b \\ c & d \end{pmatrix} \begin{pmatrix} \mathcal{G}_{\mu\nu} \\ \mathcal{F}_{\mu\nu} \end{pmatrix}, \quad (4.23)$$

Since the Maxwell equations and the Bianchi identity are

$$\nabla_{\mu} \text{Im} \mathcal{G}^{\mu\nu} = \nabla_{\mu} \text{Im} \mathcal{F}^{\mu\nu} = 0, \quad (4.24)$$

these are also invariant under $SL(2, R)$. The Maxwell contribution to the axio-dilaton equation is similarly invariant [44].

4.3.3 From $SL(2, R)$ to $SL(2, Z)$

Although $SL(2, R)$ is a larger group than bargained for, in string theory it is generically only an artefact of the classical approximation, and is broken down to a discrete subgroup by quantum effects. Since the quantum plateaux ultimately prove to be in a strongly coupled part of parameter space (over which the unbroken discrete symmetries ultimately give calculational access – see below), their properties are strongly affected by the breaking.

The low energy supergravity of Type IIB string theory has an action in 10 dimensions that is similar to the one described above, whose equations of motion are $SL(2, R)$ invariant. In this case the symmetry is broken by the presence of objects whose charges are quantized. For example, a (m, n) -string (*i.e.* a bound state of a fundamental F-string with charge m with a D-string with charge n)¹¹ has tension,

$$\tau_{m,n} = e^{\phi} (m + \chi n)^2 + e^{-\phi} n^2. \quad (4.25)$$

Under $SL(2, Z)$ transformations, the (m, n) -string transforms into a (m', n') -string, where

$$m' = dm + cn, \quad n' = bm + an. \quad (4.26)$$

Because m and n are quantized $SL(2, R)$ is broken to $SL(2, Z)$.

For holographic applications similar considerations are very likely to apply. In particular, probing the CFT at finite temperature and density require studying the AdS theory in the presence of a

¹¹We use (m, n) rather than the more traditional (p, q) to avoid notational conflict with our later use of p and q .

charged (dilaton) black hole. This becomes a dyonic black hole — with both electric and magnetic charges, Q_e and Q_m — if the CFT is probed in an external magnetic field. Although these black holes are usually studied in the classical limit, in principle the AdS/CFT duality is exact and so quantum effects can also be studied. In particular, the Dirac quantization conditions for magnetic monopoles should apply, requiring the electric and magnetic charges to be quantized relative to one another. In microscopic brane constructions, dyonic objects in the bulk can be identified as charged solitons in the boundary CFT [45].

It then suffices that there should be a minimum electric charge to learn that magnetic and electric charges must be quantized in terms of this minimum charge. As we see below, such a quantization on the AdS side naturally leads to a quantization of the Hall conductivities on the CFT side: $\sigma_{xy} \sim Q_e/Q_m \sim p/q$, for integer p and q . The precise pattern of fractions that is allowed depends on the precise discrete subgroup — possibly $SL(2, Z)$, $\Gamma_0(2)$ or $\Gamma_\theta(2)$ — of $SL(2, R)$ that is left unbroken by the full string dynamics. Since several specific stringy ultraviolet completions are likely to exist for the given low-energy action, eq. (4.16), and since different systems give rise to different discrete symmetries [46], in the phenomenological approach followed here we imagine ourselves to be free to choose this unbroken discrete symmetry.

4.3.4 Conductivities

To compute the ohmic and Hall conductivities as functions of temperature, charge density and magnetic field requires studying the response of the above AdS system to small electromagnetic perturbations about a dyonic axio-dilaton black hole. This is explored in some detail in refs. [10, 11].

Action of $SL(2, R)$

In particular, these authors compute the action of the underlying $SL(2, R)$ symmetry on the conductivities, and show that they take the form of eq. (4.6). We reproduce a version of the argument here that generalizes easily to the case of later interest.

The starting point is the AdS/CFT translation table,¹² which gives the electromagnetic current, J^a , when the CFT is perturbed by an electromagnetic field, F_{ab} . On the AdS side the perturbation is obtained by solving the linearized Maxwell equation, and evaluating the action as a function of the perturbation on the boundary. Differentiating with respect to A_μ to get the current gives a simple form when expressed in terms of $G^{\mu\nu}$:

$$J^a = \sqrt{-g} G^{va} \Big|_0, \tag{4.27}$$

¹²There is generally a choice of CFT, depending on the precise form of the boundary conditions used in AdS [47, 48]. In the present instance ref. [7] argues that one of these choices can be regarded as equivalent to treating the gauge field on the boundary as dynamical, as would be done when coupling to a statistics field in 2+1 dimensions. Furthermore, such choices are implicitly made when comparing theories related by transformations involving S -duality, $\tau \rightarrow -1/\tau$. These complications do not play a direct role in what follows.

where v is another radial coordinate (*i.e.* a function of r) for which conformal infinity lies at $v = 0$ and the horizon is at $v = v_h$.

Focusing on the spatial components, J^x and J^y , and using the (real part of the) transformation rule eq. (4.23), then implies

$$\begin{pmatrix} \mathcal{J} \\ \mathcal{E} \end{pmatrix} \rightarrow \begin{pmatrix} a & b \\ c & d \end{pmatrix} \begin{pmatrix} \mathcal{J} \\ \mathcal{E} \end{pmatrix}, \quad (4.28)$$

where¹³

$$\mathcal{J} := \left[-\tilde{G}_{tx} + i\tilde{G}_{ty} \right]_0 = \left[-\sqrt{-g} \left(G^{vy} + iG^{vx} \right) \right]_0 = -i(J^x - iJ^y), \quad (4.29)$$

and

$$\mathcal{E} := [F_{tx} - iF_{ty}]_0 = E_x - iE_y. \quad (4.30)$$

But in linear response the conductivity tensor is defined¹⁴ to be $J^i = \sigma^{ij} E_j$, or equivalently (keeping in mind $\sigma^{yx} = -\sigma^{xy}$ and $\sigma^{xx} = \sigma^{yy}$ for rotationally invariant systems),

$$\begin{aligned} \mathcal{J} = -J^y - iJ^x &= -(\sigma^{yx} E_x + \sigma^{yy} E_y) - i(\sigma^{xx} E_x + \sigma^{xy} E_y) \\ &= -(\sigma^{yx} + i\sigma^{xx})(E_x - iE_y) = \sigma_- \mathcal{E}, \end{aligned} \quad (4.31)$$

where $\sigma_- := \sigma^{xy} - i\sigma^{xx}$. Consistency of this relation with the transformation, eq. (4.28), then implies

$$\sigma_- \rightarrow \frac{a\sigma_- + b}{c\sigma_- + d}. \quad (4.32)$$

Complex conjugation – we consider here only DC conductivities, whose imaginary parts vanish – then also implies the desired transformation, eq. (4.6), for $\sigma = \sigma_+ = \sigma^{xy} + i\sigma^{xx}$.

Classical conductivities

The authors of refs. [10, 11] also show that the low-temperature properties of the conductivities predicted by this theory are relatively simple. The strategy is first to compute explicitly in the case of a purely electric black brane with a vanishing axion field. The general result for dyonic branes with an axion is then found by performing an appropriate $SL(2, R)$ transformation.

The appropriate black brane geometries have the form

$$ds^2 = -\mathfrak{h}^2(r) dt^2 + \frac{dr^2}{\mathfrak{h}^2(r)} + \mathfrak{b}^2(r) (dx^2 + dy^2), \quad (4.33)$$

¹³Our convention is $\epsilon^{txy} = +1/\sqrt{-g}$, so is opposite to [11].

¹⁴From this point on we adopt consistent tensor conventions for the conductivity, which is naturally contravariant.

for which the Maxwell field equation $\nabla_\mu G^{\mu\nu} = 0$ has solution

$$G^{rt} = -\frac{Q_e}{b^2(r)}, \quad (4.34)$$

and so using the constitutive relation, $G^{\mu\nu} = e^{-\phi}F^{\mu\nu} + \chi\tilde{F}^{\mu\nu}$, then gives (with $F_{xy} = Q_m$)

$$F = (Q_e - \chi Q_m)\frac{e^\phi}{b^2} dr \wedge dt + Q_m dx \wedge dy. \quad (4.35)$$

Given the $SL(2, R)$ transformation rules for the Maxwell field, these expressions imply an action of $SL(2, R)$ on the charges Q_e and Q_m . Our strategy is to start with an electric dilaton brane with unit electric charge, zero magnetic charge, $\phi = \hat{\phi}_0$ and $\chi = 0$. $\hat{\phi}_0$ is then chosen so that this configuration is mapped into a more general configuration with Q_e , Q_m , $\phi = \phi_0$ and $\chi = \chi_0$.

The behaviour of the purely electric brane with no axion is simple because at low temperatures and frequencies it is governed by the near-horizon limit of the near-extremal geometry, which is [49]

$$ds^2 \approx -\frac{r^2}{l^2} \left[1 - \left(\frac{r_h}{r}\right)^{2\zeta+1} \right] dt^2 + \frac{l^2 dr^2}{r^2[1 - (r_h/r)^{2\zeta+1}]} + r^{2\zeta} (dx^2 + dy^2). \quad (4.36)$$

This benefits from an attractor mechanism [50, 51] that makes the near-horizon geometry independent of the boundary data for the scalar fields at infinity. This implies that the constants l and ζ are determined by the field equations, leaving the position of the horizon, r_h , as the only important scale. The same geometry also describes the near-horizon limit when the dilaton-Maxwell action is replaced by the dilaton-DBI action discussed below (as is shown in Appendix D).

In particular, the prediction $\zeta = \frac{1}{5}$ [10, 11] — which comes from solving the field equations for the $SL(2, R)$ -invariant action given above, eq. (4.16) — is likely to be significant because the geometry of eq. (4.36) is Lifshitz-like, with different scaling assigned to time and space directions. This is true even though the asymptotic geometry near infinity is relativistic, due to the presence of the dilaton. The dynamical exponent predicted at low temperatures in this case is $z = 1/\zeta = 5$ (though the asymptotic value, $z = 1$, would apply in the UV). To the extent that this metric also describes the near-horizon limit of the background geometry in DBI-based model discussed below, we shall see in §5 that this value for z gives scaling exponents at very low temperature that agree with observations.

The dilaton also varies logarithmically with r in the purely electric solution, $e^\phi \propto r^{4\zeta}$, which vanishes on the horizon in the extremal case ($r_h \rightarrow 0$). For magnetic branes ($Q_e = 0$ and $Q_m \neq 0$) the dilaton is instead driven to the strong-coupling regime at the horizon in the extremal case. Control is nonetheless maintained in refs. [10, 11] by taking T to be nonzero but small, so the brane is not quite extremal. Then an asymptotic value for the dilaton at conformal infinity can be chosen to ensure that the coupling remains weak enough right down to $r = r_h \neq 0$. This tendency to strong coupling at low enough temperatures (for fixed dilaton) is an important feature of these dual

systems, that in later sections also limits our ability to compute conductivities directly near quantum Hall plateaux using semiclassical methods. (It is recourse to the unbroken discrete symmetries, like $SL(2, Z)$, that ultimately allow progress nonetheless.)

The explicit form obtained in this way for the AC conductivities in the limit $\omega \ll T \ll \mu$ (where μ is the chemical potential required to maintain a charge density $\rho \sim Q_e$) is [11]

$$\sigma_{xy} = \frac{\rho}{B} \left[1 + \mathcal{O}(\omega^2) \right], \quad \text{and} \quad \sigma_{xx} = \mathcal{O}(\omega) . \quad (4.37)$$

In particular, there is no DC ohmic conductivity. This ultimately vanishes because the ohmic conductivity is infinite at zero B due to translation invariance [11]. Although $SL(2, R)$ is nicely realized by the RG flow, $d\tau/dr$, of the axio-dilaton [11], it cannot directly describe the temperature flow of DC conductivities in quantum Hall systems.¹⁵ For this reason we next explore a slightly more complicated system for which $SL(2, R)$ invariance coexists with nonzero DC conductance.

4.4 Quantum Hall-ography

In order to obtain DC conductivity in an $SL(2, R)$ invariant way, we follow ref. [13] and study the case of a probe brane, described by the DBI action, situated within the background geometry of an appropriately chosen black brane. As discussed in [13], the probe limit is crucial for obtaining DC ohmic resistance because the infinite bath represented by the black brane can provide the required dissipation. Ideally, one would prefer not to have to rely on the probe approximation to achieve DC resistance, such as by incorporating disorder or some other breaking of translation invariance. We regard our reliance on the probe approximation here to be a temporary crutch that will not survive more sophisticated modeling.

4.4.1 The setup

The action for the revised model has the following form

$$S = S_{\text{grav}} + S_{\text{gauge}} , \quad (4.38)$$

where the gravitational sector is the same as before,

$$S_{\text{grav}} = - \int d^4x \sqrt{-g} \left\{ \frac{1}{2\kappa^2} \left[R - 2\Lambda + \frac{1}{2} (\partial_\mu \phi \partial^\mu \phi + e^{2\phi} \partial_\mu \chi \partial^\mu \chi) \right] \right\} + S_{\text{Lifshitz}} , \quad (4.39)$$

with the possible addition of a ‘Lifshitz’ sector, whose purpose is to build in various features of the background geometry. For instance, in [13] this sector is imagined to involve various Kalb-Ramond

¹⁵Ref. [11] also models DC conductivity due to disorder by giving the frequency a small imaginary part.

fields, $H_{\mu\nu\lambda}$, whose presence is used to generate an uncharged black-brane geometry that asymptotically scales spatial and temporal directions differently. The resulting asymmetric exponent $z = 2$ was then chosen to achieve some strange-metal properties, like a resistivity linear in temperature.

Although not strictly necessary for quantum Hall plateaux, a similar construction can be used here to build in an arbitrary value of z . What proves to be a more attractive choice, however, is instead to choose the Lifshitz sector such that its background metric is that of a dyonic black brane, whose extremal near-horizon geometry is that discussed in §3, above, or its DBI generalization discussed in Appendix D. This is attractive because we shall see that agreement with some low-temperature experiments suggests $z \simeq 5$ in the IR, while other arguments¹⁶ instead indicate $z \simeq 1$ in the UV.) Potential sources for such a background are discussed below, after describing the gauge action, S_{gauge} .

For the present purposes the main change relative to §3 is the gauge action, which replaces the dilaton-Maxwell form of eq. (4.16) with the DBI form

$$\begin{aligned}
 S_{\text{gauge}} &= -\mathcal{T} \int d^4x \left[\sqrt{-\det(g_{\mu\nu} + \ell^2 e^{-\phi/2} F_{\mu\nu})} - \sqrt{-g} \right] - \frac{1}{4} \int d^4x \sqrt{-g} \chi F_{\mu\nu} \tilde{F}^{\mu\nu} \\
 &= -\mathcal{T} \int d^4x \sqrt{-g} \left[\sqrt{1 + \frac{\ell^4}{2} e^{-\phi} F_{\mu\nu} F^{\mu\nu} - \frac{\ell^8}{16} e^{-2\phi} (F_{\mu\nu} \tilde{F}^{\mu\nu})^2} - 1 \right] \\
 &\quad - \frac{1}{4} \int d^4x \sqrt{-g} \chi F_{\mu\nu} \tilde{F}^{\mu\nu}, \tag{4.40}
 \end{aligned}$$

where the second line holds in 3+1 dimensions.

Eq. (4.40) is the unique $SL(2, R)$ -invariant generalization of the DBI action [44], and has the same form as would the action of a D3-brane written in Einstein frame if the quantity ℓ were given by

$$\ell^2 = 2\pi\alpha', \tag{4.41}$$

with \mathcal{T} representing the brane tension. However, our approach here is phenomenological and nothing would change if this action were instead to emerge as the low-energy limit of some more complicated configuration involving other kinds of branes. Although we do not try to do so here, any full string embedding would require a precise statement of the position of the relevant branes in the extra dimensions, and of what stabilizes their motion (and gives mass to any other potentially light degrees of freedom). Presumably, the DBI action describes the dynamics of 2+1 D matter fields coupled with a strongly interacting CFT modeled by the background geometry. The matter fields are also coupled with the 3+1 D $U(1)$ gauge field on the probe brane. We imagine there to be a suitable large- N limit in play, allowing us to neglect quantum fluctuations of fields on the AdS side.

This kind of dilaton-DBI action could also be used for the Lifshitz sector in the case where the background geometry is taken to be the near-horizon, near-extremal form described in §3 and

¹⁶We thank E. Fradkin and S. Kivelson for pointing out the UV evidence for $z = 1$.

Appendix D. If so, it would require a different $U(1)$ gauge potential and a parametrically larger tension $\mathcal{T} \rightarrow \sim N\mathcal{T}$ to justify the use of the probe approximation for the brane that produces the conductivity. It seems (and probably is) redundant to have the additional Lifshitz sector to produce such a background, when the same geometry would also be produced if S_{gauge} were treated beyond the probe approximation. We only do so here since we require the probe approximation in order to obtain a nonzero DC ohmic resistivity, and regard this as a feature to be improved in future iterations.

4.4.2 Duality relations

The important property of the DBI action used above is that it shares the duality invariance [44] of the dilaton-Maxwell action described earlier. The main change relative to the earlier discussion is the form of the constitutive relation between $G^{\mu\nu}$ and $F_{\mu\nu}$, which in this case is

$$\begin{aligned} G^{\mu\nu} &= -\frac{2}{\sqrt{-g}} \left(\frac{\delta S}{\delta F_{\mu\nu}} \right) \\ &= \frac{\mathcal{T} \ell^4}{X} \left[e^{-\phi} F^{\mu\nu} - \frac{\ell^4}{4} e^{-2\phi} \left(F_{\mu\nu} \tilde{F}^{\mu\nu} \right) \tilde{F}^{\mu\nu} \right] + \chi \tilde{F}^{\mu\nu}, \end{aligned} \quad (4.42)$$

where

$$X := \sqrt{1 + \frac{\ell^4}{2} e^{-\phi} F_{\mu\nu} F^{\mu\nu} - \frac{\ell^8}{16} e^{-2\phi} \left(F_{\mu\nu} \tilde{F}^{\mu\nu} \right)^2}. \quad (4.43)$$

In terms of this quantity gauge field equations and Bianchi identities have the same form as before,

$$\nabla_\mu G^{\mu\nu} = \nabla_\mu \tilde{F}^{\mu\nu} = 0. \quad (4.44)$$

It can be shown [44] that these — and the other field equations and the constitutive relation, eq. (4.42) — are invariant under the same $SL(2, R)$ transformations of the dilaton-Maxwell theory, eqs. (4.19) and (4.23):

$$\tau \rightarrow \frac{a\tau + b}{c\tau + d} \quad \text{and} \quad \begin{pmatrix} \mathcal{G}_{\mu\nu} \\ \mathcal{F}_{\mu\nu} \end{pmatrix} \rightarrow \begin{pmatrix} a & b \\ c & d \end{pmatrix} \begin{pmatrix} \mathcal{G}_{\mu\nu} \\ \mathcal{F}_{\mu\nu} \end{pmatrix}, \quad (4.45)$$

with $g_{\mu\nu}$ fixed. As before $\mathcal{F}_{\mu\nu} = F_{\mu\nu} - i\tilde{F}_{\mu\nu}$ and $\mathcal{G}_{\mu\nu} = -\tilde{G}_{\mu\nu} - iG_{\mu\nu}$.

Because the symmetry acts in the same way on $G^{\mu\nu}$ as in the last section, the same conclusion is also true for the transformation laws for the current,

$$J^a = \sqrt{-g} G^{va} \Big|_0. \quad (4.46)$$

It immediately follows that the conductivities of the dual CFT also transform as before, eq. (4.6):

$$\sigma \rightarrow \frac{a\sigma + b}{c\sigma + d}. \quad (4.47)$$

Beyond linear response

The fact that the quantities $\mathcal{G}_{\mu\nu}$ and $\mathcal{F}_{\mu\nu}$ transform under $SL(2, R)$ in the same way as they did for the dilaton-Maxwell theory carries some potentially interesting implications. In particular, since the constitutive relation, eq. (4.42), states that $G^{\mu\nu}$ is a linear combination of $F^{\mu\nu}$ and $\tilde{F}^{\mu\nu}$ (with field-dependent scalar coefficients), it can always be written in a form similar to eq. (4.21):

$$\mathcal{G}_{\mu\nu} = \bar{\tau}_{\text{eff}} \mathcal{F}_{\mu\nu}, \quad (4.48)$$

for some field-dependent quantity $\tau_{\text{eff}} = \tau_{\text{eff}}(\tau, F^2, F \cdot \tilde{F})$, satisfying $\tau_{\text{eff}}(\tau, 0, 0) = \tau$. But the invariance of this relation under $SL(2, R)$ implies that the quantity τ_{eff} must also transform under $SL(2, R)$ as

$$\tau_{\text{eff}} \rightarrow \frac{a \tau_{\text{eff}} + b}{c \tau_{\text{eff}} + d}. \quad (4.49)$$

The quantity τ_{eff} plays the role of a ‘dressed’ axio-dilaton for the DBI theory.

A similar observation also holds for the quantities $\mathcal{J} = -i(J^x - iJ^y)$ and $\mathcal{E} = E_x - iE_y$ of the CFT. These inherit from $\mathcal{G}_{\mu\nu}$ and $\mathcal{F}_{\mu\nu}$ the same transformation as for the dilaton-Maxwell theory, (4.28):

$$\begin{pmatrix} \mathcal{J} \\ \mathcal{E} \end{pmatrix} \rightarrow \begin{pmatrix} a & b \\ c & d \end{pmatrix} \begin{pmatrix} \mathcal{J} \\ \mathcal{E} \end{pmatrix}. \quad (4.50)$$

Defining the effective, field-dependent, conductivities, σ_{eff}^{xy} and σ_{eff}^{xx} , by

$$\sigma_{\text{eff}-} = \sigma_{\text{eff}}^{xy} - i\sigma_{\text{eff}}^{xx} := \frac{\mathcal{J}}{\mathcal{E}}, \quad (4.51)$$

then implies that these must transform under $SL(2, R)$ as

$$\sigma_{\text{eff}-} \rightarrow \frac{a \sigma_{\text{eff}-} + b}{c \sigma_{\text{eff}-} + d}, \quad (4.52)$$

and similarly for $\sigma_{\text{eff}} := \sigma_{\text{eff}}^{xy} + i\sigma_{\text{eff}}^{xx}$.

We see here within an AdS/CFT realization how the implications of duality can apply beyond the strict linear-response regime, to include the nonlinear dependence of the conductivities on the applied fields. This is precisely what is required to account for some of the observations discussed in §2 (see Fig. (4.4) and refs. [19, 33]).

4.4.3 Holographic DC conductivities

We next turn to the calculation of the conductivities as functions of temperature and magnetic field, to verify the presence of a nonzero DC ohmic conductivity.

Background geometry

Following [13] we take the background metric to solve the field equations generated only by S_{grav} , and regard the effects of S_{gauge} as a perturbation to this geometry (the probe-brane approximation). We return below to the limitations of the domain of validity of this approximation.

We assume the background 4D geometry sufficiently near the black hole is

$$ds^2 = L^2 \left[-h(v) \frac{dt^2}{v^{2z}} + \frac{dv^2}{v^2 h(v)} + \frac{dx^2 + dy^2}{v^2} \right], \quad (4.53)$$

where L is the length scale defined by $\Lambda = 3/L^2$ (set to unity in what follows), and the Lifshitz parameter, z , measures the difference between the scaling dimension of the space and time directions, with $z = 1$ corresponding to equal scaling.¹⁷

Not much is required to be known about the function $h(v)$, apart from that it is positive, approaches unity as $v \rightarrow 0$, and is assumed to have a simple zero, $h(v_h) = 0$ for $v_h > 0$, corresponding to the horizon of the black brane. The position of this horizon provides a temperature for the boundary theory in the usual way,

$$T = \frac{|h'(v_h)|}{4\pi v_h^{z-1}} \sim \frac{1}{v_h^z}, \quad (4.54)$$

with the approximate equality following from the assumption that $h'(v_h) \sim 1/v_h$. As before, the position of conformal infinity is taken to be $v = 0$.

If the black brane of the background geometry does not couple to a Maxwell field, as for the Lifshitz sector of ref. [13], then the dilaton and axion fields can be taken to be constants: $\phi = \phi_0$ and $\chi = \chi_0$. In this case the parameter z can be taken to be a knob to be dialed essentially at will. Alternatively, if the background geometry carries a charge and so approaches an extremal black brane at low temperature with an attractor form, then ϕ generically has a nontrivial profile. When necessary we take this to be $e^\phi \propto 1/v^4$ (suggested by the dilaton-Maxwell solution of [49, 10] or the dilaton-DBI solution described in Appendix D). In either case the axion can be set to zero and then later regenerated by performing an $SL(2, R)$ transformation.

¹⁷As discussed in [13] the presence of z complicates the discussion of the boundary conditions (see also footnote 11), particularly once $z \gtrsim 2$. Following [7], we expect these to be automatically incorporated into the duality transformations, but do not expect them to affect our conductivity calculations in any case. In particular, we expect the large value $z \simeq 5$ indicated by experiments to be generated in the far IR by an attractor mechanism for near-extremal black holes, without requiring $z \neq 1$ at conformal infinity.

Conductivity calculation

We proceed following closely the steps of ref. [13] (see also refs. [52, 53]). The field equations for the gauge field are $\nabla_\mu G^{\mu\nu} = 0$, with $G^{\mu\nu}$ given by (4.42). Those for the axio-dilaton are

$$\begin{aligned} 0 &= \square\phi + \frac{\kappa^2 \mathcal{T} \ell^4}{2X} \left[e^{-\phi} F_{\mu\nu} F^{\mu\nu} - \frac{\ell^4}{4} e^{-2\phi} \left(F_{\mu\nu} \tilde{F}^{\mu\nu} \right)^2 \right] - e^{2\phi} \partial_\mu \chi \partial^\mu \chi \\ &= \square\phi + \frac{\kappa^2}{2} \left[G^{\mu\nu} - \chi \tilde{F}^{\mu\nu} \right] F_{\mu\nu} - e^{2\phi} \partial_\mu \chi \partial^\mu \chi \end{aligned} \quad (4.55)$$

and

$$\nabla_\mu \left(e^{2\phi} \nabla^\mu \chi \right) - \frac{\kappa^2}{2} F_{\mu\nu} \tilde{F}^{\mu\nu} = 0. \quad (4.56)$$

The strategy in the probe limit is to solve the Maxwell equation, but neglect the corrections to the background metric and dilaton. The above equations show this requires the neglect of quantities like $\kappa^2 \mathcal{T}/X$ and $\kappa^2 F_{\mu\nu} \tilde{F}^{\mu\nu}$ relative to $1/L^2$ (which itself must satisfy $1/L^2 \ll 1/\ell^2$). Because $\kappa^2 \sim \ell^8/\Omega \ll \ell^2$ — with Ω the volume of the extra dimensions not made explicit here — these conditions need not imply that quantities like $\ell^4 e^{-\phi} F_{\mu\nu} F^{\mu\nu}$ are also small, so it remains consistent to keep the nonlinearities in the DBI action. In addition to these conditions are the more ‘stringy’ conditions for weak coupling, $e^\phi \ll 1$, and the absence of runaway string pair-production [54] (more about the domain of validity later).

It suffices to compute the ohmic conductivity in the absence of a magnetic field and axion, since the general case can then be recovered by performing an appropriate $SL(2, R)$ transformation. To this end we require the solution to the Maxwell equation subject to the ansatz

$$A = \Phi(v) dt + \left[\mathcal{A}(v) - Et \right] dx. \quad (4.57)$$

The corresponding components to the field strength then are

$$\text{and} \quad \begin{aligned} F_{vt} &= \Phi', & F_{vx} &= \mathcal{A}', & F_{tx} &= E \\ \tilde{F}^{xy} &= -\frac{\Phi'}{\sqrt{-g}}, & \tilde{F}^{ty} &= \frac{\mathcal{A}'}{\sqrt{-g}}, & \tilde{F}^{vy} &= -\frac{E}{\sqrt{-g}}, \end{aligned} \quad (4.58)$$

and so $F_{\mu\nu} \tilde{F}^{\mu\nu} = 0$.

Since the equations of motion can be written $\partial_\nu [\sqrt{-g} G^{\nu\mu}] = 0$, the equations corresponding to $\mu = a = \{x, y, t\}$ immediately integrate to give $\sqrt{-g} G^{va} = C^a$, where C^a are three v -independent integration constants. The absence of an axion allows the choice $C^y = 0$, but the other two equations determine Φ' and \mathcal{A}' in terms of C^t and C^x , as follows:

$$\sqrt{-g} \left(\frac{\mathcal{T} \ell^4 e^{-\phi}}{X} \right) g^{vv} g^{tt} \Phi' = C^t \quad \text{and} \quad \sqrt{-g} \left(\frac{\mathcal{T} \ell^4 e^{-\phi}}{X} \right) g^{vv} g^{xx} \mathcal{A}' = C^x, \quad (4.59)$$

where

$$X = \sqrt{1 + \ell^4 e^{-\phi} \left[g^{vv} g^{tt} (\Phi')^2 + g^{vv} g^{xx} (\mathcal{A}')^2 + g^{tt} g^{xx} E^2 \right]}. \quad (4.60)$$

Using these expression to eliminate Φ' and \mathcal{A}' gives the following result for X as a function of C^t and C^x :

$$X = \sqrt{\frac{N}{D}}, \quad (4.61)$$

with

$$\begin{aligned} N &:= 1 + \ell^4 e^{-\phi} \left(\frac{E^2}{g_{tt} g_{xx}} \right) \\ D &:= 1 + \frac{e^\phi}{\mathcal{T}^2 \ell^4} \left[\frac{(C^t)^2}{g_{xx}^2} + \frac{(C^x)^2}{g_{tt} g_{xx}} \right]. \end{aligned} \quad (4.62)$$

Notice that when $v \rightarrow 0$ all of the metric functions diverge, and so both N and D approach unity. But when $v \rightarrow v_h$ we instead have $g_{tt} \rightarrow 0^-$ and $g_{vv} \rightarrow \infty$, while g_{xx} and $\sqrt{-g}$ remain finite. This implies both N and D approach $-\infty$ in this limit, requiring they both change sign somewhere in the interval $0 < v < v_h$. A quick way to solve for the relation between C^a and E is the observation [52] that the reality of the action requires both N and D to change sign at the same point, $v = v_*$, implying

$$-(g_{tt} g_{xx})_\star = \frac{h(v_\star)}{v_\star^{2(z+1)}} = \ell^4 e^{-\phi_\star} E^2, \quad (4.63)$$

and

$$-\frac{(C^x)^2}{(g_{tt} g_{xx})_\star} = \frac{(C^t)^2}{(g_{xx}^2)_\star} + \mathcal{T}^2 \ell^4 e^{-\phi_\star}. \quad (4.64)$$

The first of these can be used to infer the value of v_* as a function of E , and the second then imposes an E -dependent relation between C^x and C^t . Notice that as $E \rightarrow 0$, eq. (4.63) implies $v_\star \rightarrow v_h \propto T^{-1/z}$.

Now the usual AdS/CFT translation tells us that the integration constants found above are the currents¹⁸ in the CFT: $J^a = C^a$, so using $C^x = J^x = \sigma^{xx} E$ and $C^t = J^t = \rho$ in the last equation gives the ohmic conductivity as

$$\begin{aligned} \sigma^{xx} &= \sqrt{(\mathcal{T} \ell^4 e^{-\phi_\star})^2 + (\ell^4 e^{-\phi_\star}) \rho^2 / (g_{xx}^2)_\star} \\ &= \sqrt{(\mathcal{T} \ell^4 e^{-\phi_\star})^2 + v_\star^4 (\ell^2 \rho)^2 e^{-\phi_\star}}, \end{aligned} \quad (4.65)$$

where the last line uses the explicit form of the metric, eq. (4.53). The absence of a magnetic field and axion in this case also require vanishing Hall conductivity $\sigma^{xy} = 0$. Notice the limiting forms,

¹⁸A note on units of charge: this can be changed for the carriers in the CFT by rescaling $A_\mu \rightarrow \xi A_\mu$. This is a symmetry of the action — contained in $SL(2, R)$ — if $e^{-\phi} \rightarrow \xi^{-2} e^{-\phi}$ and $\chi \rightarrow \xi^{-2} \chi$. Under this rescaling $G^{\mu\nu} \rightarrow \chi^{-1} G^{\mu\nu}$, $J^\mu \rightarrow \xi^{-1} J^\mu$ and $\sigma^{ab} \rightarrow \xi^{-2} \sigma^{ab}$.

depending on the relative size of v_\star^4 and $v_c^4 := e^{-\phi_\star} (\mathcal{T}\ell^2/\rho)^2 \gg 1$,

$$\begin{aligned}\sigma^{xx} &\simeq \mathcal{T}\ell^4 e^{-\phi_\star} && \text{if } v_\star \ll v_c \\ \sigma^{xx} &\simeq v_\star^2 (\ell^2 \rho) e^{-\phi_\star/2} && \text{if } v_\star \gg v_c.\end{aligned}\tag{4.66}$$

Provided $\mathcal{T}\ell^4 \simeq \mathcal{O}(1)$, as would be true for a D3 brane, this shows that weak coupling (*i.e.* $e^{-\phi_\star} \gg 1$) implies σ^{xx} starts at a fixed, large value — $\sigma^{xx} \simeq \mathcal{O}(e^{-\phi_\star}) \gg 1$ for $v_\star < v_c$, and then climbs to still larger values with growing v_\star . As shown in Appendices C and D, for sufficiently large σ^{xx} the probe-brane limit can eventually fail, corresponding to the need for a better approximation to understand the limit of vanishing T .

The temperature-dependence of this expression is encoded in the value of v_\star , whose determination requires a fuller specification of the metric function $h(v)$. For small E we know $v_\star^{-4} \simeq v_h^{-4} \simeq CT^{4/z}$. This implies

$$\sigma^{xx} \simeq \frac{e^{-\phi_\star/2}}{\sqrt{C} T^{2/z}} \sqrt{(\ell^2 \rho)^2 + C(\mathcal{T}\ell^4)^2 e^{-\phi_\star} T^{4/z}},\tag{4.67}$$

and so σ^{xx} asymptotes to the fixed, large value $\mathcal{T}\ell^4 e^{-\phi_\star}$ for high T , but grows with falling temperature, like $\sigma^{xx} \propto T^{-2/z}$ for temperatures $T \ll T_c$, where $T_c = T(v_c) \ll 1/L$ because $v_c \gg 1$. This shows that it is indeed small T that corresponds to large σ^{xx} , and so the breakdown of the probe-brane approximation.

Validity of the probe approximation

It turns out that the details of the domain of validity of the probe-brane approximation differ for the cases where the background geometry describes a neutral black brane (with constant dilaton and z arbitrary), or when it is that of a charged, near-extremal black brane (with a dilaton profile and an attractor value $z = 5$). As is argued in detail in Appendix C, a necessary condition for the probe approximation is

$$\rho \ll \left(\frac{\ell^2}{\kappa^2 L^2} \right) \frac{e^{-\phi_\star/2}}{v_\star^2},\tag{4.68}$$

where ρ is the charge density and $\phi_\star := \phi(v_\star)$ with v_\star (defined above) approaching the horizon, $v_\star \rightarrow v_h$, for small applied electric fields, E . Since $v_\star \leq v_h$, the probe approximation can work well right down to the horizon, $v = v_h$, provided v_h is not too large (and so temperatures are not too close to zero).

For neutral branes, where ϕ is constant, the probe approximation ultimately fails for small enough temperatures because eventually $v_\star \simeq v_h$ is large enough to invalidate eq. (4.68).

If, on the other hand, the source brane is charged then the above bound is more complicated because ϕ_\star depends nontrivially on v_\star (and so also on T). In particular, in the very low temperature limit the near-horizon geometry can be independent of the asymptotic values of the dilaton and axion, and in the dilaton-Maxwell described above [11] (and the dilaton-DBI system of Appendix

D), $e^{-\phi_\star/2} \propto v_\star^2$. This makes the right-hand-side of eq. (4.68) constant, and so it need not be violated at very small T . Appendix D explores the value, X_h , approached by X in the near-horizon, near-extremal geometry; showing that if the background geometry is supported by a DBI action with tension $N\mathcal{T}$, then $\kappa^2 N\mathcal{T}/X_h > 1$, although $\kappa^2 \mathcal{T}/X_h$ can be small if N is sufficiently large.

Conductivities with nonzero magnetic fields

To obtain the conductivities for general magnetic fields and asymptotic axion fields, we act on the previous result using an $SL(2, R)$ transformation. Notice in particular that this automatically ensures that the result found for $\sigma(\rho, B, T)$ has a temperature flow that commutes with the action of the group, as assumed in §2 to reproduce the observed phenomenology from a discrete duality group — see Fig. 4.6.

The transformation law, $\sigma \rightarrow (a\sigma + b)/(c\sigma + d)$, implies that the ohmic and Hall conductivities obtained starting from $\sigma_0^{xy} = 0$ and $\sigma_0^{xx} := \sigma_0$ (with σ_0 given in eq. (4.65)) are

$$\sigma^{xx} = \frac{\sigma_0}{d^2 + c^2 (\sigma_0)^2} \quad \text{and} \quad \sigma^{xy} = \frac{ac(\sigma_0)^2 + bd}{d^2 + c^2 (\sigma_0)^2}. \quad (4.69)$$

We require only the values of the parameters a, b, c , and d that are required to take the pure dilatonic electric case to a general axion and dyonic field.

The required transformation is computed in Appendix A, and has parameters $a = 1$, $c = -B/\rho = 1/\nu$ (where $\nu = -\rho/B$ is the filling fraction appropriate for a negatively charged particle) and

$$b = \frac{\nu [\chi(\nu - \chi) - e^{-2\phi}]}{(\nu - \chi)^2 + e^{-2\phi}} \quad \text{and} \quad d = \frac{\nu(\nu - \chi)}{(\nu - \chi)^2 + e^{-2\phi}}. \quad (4.70)$$

These lead to the conductivities

$$\sigma^{xx} = \frac{\nu^2 [(\chi - \nu)^2 + e^{-2\phi}]^2 \sigma_0}{\nu^4 (\chi - \nu)^2 + [(\chi - \nu)^2 + e^{-2\phi}]^2 (\sigma_0)^2} \quad (4.71)$$

$$\sigma^{xy} = \frac{\nu [(\chi - \nu)^2 + e^{-2\phi}]^2 (\sigma_0)^2 + \nu^4 (\chi - \nu) [\chi(\chi - \nu) + e^{-2\phi}]}{\nu^4 (\chi - \nu)^2 + [(\chi - \nu)^2 + e^{-2\phi}]^2 (\sigma_0)^2}. \quad (4.72)$$

where σ_0 is the ρ - and T -dependent, but B -independent, result given in eq. (4.65) (corresponding to the $\nu \rightarrow \infty$ limit of σ^{xx}). The temperature-dependence is simplest to describe in the regime of small E , in which case eq. (4.67) can be used. In particular, for small temperatures in this case $\sigma_0 \simeq C' \rho/T^{2/z}$ and so is large for small T .

These expressions are graphed in Fig. 4.8, which plots σ^{xx} on the vertical axis against σ^{xy} on the horizontal. Each curve corresponds to an integer choice for ν , stepping between the values $\nu = 1$ and $\nu = 10$, while the parameter σ_0 varies along each curve. Each curve approaches $\sigma^{xy} = \nu$ in

the large- σ_0 limit (see below), and is a semi-circle centred on the $\sigma^{xx} = 0$ axis that passes through the point $\sigma^{xy} = \chi$ and $\sigma^{xx} = e^{-\phi}$ (so $\sigma = \tau$). Each is a semi-circle because it is the image under $SL(2, R)$ of the straight line $\sigma^{xy} = 0$, obtained for $\chi = B = 0$. Each curve passes through $\sigma = \tau$ because σ and τ transform the same way under $SL(2, R)$ and there is always a choice for σ_0 for which the initial value of σ^{xx} agrees with $e^{-\phi}$.

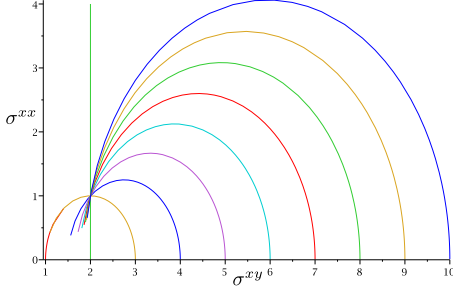


Figure 4.8. The conductivities (σ^{xx} plotted vs σ^{xy}), as computed using eqs. (4.71) and (4.72) with $\tau = 2 + i$. Each curve corresponds to a different choice for ν , stepping from $\nu = 1$ to $\nu = 10$ through integer values. σ_0 is the parameter along each curve, with $\sigma^{xy} \rightarrow \nu$ in the limit of large σ_0 . All lines are semi-circles centred on the real axis, and all pass through the point $\sigma = \tau$, for the reasons explained in the text (colour online).

There are several limits for which the conductivities take a particularly simple form.

1. If $e^{-2\phi} \gg \nu^2, (\chi - \nu)^2$ (or if $\chi = \nu$, or $\nu \ll 1$, or if σ_0 is sufficiently large) then

$$\sigma^{xx} = \frac{\nu^2}{\sigma_0} \quad \text{and} \quad \sigma^{xy} = \nu. \quad (4.73)$$

In particular, unless ν or χ are taken to be parametrically large, this result holds to the extent that we neglect loop corrections, which are controlled by powers of e^ϕ . In particular, using the large- σ_0 limit obtained at small T gives the form:

$$\sigma^{xx} = \frac{\nu^2}{\sigma_0} \simeq \frac{\rho T^{2/z}}{C' B^2} \quad \text{and} \quad \sigma^{xy} = \nu = -\frac{\rho}{B}. \quad (4.74)$$

2. The limits of weak and strong magnetic field are also simple. Weak magnetic field corresponds to $\nu \rightarrow \infty$, which gives

$$\sigma^{xx} \rightarrow \sigma_0 \left[1 - \frac{2\chi}{\nu} + \dots \right] \quad \text{and} \quad \sigma^{xy} \rightarrow \chi + \frac{(\sigma_0)^2 - e^{-2\phi}}{\nu} + \dots, \quad (4.75)$$

where the ellipses denote terms that are of relative order χ^2/ν^2 , $e^{-2\phi}/\nu^2$ and σ_0^2/ν^2 . This generalizes the calculation of the previous section to nonzero χ . By contrast, both conductivities vanish, $\sigma^{xx} = \sigma^{xy} = 0$, in the limit of large B (or vanishing density) corresponding to $\nu \rightarrow 0$. The approach to zero for small ν is given by eq. (4.73).

4.4.4 Plateaux, semi-circles and the low-temperature limit

Although remarkable, at face value the formulae of eqs. (4.71) and (4.72) do not generically describe quantum Hall plateaux, which should have vanishing ohmic conductivity, $\sigma^{xx} = 0$, combined with the defining plateau behaviour for which σ_{xy} does not change as B varies. By contrast, the generic low-temperature limit of the above formulae produce a Hall conductivity that takes a continuous

range of values, $\sigma^{xy} = \nu$, as B is varied, and so does not show the characteristic plateau-like feature of remaining constant as B varies over a finite range. As a result, at low temperatures and magnetic fields the fluid has an ohmic conductivity that tracks the temperature and a Hall conductivity that tracks the magnetic field (or filling fraction), as shown in the left panel of Fig. 4.9.

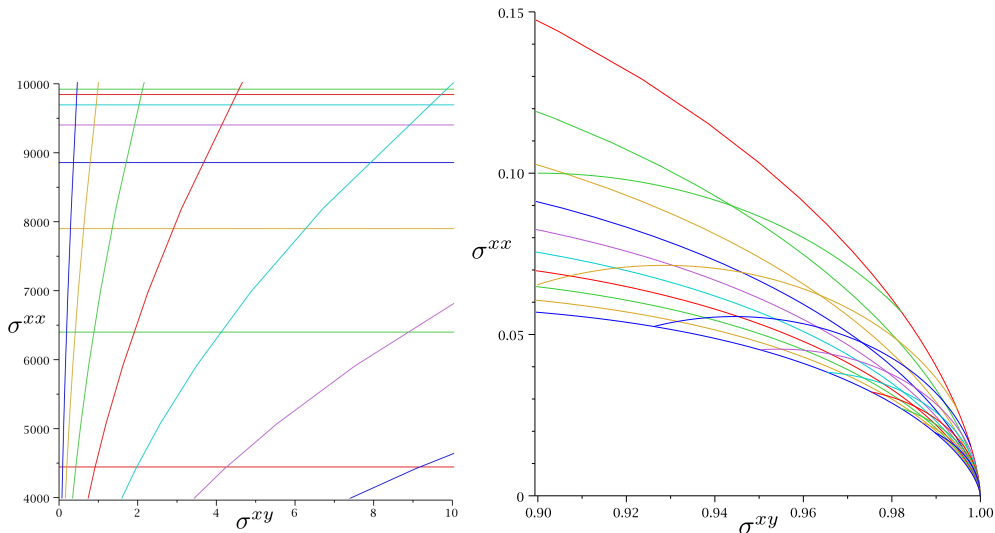


Figure 4.9. Left panel: Curves of constant σ_0 and ν as computed semiclassically using the holographic model in the regime $\nu \gg \sigma_0^2$, $e^{-2\phi} \gg 1$. Horizontal lines represent loci of fixed σ_0 (and so also temperature), while the sloped lines describe those of fixed ν (and so also fixed magnetic field). Right panel: the same curves mapped to the strongly interacting near-plateau regime using an element of $SL(2, Z)$. The semi-circles radiating from the tip of the fan at the real axis represent lines of constant B , along which T varies. Those transverse to these are lines of constant T . These illustrate a plateau behaviour inasmuch as all curves converge to the same values of σ^{xx} and σ^{xy} for all values of magnetic field at low temperatures (colour online).

The special point, $\sigma = \tau$, in Fig. 4.8 where the many semi-circles cross is more plateau-like, however. It is plateau-like in the following specific sense: once the temperature is adjusted to sit at the point $\sigma = \tau$, changes in ν do not change the value of the conductivity. What differs between this point and those observed in quantum Hall systems is that for real systems the ohmic conductivity should also vanish, corresponding to taking $\text{Im } \tau = e^{-\phi} \rightarrow 0$. Although plateaux with $\text{Im } \tau \neq 0$ cannot describe quantum Hall systems, it would be of great interest to compute their full electromagnetic response to better understand their properties.

Clearly real quantum Hall systems (with $\text{Im } \tau \rightarrow 0$) cannot be captured by the semiclassical limit, for which $SL(2, R)$ is a good symmetry. Another hint that strong coupling should play a role comes from the recognition that the classical near-horizon configuration for $e^{-\phi}$ vanishes for extremal magnetic black holes. Similarly, ref. [11] computes the compressibility of the fluid for the dilaton-Maxwell system of S3, and find that it is generically compressible, but would be incompressible at strong coupling if the weak-coupling formulae were simply formally extrapolated into the strong-coupling regime.

Happily, there is a way to probe strong coupling if it is assumed that a discrete symmetry like $\Gamma = PSL(2, Z)$ (or one of its subgroups) survives in the strong-coupling limit. In this case the behaviour near $\sigma^{xx} = 0$ is often the image under Γ of a calculable region with much larger σ^{xx} for which the above calculations are valid. This is possible to the extent that it is only the weak-coupling approximation that fails, since this is controlled by $e^{-\phi} = \text{Im } \tau \gg 1$ and Γ maps regions with large $\text{Im } \tau$ to regions where it is small (precisely as it does for $\text{Im } \sigma$).

For instance, imagine starting from $\sigma = i\sigma_0$ at $B = 0$ and performing the transformations, eq. (4.69), with $a = p$, $b = r$, $c = q$ and $d = s$ restricted to be integers, which yields

$$\sigma^{xx} = \frac{\sigma_0}{s^2 + q^2 (\sigma_0)^2} \quad \text{and} \quad \sigma^{xy} = \frac{pq (\sigma_0)^2 + rs}{s^2 + q^2 (\sigma_0)^2}, \quad (4.76)$$

where the domain of validity is large σ_0 , as before, and the assumed exact validity of the discrete transformation. In particular, although we cannot compute the explicit T -dependence of σ_0 very close to $T = 0$, we need not be able to do so in order to explore the implications of the $SL(2, R)$ and $SL(2, Z)$ transformations so long as $\sigma_0 \rightarrow \infty$ as $T \rightarrow 0$. In this limit

$$\sigma^{xx} \simeq \frac{1}{q^2 \sigma_0} \left[1 + \mathcal{O} \left(\frac{1}{\sigma_0^2} \right) \right] \quad \text{and} \quad \sigma^{xy} \simeq \frac{p}{q} \left[1 + \mathcal{O} \left(\frac{1}{\sigma_0^2} \right) \right], \quad (4.77)$$

where $\sigma_0 \gg 1$. These show that as $T \rightarrow 0$ the Hall conductivity, σ^{xy} , assumes a B and T -independent quantized fractional value, p/q , while σ^{xx} vanishes. The behaviour near this point as ν and σ_0 are varied over values $\nu \gg \sigma_0 \gg 1$ is illustrated on the right-hand panel of Fig. 4.9, which plots the image of the left panel under the discrete transformation, $\sigma \rightarrow \sigma/(\sigma + 1)$, that maps $\sigma = \infty$ to $\sigma = 1$.

These fractional values become *bona fide* quantum Hall plateaux if we also take $e^{-\phi} \rightarrow \infty$ together with $\sigma_0 \rightarrow \infty$, since then the same discrete transformation that maps $\sigma \rightarrow \sigma' = \sigma/(\sigma + 1)$ also takes $\tau \rightarrow \tau' = \tau/(\tau + 1)$ as well as $\nu \rightarrow \nu' = \nu/(\nu + 1)$. This ensures that the ν' -independent plateau at $\sigma' = \tau'$ occurs for $\text{Im } \tau' = \text{Im } \sigma' = 0$, rather than off in the interior of the σ -plane as was the case for Fig. 4.8.

The precise values of p and q appearing in the fraction depend on the discrete group that is assumed to be valid, and ref. [7] argues this generically to be $SL(2, Z)$ (generated by S and T – see Appendix A) in the presence of a spin structure, or $\Gamma_\theta(2) \subset SL(2, Z)$ (generated by S and T^2) for no spin structure. In neither case does the above expression agree with real non-degenerate quantum Hall systems, since $SL(2, Z)$ allows arbitrary p , q , r and s , subject only to $ps - qr = 1$ and $\Gamma_\theta(2)$ requires both r and q to be even (in which case p and s must be odd), or both r and q to be odd (with both p and s even). Both cases allow even q , unlike the usual situation in Zeeman-split quantum Hall systems.¹⁹

In particular, for spin-split systems with unbroken $\Gamma_\theta(2)$ symmetry this predicts Hall plateaux

¹⁹There is evidence for some Hall states with even denominators, but these are the exception rather than the rule in the absence of more than one electron label (like spin, or layer number for bilayers or band label in graphene), for which $SL(2, Z)$ is the appropriate group.

at fractions $\sigma^{xy} = p/q$ where p is odd and q is even, or with p even and q odd. This is precisely the duality group and Hall plateaux predicted [6] for bosonic Hall systems, described in §2 — *c.f.* eq. (4.14) — suggesting the CFT is a strongly coupled analog of scalar electrodynamics.

Fermionic quantum Hall systems

Given this identification of the the CFT as a bosonic Hall system, it is clear what is required to obtain a fermionic candidate to describe real quantum Hall systems. This is obtained from a bosonic system by coupling to a boundary statistics field having an odd statistics parameter, $\vartheta = \pi$, as in §2. Within the present framework this is most easily done by performing the $SL(2, Z)$ transformation, eq. (4.15), that implements the addition of such a flux: $g = ST^{-1}S$. The duality group that survives to strong couplings for the fermionic system is then $\Gamma_F = g\Gamma_B g^{-1}$, where Γ_B is the corresponding group in the boson system before the addition of the statistics flux. Assuming, as before, that $\Gamma_B = \Gamma_\theta(2)$ for the bosonic system leads to the fermionic group $\Gamma_F = g\Gamma_\theta(2)g^{-1} = \Gamma_0(2)$ (generated by ST^2S and T), as is shown in Appendix A. This is precisely the group (defined by the condition that q be even, and so for which p and s must also be odd) multiply proposed over the years [24, 27, 6] as providing a good phenomenological description of quantum Hall systems.

To find the T and B dependence of the conductivities in this case, first act on the initial bosonic conductivity with $g = ST^{-1}S$, for which $p = s = q = -1$ and $r = 0$. Starting with the dilaton-DBI result without a magnetic field, $\sigma_0^{xy} = 0$ and $\sigma_0^{xx} = \sigma_0$ given by eq. (4.67), then gives the fermionic archetype:

$$\sigma_0^{xx} = \frac{\sigma_0}{1 + \sigma_0^2} \quad \text{and} \quad \sigma_0^{xy} = \frac{\sigma_0^2}{1 + \sigma_0^2}, \quad (4.78)$$

which in the low-temperature regime approaches an integer quantum Hall level, $\sigma_0^{xy} \rightarrow 1$.

The expression for general χ and B can then be found in one of two equivalent ways. One can either directly act with $ST^{-1}S$ on the general bosonic result, eqs. (4.71) and (4.72); or one can act on eq. (4.78) using the fermion $SL(2, R)$ transformation obtained by conjugating the boson duality transformation, (4.70), using $g = ST^{-1}S$. This latter is obtained by using

$$g \begin{pmatrix} a & b \\ c & d \end{pmatrix} g^{-1} = \begin{pmatrix} a - b & b \\ a - b + c - d & b + d \end{pmatrix}. \quad (4.79)$$

The plateaux themselves for the fermionic system can be found by acting on the basic case, eq. (4.78), using a $\Gamma_0(2)$ transformation. Defining $\hat{\sigma} = \sigma_0^{xx} + i\sigma_0^{xy}$, with components taken from (4.78), the conductivity near a plateau is

$$\sigma = \frac{p\hat{\sigma} + r}{q\hat{\sigma} + s}, \quad (4.80)$$

where q is even (and so p and s are odd). In the low-temperature limit, where $\sigma_0 \rightarrow \infty$ we have

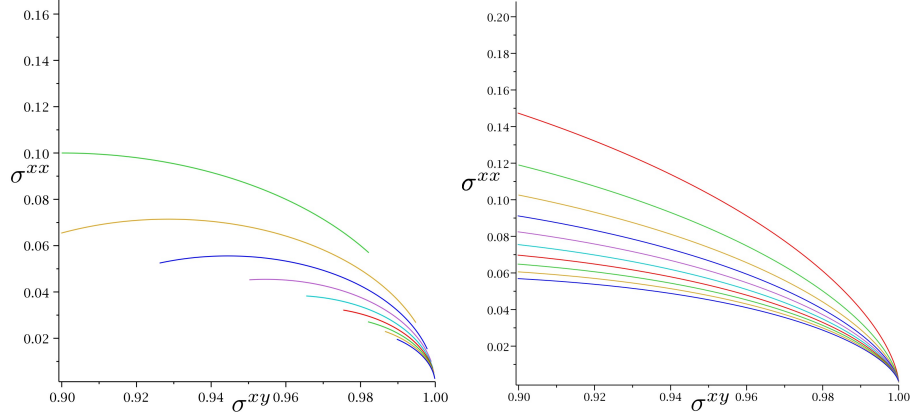


Figure 4.10. Left panel: Curves of constant magnetic field (or $\nu' = g(\nu)$) as computed semiclassically using the holographic model and mapped onto a plateau using an element $g \in PSL(2, Z)$. Right panel: the same curves for lines of constant T (or σ_0). Constant B lines are semicircles, while those along which B varies become semicircles at sufficiently low temperatures (colour online).

$\hat{\sigma} \rightarrow 1$ and so

$$\sigma \rightarrow \frac{p+r}{q+s}, \quad (4.81)$$

which clearly always has an odd denominator. The plateau-like behaviour is as illustrated on the right-hand panel of Fig. 4.9.

Semicircles

The generation of conductivities using $PSL(2, R)$, followed by mapping weak to strong coupling using a discrete symmetry also naturally ensures the observed semicircle behaviour as one approaches a quantum Hall plateau. This can be seen in Fig. 4.10, which plots how lines of constant ν and T approach the plateau. Lines of constant ν obtained in this way are always semi-circles because they are the images under $PSL(2, R)$ and $PSL(2, Z)$ of the straight line along which only σ^{xx} varies when $B = 0$. Experiments varying B at sufficiently small T are also semicircles because these coincide with semicircular temperature flow lines. This can be seen in Fig. 4.7.

4.5 Discussion and conclusions

We see that the DBI-based model examined here provides an example of a 3+1 dimensional gravitational system that has two desirable properties: (i) it admits an $SL(2, R)$ duality group at the classical level; and (ii) it has nonzero DC ohmic and Hall conductivities. The model is phenomenological, in that it is not part of an explicit string construction, but this is also unlikely to be relevant for low-energy purposes so long as all of the other string ingredients do not play an important role and so can be integrated out. These other stringy ingredients do play one important role, however,

and that is to break the classical $SL(2, R)$ group down to a discrete subgroup. The general properties of 2+1 dimensional CFTs make this subgroup generically likely to be $SL(2, Z)$ in situations where a spin structure is relevant, or $\Gamma_\theta(2) \subset SL(2, Z)$ if a spin structure is not relevant.

These two properties are the minimal two things that would be required for a candidate description of low-energy quantum Hall systems, based on the phenomenological evidence in these systems for an emergent discrete duality symmetry (summarized in §2). Any system with these properties automatically captures all of the implications of the discrete symmetry that survives in the strongly coupled regime, and in particular those enjoying an unbroken $\Gamma_0(2)$ duality group merit a closer inspection to see how well they capture other properties of real quantum Hall systems. This section discusses several kinds of observables of this type that are *not* simply consequences of duality.

4.5.1 A model-building wish list

There are two kinds of predictions made by the specific dilaton-DBI model examined here, that are typical of the kinds of comparisons that can be made that go beyond the implications of the duality groups.

Approach to zero temperature

Although having a duality group commute with the RG flow to low temperatures predicts the properties of some of the trajectories, $\sigma(B, T)$, in the conductivity plane [30], it does not predict them all. The duality itself also does not predict the dependence on T along the flow lines, although these are often reasonably well-measured (*c.f.* eq. (4.2), for example). Since specific models predict this dependence in detail, comparison with the measurements can help sort out those models that provide the best description.

For instance, Fig. 4.11 shows how the ohmic DC conductivity drops exponentially with T as one approaches various quantum Hall plateaux, $\propto e^{-\Delta/T}$, over a wide range of temperatures. Like the incompressibility of the quantum Hall state, this is consistent with the existence of a gap at low energies. By contrast, the CFT corresponding to the gravity dual described above predicts a power-law for this approach, such as the dependence $\sigma^{xx} \propto T^{2/z}$ seen near $\sigma^{xy} = 1$ in eq. (4.77).

When the background describes a neutral brane, the probe-brane approximation prevents our direct exploration of the $T \rightarrow 0$ limit and so cannot exclude a crossover to exponential behaviour at very low temperatures. The same need not be true for the near-horizon extremal geometry explored in §3 and Appendix D, however, and does not appear to indicate such a crossover. It is possible

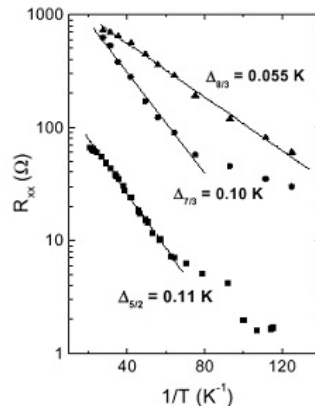


Figure 4.11. Experimental plots, reproduced from ref. [55], of the temperature dependence of the approach to various quantum Hall plateaux, showing an exponential form.

that this exponential is associated with the approach to the low-energy 2D surface in coupling space. It is also intriguing that Fig. 4.11 shows deviations from an exponential form at sufficiently low temperatures (although this may equally well just prove to be an experimental issue). This motivates a more detailed study of the very low-temperature limit, as well as AdS/CFT systems having gaps like the D7 system studied in [13]. We leave it as an open problem whether an alternative brane construction could be made that leads to a duality-invariant form for the low-energy 4D effective action consistent with an exponential temperature dependence.

Critical exponents

Another experimentally accessible feature not purely dictated on symmetry grounds is the powers, α and β , governing the scaling of the resistivities in the low-temperature limit (*c.f.* eq. (4.5)) and Fig. 4.5. As discussed in §2, these are measured to satisfy $\beta \simeq \alpha \simeq 0.42 \pm 0.04$ [21], a result that can be usefully compared with the predictions of a particular CFT. How does the dilaton-DBI gravity dual described above do on this score?

The numerical equivalence $\alpha \simeq \beta$ would be easy to understand if the resistivity, ρ_{ab} , near the critical field, $B = B_c + \Delta B$, depended only on T and ΔB through the one scaling combination

$$\rho_{ab} \simeq \rho_{ab}(x) \quad \text{with} \quad x := \frac{\Delta B}{T^p}, \quad (4.82)$$

for some power p . This dependence implies

$$\left(\frac{d\rho_{xy}}{dB} \right)_{B_c} = \frac{1}{T^p} \left(\frac{d\rho_{xy}}{dx} \right)_{x=0}. \quad (4.83)$$

Similarly, if ΔB is defined by the shape difference $\Delta\rho_{xx} = \rho_{xx}(x + \Delta x) - \rho_{xx}(x - \Delta x)$, for a fixed Δx , then

$$\Delta B \propto T^p \Delta x. \quad (4.84)$$

Comparing these two equations gives the prediction $\alpha = \beta = p$.

Does this follow from the CFT explored above, and if so what is the predicted numerical size of p ? In the present instance σ^{ab} and ρ_{ab} come as functions of ν and σ_0 , and for small E we have $\sigma_0 = \sigma_0(\rho/T^{2/z})$. For a neutral background brane z is a parameter that is free to be dialed by adjusting the ‘Lifshitz sector’ that sets the background geometry, but the prediction $\sigma_0 = \sigma_0(\rho/T^{2/z})$ eventually breaks down for sufficiently small T . Alternatively, for a charged background brane this prediction survives to lower temperatures, and the near-horizon, near-extremal geometry gives the universal value $z = 5$ along the lines described in §3 and Appendix D. In either case we have the following scaling form for the conductivities

$$\sigma^{ab} = \sigma^{ab}(\nu, \sigma_0) = \sigma^{ab} \left(\frac{\rho}{T^{2/z}}, \frac{B}{T^{2/z}} \right), \quad (4.85)$$

where the same power of T appears with both the charge density, ρ , and magnetic field, B , because both have no anomalous dimension (since both J^μ and $\epsilon^{\mu\nu\lambda}F_{\nu\lambda}$ are conserved currents in 2+1 dimensions). Near a critical field, $B = B_c + \Delta B$, this is a function of two variables

$$\sigma^{ab} \simeq \sigma^{ab} \left(\Delta\nu, \frac{\Delta B}{T^{2/z}} \right), \quad (4.86)$$

and so has the form of eq. (4.82) for temperatures small enough that $\Delta B/T^{2/z} \gg \Delta\nu$. This regime then predicts $\alpha \simeq \beta \simeq p \simeq 2/z$. The observed exponent, $p \simeq 0.4$, corresponds to the choice $z \simeq 5$ for the dynamical exponent. Remarkably, this is precisely the universal value found for z in §3 and Appendix D for the near-horizon geometry of the near-extremal black hole.

Summary

Quantum Hall systems are characterized by an impressive suite of phenomena — quantization of the Hall conductivity; selection rules for allowed transitions between plateaux; semi-circle behaviour; $\rho_{xx} \rightarrow 1/\rho_{xx}$ duality — that control the properties of, and the transitions between, quantum Hall plateaux. The observational evidence for these phenomena is remarkably robust; more robust than the extant theoretical explanations that are based directly on the detailed dynamics of the underlying electrons.

All of these phenomena would be robustly explained if the very low-energy approach to the quantum Hall plateaux were controlled by the RG flow through an approximately two-dimensional subspace of the space of couplings, that commutes with the duality group $\Gamma_0(2) \subset SL(2, Z)$. There is good evidence that duality groups of this type can robustly emerge within 2+1 dimensional CFTs. What has been missing is an explicit class of CFTs within which this hypothesis can be made precise, and compared in more detail with the extant experiments.

The advent of AdS/CFT models including both a discrete duality group and nonzero DC ohmic and Hall conductivities opens up the first class of models of the required type, and so opens up a new way to describe the low-energy behaviour of quantum Hall systems. We provide an explicit calculation of the DC conductivities in a simple example of this class, and describe its predictions for the low-energy approach to the quantum Hall plateaux. It generically predicts an approach for which the ohmic conductivity vanishes as a power $T^{2/z}$, and some observations suggest $z \simeq 5$. Most remarkably, $z = 5$ is precisely the value predicted at low temperatures if the background is described by a charged dilaton-Maxwell or dilaton-DBI brane. Better yet, in this case the near-horizon, near-extremal geometry predicts $z = 5$ in the far IR even if $z = 1$ in the asymptotic geometry describing the UV.

The dilaton-DBI model examined here has several attractive ingredients likely to be worth incorporating into future AdS/CFT modeling of quantum Hall systems: the presence of the $SL(2, R)$ symmetry, broken by quantum effects to $SL(2, Z)$ or a subgroup; a DBI-like dynamics that natu-

rally incorporates nonlinear effects that go beyond linear response; and the attractor near-horizon, near-extremal geometry that can make universal predictions (like $z = 5$) for very low energies if taken beyond the probe approximation. Its main drawback is the necessity to work within the probe approximation to obtain a DC resistance, requiring the invocation of a separate ‘Lifshitz’ sector whose sole purpose is to generate the same background geometry.

But more interesting than this particular example is probably the opening up of a class of modular models, within which the drawbacks can be removed and a variety of more detailed comparisons with observations can begin to be explored.

Acknowledgements

We thank Shamit Kachru for giving a head’s up about ref. [11], and Sean Hartnoll, Gary Horowitz, Clifford Johnson, Rob Myers and Al Shapere for useful conversations. CB thanks summer students A. Chan, U. Hussein, Z.Y. Niu and Y.F. Wang for their help, and the Aspen Center for Physics for providing the spectacular environment where parts of this work were done, and BD thanks McMaster University and the Perimeter Institute for hospitality as work progressed. This research has been supported in part by funds from the Natural Sciences and Engineering Research Council (NSERC) of Canada. Research at the Perimeter Institute is supported in part by the Government of Canada through NSERC and by the Province of Ontario through the Ministry of Research and Information (MRI).

4.A Some useful properties of $SL(2, R)$ and $SL(2, Z)$

The purpose of this appendix is to group together useful facts about the groups $SL(2, R)$, $PSL(2, R)$ and their subgroups.

The group $SL(2, R)$ consists of real-valued (or, for $SL(2, Z)$, integer-valued) two-by-two matrices with unit determinant:

$$M := \begin{pmatrix} a & b \\ c & d \end{pmatrix}, \quad (4.87)$$

where $\det M = 1$ requires $ad - bc = 1$.

The group $PSL(2, R)$

Complex quantities can contain the action of this group through fractional-linear transformations,

$$z \rightarrow \frac{az + b}{cz + d}. \quad (4.88)$$

As is easily checked, repeated applications of this transformation rule reproduces the same group multiplication law as is obtained by multiplying the matrix representation M . Because eq. (4.88)

is invariant under a simultaneous change of sign in all four parameters, a , b , c and d , it is more properly regarded as a realization of the group $PSL(2, R)$ obtained from $SL(2, R)$ by identifying group elements that are related by $M \rightarrow -M$.

The real and imaginary parts of eq. (4.88) arise often in the main text, and are given by

$$z_1 \rightarrow \frac{ac(z_1^2 + z_2^2) + (ad + bc)z_1 + bd}{c^2(z_1^2 + z_2^2) + 2cdz_1 + d^2} \quad (4.89)$$

$$z_2 \rightarrow \frac{z_2}{c^2(z_1^2 + z_2^2) + 2cdz_1 + d^2}, \quad (4.90)$$

where $z := z_1 + iz_2$. The second of these equations is simplified using $ad - bc = 1$.

The group $SL(2, Z)$ and some of its subgroups

Any element of the group obtained when the elements of M are integer-valued can be generated as a product of powers of two specific elements, traditionally called

$$S := \begin{pmatrix} 0 & 1 \\ -1 & 0 \end{pmatrix} \quad \text{and} \quad T := \begin{pmatrix} 1 & 1 \\ 0 & 1 \end{pmatrix}, \quad (4.91)$$

for which the fraction-linear transformation, (4.88), becomes

$$S(z) = -\frac{1}{z} \quad \text{and} \quad T(z) = z + 1. \quad (4.92)$$

Direct matrix multiplication shows these have the property $(ST)^3 = 1$.

Regarded as acting on the complex variable z , the group $PSL(2, Z)$ maps the upper half-plane onto itself since both S and T preserve the sign of z_2 . Any point in the upper half-plane can be reached from a ‘fundamental domain’, which can be taken as the intersections of the regions $-\frac{1}{2} \leq z_1 \leq \frac{1}{2}$ and $|z| \geq 1$.

The subgroup $\Gamma_\theta(2)$

The subgroup²⁰ $\Gamma_\theta(2)$ can be defined as that subgroup of $SL(2, Z)$ that is generated by S and T^2 , rather than S and T . Since T^2 written explicitly is

$$T^2 := \begin{pmatrix} 1 & 2 \\ 0 & 1 \end{pmatrix}, \quad (4.93)$$

it is clear that both S and T^2 have the property that either b and c are both odd, or they are both even. Since this property is preserved under matrix multiplication, it is true for all of the elements of $\Gamma_\theta(2)$, and it can be regarded as an alternative definition of the group.

²⁰Our notation is taken from [56].

A fundamental domain for $\Gamma_\theta(2)$, from which the entire upper half-plane can be generated, can be taken as the intersection of the regions $-1 \leq z_1 \leq 1$ and $|z| \geq 1$.

The subgroup $\Gamma_0(2)$

The subgroup of $SL(2, Z)$ whose properties are relevant to fermions (and so to real quantum Hall systems) is $\Gamma_0(2)$. It can be defined, as in the main text, as that group obtained by conjugating the elements of $\Gamma_\theta(2)$ by the element $g = ST^{-1}S \in SL(2, Z)$:

$$\Gamma_0(2) = g\Gamma_\theta(2)g^{-1}. \quad (4.94)$$

To see what the generators of $\Gamma_0(2)$ are it suffices to conjugate the two generators of $\Gamma_\theta(2)$, to get:

$$\begin{aligned} gSg^{-1} &= (ST^{-1}S)S(STS) = ST^{-1}STS = ST^{-1}(ST)^{-2}S \\ &= ST^{-1}(T^{-1}S)^2S = ST^{-2}ST^{-1}, \end{aligned} \quad (4.95)$$

which uses $(ST)^3 = 1$ to write $ST = (ST)^{-2}$. Similarly,

$$\begin{aligned} gT^2g^{-1} &= (ST^{-1}S)T^2(STS) = ST^{-1}ST^2(ST)^{-2}S \\ &= ST^{-1}ST^2(T^{-1}S)^2S = ST^{-1}STST^{-1} \\ &= ST^{-2}ST^{-2}. \end{aligned} \quad (4.96)$$

But any group element that can be obtained from products of powers of these generators can equally well be generated by products of powers of the more usually chosen generators

$$ST^2S = \begin{pmatrix} -1 & 0 \\ -2 & -1 \end{pmatrix} \quad (4.97)$$

and T . Notice that both ST^2S and T have the property that the lower-left element c is even, and since this is preserved under group multiplication it is true for all of the elements of $\Gamma_0(2)$. The condition $ad - bc = 1$ then implies that both a and d must be odd. The condition of even c turns out to provide an equivalent definition of the group.

A fundamental domain for the group $\Gamma_0(2)$ can be taken as the intersections of the region $0 \leq z_1 \leq 1$ and $|z - \frac{1}{2}| \geq \frac{1}{2}$.

The group element as a function of B , χ and ρ

In §4 of the text the $SL(2, R)$ transformation is required that maps the special case of $B = \chi = 0$ onto the general case. This subsection determines the required transformations.

Starting with the xy -component of (4.23), we see

$$\begin{aligned} F_{xy} &= d(F_{xy})_0 - c(\tilde{G}_{xy})_0 \\ -\tilde{G}_{xy} &= b(F_{xy})_0 - a(\tilde{G}_{xy})_0, \end{aligned} \quad (4.98)$$

so using $F_{xy} = B$ and $\tilde{G}_{xy} = -\epsilon_{tvyx}G^{vt} = \sqrt{-g}G^{vt} = \rho$, and $B_0 = 0$, gives the relations

$$c = -\frac{B}{\rho_0} \quad \text{and} \quad a = \frac{\rho}{\rho_0}. \quad (4.99)$$

Finally, performing the inverse transformation to

$$e^{-\phi} = \frac{e^{-\phi_0}}{d^2 + c^2 e^{-2\phi_0}} \quad \text{and} \quad \chi = \frac{ac e^{-2\phi_0} + bd}{d^2 + c^2 e^{-2\phi_0}}. \quad (4.100)$$

gives

$$\chi_0 = 0 = \frac{-dc(\chi^2 + e^{-2\phi}) - ab + (ad + bc)\chi}{(a - c\chi)^2 + c^2 e^{-2\phi}}, \quad (4.101)$$

which can be solved for d once $b = (ad - 1)/c$ is used, giving

$$d = \rho_0 \left[\frac{\rho + B\chi}{(\rho + B\chi)^2 + B^2 e^{-2\phi}} \right], \quad (4.102)$$

and so $b = (ad - 1)/c$ is

$$b = \rho_0 \left[\frac{\chi(\rho + B\chi) + B e^{-2\phi}}{(\rho + B\chi)^2 + B^2 e^{-2\phi}} \right]. \quad (4.103)$$

The final form for the conductivities is therefore found by choosing $\rho = \rho_0^{21}$ and therefore $a = 1$, leading to $c = -B/\rho = 1/\nu$, where $\nu = -\rho/B$ is the filling fraction (with the sign appropriate for a negatively charged particle). The remaining two parameters then are

$$b = \frac{\nu [\chi(\nu - \chi) - e^{-2\phi}]}{(\nu - \chi)^2 + e^{-2\phi}} \quad \text{and} \quad d = \frac{\nu(\nu - \chi)}{(\nu - \chi)^2 + e^{-2\phi}}, \quad (4.104)$$

These are the results quoted in section §4.

4.B DBI thermodynamics

This section reproduces some of the thermodynamic properties of the dilaton-DBI system, which do not differ significantly from the non-dilaton case studied in ref. [13].

²¹As discussed in the main text, keeping $\rho \neq \rho_0$ allows the formulae to be generalized to arbitrary values for the charges of the carriers in the CFT.

Free Energy

The free energy (density) is found by evaluating the bulk action at the classical solution, and regarding the result as a function of the boundary values. Since the asymptotic value of A_t gives the chemical potential, the result is naturally viewed as a thermodynamic potential whose variables are T , μ , and B . It is convenient to instead work at fixed charge density, so we follow [13] (see also [57]) by performing the Legendre transformation to obtain the potential whose natural variables are T , ρ and B :

$$f(T) = \frac{TS_{\text{gauge}}}{V_2} + \mu J^t. \quad (4.105)$$

For the purposes of thermodynamics it suffices to work with the following gauge field ansatz,

$$A = \Phi(v) dt + Bx dy. \quad (4.106)$$

The solution to the field equations for Φ is then

$$F_{vt} = \Phi' = \frac{1}{v^{1+z}} \frac{C}{\sqrt{v^{-4} + \left(\frac{\ell^2}{L^2}\right)^2 (B^2 + C^2)}}, \quad (4.107)$$

where C is an integration constant. Eq. (4.107) can be integrated, to obtain

$$\Phi(v) = \mu(v_h) + \int_\epsilon^v \frac{d\hat{v}}{\hat{v}^{1+z}} \frac{C}{\sqrt{\hat{v}^{-4} + \left(\frac{\ell^2}{L^2}\right)^2 (B^2 + C^2)}}. \quad (4.108)$$

Here μ is another integration constant, to be interpreted as the chemical potential, whose value is determined by the condition that $\Phi(v_h) = 0$ at the black hole horizon. This gives the following expression for the chemical potential as a function of horizon position (temperature),

$$\mu(T) = \int_\epsilon^{v_h} \frac{d\hat{v}}{\hat{v}^{1+z}} \frac{C}{\sqrt{\hat{v}^{-4} + \left(\frac{\ell^2}{L^2}\right)^2 (B^2 + C^2)}}. \quad (4.109)$$

Expanding the solution near the conformal boundary, $v = 0$, gives

$$\Phi = \mu - \frac{1}{v^{z-2}} \left(\frac{C}{z-2} \right) + \dots, \quad (4.110)$$

which shows that the constant, C is related to the boundary charge density by

$$J^t = \mathcal{T} \ell^4 C. \quad (4.111)$$

The free energy becomes

$$f(T) = -\mathcal{T} L^4 \int_{\epsilon}^{v_h} \frac{dv}{v^{1+z}} \frac{v^{-4} + \left(\frac{\ell^2}{L^2}\right)^2 B^2}{\sqrt{v^{-4} + \left(\frac{\ell^2}{L^2}\right)^2 (B^2 + C^2)}} + \mu(T) J^t, \quad (4.112)$$

with the second term evaluated using eq. (4.109). The resulting integral diverges, but since these divergences are independent of temperature they can be regulated by subtracting the free-energy at zero temperature, giving the finite result

$$\begin{aligned} \Delta f &:= f(T) - f(0) \\ &= -\mathcal{T} L^4 \int_{\infty}^{v_h} \frac{dv}{v^{1+z}} \sqrt{v^{-4} + \left(\frac{\ell^2}{L^2}\right)^2 (B^2 + C^2)} \end{aligned} \quad (4.113)$$

$$\propto \mathcal{T} \ell^2 L^2 T \sqrt{B^2 + C^2} + \frac{\mathcal{T} L^6 T^{1+4/z}}{\ell^2 \sqrt{B^2 + C^2}} + \dots, \quad (4.114)$$

where the ellipses denote higher orders in temperature. Without an exact form for $h(v)$ it is impossible to keep track of numerical factors in these expressions.

First and Second Order Quantities

Differentiating eq. (4.114) gives various thermodynamic quantities. The entropy is

$$S = -\frac{\partial f}{\partial T} \propto \mathcal{T} \ell^2 L^2 \sqrt{B^2 + C^2} + \frac{\mathcal{T} L^6}{\ell^2 \sqrt{B^2 + C^2}} T^{4/z}, \quad (4.115)$$

while the specific heat is

$$c_v = -T \frac{\partial^2 f}{\partial T^2} \propto \frac{\mathcal{T} L^6 T^{4/z}}{\ell^2 \sqrt{B^2 + C^2}}, \quad (4.116)$$

at low temperatures.

The regularization described above, simply subtracting the zero-temperature result, is insufficient to render the magnetization density finite since this doesn't involve differentiating with respect to temperature. It consequently receives a contribution from the diverging zero-temperature terms. The required integral is a hypergeometric function, which at low temperatures gives

$$m = -\frac{1}{V_2} \frac{\partial f}{\partial B} \propto \mathcal{T} \ell^2 L^2 \frac{T}{\sqrt{B^2 + C^2}} + \mathcal{T} \ell^2 L^2 B \epsilon^{-z+2}, \quad (4.117)$$

where ϵ is a cutoff representing the UV sensitivity of the temperature-independent contribution. Finally the magnetic susceptibility is (at zero magnetic field)

$$-\frac{1}{V_2} \frac{\partial^2 f}{\partial B^2} \propto \frac{\mathcal{T} \ell^2 L^2 T}{C} + \mathcal{T} \ell^2 L^2 \epsilon^{-z+2}, \quad (4.118)$$

where numerical factors are not followed in the relative normalization between the two terms.

4.C Validity of the Probe-brane Approximation

Here we investigate the region in which the probe brane approximation is valid, closely following [13]. We vary the action with respect to g_{tt} to find the energy density, and insist it must be less than the background energy density $\sim \frac{1}{\kappa^2 L^2}$.

Our action (assuming ohmic conductivity and a constant electric field) takes the form

$$S_{\text{gauge}} = -\mathcal{T} \int d^4x \sqrt{-g} \sqrt{1 + \ell^4 e^{-\phi} (g^{tt} g^{vv} (\Phi')^2 + g^{vv} g^{xx} (\mathcal{A}')^2 + g^{tt} g^{xx} E^2)} \quad (4.119)$$

$$= -\mathcal{T} \int d^4x \sqrt{-g} X. \quad (4.120)$$

Varying this action with respect to g_{tt} gives

$$\frac{\mathcal{T}}{\sqrt{-g} X} (g_{xx}^2 g_{vv} + \ell^4 e^{-\phi} (\mathcal{A}')^2 g_{xx}), \quad (4.121)$$

Similarly, the background energy density is found from varying $\sqrt{-g} \frac{1}{\kappa^2 L^2}$. This gives

$$\frac{g_{xx}^2 g_{vv}}{\sqrt{-g}} \frac{1}{\kappa^2 L^2}. \quad (4.122)$$

The probe brane condition is therefore

$$\gamma := \frac{1}{X} (1 + \ell^4 e^{-\phi} (\mathcal{A}')^2 g^{vv} g^{xx}) \ll \frac{1}{\kappa^2 L^2 \mathcal{T}}. \quad (4.123)$$

Since we're only interested in the conductivity calculation, this condition only needs to hold at v_* .

We evaluate γ using equation (4.22) of the main text,

$$\sqrt{-g} \frac{\mathcal{T} \ell^4 e^{-\phi}}{X} g^{vv} g^{xx} \mathcal{A}' = C^x \quad \text{and} \quad \sqrt{-g} \frac{\mathcal{T} \ell^4 e^{-\phi}}{X} g^{vv} g^{tt} \Phi' = C^t, \quad (4.124)$$

and plug this into the definition of γ . As in the conductivity calculation, we opt to trade the functions, Φ and \mathcal{A} , for the conserved quantities, C^t and C^x . This gives us

$$\gamma = X \left(\frac{1}{X^2} - \frac{(C^x)^2 g_{xx} g_{vv}}{g \mathcal{T}^2 \ell^4 e^{-\phi}} \right) \quad (4.125)$$

$$= X \left(\frac{1}{X^2} - \frac{(C^x)^2}{g_{tt} g_{xx} \mathcal{T}^2 \ell^4 e^{-\phi}} \right) \quad (4.126)$$

$$= \sqrt{\frac{N}{D}} \left(\frac{D}{N} - D + 1 + \frac{(C^t)^2}{\mathcal{T}^2 \ell^4 e^{-\phi} g_{xx}^2} \right), \quad (4.127)$$

where

$$N := 1 + \ell^4 e^{-\phi} \left(\frac{E^2}{g_{tt}g_{xx}} \right) \quad (4.128)$$

$$D := 1 + \frac{1}{\mathcal{T}^2 \ell^4 e^{-\phi}} \left[\frac{(C^t)^2}{g_{xx}^2} + \frac{(C^x)^2}{g_{xx}g_{tt}} \right] \quad (4.129)$$

$$X = \sqrt{\frac{N}{D}}. \quad (4.130)$$

For small electric fields the conductivity is evaluated at $v_\star \simeq v_h$. Near the horizon $g_{tt} \rightarrow 0$ and so

$$X = \sqrt{\frac{N}{D}} \rightarrow \frac{\ell^4 e^{-\phi} \mathcal{T}}{\sigma^{xx}} \quad \text{as } v \rightarrow v_h. \quad (4.131)$$

We still haven't assumed that $v = v_\star$ yet. When we assume $v = v_\star$, $N = D = 0$. Finally, taking $v_\star \rightarrow v_h$, γ becomes

$$\gamma_{v_\star} = \left[\left(\frac{\sigma^{xx}}{\ell^4 e^{-\phi_\star} \mathcal{T}} \right) + \frac{\ell^4 e^{-\phi_\star} \mathcal{T}}{\sigma^{xx}} + \frac{(C^t)^2}{\mathcal{T} \sigma^{xx} g_{xx\star}^2} \right]. \quad (4.132)$$

The conductivity itself is given by

$$\sigma^{xx} = \sqrt{(\mathcal{T} \ell^4 e^{-\phi_\star})^2 + \ell^4 e^{-\phi_\star} (C^t)^2 / (g_{xx\star}^2)}, \quad (4.133)$$

allowing us to write γ_\star in terms of the ohmic conductivity as

$$\gamma_\star = \frac{2\sigma^{xx}}{\ell^4 e^{-\phi_\star} \mathcal{T}}. \quad (4.134)$$

We can now put a constraint on the conductivity, σ^{xx} , instead of γ_\star . Using (4.123), our condition is (dropping factors of order unity)

$$\sigma^{xx} \ll \frac{\ell^4 e^{-\phi_\star}}{L^2 \kappa^2}. \quad (4.135)$$

To be clear, we took the limit $v \rightarrow v_\star$, and used the fact that $N = D = 0$ in this limit, while keeping their ratio undetermined. We then took the limit²² $v_\star \rightarrow v_h$, which then fixes the ratio $\frac{N}{D}$ in terms of the conductivity, σ^{xx} . Notice how this condition on σ^{xx} is independent of brane tension and just on the ratio of the coupling strengths of the gauge and gravity sector.

We can use this relation to put a constraint on the charge density instead. Since we know at low temperatures, σ^{xx} behaves as

$$\sigma^{xx} \simeq v_\star^2 \ell^2 \rho e^{-\phi_\star/2}, \quad (4.136)$$

there is a condition on rho,

$$\rho \ll \frac{\ell^2 e^{-\phi_\star/2}}{v_\star^2 \kappa^2 L^2}. \quad (4.137)$$

²²The alert reader will notice that the argument above takes these limits in the opposite order, but the same result can be obtained by first letting $v \rightarrow v_\star$ provided l'Hôpital's rule is used to resolve the limit $N/D = N'/D'$ that arises in the result.

This ensures that we can not go to zero temperature ($v_* \sim v_h \rightarrow \infty$) for finite values of ρ without taking our gauge coupling, $\ell^2 e^{-\phi}$ to infinity (weak coupling).

Dilaton Field Equations

We can now ask what happens to the dilaton equations of motion near the horizon. We again focus on $\chi = 0$ and an ohmic conductivity with a constant electric field. Looking at the source term of the dilaton equation,

$$\square\phi = -\frac{\kappa^2 \mathcal{T} \ell^4 e^{-\phi}}{4X} [g^{tt} g^{vv} (\Phi')^2 + g^{vv} g^{xx} (\mathcal{A}')^2 + g^{tt} g^{xx} E^2], \quad (4.138)$$

we can again trade out the gauge functions for the conserved quantities. This makes the source of the dilaton equation,

$$\square\phi = -\frac{\kappa^2 \mathcal{T} (X^2 - 1)}{4X}. \quad (4.139)$$

We take the near-horizon limit and use (4.131) to express this in terms of the ohmic conductivity,

$$\frac{4\square\phi}{\kappa^2} = -\frac{\mathcal{T}^2 \ell^4 e^{-\phi}}{\sigma^{xx}} + \frac{\sigma^{xx}}{e^{-\phi} \ell^4}. \quad (4.140)$$

This is actually quite interesting - it seems that the dilaton is driven to strong or weak coupling depending on the initial value of the dilaton and the conductivity. In fact, with too large a conductivity the dilaton is driven to strong coupling, ruining our probe brane approximation near the horizon. Of course, this can always be remedied by choosing a sufficiently weak coupling as our initial value of the dilaton when integrating the equations of motion.

4.D DBI near-horizon extremal geometry

In this section we compute the attractor exponent z for the near-horizon geometry of the extremal black hole using the dilaton-DBI action beyond the probe-brane approximation, verifying that $z = 5$ as for the dilaton-Maxwell case. Although our real interest is the near-extremal case in order to maintain calculational control, the simpler extremal geometry suffices for the purpose of identifying z . For simplicity we work with the purely electric black brane in dilaton-DBI gravity, with both the magnetic and axion fields set to zero. We return to generalizing to near-extremal and nonzero magnetic and axion fields at the end.

Action and field equations

With the axion set to zero the action becomes

$$S = - \int d^4x \sqrt{-g} \left\{ \frac{1}{2\kappa^2} \left[R - 2\Lambda + \frac{1}{2} \partial_\mu \phi \partial^\mu \phi \right] + \mathcal{T}(X - 1) \right\}, \quad (4.141)$$

with

$$X = \sqrt{1 + \frac{\ell^4}{2} e^{-\phi} F^2 - \frac{\ell^8}{16} e^{-2\phi} (F\tilde{F})^2}, \quad (4.142)$$

as before. The field equations for this action are

$$\nabla_\mu G^{\mu\nu} = 0, \quad (4.143)$$

$$\square\phi + \frac{\kappa^2}{4} G^{\mu\nu} F_{\mu\nu} = 0, \quad (4.144)$$

with

$$G^{\mu\nu} = \frac{\mathcal{T}\ell^4}{X} \left[e^{-\phi} F^{\mu\nu} - \frac{\ell^4}{4} e^{-2\phi} (F\tilde{F})\tilde{F}^{\mu\nu} \right], \quad (4.145)$$

and

$$R_{\mu\nu} + \frac{1}{2} \partial_\mu \phi \partial_\nu \phi - \Lambda g_{\mu\nu} + \frac{\kappa^2 \mathcal{T}}{X} \left[\ell^4 e^{-\phi} F_{\mu\lambda} F_\nu{}^\lambda - (X - 1) g_{\mu\nu} \right] = 0. \quad (4.146)$$

Radial ansatz

We seek solutions to these equations subject to the ansatz $\phi = \phi(r)$ and $F = F_{rt}(r) dr \wedge dt$, with metric

$$ds^2 = -h(r) e^{-\xi(r)} dt^2 + \frac{dr^2}{h(r)} + r^2(dx^2 + dy^2). \quad (4.147)$$

These coordinates are related to those in the main text by $r = 1/v$, so conformal infinity is at $r \rightarrow \infty$ and the horizon is at $r = 0$ (for an extremal black brane).

The Maxwell equation, eq. (4.143), integrates to give

$$G^{rt} = - \frac{Q_e e^{\xi/2}}{r^2}, \quad (4.148)$$

where Q_e is an integration constant. Combining this with the constitutive relation, eq. (4.145), then gives (after some algebra)

$$-e^{-\phi} F^2 = \frac{4Q_e^2}{2Q_e^2 \ell^4 + \frac{1}{4} (T\ell^4)^2 r^4 e^{-\phi}}. \quad (4.149)$$

The dilaton equation, eq. (4.144), evaluated using the above ansatz becomes

$$\left(r^2 e^{-\xi/2} h \phi' \right)' - \frac{\kappa^2 Q_e}{4} F_{rt} = 0, \quad (4.150)$$

where primes denote differentiation with respect to r . Evaluation of the Einstein equations requires the following components of the Ricci tensor,

$$\begin{aligned} g^{tt}R_{tt} &= \frac{h''}{2} - \frac{3h'\xi'}{4} - \frac{h\xi''}{2} + \frac{h(\xi')^2}{4} + \frac{h'}{r} - \frac{h\xi'}{r}, \\ g^{rr}R_{rr} &= \frac{h''}{2} - \frac{3h'\xi'}{4} - \frac{h\xi''}{2} + \frac{h(\xi')^2}{4} + \frac{h'}{r}, \\ g^{xx}R_{xx} = g^{yy}R_{yy} &= \frac{h'}{r} - \frac{h\xi'}{2r} + \frac{h}{r^2}. \end{aligned} \quad (4.151)$$

With these, the $(tt) - (rr)$ Einstein equation becomes

$$\xi' + \frac{r}{2} (\phi')^2 = 0, \quad (4.152)$$

while the (xx) and (yy) Einstein equations give

$$\frac{h'}{r} - \frac{h\xi'}{2r} + \frac{h}{r^2} = \Lambda + \kappa^2 \mathcal{T} \left(\frac{X-1}{X} \right). \quad (4.153)$$

Solutions

Eq. (4.153) has a simple power-law solution for any region where X is approximately constant. These resemble the known solutions [49] for the pure dilaton-Maxwell case, which are included here as the special case $r \rightarrow \infty$ since $e^{-\phi} F^2 \rightarrow 0$ implies $X \rightarrow 1$ in this regime. The power-law solution is

$$h \propto r^2 \quad \text{and} \quad e^{-\xi} \propto r^{\omega_\xi}, \quad (4.154)$$

for any ω_ξ . Eq. (4.152) then implies ϕ is also described by a power law,

$$e^\phi \propto r^{\omega_\phi}, \quad (4.155)$$

with $\omega_\xi = \frac{1}{2} \omega_\phi^2$. There are two ways that F_{rt} can then scale consistent with having X constant, and these define the regimes of large and small r that are of particular interest.

Large- r regime

The large- r regime exploits the above solution by choosing $\omega_\phi = \omega_\xi = 0$, which implies $r^4 e^{-\phi} \rightarrow \infty$ as $r \rightarrow \infty$ and so — from eq. (4.149) — we have $e^{-\phi} F^2 \propto 1/r^4 \rightarrow 0$ and so $X \rightarrow 1$. In this limit eq. (4.145) implies the Maxwell field falls off as

$$F_{rt} \propto \frac{1}{r^2}, \quad (4.156)$$

which, when used in the dilaton equation, eq. (4.150), gives the sub-dominant fall-off: $\phi - \phi_\infty \propto 1/r^4$. This gives the asymptotic geometry

$$ds^2 \simeq h_\infty r^2 dt^2 + \frac{dr^2}{h_0 r^2} + r^2(dx^2 + dy^2), \quad (4.157)$$

and so defining the anisotropic exponent z by $g_{tt} \propto r^{2z}$ when $g_{xx} = g_{yy} \propto r^2$ shows that $z = 1$ in the UV (large- r) limit.

Small- r regime

The other regime of constant X is the near-horizon limit, $r \rightarrow 0$. In this case X can be constant if $e^\phi \propto r^4$ as $r \rightarrow 0$, so that $r^4 e^{-\phi}$ in the denominator of eq. (4.149) approaches a constant. The same arguments as given above using the Einstein equations then show $h \propto r^2$ and $e^{-\xi} \propto r^8$. The constitutive equation, (4.145), then implies $F_{rt} \propto r^6$, which when used in the dilaton equation, eq. (4.150), gives the consistency condition

$$\left(r^4 e^{-\xi/2} \phi'\right)' \propto r^6, \quad (4.158)$$

which is consistent with the above choices: $\phi' \propto 1/r$ and $e^{-\xi/2} \propto r^4$.

This gives the asymptotic near-horizon geometry as

$$ds^2 \simeq h_0 r^{10} dt^2 + \frac{dr^2}{h_0 r^2} + r^2(dx^2 + dy^2). \quad (4.159)$$

Again defining the anisotropic exponent z by $g_{tt} \propto r^{2z}$ when $g_{xx} = g_{yy} \propto r^2$ shows that $z = 5$ in the IR (near-horizon) limit.

Once these powers are chosen the values of the pre-multiplying constants are also fixed by the field equations. That is, if $h \simeq h_h r^2$, $e^\phi \simeq e^{\phi_h} r^4$ and $e^{-\xi} \simeq e^{-\xi_h} r^8$ then the constants h_h , ϕ_h and ξ_h can be computed using the field equations. This implies a prediction, in particular for the value, X_h , obtained by the function X as $r \rightarrow 0$, given by

$$X_h = \frac{\sqrt{(6 + 2\hat{\mathcal{T}})^2 + 5\hat{\mathcal{T}}^2} - (6 + 2\hat{\mathcal{T}})}{\hat{\mathcal{T}}}, \quad (4.160)$$

where $\hat{\mathcal{T}} := \kappa^2 L^2 \mathcal{T}$ is a dimensionless brane tension. Notice this has the property that $0 \leq X_h \leq 1$, with X_h varying from zero to unity as $\hat{\mathcal{T}}$ varies from zero to infinity, and always satisfies $\kappa^2 L^2 \mathcal{T} / X_h > 1$.

Generalizations

We next record in passing several easy generalizations to these solutions.

Near-extremal black hole

There is a simple generalization of the $r \rightarrow 0$ solution to include a nonzero temperature. This comes from the recognition that $h \propto r^2$ is not the only solution to eq. (4.153) in the regime where X is constant. Since this equation is linear in h a more general solution is obtained by adding to this the solution to the homogeneous equation,

$$\frac{h'}{r} - \frac{h\xi'}{2r} + \frac{h}{r^2} = \frac{h'}{r} + \frac{5h}{r^2} = 0, \quad (4.161)$$

where the first equality uses the same solution for ξ as before: $\xi' = -8/r$. The more general solution is then clearly

$$h = h_0 r^2 \left[1 - \left(\frac{r_h}{r} \right)^7 \right], \quad (4.162)$$

where the integration constant, r_h , denotes the nonzero position of the horizon of the now non-extremal black hole.

Since only $h(r)$ is modified, eqs. (4.152) and (4.149) remain solved using the previous solutions $e^\phi \propto r^4$ and $e^{-\xi} \propto r^8$. Furthermore, since F^2 is independent of $h(r)$ it is still true that X is constant for this new solution. All that remains is to check the dilaton equation, eq. (4.150), which is easily seen to be solved because r_h drops out of

$$\left(r^2 e^{-\xi/2} h \phi' \right)' = 4h_0 e^{-\xi_0/2} \left\{ r^7 \left[1 - \left(\frac{r_h}{r} \right)^7 \right] \right\}' = 28h_0 e^{-\xi_0} r^6. \quad (4.163)$$

This solution provides the near-horizon, near-extremal geometry that governs the low-temperature limit. In particular, it verifies that the presence of a nonzero temperature does not change the value found earlier for $z = 5$ in the far IR.

Nonzero axion and magnetic field

Another trivial generalization is to act on the above near-horizon solutions with $SL(2, R)$ to generate their analogs having nonzero axion and magnetic fields. Because the field equations and Bianchi identities demand $\tilde{G}_{xy} = \sqrt{-g} G^{rt} = -Q_e$ and $F_{xy} = Q_m$ are constants, it is useful to use the $SL(2, R)$ transformations

$$(-\tilde{G}_{xy}) = a(-\tilde{G}_{xy})_0 + b(F_{xy})_0 \quad \text{and} \quad (F_{xy}) = c(-\tilde{G}_{xy})_0 + d(F_{xy})_0, \quad (4.164)$$

to learn $a = 1$ (if we demand we do not change Q_e) and $c = Q_m/Q_e$ (if we start from zero magnetic charge, $Q_m = 0$). Then after transforming the axion and dilaton become

$$e^\phi = c^2 e^{-\phi_0} + d^2 e^{\phi_0} \quad \text{and} \quad \chi = \frac{ac + bd e^{2\phi_0}}{c^2 + d^2 e^{2\phi_0}} \simeq \frac{Q_e}{Q_m} [1 + \mathcal{O}(r^8)], \quad (4.165)$$

which uses $e^{\phi_0(r)} \propto r^4$ as $r \rightarrow 0$. This shows that e^ϕ is driven to strong coupling (for which the above classical arguments break down) as soon as $Q_m \neq 0$. The axion is similarly driven to $\chi \rightarrow Q_e/Q_m$ as $r \rightarrow 0$, and although this classical conclusion cannot be trusted in the strong-coupling limit, the attraction to quantized fractions is an exact consequence of unbroken $PSL(2, Z)$ (or one of its subgroups).

Bibliography

- [1] J. M. Maldacena, Adv. Theor. Math. Phys. **2** (1998) 231 [Int. J. Theor. Phys. **38** (1999) 1113] [hep-th/9711200];
S. S. Gubser, I. R. Klebanov and A. M. Polyakov, Phys. Lett. B **428** (1998) 105 [hep-th/9802109];
E. Witten, “Anti-de Sitter space and holography,” Adv. Theor. Math. Phys. **2** (1998) 253 [hep-th/9802150].
- [2] For a particularly good introduction to nonspecialists see: G. T. Horowitz and J. Polchinski, “Gauge / gravity duality,” [gr-qc/0602037];
- [3] O. Aharony, S. S. Gubser, J. M. Maldacena, H. Ooguri and Y. Oz, “Large N field theories, string theory and gravity,” Phys. Rept. **323** (2000) 183 [hep-th/9905111];
I. R. Klebanov, “TASI lectures: Introduction to the AdS/CFT correspondence,” [hep-th/0009139].
- [4] S. A. Hartnoll, “Lectures on holographic methods for condensed matter physics,” Class. Quant. Grav. **26** (2009) 224002 [arXiv:0903.3246 [hep-th]];
C. P. Herzog, “Lectures on Holographic Superfluidity and Superconductivity,” J. Phys. A **42** (2009) 343001 [arXiv:0904.1975 [hep-th]];
J. McGreevy, “Holographic duality with a view toward many-body physics,” arXiv:0909.0518 [hep-th];
S. Sachdev, “Condensed matter and AdS/CFT,” arXiv:1002.2947 [hep-th].
- [5] The literature is vast; for a good (but fairly old) review see S.M. Girvin, cond-mat/9907002.
- [6] C.P. Burgess and B.P. Dolan, *Particle-Vortex Duality and the Modular Group: Applications to the quantum Hall Effect and Other 2-D Systems*, Phys. Rev. **B63** 155309 (2001), [hep-th/0010246]
- [7] E. Witten, “SL(2,Z) Action On Three-Dimensional Conformal Field Theories With Abelian Symmetry,” in Shifman, M. (ed.) et al.: *From fields to strings*, vol. 2, 1173-1200, [hep-th/0307041].

- [8] C. P. Herzog, P. Kovtun, S. Sachdev and D. T. Son, “Quantum critical transport, duality, and M-theory,” *Phys. Rev. D* **75** (2007) 085020 [hep-th/0701036].
- [9] S. A. Hartnoll and C. P. Herzog, “Ohm’s Law at strong coupling: S duality and the cyclotron resonance,” *Phys. Rev. D* **76** (2007) 106012 [arXiv:0706.3228 [hep-th]].
- [10] K. Goldstein, S. Kachru, S. Prakash and S. P. Trivedi, “Holography of Charged Dilaton Black Holes,” arXiv:0911.3586 [hep-th].
- [11] K. Goldstein, N. Iizuka, S. Kachru, S. Prakash, S. P. Trivedi and A. Westphal, “Holography of Dyonic Dilaton Black Branes,” arXiv:1007.2490 [hep-th].
- [12] S. A. Hartnoll and P. Kovtun, “Hall conductivity from dyonic black holes,” *Phys. Rev. D* **76** (2007) 066001 [arXiv:0704.1160 [hep-th]];
J. L. Davis, P. Kraus and A. Shah, “Gravity Dual of a Quantum Hall Plateau Transition,” *JHEP* **0811** (2008) 020 [arXiv:0809.1876 [hep-th]];
O. Bergman, N. Jokela, G. Lifschytz and M. Lippert, “Quantum Hall Effect in a Holographic Model,” arXiv:1003.4965 [hep-th];
F. Aprile, S. Franco, D. Rodriguez-Gomez and J. G. Russo, “Phenomenological Models of Holographic Superconductors and Hall currents,” *JHEP* **1005** (2010) 102 [arXiv:1003.4487 [hep-th]];
T. Albash and C. V. Johnson, “Landau Levels, Magnetic Fields and Holographic Fermi Liquids,” *J. Phys. A* **43** (2010) 345404 [arXiv:1001.3700 [hep-th]];
J. Tarrío, “Holographic operator mixing - the Hall experiment,” arXiv:0911.4976 [hep-th];
J. Alanen, E. Keski-Vakkuri, P. Kraus and V. Suur-Uski, “AC Transport at Holographic Quantum Hall Transitions,” *JHEP* **0911** (2009) 014 [arXiv:0905.4538 [hep-th]].
- [13] S. A. Hartnoll, J. Polchinski, E. Silverstein and D. Tong, “Towards strange metallic holography,” *JHEP* **1004**, 120 (2010) [arXiv:0912.1061 [hep-th]].
- [14] H.L. Stormer, *Physica B*177 (1992) 401.
- [15] M. Hilke *et.al.*, *Europhysics Letters*, 46 (1999) 775-779; [cond-mat/9810217].
- [16] M. Hilke *et.al.*, *Nature*, **395** (1998) 675-677; [cond-mat/9810172].
- [17] B.P. Dolan, *Phys. Rev.* **B62**, 10278 (2000), [cond-mat/0002228] ;
B. P. Dolan, “Modular symmetry and temperature flow of conductivities in quantum Hall systems with varying Zeeman energy,” arXiv:1006.5361 [cond-mat.str-el].
- [18] K. Yang *et.al.*, *Journal of Physics: Condensed Matter*, **12** (2000) 5343-5360; [cond-mat/9805341].

- [19] D. Shahar *et.al.*, *Science* 274 (1995) 589, [cond-mat/9510113].
- [20] B. Huckestein, *Reviews of Modern Physics* **67** (1995) 357-396; [cond-mat/9501106].
- [21] H.P. Wei *et.al.*, *Phys. Rev. Lett.* 61 (1988) 1294;
P.T. Coleridge, *Phys. Rev.* B60, 4493 (1999);
P.T. Coleridge, *Solid State Comm.* 112, 241 (1999).
- [22] D. Shahar *et.al.*, *Solid State Comm.* 107 (1998) 19-23, [cond-mat/9706045].
- [23] J. L. Cardy and E. Rabinovici, “Phase Structure Of Z(P) Models In The Presence Of A Theta Parameter,” *Nucl. Phys. B* **205** (1982) 1.
- [24] C.A. Lütken and G.G. Ross, *Phys. Rev.* **B45**, 11837 (1992).
- [25] C.A. Lütken and G.G. Ross, *Phys. Rev.* **B48**, 2500 (1993).
- [26] C.A. Lütken, *J. Phys.* **A26** L811 (1993); *Nuc. Phys.* **B396** 670 (1993);
C.P. Burgess and C.A. Lutken, “One-dimensional flows in quantum Hall systems,” *Nuc. Phys.* **500** (1997) 367, [cond-mat/9611118];
“On the Implications of Discrete Symmetries for the β -function of quantum Hall Systems,”
C.P. Burgess and C.A. Lutken, *Phys. Lett.* **B451** 365 (1999), [cond-mat/9812396].
- [27] D-H. Lee, S. Kivelson and S-C. Zhang, *Phys. Lett.* **68**, 2386 (1992);
S. Kivelson, D-H. Lee and S-C. Zhang, *Phys. Rev.* **B46**, 2223 (1992).
- [28] J.K Jain, S.A. Kivelson and N. Trivedi, *Phys. Rev. Lett.* **64** (1990) 1927;
J.K. Jain and V.J. Goldman, *Phys. Rev.* **B45** 1255 (1992)
- [29] E. Fradkin and S. Kivelson, “Modular invariance, self-duality and the phase transitions between quantum Hall plateaus,” *Nucl. Phys.* **B474** (FS) (1996) 543–574.
- [30] C.P. Burgess, Rim Dib and B.P. Dolan, “Derivation of the Semi-circle Law from the Law of Corresponding States,” *Phys. Rev.* **B62** 15359 (2000), [cond-mat/9911476];
- [31] B.P. Dolan, *J. Phys.* **A32** L243 (1999), [cond-mat/9805171].
- [32] C.F. Huang *et al.*, “An experimental study on $\Gamma(2)$ modular symmetry on the quantum Hall system with a small spin-splitting,” *Journal of Physics: Condensed Matter* **19** (2007) 026205; [cond-mat/0609310].
- [33] C. P. Burgess and B. P. Dolan, “Duality and Non-linear Response for Quantum Hall Systems,” *Phys. Rev. B* **65**, 155323 (2002) [cond-mat/0105621].

- [34] C. P. Burgess and B. P. Dolan, “The Quantum Hall Effect in Graphene: Emergent Modular Symmetry and the Semi-circle Law,” *Phys. Rev. B* **76** (2007) 113406 [cond-mat/0612269].
- [35] M.P.A. Fisher and D.H. Lee, *Physical Review B* **39**, 2756 (1989).
- [36] A. Shapere and F. Wilczek, *Nuc. Phys.* **B320** 669 (1989);
S. J. Rey and A. Zee, “Selfduality of Three-Dimensional Chern-Simons Theory,” *Nucl. Phys. B* **352** (1991) 897.
- [37] C. P. Burgess and B. P. Dolan, “Duality, the Semi-Circle Law and Quantum Hall Bilayers,” *Phys. Rev. B* **76** (2007) 155310 [cond-mat/0701535].
- [38] For a review with references see: S-C. Zhang, *Int. J. Mod. Phys. B* **6**, 25 (1992).
- [39] For a review of the composite fermion picture see e.g. *Composite Fermions: A unified view of the Quantum Hall Regime* ed. O. Heinonen, (1998) World Scientific.
- [40] D. Bak and S. J. Rey, “Composite Fermion Metals from Dyon Black Holes and S-Duality,” arXiv:0912.0939 [hep-th].
- [41] F. Wilczek, *Lectures on Fractional Statistics and Anyon Superconductivity*, http://ccdb4fs.kek.jp/cgi-bin/img_index?9009083;
E.H. Fradkin, *Field theories of condensed matter systems*, Addison-Wesley (1991) (Frontiers in physics, 82).
- [42] S. Weinberg, *Gravitation and Cosmology: principles and applications of the general theory of relativity*, John Wiley & Sons (New York) 1972.
- [43] C.W. Misner, K.S. Thorne and J.A. Wheeler, *Gravitation*, W.H. Freeman (San Francisco) 1973.
- [44] G. W. Gibbons and D. A. Rasheed, “SL(2,R) Invariance of Non-Linear Electrodynamics Coupled to An Axion and a Dilaton,” *Phys. Lett. B* **365** (1996) 46 [hep-th/9509141].
- [45] D. K. Hong and H. U. Yee, “Holographic aspects of three dimensional QCD from string theory,” *JHEP* **1005** (2010) 036 [arXiv:1003.1306 [hep-th]].
- [46] N. Seiberg and E. Witten, “Monopole Condensation, And Confinement In N=2 Supersymmetric Yang-Mills Theory,” *Nucl. Phys. B* **426** (1994) 19 [Erratum-ibid. B **430** (1994) 485] [hep-th/9407087];
“Monopoles, duality and chiral symmetry breaking in N=2 supersymmetric QCD,” *Nucl. Phys. B* **431** (1994) 484 [hep-th/9408099].
- [47] P. Breitenlohner and D.Z. Freedman, “Stability in Gauged Extended Supergravity,” *Ann. Phys.* **144** (1982) 249.

- [48] I.R. Klebanov and E. Witten, “AdS/CFT Correspondence and Symmetry Breaking,” Nucl. Phys. **B536** (1998) 199 [hep-th/9905104];
E. Witten, “Multi-trace Operators, Boundary Conditions and AdS/CFT Correspondence,” [hep-th/0112258];
M. Berkooz, A. Sever and A. Shomer, “Double-trace Deformations, Boundary Conditions and Spacetime Singularities,” JHEP 05 (2002) 034 [hep-th/0112264];
P. Minces, “Multi-trace Operators and the Generalized AdS/CFT Prescription,” [hep-th/0201172];
V.K. Dobrev, “Intertwining Operator Realization of the AdS/CFT Correspondence,” Nucl. Phys. **B553** (1999) 559 [hep-th/9812194].
- [49] M. Taylor, [arXiv:0812.0530].
- [50] S. Ferrara, R. Kallosh and A. Strominger, “N=2 extremal black holes,” Phys. Rev. D **52** (1995) 5412 [hep-th/9508072].
- [51] For a review see: S. Bellucci, S. Ferrara, R. Kallosh and A. Marrani, “Extremal Black Hole and Flux Vacua Attractors,” Lect. Notes Phys. **755** (2008) 115 [arXiv:0711.4547 [hep-th]].
- [52] A. Karch and A. O’Bannon, “Metallic AdS/CFT,” JHEP **0709** (2007) 024 [arXiv:0705.3870 [hep-th]];
- [53] A. O’Bannon, “Hall Conductivity of Flavor Fields from AdS/CFT,” Phys. Rev. D **76** (2007) 086007 [arXiv:0708.1994 [hep-th]];
K. B. Fadafan, “Drag force in asymptotically Lifshitz spacetimes,” arXiv:0912.4873 [hep-th].
- [54] C. P. Burgess, “Open String Instability in Background Electric Fields,” Nucl. Phys. B **294** (1987) 427;
V.V. Nesterenko, “The Dynamics of Open Strings in a Background Electric Field,” Int. J. Mod. Phys. **A4** (1989) 2627;
C. Bachas and M. Porrati, “Pair Creation of Open Strings in an Electric Field,” Phys. Lett. **B296** (1992) 77 [hep-th/9209032].
- [55] W. Pan *et.al.*, “Exact Quantization of Even-Denominator Fractional Quantum Hall State at $\nu = \frac{5}{2}$ Landau Level Filling Factor,” Phys. Rev. Lett. **83** (1999) 3530, cond-mat/9907356.
- [56] N. Koblitz, *Introduction to Elliptic Curves and Modular Forms*, Springer-Verlag 1984 (2nd edition 1993).
- [57] S.W. Hawking and S.F. Ross, “Duality between Electric and Magnetic Black Holes,” Phys. Rev. **D52** (1995) 5865 [hep-th/9504019].

Chapter 5

Holographic Finite Scaling

Preface

While the preceding paper in chapter 4 presents a model for the quantum Hall effect using gauge-gravity duality that captures much of the experimental physics, a number of issues still remain. One of these issues is the experimental observation that the dynamical critical exponent in quantum Hall systems has been measured to be $z = 1$ in a number of experiments. However, the quantum Hall model which predicts $p = 0.4 = 2/z$ requires that $z = 5$. This apparent contradiction creates a potential problem for the Hall-ographic model. One of these experiments measuring $z = 1$ is quickly resolved when it is understood that the measurement is done in the UV [24], which is in agreement with the quantum Hall-ography since $z = 1$ in the UV. Another experiment measuring $z = 1$ is done through the measurement of the finite size scaling of the quantum Hall system [25]. The purpose of this paper is first and foremost to develop a framework in which to treat finite size effects in AdS/CMT, and then applying it to our quantum Hall-ography model. In particular, the finite size scaling paper is to see whether it is possible to produce the results of [25] while still maintaining the $z = 5$ result in the IR. It turns out in the purely scale-invariant case, our framework does not agree with experiment. This is due to very basic scaling arguments in which the only parameters entering the system are temperature, system size, and charge density. However, this paper does leave the door open for interesting scaling behaviour in the non-scale invariant case, in which an additional dimensionful parameter becomes a relevant quantity in the system. While this paper doesn't have a definite conclusion in which way this new parameter affects the scaling, its existence leads to potential future research programs to better understand the field theory corresponding to our quantum Hall-ography model.

Abstract

At low temperatures observations of the Hall resistance for Quantum Hall systems at the interface between two Hall plateaux reveal a power-law behaviour, $dR_{xy}/dB \propto T^{-p}$ (with $p = 0.42 \pm 0.01$); changing at still smaller temperatures, $T < T_s$, to a temperature-independent value. Experiments also show that the transition temperature varies with sample size, L , according to $T_s \propto 1/L$. These experiments pose a potential challenge to the holographic AdS/QHE model recently proposed in [arXiv:1008.1917](#). This proposal, which was motivated by the natural way AdS/CFT methods capture the emergent duality symmetries exhibited by quantum Hall systems, successfully describes the scaling exponent p by relating it to an infrared dynamical exponent z with $p = 2/z$. For a broad class of models z is robustly shown to be $z = 5$ in the regime relevant to the experiments (though becoming $z = 1$ further in the ultraviolet). By incorporating finite-size effects into these models we show that they reproduce a transition to a temperature-independent regime, predicting a transition temperature satisfying $T_s \propto 1/L^{n+1}$, even though $z = 5$ governs the temperature dependence of the conductivity in all cases. The parameter n depends on how a brane tension, \mathcal{T} , scales as L varies, with $n = 4$ (so $T_s \propto 1/L^5$) if the tension is negligible or scale invariant. $T_s \propto 1/L$ corresponds to $\mathcal{T} \propto L^2$. The possibility of a deviation from naive $z = 5$ scaling arises because the brane tension introduces a new scale, which alters where the transition between UV and IR scaling occurs, in an L -dependent way. The AdS/CFT calculation indicates the two regimes of temperature scaling are separated by a first-order transition, suggesting new possibilities for testing the picture experimentally. Remarkably, in this interpretation the gravity dual of the transition from temperature scaling to temperature-independent resistance is related to the Chandrasekhar transition from a star to a black hole with increasing mass.

5.1 Introduction

In essence the AdS/CFT correspondence asserts that the space of field theories is smaller than had been previously thought: two theories previously believed to be unrelated to one another turn out to be different descriptions of the same physics [1]. This equivalence was not understood earlier because it is the strongly coupled limit of one theory in the pair that is equivalent to the weakly coupled limit of the other, and vice versa. What is most remarkable is how dramatically different the two related theories superficially are: a non-gravitational theory in d dimensions is equivalent to a gravitational theory in $d + 1$ dimensions. See ref. [2] (or refs. [3]) for an intuitive (or more detailed) review.

This observation has generated considerable recent interest in applying AdS/CFT methods to condensed matter systems (for reviews, see [4]). The desired end-game for these studies is to find a gravity dual that correctly predicts the properties of a system of strongly correlated electrons. The hope is that AdS/CFT methods might shed light on dynamics to which current tools have no access by providing a new class of relatively simple physical models of strongly interacting systems. Quantum Hall systems — for which strongly correlated electrons exhibit a variety of surprising and remarkable properties [5] — provide a promising point of potential contact for AdS/CFT methods [6].

For this paper our interest is in a particular AdS/QHE approach, ref. [7], which starts from the observation that transitions among quantum Hall plateaux exhibit a number of robust experimental properties [8, 9] that have a simple and universal phenomenological interpretation [10] in terms of a class of emergent ‘symmetries’ [11]. These symmetries act directly on the Ohmic and Hall conductivities: if $\sigma = \sigma_{xy} + i\sigma_{xx}$ is measured in units of e^2/h , then a variety of remarkable observations are consistent with (and derivable from) the statement that the flow of σ with changing temperature commutes with the action of a discrete duality group: $\sigma \rightarrow (a\sigma + b)/(c\sigma + d)$, with integers a , b , c and d satisfying $ad - bc = 1$, with c even. Although evidence has been accumulating over many years [12] that (2+1)-dimensional conformal systems very often enjoy such symmetries, this property turns out to be particularly manifest within the AdS/CFT framework [13, 14].

Of course, given a class of theories that capture these symmetries, the acid test is to find models that also get other experiments right that do not follow immediately from symmetry considerations. An encouraging feature of the proposal of ref. [7] is that it correctly models a measured scaling exponent whose numerical value is not simply a consequence of the emergent symmetries. Specifically, as described more fully below, between two Hall plateaux the differential Hall resistance at low temperatures behaves as

$$\left(\frac{dR_{xy}}{dB}\right)_{B_c} \propto T^{-p}, \quad (5.1)$$

with p measured to be $p = 0.42 \pm 0.01$ [9, 15]. In [7] this is predicted to be $p \simeq 2/z$, where z is an infrared dynamical exponent [18] whose value evaluates (for a broad class of models – see below) to 5.

But the real power of having an explicit model is that it allows different measurements to be related to one another. In particular, because z is a dynamical exponent (*i.e.* describes the relative scaling of time and space as one coarse-grains high-frequency modes), a prediction for z can be tested in other ways besides through its implications for p , and these must also agree with experiment. And for quantum Hall systems several other measurements appear to indicate $z = 1$ [15, 17].

Our purpose in this paper is to argue that the experimental evidence for $z = 1$ is consistent with the AdS/QHE framework proposed in [7], including its successful description of p . There are two separate reasons for this, both of which come down to the precise domain of validity of the theory's reproduction of $z = 5$. First, although the theory allows $z = 5$ for the dynamical scaling exponent in the far infrared, it also predicts a crossover to $z = 1$ in the ultraviolet. So experiments that indicate $z = 1$ in the ultraviolet, such as AC conductivity measurements [17], do not actually disagree, even at face value, with the $z = 5$ temperature scaling found in the deep infrared by [7].

More problematic are experiments like [15], that find evidence for $z = 1$ directly in the same regime where p is measured. As described in more detail below, these measurements find that at small enough temperatures the scaling behaviour, eq. (5.1), eventually stops, with dR_{xy}/dB becoming T -independent for $T < T_s$. The evidence for $z = 1$ comes because the crossover temperature between the scaling and T -independent regimes is observed to vary with system size, L , as $T_s \propto 1/L$.

To address these measurements we extend the analysis of [7] to include finite-size effects, in order to see if the AdS/QHE model properly captures the onset of a T -independent regime. We find that it does, predicting a transition to a T -independent (but L -dependent) Hall resistance for $T < T_s$. More remarkably, we find that the transition between dR_{xy}/dB being T -independent and scaling like $T^{-2/5}$ occurs at a transition temperature that scales as $T_s \propto 1/L^{n+1}$. The system contains a space-filling brane that is required on the AdS side to describe the charge carriers, and the parameter n parameterizing how the brane tension, \mathcal{T} , varies with L : $\mathcal{T} \propto L^{2-n}$.

Ultimately, the possibility for having two kinds of L -scaling for T_s without changing the T -scaling of the Hall resistance can be traced to the presence of this brane tension, which provides an intrinsic scale to the problem and so causes deviations from naive scaling behaviour. In particular, we find that \mathcal{T} causes the transition point between the IR and UV scaling regimes to vary in an L -dependent (but not T -dependent) way. When the tension is negligible (or scale-invariant, in a sense described in detail below) we find $n = 4$ and so $T_s \propto 1/L^5$, as expected for simple scaling with $z = 5$. We find $T_s \propto 1/L$ when $\mathcal{T} \propto L^2$.

We incorporate finite-size effects by generalizing standard AdS/CFT methods introduced by ref. [19], which argues that black holes are not the appropriate solution for describing finite-size systems at sufficiently low temperatures. In the absence of a chemical potential in the CFT (which corresponds on the gravity side to a black hole with no charge) ref. [19] argues that the better low-temperature solution — *i.e.* the one with lower free energy — is empty anti-de Sitter space. Entropy density is discontinuous across the transition to the low-temperature phase indicating that

the transition is first order.

Our main generalization of this argument is to the case of nonzero chemical potential, for which the preferred low-temperature solution is instead an electrically charged star, rather than empty anti-de Sitter space. (See [21, 22] for similar considerations with a chemical potential in the infinite-volume limit.) Remarkably, this links the quantum Hall transition from temperature-scaling to temperature-independence with the Chandrasekhar transition from a star to a black hole as its mass is increased. The transition between the black-hole and stellar phases is again first order, suggesting the possibility of there being experimental tests of this picture if the thermal properties of the electron gas can be accessed (certainly a difficult experimental challenge for samples this small).

We organize our presentation as follows. The remainder of this section does two things: first §5.1.1 summarizes the AdS/QHE proposal of ref. [7]; and then §5.1.2 outlines the finite-size experimental results of [15]. §5.2 then describes how to incorporate finite-size effects into an AdS/CFT framework, starting in §5.2.1 with a summary of ref. [19]’s analysis in terms of a Hawking-Page transition. §5.2.2 then describes the extension of this analysis to the AdS/QHE system, for which the main complication is the nonzero chemical potential. For nonzero chemical potential the transition at low temperatures on the gravity side is pictured to be into a phase described by a charged star. §5.3 develops the gravity description of the star and what its properties imply for the AdS/QHE system. §5.3.2 calculates the free energies of the two phases and demonstrates that the new stellar phase is preferred at sufficiently low temperatures, $T < T_s$. §5.3.3 then shows that the transition is related to system size by $T_s \propto 1/L^5$ when brane tension is negligible or $T_s \propto 1/L^{n+1}$ otherwise, while also identifying specific parts of parameter space for which this behaviour could break down. Finally, §5.4 briefly summarizes our results together with potential future directions.

5.1.1 The AdS/QHE system

The action for the AdS/QHE model proposed in ref. [7] has the following form

$$S = S_{\text{grav}} + S_{\text{matter}} + S_{\text{probe}} , \tag{5.2}$$

where the equations of motion for $S_{\text{grav}} + S_{\text{matter}}$ give the black-brane solution that describes the CFT’s thermal properties at infinite volume. S_{probe} describes a probe brane whose charge carriers give rise to the Ohmic and Hall conductivities of interest for quantum Hall phenomenology. By assumption S_{probe} only responds to, and does not perturb, the fields sourced by $S_{\text{grav}} + S_{\text{matter}}$ (we comment below on the necessity for both S_{matter} and S_{probe}).

The bulk

With duality in mind the gravitational sector is chosen to be $SL(2, R)$ invariant,¹

$$S_{\text{grav}} = - \int d^4x \sqrt{-g} \left\{ \frac{1}{2\kappa^2} \left[R - \frac{6}{L^2} + \frac{\zeta}{2} \left(\partial_\mu \tilde{\phi} \partial^\mu \tilde{\phi} + e^{2\tilde{\phi}} \partial_\mu \chi \partial^\mu \chi \right) \right] \right\}, \quad (5.3)$$

with $SL(2, R)$ acting according to

$$\tau \rightarrow \frac{a\tau + b}{c\tau + d} \quad \text{and} \quad g_{\mu\nu} \rightarrow g_{\mu\nu}, \quad (5.4)$$

where a, b, c and d are arbitrary real numbers that satisfy the $SL(2, R)$ condition $ad - bc = 1$ and

$$\tau := \chi + ie^{-\tilde{\phi}}. \quad (5.5)$$

We choose $\zeta = 1$, as supersymmetry would require if we were to embed this into a more complete description.

For the matter sector we take a Maxwell field, B_μ , governed by the $SL(2, R)$ -invariant Dirac-Born-Infeld (DBI) lagrangian

$$S_{\text{matter}} = - \int d^4x \sqrt{-g} \mathcal{T}(X - 1) - \frac{1}{4} \int d^4x \sqrt{-g} \chi F_{\mu\nu} \tilde{F}^{\mu\nu}$$

with $X := \sqrt{1 + \frac{\ell^4}{2} e^{-\tilde{\phi}} F_{\mu\nu} F^{\mu\nu} - \frac{\ell^8}{16} e^{-2\tilde{\phi}} (F_{\mu\nu} \tilde{F}^{\mu\nu})^2}$, (5.6)

where $F := dB$ is the usual 2-form Maxwell field strength and² $\tilde{F}_{\mu\nu} := \frac{1}{2} \epsilon_{\mu\nu\lambda\rho} F^{\lambda\rho}$.

Notice that the square-root term reduces to the usual Maxwell action (with a non-minimal dilaton coupling) in the limit $\ell \rightarrow 0$ with $\mathcal{T}\ell^4$ fixed. Unlike the Maxwell action, the DBI action has the advantage of being able to handle nonlinear situations where the conductivities themselves depend on the applied potentials. The action of $SL(2, R)$ on the Maxwell field is most simply written as [23]

$$\begin{pmatrix} \mathcal{G}_{\mu\nu} \\ \mathcal{F}_{\mu\nu} \end{pmatrix} \rightarrow \begin{pmatrix} a & b \\ c & d \end{pmatrix} \begin{pmatrix} \mathcal{G}_{\mu\nu} \\ \mathcal{F}_{\mu\nu} \end{pmatrix}, \quad (5.7)$$

where script fields denote the complex quantities

$$\mathcal{F}_{\mu\nu} := F_{\mu\nu} - i\tilde{F}_{\mu\nu} \quad \text{and} \quad \mathcal{G}_{\mu\nu} := -\tilde{G}_{\mu\nu} - iG_{\mu\nu}, \quad (5.8)$$

with

$$G^{\mu\nu} := -\frac{2}{\sqrt{-g}} \left(\frac{\delta S}{\delta F_{\mu\nu}} \right) = \frac{\mathcal{T}\ell^4}{X} \left[e^{-\tilde{\phi}} F^{\mu\nu} - \frac{\ell^4}{4} e^{-2\tilde{\phi}} (F_{\lambda\rho} \tilde{F}^{\lambda\rho}) \tilde{F}^{\mu\nu} \right] + \chi \tilde{F}^{\mu\nu}. \quad (5.9)$$

¹Strictly speaking, $SL(2, R)$ is a classical symmetry, and only a discrete subgroup like $SL(2, Z)$ or a smaller subgroup is expected to survive quantum effects [7].

²In our conventions the Levi-Civita symbol, $\epsilon_{\mu\nu\lambda\rho}$ transforms as a tensor rather than a tensor density.

$SL(2, R)$ invariance of the field equations allows a great simplification when seeking black-brane/black-hole solutions, since they can always be used to set χ and any magnetic charge, Q_m , to zero. It suffices therefore to consider black branes with electric charge, Q , (defined more precisely by (5.33), below) in the presence of a nonvanishing dilaton field. Some simplifications are possible even in this case, however, since the $SL(2, R)$ transformation with $b = c = 0$, $a = 1/d$ preserves the choice $\chi = Q_m = 0$, while transforming

$$\tilde{\phi} \rightarrow \tilde{\phi} - 2 \log a \quad \text{and} \quad Q \rightarrow a Q. \quad (5.10)$$

This shows that Q and $\tilde{\phi}$ should only appear in the invariant combination $Q^2 e^{\tilde{\phi}}$.

The field equations for this action admit charged black-brane solutions [7] that have the following large- and small- r forms³

$$\begin{aligned} ds^2 &\simeq h_\infty \tilde{r}^2 dt^2 + \frac{d\tilde{r}^2}{h_\infty \tilde{r}^2} + \tilde{r}^2 (dx^2 + dy^2) && \text{(large } \tilde{r} \text{ or UV)} \\ ds^2 &\simeq h_0 r^{10} dt^2 + \frac{d\tilde{r}^2}{h_0 \tilde{r}^2} + \tilde{r}^2 (dx^2 + dy^2) && \text{(small } \tilde{r} \text{ or IR),} \end{aligned} \quad (5.11)$$

where h_0 and h_∞ are constants. These solutions closely resemble those found for the non-DBI Maxwell-axio-dilaton theory in ref. [14]. Notice in particular they are invariant under rescalings $x \rightarrow \lambda x$ and $y \rightarrow \lambda y$ provided h_0 and h_∞ are fixed while $\tilde{r} \rightarrow \tilde{r}/\lambda$ and $t \rightarrow \lambda^z t$, with $z = 1$ in the UV (large- \tilde{r}) and $z = 5$ in the IR (small- \tilde{r}) limits.

The probe

The probe system couples to the real electromagnetic field, A_μ , for which we again choose precisely the same DBI action as given in eq. (5.6).

$$S_{\text{probe}}(A_\mu) = S_{\text{matter}}(B_\mu \rightarrow A_\mu), \quad (5.12)$$

but with a much smaller tension (to justify the probe approximation).

It might seem redundant to have two almost identical sectors, S_{matter} and S_{probe} , and it probably is. Both sectors are needed in [7] in order to achieve a finite DC conductivity for general magnetic fields, with the CFT described by the black brane providing a source of dissipation for the charge carriers described by S_{probe} [24]. Without the probe sector the remaining black brane does not break translation invariance and so conservation of momentum suppresses the dissipation required for generating a generic DC resistance.

However from the point of view of the long game this likely only reflects how poorly developed is the present state of the holographic art. It would seem more efficient to drop S_{matter} altogether

³The near-brane form shown here relies on the choice $\zeta = 1$, made above.

while simultaneously dropping the probe approximation for S_{probe} , so that S_{probe} can play S_{matter} 's role in shaping the form of the black-hole geometry. It is likely that S_{matter} could be dropped in this way once an efficient formulation of disorder becomes available for AdS/CFT systems [25].

Domain of approximation

Since our analysis is semiclassical, we must stake out its domain of validity. The first approximation required is weak coupling, which amounts to the requirement

$$e^{\tilde{\phi}} \ll 1. \tag{5.13}$$

Next comes the low-energy/small-curvature approximation that allows one to work within a low-energy field theoretic (gravity) description. As discussed in [24] this requires the curvature radius, L , to be much larger than the string length, ℓ/X , in the presence of the background Maxwell field: $L \gg \ell/X$.

Of particular interest in what follows are situations where the near-horizon geometry is well-described by the near-horizon $z = 5$ solution given above, for which the dilaton profile satisfies $e^{\tilde{\phi}} \propto \tilde{r}^4$. In this case X is approximately \tilde{r} -independent and the condition $L \gg \ell/X$ simplifies to

$$1 \gg \frac{\ell^2}{X^2 L^2} \simeq \frac{\ell^2}{L^2} \left(1 + \frac{Q^2 e^{\tilde{\phi}}}{\mathcal{T}^2 \ell^4 \tilde{r}^4} \right) \simeq \frac{Q^2 e^{\tilde{\phi}}}{\mathcal{T}^2 L^2 \ell^2 \tilde{r}^4} \simeq \frac{Q^2 e^{\tilde{\phi}_h}}{\mathcal{T}^2 L^2 \ell^2 \tilde{r}_h^4}, \tag{5.14}$$

where \tilde{r}_h represents the position of the black brane horizon and $\tilde{\phi}_h := \tilde{\phi}(r_h)$. Eq. (5.14) uses the approximate expression for X , eq. (5.37), that we find from the near-horizon solutions of later sections, together with the observation that $\frac{Q^2 e^{\tilde{\phi}}}{\mathcal{T}^2 \ell^4 \tilde{r}^4}$ is typically large in the asymptotic near-horizon regime of interest.

In principle this represents a lower bound as to how small L can be made, which is of interest in the finite-volume case for which L ends up playing the role of system size. In practice, however, no matter how tiny L becomes eq. (5.14) can always be satisfied by demanding the gauge coupling $g^2 := e^{\tilde{\phi}_h}/(\mathcal{T} \ell^4)$ to be sufficiently small. It turns out that the dilaton profile grows monotonically with \tilde{r} , and so $e^{\tilde{\phi}_h} < e^{\tilde{\phi}_0}$, where $\tilde{\phi}_0$ is the asymptotic dilaton value at large \tilde{r} . This ensures that small $e^{\tilde{\phi}_h}$ can be ensured by choosing $e^{\tilde{\phi}_0}$ to be sufficiently small.

The probe approximation, which we use when calculating the conductivity (see appendix 5.A), imposes additional constraints. Denoting the probe-brane tension by⁴ \mathcal{T}_p , we must demand $\kappa^2(\mathcal{T}_p/X) \ll 1/L^2$, where \mathcal{T}_p/X is the size of the DBI brane stress energy and $1/L^2$ is a typical background cur-

⁴For instance, if the matter source is a stack of N identical branes then $\mathcal{T} = N\mathcal{T}_p$, for some large N .

vature. Equivalently, $\kappa^2 L^2 \mathcal{T}_p \ll X$ or

$$\hat{\mathcal{T}}_p \ll \left[1 + \frac{Q^2 e^{\tilde{\phi}}}{\mathcal{T}^2 \ell^4 \tilde{r}^4} \right]^{-1/2}, \quad (5.15)$$

where $\hat{\mathcal{T}}_p := \kappa^2 L^2 \mathcal{T}_p$.

5.1.2 Experimental finite-size effects

This section briefly summarizes the measurements of ref. [15], mentioned in the introduction, that provide evidence for $z = 1$ through the low-energy temperature dependence of the Hall resistance midway between two plateaux.

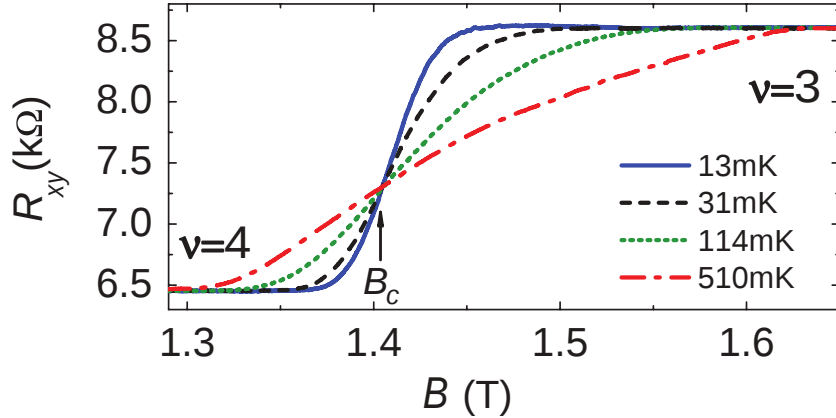


Figure 5.1. Hall resistance vs magnetic field for various temperatures, reproduced from [15]. B_c is the critical magnetic field where resistance doesn't change as temperature varies (colour online).

The measurements in question are performed at the critical inter-plateaux magnetic field, B_c , defined as the field for which the Hall resistance remains constant as the temperature varies (see figure 5.1). The quantity of interest is the slope of the resistance profile evaluated at the critical field, $(\partial R_{xy}/\partial B)_{B_c}$.

This quantity is observed to be fairly sensitive to the amount of doping, x , in the $\text{Al}_x\text{Ga}_{1-x}\text{As}/\text{Al}_{0.32}\text{Ga}_{0.68}\text{As}$ heterostructure, but for $0.6\% < x < 1.6\%$ a power-law behaviour

$$\left(\frac{\partial R_{xy}}{\partial B} \right)_{B_c} \propto T^{-p}, \quad (5.16)$$

is observed over two decades of temperature. Whenever this broad a range of scaling is seen the power is given by $p = 0.42 \pm 0.01$. This is seen in the top panel of figure 5.2.

The significance of the sensitivity to doping is not yet clear, but deviations from $p = 0.42$ only arise when the power-law behaviour does not apply over as large a temperature range. The range of doping for which the robust scaling occurs reflects a regime where short-range scattering from the

doped Al disorder dominates [15, 16], and further studies of this doping dependence could shed light on the domain over which the low-energy behaviour is universal, and so described by the CFT dual to our AdS description.⁵

Finite-size effects are observed when the derivative $(\partial R_{xy}/\partial B)_{B_c}$ is measured for samples small enough that the system size can compete with temperature effects in charge transport. The experiments find that at small enough system size, there exists a temperature, T_s , below which $(\partial R_{xy}/\partial B)_{B_c}$ becomes independent of temperature. By repeating the measurements for samples of different size (see the bottom panel in figure 5.2), it is found that the transition temperature varies inversely with system size,

$$T_s \propto 1/L, \quad (5.17)$$

where L is the sample width.

This relation has an interpretation in terms of critical scaling exponents [18]. At a critical point coherence length, ξ , and temperature are related by a power law, $\xi \propto T^{-s/2}$. If we follow ref. [15] and assume the coherence length saturates at the system size, $\xi \propto L$, for low enough temperatures, then eq. (5.17) implies $s = 2$. On the other hand, a dynamical scaling exponent z would give $L \propto T^{1/z}$ and so comparison shows $z = 2/s$, and so $z = 1$. The connection to temperature scaling of conductivities comes through the localization length, which scales as a function of the magnetic field as $\zeta \propto |B - B_c|^{-\nu}$. If physical quantities like conductivities depend only on the ratio ξ/ζ then they depend only on the scaling combination $|B - B_c|/T^{s/2\nu}$. This implies $p = s/(2\nu)$.

It is the apparent mismatch between this evidence for $z = 1$ and the use of $z = 5$ of the model in [7] that we set out to understand in the next sections.

5.2 Finite-size effects in AdS/CFT systems

In this section we describe how finite-size effects are included into the holographic system of interest. Because the size introduces a new scale, L , this can be combined into a scale-invariant combination

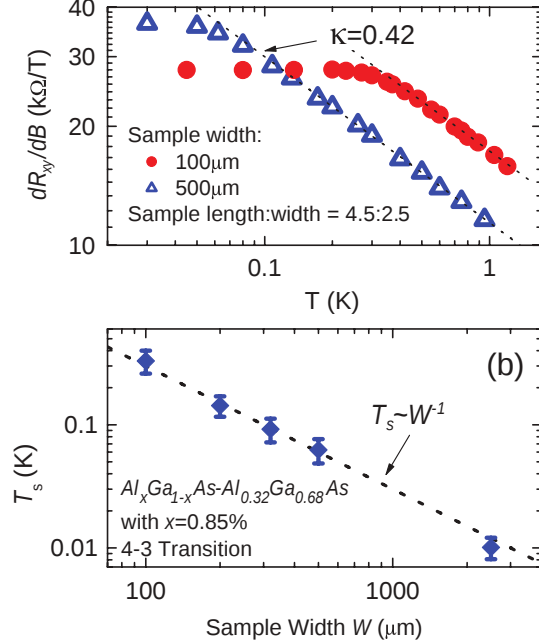


Figure 5.2. Top panel: $\partial R_{xy}/\partial B$ measured at $B = B_c$, as a function of temperature (reproduced from [15]), showing the transition from power-law temperature dependence to temperature-independence. Bottom panel: The transition temperature between these regimes vs system size (colour online).

⁵We thank Michael Hilke and Gabor Cs athy for helpful conversations on this point.

with temperature, T , allowing physical quantities to depend on these variables in a complicated way, even for scale invariant systems (like CFTs). In §5.2.1 we first briefly review standard arguments about how finite-size effects can be used to describe a transition [19] for AdS/CFT systems in the absence of a chemical potential. We then describe in §5.2.2 how this argument generalizes to the AdS/QHE case, where a chemical potential plays an important role.

5.2.1 Finite size with no chemical potential

In this section we briefly summarize the discussion of ref. [19], which discusses how to include finite-size effects for the simplest AdS/CFT system, and how these can change the low temperature properties of the system. Following [19], consider the following bulk action

$$S = -\frac{1}{2\kappa^2} \int d^4x \sqrt{-g} \left(R - \frac{6}{L^2} \right), \quad (5.18)$$

whose equations are solved by the black-hole metric

$$ds^2 = -h(\tilde{r}) dt^2 + \frac{d\tilde{r}^2}{h(\tilde{r})} + \tilde{r}^2 d\Omega^2, \quad (5.19)$$

with $d\Omega^2 = d\theta^2 + \sin^2 \theta d\phi^2$ and

$$h(\tilde{r}) = \frac{\tilde{r}^2}{L^2} - \frac{\tilde{r}_h^3}{\tilde{r}L^2} + \left(1 - \frac{\tilde{r}_h}{\tilde{r}} \right). \quad (5.20)$$

Here the integration constant is chosen so that $h(\tilde{r}_h) = 0$.

This differs from the translation-invariant black-brane solutions because the asymptotic, large- \tilde{r} , geometry is a sphere rather than a plane. Because the radius of the sphere provides a scale, this asymptotic geometry only becomes scale invariant at large \tilde{r}/L . Consequently the AdS radius, L , enters differently into observables, and ultimately plays the role of the CFT system size (as we now clarify).

CFT system size

Let us be a little more precise about what we mean by the system size for the CFT dual to the black-hole geometry, eq. (5.19). To this end consider the limit of large \tilde{r} in (5.19), for which the metric along slices of constant \tilde{r} is

$$ds_r^2 \simeq -\frac{\tilde{r}^2}{L^2} dt^2 + \tilde{r}^2 d\Omega^2 = \frac{\tilde{r}^2}{L^2} \left(-dt^2 + L^2 d\Omega^2 \right). \quad (5.21)$$

ds_r^2 is not quite the metric of the CFT, since the circumference of the time circle must be $1/T$ for a CFT at temperature T . Rather, ds_r^2 is conformal to the CFT metric, which is given by

$$ds_{CFT}^2 = -dt^2 + L^2 d\Omega^2. \quad (5.22)$$

Clearly this metric describes a finite-size system with a real-space circumference of $2\pi L$, giving the precise relationship between system size and the AdS scale. Notice how this argument is independent of the small- r geometry, so as long as the system is asymptotically AdS.

Temperature and system size

An important consequence of having a finite system size can be seen from the expression for the Hawking temperature for this metric,

$$4\pi T = h'(\tilde{r}_h) = \frac{3\tilde{r}_h}{L^2} + \frac{1}{\tilde{r}_h}. \quad (5.23)$$

This expression is obtained, for example, by going to euclidean signature and requiring the time coordinate to be periodic, $t \simeq t + \beta$, with $\beta = 1/T$ chosen to remove the conical singularity that would otherwise appear at $\tilde{r} = \tilde{r}_h$.

What is noteworthy about eq. (5.23) is that it has a minimum at $\tilde{r}_h^2 = L^2/3$, with the temperature bounded below, $T \geq T_*$, with

$$4\pi T_* = \frac{2\sqrt{3}}{L}. \quad (5.24)$$

The system has a minimum temperature inversely proportional to the system size. But if the black hole does not describe temperatures lower than T_* , what does? Ref. [19] proposes the system is better described by the alternative solution corresponding to $\tilde{r}_h = 0$, for which $h(\tilde{r}) = 1 + \tilde{r}^2/L^2$ does not vanish. In this case the periodicity, β' , of the euclidean time direction can be arbitrary (and so in particular can describe arbitrarily low temperatures).

To determine which solution the system prefers for any given temperature and system size we compare the two free energies, $F(T)$, for these solutions, using the AdS/CFT prescription that $F(T) = -TS_{\text{on-shell}}$. (Here $S_{\text{on-shell}}$ denotes the classical action evaluated at the classical solution, regarded as a function of its boundary values at large \tilde{r} .) Since the Einstein equation implies $R = 12/L^2$ for both solutions we have

$$F_{\beta'}(T) = \frac{3T}{\kappa^2 L^2} \int_0^{\beta'} dt \int_0^{\tilde{r}_\infty} d\tilde{r} \int d^2\Omega \tilde{r}^2 = \frac{8\pi T \beta' \tilde{r}_\infty^3}{\kappa^2 L^2}, \quad (5.25)$$

and

$$F_\beta(T) = \frac{3T}{\kappa^2 L^2} \int_0^\beta dt \int_{\tilde{r}_h}^{\tilde{r}_\infty} d\tilde{r} \int d^2\Omega \tilde{r}^2 = \frac{8\pi T \beta (\tilde{r}_\infty^3 - \tilde{r}_h^3)}{\kappa^2 L^2}, \quad (5.26)$$

with \tilde{r}_∞ being a temporary regulator that is ultimately taken to infinity.

The parameters β and β' are related to one another in an \tilde{r}_∞ -dependent way, by the condition that both actions describe the same temperature, T , since this requires their euclidean time directions must have the same circumference for large \tilde{r} . That is, using the form of the two metrics at $\tilde{r} = \tilde{r}_\infty$,

$$\beta' \sqrt{(\tilde{r}_\infty)^2/L^2 + 1} = \beta \sqrt{(\tilde{r}_\infty)^2/L^2 - r_h^3/(\tilde{r}_\infty L^2) + (1 - \tilde{r}_h/\tilde{r}_\infty)}$$

to give us the same CFT temperature at infinity, (that is, the S^1 's from the time component have the same circumference.) Using this in the free-energy expressions gives

$$\begin{aligned} \Delta F := F_\beta(T) - F_{\beta'}(T) &= \frac{4\pi T}{\kappa^2 L^2} [(\beta - \beta') \tilde{r}_\infty^3 - \beta \tilde{r}_h^3] \\ &= \frac{4\pi \beta T}{\kappa^2 L^2} \left[\tilde{r}_\infty^3 \left(1 - \sqrt{1 - \frac{\tilde{r}_h(r_h^2/L^2 + 1)}{\tilde{r}_\infty(\tilde{r}_\infty^2/L^2 + 1)}} \right) - \tilde{r}_h^3 \right] \\ &= \frac{2\pi \tilde{r}_h}{\kappa^2} \left(\frac{L^2 - \tilde{r}_h^2}{L^2} \right), \end{aligned} \quad (5.27)$$

where \tilde{r}_∞ is taken to infinity in the last line. This calculation indicates a transition at $\tilde{r}_h = L$, with the black-hole solution having lower free energy at larger \tilde{r}_h (or higher temperatures), while the other solution has lower free energy for smaller temperatures. Notice in particular that this transition happens above the minimum temperature of the black-hole solution, which occurs at $\tilde{r}_h = L/\sqrt{3}$.

The value of the transition temperature can be seen by writing ΔF in terms of T , using (5.23):

$$\Delta F = \frac{4\pi \tilde{r}_h}{\kappa^2} \left[1 - \frac{L^2}{36} \left(4\pi T + \sqrt{(4\pi T)^2 - \frac{12}{L^2}} \right)^2 \right], \quad (5.28)$$

which shows that $\Delta F = 0$ occurs at a transition temperature inversely proportional to the system size: $T_s \propto 1/L$.

5.2.2 Finite size AdS/QHE black holes

We now repeat the above finite-size analysis for the quantum Hall-ography model. This involves several steps: construct the black hole solutions for asymptotic spherical geometries and see whether they have a minimum temperature; and if so, identify a candidate alternative gravity dual that describes the low-temperature phase. Once a low-temperature description is found we check whether its conductivity is temperature independent, and find how the temperature, T_s , changes with system size.

Field equations

We start with the Hall-ography action of §5.1.1, and use the $SL(2, R)$ freedom to set $\chi = B = 0$, so

$$S_{\text{grav}} + S_{\text{matter}} = - \int d^4x \sqrt{-g} \left[\frac{1}{2\kappa^2} \left(R - \frac{6}{L^2} + \frac{1}{2} \partial_\mu \tilde{\phi} \partial^\mu \tilde{\phi} \right) + \mathcal{T}(X - 1) \right], \quad (5.29)$$

and seek black hole solutions with spherical geometry at fixed radius and time. Adopting a dimensionless radial coordinate,

$$\tilde{r} = Lr, \quad (5.30)$$

and using the metric ansatz

$$ds^2 = \left[-h(r) e^{\xi(r)} dt^2 + \frac{L^2 dr^2}{h(r)} + L^2 r^2 d\Omega^2 \right] \quad \text{and} \quad \tilde{\phi} = \tilde{\phi}(r), \quad (5.31)$$

we find (as above) that it is L that plays the role of the CFT system size, with the CFT metric conformal to the asymptotic bulk metric. The temperature associated with this metric is

$$4\pi T = \frac{1}{L} e^{\xi(r_h)/2} h'(r_h), \quad (5.32)$$

where $h(r_h) = 0$.

The Maxwell field equation integrates simply to give

$$G^{rt} = \frac{\mathcal{T} \ell^4}{X} e^{-\phi} F^{rt} = \frac{Q e^{-\xi/2}}{L^3 r^2} \quad (5.33)$$

where Q is the black hole electric charge. It is shown in [7] that the CFT current density is given by $J^i = \sqrt{-g} G^{ri}|_\infty$, and keeping in mind that $g_{\mu\nu}$ is only asymptotically conformal to the CFT metric in the finite-volume case, the CFT charge density turns out to be related to Q by

$$Q = L^2 \rho_{\text{CFT}}. \quad (5.34)$$

Consequently Q scales like L^2 if L is varied with fixed CFT charge density. Since this expression also shows that Q counts the total number of charge carriers in the CFT, $Q \gg 1$ is the regime appropriate to real quantum Hall systems. How finite size affects the conductivity calculation for this system is explored in appendix 5.A.

The field equations differ slightly from the black brane case solved in [7], because of the curvature of the surfaces of fixed r and t , which appears in the $\theta\theta$ Einstein equation. This difference is less and less important for larger r . The field equations to solve are

$$r\xi' - \frac{1}{2}(r\phi')^2 = 0, \quad (5.35)$$

and

$$\begin{aligned} \frac{h'}{r} + \frac{h\xi'}{2r} + \frac{h}{r^2} - \frac{1}{r^2} - 3 - \hat{\mathcal{T}} \left(\frac{X-1}{X} \right) &= 0 \\ \frac{e^{-\xi/2}}{r^2} \left(e^{\xi/2} r^2 h \phi' \right)' + \frac{\hat{\mathcal{T}}}{X} (X^2 - 1) &= 0, \end{aligned} \quad (5.36)$$

where r is the dimensionless radial coordinate, and the other quantities in these equations are

$$X^{-2} = 1 + \frac{Q^2 e^\phi}{\hat{\mathcal{T}}^2 r^4}, \quad (5.37)$$

$$\hat{\mathcal{T}} = \kappa^2 L^2 \mathcal{T} \text{ and } \phi = \tilde{\phi} - 4 \log(\ell/\kappa).$$

Asymptopia: the far-field $z = 1$ region

The first region of interest is the asymptotic far-field regime, for which $r \gg 1$. An approximate solution in this regime is obtained by expanding fields in powers of $1/r$ plugging the result into (5.36). The approximate solution obtained in this way is $\xi(r) \simeq 0$,

$$\begin{aligned} h(r) &\simeq r^2 \left(1 + \frac{1}{r^2} - \frac{r_b^3}{r^3} + \frac{Q^2 e^{\phi_0}}{2\hat{\mathcal{T}} r^4} \right) \\ &= r^2 \left[1 - \frac{r_h^3}{r^3} + \left(\frac{1}{r^2} - \frac{r_h}{r^3} \right) + \frac{Q^2 e^{\phi_0}}{2\hat{\mathcal{T}}} \left(\frac{1}{r^4} - \frac{1}{r_h r^3} \right) \right] \\ \text{and } \phi &\simeq \phi_0 + \frac{\phi_1}{r^3} + \frac{Q^2 e^{\phi_0}}{4\hat{\mathcal{T}} r^4}, \end{aligned} \quad (5.38)$$

where ϕ_0 and ϕ_1 are boundary data to be specified, and r_b is an integration constant that is traded in the second line for r_h , defined as the position satisfying $h(r_h) = 0$.

More specifically, this solution assumes that

$$\frac{1}{r^2} \sim \frac{Q^2 e^{\phi_0}}{\hat{\mathcal{T}}^2 r^4} \sim \frac{\phi_1}{r^3} \ll 1, \quad (5.39)$$

so that anything quadratic in these quantities can be neglected. But we can only use eq. (5.38) to infer that $h(r)$ vanishes for some r if r_h is large enough to ensure that eqs. (5.39) is valid for all $r_h < r < \infty$. When this is true a horizon exists in this region, terminating the solution at $r = r_h$. Using equation (5.32) the temperature for this metric becomes

$$4\pi T = \frac{1}{L} \left(2r_h + \frac{1}{r_h} - \frac{Q^2 e^{\phi_0}}{2\hat{\mathcal{T}} r_h^3} \right). \quad (5.40)$$

Attractor: the near-horizon $z = 5$ region

A different solution describes the near-horizon geometry if $Q^2 e^{\phi_0} / \hat{T}^2 r_h^4$ is not much smaller than unity, and provided r_h is still large enough to be in the large- r limit. Then what was an exact solution for the black brane in ref. [7],

$$h(r) = h_0 r^2 \left(1 - \frac{r_h^7}{r^7}\right), \quad \xi(r) = 8 \ln \left(\frac{r}{r_c}\right) \quad \text{and} \quad \phi(r) = 4 \ln \left(\frac{r}{r_c}\right) + \phi_0, \quad (5.41)$$

also solves eqs. (5.36), provided we drop terms of relative order r^{-2} . In these expressions r_c is an integration constant, which is ultimately fixed by matching to the large- r $z = 1$ region below (*c.f.* eq. (5.44)).

For this solution the quantity X evaluates to a constant,

$$X := X_h = \frac{-(6 + 2\hat{T}) + \sqrt{(6 + 2\hat{T})^2 + 5\hat{T}^2}}{\hat{T}}, \quad (5.42)$$

which has the limits $X_h \rightarrow 1 - 2/\hat{T} + \mathcal{O}(1/\hat{T}^2)$ as $\hat{T} \rightarrow \infty$ and $X_h \rightarrow \frac{5}{12} \hat{T} + \mathcal{O}(\hat{T}^2)$ as $\hat{T} \rightarrow 0$. The equations of motion then fix the quantity h_0 to be

$$7h_0 = 3 + \hat{T} \left(\frac{X_h - 1}{X_h}\right). \quad (5.43)$$

Notice that $h_0 \simeq 3/35$ when $\hat{T} \ll 1$ and $h_0 \simeq 1/7$ for $\hat{T} \gg 1$.

As discussed⁶ in ref. [14], this solution is an attractor inasmuch as all solutions eventually approach this one in the near-horizon limit, regardless of their boundary conditions at large r . We have checked numerically that these solutions exist, and fig. 5.3 shows two examples where $\phi(r)$ asymptotes to eqs. (5.38) for very large r , but then crosses over to the attractor form, eq. (5.41), as the horizon is approached. The figure also shows how the solution for $\phi(r)$ crosses quite quickly from the logarithmic behaviour of eq. (5.41) to the asymptotically constant limit of eq. (5.38) (similar to what was also found in ref. [14]).

In what follows it is crucial to determine how the integration constant r_c depends on system parameters like L and ρ_{CFT} , a dependence that arises when the attractor solution is matched onto the solution at asymptotically large r . To this end it is useful to treat the transition between (5.38) to

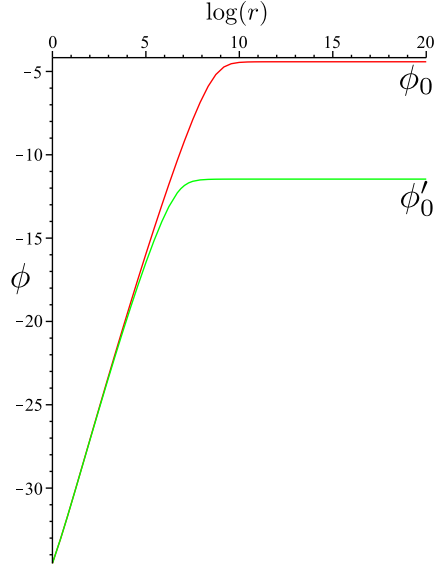


Figure 5.3. Semi-log plot of the dilaton profile for $Q = 1000$ and $\hat{T} = 10^{-5}$, for two asymptotic initial conditions (colour online).

⁶Although ref. [14] uses the Maxwell action, ref. [7] shows their attractor solution also applies for black branes with the DBI action, and so also in the present case for large enough black holes.

(5.41) as occurring at a specific transition radius, since fig. 5.3 shows this to be a good approximation. Since $\xi = 0$ in the asymptotic region, matching $\xi(r)$ using eq. (5.41), shows this transition radius is given by $r = r_c$. The dependence of r_c on other parameters is then obtained by similarly demanding continuity of $\phi(r)$ at $r = r_c$, leading to

$$\begin{aligned} \frac{Q^2 e^{\phi_0}}{r_c^4} &= \frac{\hat{\mathcal{T}}^2(1 - X_h^2(\hat{\mathcal{T}}))}{X_h^2(\hat{\mathcal{T}})} \simeq 4\hat{\mathcal{T}} + \mathcal{O}(1) && \text{if } \hat{\mathcal{T}} \gg 1 \\ &\simeq \frac{119}{25} [1 + \mathcal{O}(\hat{\mathcal{T}})] && \text{if } \hat{\mathcal{T}} \ll 1. \end{aligned} \quad (5.44)$$

Notice in particular that no choice for $\hat{\mathcal{T}} > 0$ allows $Q e^{\phi_0/2}/r_c^2 \ll 1$.

Eliminating Q using $Q = \rho_{CFT} L^2$ and using the definition $\hat{\mathcal{T}} = \kappa^2 L^2 \mathcal{T}$ in eq. (5.44) then gives

$$\begin{aligned} r_c^4 &\simeq \frac{L^2 \rho_{CFT}^2 e^{\phi_0}}{4\kappa^2 \mathcal{T}} && \text{if } \hat{\mathcal{T}} \gg 1 \\ &\simeq \frac{25}{119} \rho_{CFT}^2 e^{\phi_0} L^4 && \text{if } \hat{\mathcal{T}} \ll 1 \end{aligned} \quad (5.45)$$

which shows how r_c depends on L . For fixed ϕ_0 and ρ_{CFT} , r_c^4 scales as L^4 when $\hat{\mathcal{T}}$ is small. By contrast, for large $\hat{\mathcal{T}}$ we have $r_c^4 \propto L^2/\mathcal{T}$ and so in order to know how r_c varies with system size in the CFT we must know how \mathcal{T} varies with L .

From the AdS point of view the possibility that \mathcal{T} could depend on L is very natural, since within an explicit embedding into string theory the branes in question could wrap cycles in any additional ‘internal’ dimensions, whose size typically is also set by L . (See refs. [20] for more explicit examples of this type involving D5 and D7 branes in a top-down AdS/CFT construction.) In the absence of such a construction we parameterize the scaling of tension with system size as $\mathcal{T} = \mathcal{T}_n L^{2-n}$, which implies the crossover radius scales as

$$r_c^4 \propto L^n \quad (5.46)$$

when $\hat{\mathcal{T}} \gg 1$. Notice that any choice but $n = 4$ breaks scale invariance in the IR, since scale invariance of the metric of eq. (5.11) requires h_0 to be held fixed, and this in turn requires $\hat{\mathcal{T}}$ be fixed (*c.f.* eq. (5.43)).

This L -dependence of r_c is of interest because it enters into the relation between the temperature and r_h . Using eq. (5.32) as before to connect T and r_h , using the $z = 5$ attractor geometry gives

$$4\pi T = \frac{7h_0 r_h^5}{L r_c^4}, \quad (5.47)$$

where the r_c dependence arises from the form of $\xi(r)$ in (5.41). Finally, using eqs. (5.45) to eliminate

r_c in (5.47) gives a form which makes the scaling of the $T-r_h$ relation with system size more explicit:

$$\begin{aligned}
 4\pi T &= \left(\frac{4\kappa^2 \mathcal{T}_n r_h^5}{\rho_{CFT}^2 e^{\phi_0}} \right) \frac{7h_0}{L^{n+1}} && \text{if } \hat{\mathcal{T}} \gg 1 \\
 4\pi T &= \left(\frac{119}{25} \frac{r_h^5}{\rho_{CFT}^2 e^{\phi_0}} \right) \frac{7h_0}{L^5} && \text{if } \hat{\mathcal{T}} \ll 1.
 \end{aligned} \tag{5.48}$$

This last pair of equations has two important consequences if we anticipate two results from subsequent sections.

1. *Temperature scaling:*

First, as is shown in Appendix 5.A (and ref. [7]), the power-law temperature dependence of the Hall conductivity (and resistivity) arises because it scales proportional to $1/r_h^2$. Whenever $r_c > r_h$ eq. (5.48) then implies a temperature scaling proportional to $T^{-2/5}$, for *both* large and small $\hat{\mathcal{T}}$.

What is required to ensure⁷ $r_c > r_h \gg 1$? For $\hat{\mathcal{T}}$ large inspection of eq. (5.44) shows this requires $1 \ll r_h^2 \ll Q e^{\phi_0/2}/\hat{\mathcal{T}}$, which is a non-empty region only if $\hat{\mathcal{T}} \ll Q e^{\phi_0/2}$. In particular if $\hat{\mathcal{T}} \gg 1$ a large- r crossover between the two solutions requires Q must be even larger, since the use of semi-classical reasoning requires $e^{\phi_0} \ll 1$. Happily, as mentioned earlier, large Q is the regime of interest for real quantum Hall systems.

2. *Scaling with System Size:*

The second important consequence of eq. (5.48) is what it says about how T scales with L when r_h is fixed. Fixed r_h is of interest because this is what subsequent sections show is required for the transition temperature, T_s .

Eq. (5.48) shows that if $\hat{\mathcal{T}}$ is negligible then T varies with L (for fixed r_h) as expected for $z = 5$ scaling: $T \propto 1/L^5$. The same is true for $\hat{\mathcal{T}} \gg 1$ if we make the scale-invariant choice, $n = 4$. In either case the only scales that arise are those characterizing the CFT, such as ρ_{CFT} , T and L .

However, more generally the presence of \mathcal{T} introduces an additional scale and so changes the L -dependence of both r_c and T , with $T \propto 1/L^{n+1}$ when r_h is held fixed. In particular, $T \propto 1/L$ when $n = 0$ (*i.e.* when $\mathcal{T} \propto L^2$).

Relaxing the large- r approximation

This section describes how the black hole temperature is related to r_h and other system parameters in the regime where the above approximate forms need not apply because we no longer neglect the $1/r^2$ term in (5.36); *i.e.* where the black hole solutions can differ from the black-brane solutions of ref. [7]. Our goal is to motivate the existence of a transition to a new regime by showing that $T(r_h)$ is bounded from below, with a minimum temperature, T_* , below which some other solution must replace the black-hole description.

⁷Recall the condition $r_h \gg 1$ is required to use the large- r black-hole solution described above. (The discussion of later sections examines what happens if this condition is relaxed.)

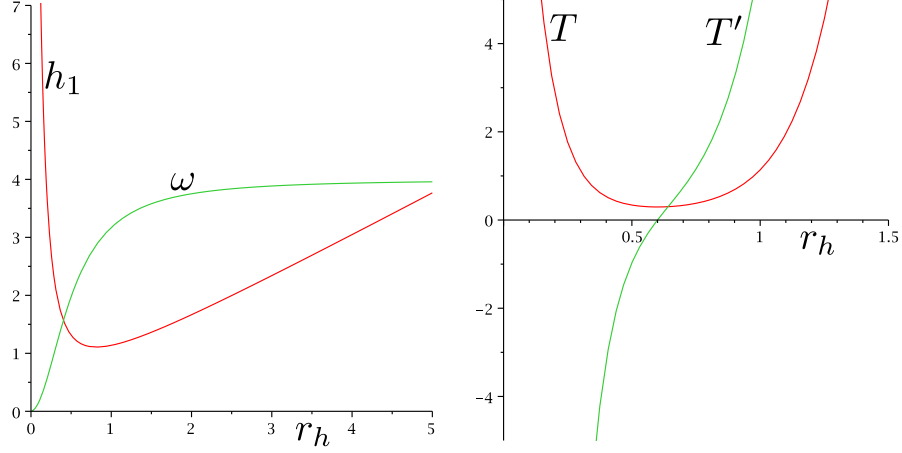


Figure 5.4. Left panel: A plot of h_1 and ω as functions of r_h . Note that h_1 diverges and $\omega \rightarrow 0$ as $r_h \rightarrow 0$, a reflection of the minimum temperature discussed in the main text. Also note that $\omega \rightarrow 4$ and $h_1 \rightarrow r_h$ at large r_h , in agreement with the analytic large- r_h solution in the $z = 5$ region. Right panel: A plot of $T(r_h)$ and $dT/dr_h(r_h)$ against r_h showing that temperature has a minimum for the black hole solution. In both cases we choose the value $\hat{\mathcal{T}} = 1$ (colour online).

Although we don't have the luxury of an explicit solution in the general case, because our main interest is in how the temperature depends on other parameters like r_h we can proceed by expanding the metric in powers of $r - r_h$, as follows

$$\begin{aligned}
 h(r) &= h_1(r - r_h) + h_2(r - r_h)^2 + \dots \\
 \phi(r) &= \phi_h + \frac{\omega}{r_h}(r - r_h) + \dots \\
 \xi(r) &= \xi_h - \frac{\omega^2}{2r_h}(r - r_h) + \dots,
 \end{aligned}
 \tag{5.49}$$

where we define $\phi_1 := \omega/r_h$ and eq. (5.35) is used to relate the linear terms in ϕ and ξ to one another. In the special case where $r_h \gg 1$ the solutions of the previous sections apply, with the solutions of eqs. (5.38) corresponding to the choices $\omega \simeq \xi_h \simeq 0$ and $\phi_h \simeq \phi_0$, while those of eqs. (5.41) being captured by $\omega \simeq 4$, $\phi_h \simeq \phi_0 + 4 \ln(r_h/r_c)$ and $\xi_h \simeq 8 \ln(r_h/r_c)$.

Since eq. (5.35) has been used already to relate ξ to ϕ , there are only two other field equations to solve. Expanding equations (5.36) about $r = r_h$ gives

$$\begin{aligned}
 \frac{h_1}{r_h} - 3 - \frac{1}{r_h^2} + \frac{\hat{\mathcal{T}}}{X_h}(1 - X_h) \\
 + \left[\frac{2h_2}{r_h} + \frac{2}{r_h^3} + \frac{\omega^2 h_1}{4r_h^2} - \frac{(4 - \omega)Q^2 e^{\phi_h} X_h}{2r_h^{5-\omega} \hat{\mathcal{T}}} \right] (r - r_h) + \dots = 0,
 \end{aligned}
 \tag{5.50}$$

and

$$\frac{\omega h_1}{r_h} + \frac{\hat{\mathcal{T}}}{X_h}(1 - X_h^2) + \left[\frac{2\omega h_2}{r_h} + \frac{h_1 \omega^3}{4r_h^2} + \frac{(4 - \omega)Q^2 e^{\phi_h}}{r_h^{5-\omega} \hat{\mathcal{T}}} X_h (1 + X_h^2) \right] (r - r_h) + \dots = 0, \quad (5.51)$$

where

$$X_h^{-2} = 1 + \frac{Q^2 e^{\phi_h}}{\hat{\mathcal{T}}^2 r_h^{4-\omega}}. \quad (5.52)$$

Since these equations hold for all r satisfying $|r - r_h| \ll 1$, the coefficient of each power of $r - r_h$ must separately vanish. Working to linear order in $r - r_h$ then implies four conditions, which we solve for h_1, ω, h_2 , and ϕ_h as functions of r_h . The left panel of figure 5.4 plots sample numerical solutions for h_1 and ω obtained in this way, as functions of r_h . In principle this can be continued to higher orders in $(r - r_h)$, though the higher terms have no bearing on how the temperature of the system depends on r_h .

While these equations don't all have analytic solutions, the equation for h_1 is a quartic equation and so does have a closed-form solution in principle. This allows a check on our numeric solutions, since one can compare with the known $z = 1$ and $z = 5$ solutions found earlier by taking the large- r_h limit. To obtain $z = 1$ take $Q \rightarrow 0$, to find

$$h_1 = 3r_h + \frac{1}{r_h} \quad \text{and} \quad \omega = 0, \quad (5.53)$$

agreeing with eqs. (5.38). Similarly, to get the $z = 5$ solution take $r_h \gg 1$ while ensuring that $Q^2 e^{\phi_0} / \hat{\mathcal{T}}^2 \gtrsim r_h^4$, in which case $\omega = 4$ and the value found for h_1 agrees with (5.41) (as is also seen from the left panel of fig. 5.4).

In terms of these quantities the temperature for the system is given by eq. (5.32),

$$4\pi T = e^{\xi_h/2} \frac{h_1}{L}, \quad (5.54)$$

where we keep in mind that this expression implicitly depends on the quantities $\hat{\mathcal{T}}$ and Q through their appearance in ξ_h and h_1 . A plot of this expression for T (and its derivative with respect to r_h) is shown in the right panel of figure 5.4, which explicitly shows how T has a minimum at a particular value $r_h = r_{h\star}$.

The upshot is that there is a minimum temperature the black hole can describe, and so some other solution must describe the physics below this temperature, similar to the discussion in section

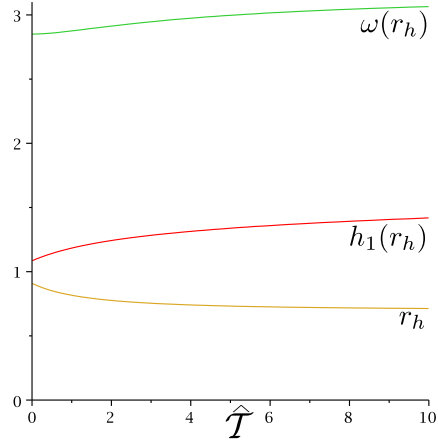


Figure 5.5. Plots, from top to bottom, of $\omega_\star, h_{1\star}$ and $r_{h\star}$ vs $\hat{\mathcal{T}} = \kappa^2 L^2 \mathcal{T}$, where ‘ \star ’ denotes evaluation at the r_h that minimizes the temperature $T(r_h)$. (colour online).

§5.2.1. In the present instance this new solution cannot simply be anti-de Sitter space because of the existence of the black hole charge. Our proposal for this new solution is a ‘stellar’ configuration, described in section §5.3 below.

***L*-dependence of the minimum temperature**

Before turning to what describes the very low-temperature regime, we first pause to examine how the minimum temperature, T_* , varies with L (when ρ_{CFT} , ϕ_0 and are fixed). We do so as a warm-up to a similar discussion for the transition temperature, T_s , between the high- and low-temperature regimes.

Naively, eq. (5.54) suggests that T_* is inversely proportional to L , however this ignores the potential L -dependence that the parameters ξ_{h_*} and h_{1*} might acquire due to their implicit dependence on the quantities $Q = \rho_{CFT}L^2$ and $\hat{\mathcal{T}} = \kappa^2L^2\mathcal{T}$ appearing in eqs. (5.50) and (5.51), as well as through the dependence on r_c that ξ_h implicitly acquires once the solution is matched onto the solution at infinity.⁸

The dependence on Q can be understood analytically as follows. In general we can regard (5.50) and (5.51) as being solved for h_1 , h_2 , ω and $Q^2e^{\phi_h}$ as functions of r_h and $\hat{\mathcal{T}}$: *i.e.* $h_1 = h_1(r_h, \hat{\mathcal{T}})$ and so on. In particular, it follows that none of h_1 , h_2 or ω can depend on Q at all if r_h and $\hat{\mathcal{T}}$ are fixed.

Furthermore, the $\hat{\mathcal{T}}$ dependence of h_1 , h_2 and ω is also usually weak. The dependence of r_{h_*} , h_{1*} , and ω_* on $\hat{\mathcal{T}}$ as computed numerically is plotted in figure 5.5, showing this dependence to be comparatively weak, and becoming weaker for larger $\hat{\mathcal{T}}$.

To see why this is so, recall that eq. (5.42) shows that $X_h = \mathcal{O}(\hat{\mathcal{T}})$ for small $\hat{\mathcal{T}}$ and $X_h = 1 + \mathcal{O}(1/\hat{\mathcal{T}})$ when $\hat{\mathcal{T}}$ is large, and so the quantity $\hat{\mathcal{T}}(1 - X_h)/X_h$ is independent of $\hat{\mathcal{T}}$ in both of these limits.⁹ When this is true the only other relevant $\hat{\mathcal{T}}$ -dependence comes from the combination $Q^2e^{\phi_h}X_h/\hat{\mathcal{T}}$, which is again independent of $\hat{\mathcal{T}}$ when $\mathcal{T} \ll 1$. By contrast, when it is large $\hat{\mathcal{T}}$ only appears in the combination $y := Q^2e^{\phi_h}/\hat{\mathcal{T}}$, in which case eqs. (5.50) and (5.51) give y , h_1 , h_2 and ω as a function of r_h only.

We see in particular that the factor h_1 appearing in eq. (5.54) is independent of Q and becomes approximately independent of $\hat{\mathcal{T}}$ when $\hat{\mathcal{T}}$ is very large or small. The only remaining potential L -dependence in T_* can only appear through ξ_{h_*} .

To address this, return to the exact equations, eqs. (5.35) through (5.37), governing $\xi(r)$, $\phi(r)$ and $h(r)$. The first observation is that these equations have a symmetry under which ξ is shifted by a constant, and the constant part of ϕ only appears in eq. (5.37), which can be written

$$X^{-2} = 1 + \frac{Q^2e^{\phi_h}}{\hat{\mathcal{T}}^2r^4} e^{\Phi(r)} = 1 + \frac{\mathcal{C}(r_h, \hat{\mathcal{T}})}{\hat{\mathcal{T}}^2r^4} e^{\Phi(r)}, \quad (5.55)$$

⁸See, for example, the discussion below eq. (5.49) showing $\xi_h \simeq 8 \ln(r_h/r_c)$ in the large- r_h limit.

⁹Strictly speaking, these asymptotic limits assume $r_h \gg 1$, however they can be checked ex-post-facto also in the small- r_h limit.

if we redefine $\phi(r) = \phi_h + \Phi(r)$. In this case $\Phi(r_h) = 0$ and eq. (5.55) uses that the quantity $Q^2 e^{\phi_h} = \mathcal{C}(r_h, \hat{\mathcal{T}})$ can be found by solving eqs. (5.50) and (5.51), and so is a function only of r_h and $\hat{\mathcal{T}}$. Furthermore, we also saw that \mathcal{C} is independent of $\hat{\mathcal{T}}$ when $\hat{\mathcal{T}} \ll 1$ while $\mathcal{C}/\hat{\mathcal{T}}$ is independent of $\hat{\mathcal{T}}$ when $\hat{\mathcal{T}} \gg 1$.

If we now solve eqs. (5.35), (5.36) and (5.55) for $\xi(r)$, $\Phi(r)$ and $h(r)$, it is clear that the results must be independent of Q . They must also be largely independent of $\hat{\mathcal{T}}$, when this is very large or small, as may be seen either from (5.55) using the limiting forms of $\mathcal{C}(r_h, \hat{\mathcal{T}})$, or (in the attractor regime, but for larger r) by using the large- or small- $\hat{\mathcal{T}}$ limits of eq. (5.42).

The result is a set of universal profiles for ξ , Φ and h in the attractor region, which then fan out to different Q - and $\hat{\mathcal{T}}$ -dependent asymptotic forms at $r > r_c$ to satisfy the boundary conditions at infinity. This is shown numerically in fig. 5.6, which shows how $X(r)$ takes a universal profile for $r < r_c$ for different values Q . Finally, the L -dependence of ξ_h is fixed by this matching to the asymptotic region at r_c , and since r_c is large we may do this matching as before using the approximate expression, (5.41), to obtain $e^{\xi_h/2} = K(r_h)(r_h/r_c)^4$, where $K(r_h)$ is a function whose form we do not need in what follows.

Using this in 5.54, our temperature has the form

$$4\pi LT = \left(\frac{r_h}{r_c}\right)^4 h_1(r_h)K(r_h), \quad (5.56)$$

for small $r_h \ll r_c$. We see that we find the same r_c dependence as found earlier even when $r_h \sim 1$.

From here on the argument proceeds as in the discussion below eqs. (5.48): processes taking place at fixed

$$r_h = r_h(LTr_c^4), \quad (5.57)$$

lead to a T vs L relation of the form $T \propto 1/Lr_c^4$, which becomes $T \propto 1/L^5$ in the scale invariant case or $T \propto 1/L^{n+1}$ more generally, depending on the size and scaling behaviour of the tension.

Fig. 5.7 gives a cartoon of the finite-size picture. This figure plots cartoon profiles of r_h/L and r_c/L as a function of system size for fixed temperature and charge density. The quantity $r/L = \tilde{r}/L^2$ is drawn because it is what tracks the energy scale of the CFT. In both panels the upper r_h curve uses a temperature corresponding to the $z = 1$ regime (*i.e.* $r_h > r_c$) and the lower curve one for the $z = 5$ region ($r_h < r_c$). The left panel chooses \mathcal{T} small enough that $\hat{\mathcal{T}} \ll 1$ throughout, showing how

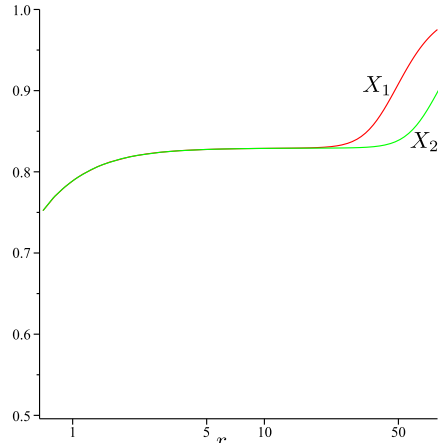


Figure 5.6. Here we plot the function $X(r)$ defined in (5.37) for two different values of Q with $\hat{\mathcal{T}} = 10$. (X_1 uses $Q = 200000$ and X_2 uses $Q = 800000$.) In the attractor region X is approximately constant, $X(\hat{\mathcal{T}})$, until r becomes sufficiently small that the large- r approximation fails. Even when $r \sim 1$ X remains Q -independent, and Q only determines where the crossover between the $z = 5$ and $z = 1$ regions occurs.

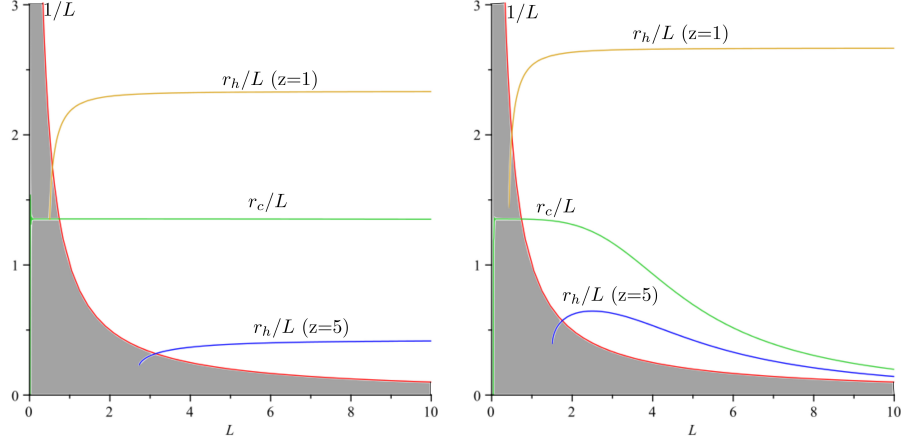


Figure 5.7. Two cartoons of r_h/L and r_c/L as a function of system size for fixed temperature and charge density. The upper (lower) r_h curve uses a temperature corresponding to the $z = 1$ ($z = 5$) region. The shaded area marked $1/L$ shows where finite-size effects become important. The curves for $r_h(L)$ stop for small L due to the existence of a minimum temperature. The left panel chooses \mathcal{T} small enough that $\hat{\mathcal{T}} \ll 1$ throughout, while in the right panel \mathcal{T} is larger so $\hat{\mathcal{T}}$ is negligible only to the far left. The curves assume $n = 0$ (i.e. $\mathcal{T} \propto L^2$).

both r_h and r_c are proportional to L in this regime. In the right panel \mathcal{T} is larger so $\hat{\mathcal{T}}$ is negligible only to the far left, and we choose $n = 0$ in the figure so $\mathcal{T} \propto L^2$. The shaded area marked $1/L$ in the figure shows in the same units where $r < 1$ and so where finite size effects become important. In particular, for each temperature the curve $r_h(L)$ becomes undefined for sufficiently small L in this region, due to the existence of a minimum temperature for the black hole. This also shows how the large- L limit gives us back the black brane case, as the finite size effects coming from the energy scale $1/L$ become vanishingly small in the infinite system limit.

5.3 The low-temperature phase: a charged star

We now describe the alternative solution that describes the AdS/QHE system for small temperatures. This cannot be the empty AdS solution considered in ref. [19] because of the requirement that the solution carry electric charge Q . For this reason in this section we propose a charged star as the alternative low-temperature solution, and interpret the transition between the low-temperature and high-temperature phases of the CFT as corresponding on the gravity side to the transition, with increasing mass, from a stellar solution to a black hole solution.

This section develops this proposal in three steps. First §5.3.1 solves the equations of hydrostatic equilibrium to obtain the properties of a charged star. Then §5.3.2 compares the free energy of this solution with the corresponding black hole solutions, identifying in particular the temperature, T_s , at which the transition between a star and a black hole occurs. Finally, §5.3.3 examines how T_s changes with L .

5.3.1 Hydrostatic equilibrium for a charged star

To find the new low-temperature solution we solve the Tolman-Oppenheimer-Volkoff (TOV) equations for a charged star in asymptotically AdS space. We ultimately solve these equations numerically, using values for the stellar mass and charge (and asymptotic dilaton) corresponding to those used in calculating the free energies for both the black hole and stellar solutions in later sections.

For the action of a charged perfect fluid in the stellar interior we follow [21] and use

$$\mathcal{L}_{\text{fluid}} = -\sqrt{-g} \left[\rho_m + \lambda_1 (u^\mu u_\mu + 1) + \rho_c u^\mu (\nabla_\mu \lambda_2 + A_\mu) \right], \quad (5.58)$$

where u^μ is the fluid's 4-velocity, and ρ_m and ρ_c are its mass and charge densities. λ_1, λ_2 are Lagrange multipliers, introduced to enforce the 4-velocity condition $u^\mu u_\mu = -1$ and conservation of charge $\nabla_\mu (\rho_c u^\mu) = 0$.

The stress-energy tensor for this action is

$$T_{\mu\nu}^f = (\rho_m + p) u_\mu u_\nu + p g_{\mu\nu}, \quad (5.59)$$

to which we add the energy-momentum tensor for the dilaton and the DBI action,

$$T_{\mu\nu}^{DBI} = \frac{2}{\sqrt{-g}} \left(\frac{\partial \mathcal{L}_{DBI}}{\partial g^{\mu\nu}} \right), \quad (5.60)$$

to obtain the full energy momentum tensor for our DBI-charged star,

$$\begin{aligned} T_{\mu\nu} = & (\rho_m + p) u_\mu u_\nu + p g_{\mu\nu} - \frac{1}{4\kappa^2} [g_{\mu\nu} \partial^\lambda \phi \partial_\lambda \phi - 2 \partial_\mu \phi \partial_\nu \phi] \\ & - g_{\mu\nu} \mathcal{T}(X - 1) + G_\mu^\lambda F_{\nu\lambda}. \end{aligned} \quad (5.61)$$

Because $SL(2, R)$ invariance requires the stress tensor to be invariant, we imagine ρ_m, p and u^μ to be $SL(2, R)$ invariant. We cannot also do so for the charge density, ρ_c , because we know that the Maxwell field (and in particular the total electric charge Q) transforms. For general transformations electric charge gets mapped into magnetic charge, and so specifying a fully $SL(2, R)$ invariant fluid would require having both electric and magnetic charge densities. We side-step this issue here, and for the purposes of comparing to black hole solutions with axion and magnetic fields turned off we consider only electrically charged matter and ignore the axion.

The Einstein equation is as before (but using this new stress energy tensor); the dilaton field equation remains unchanged; and the Maxwell equation inside the star is modified to

$$\nabla_\mu G^{\mu\nu} = J^\nu = \rho_c u^\nu. \quad (5.62)$$

The field equation describing the motion of the fluid is given by conservation of energy-momentum

$$\begin{aligned}
 \nabla_\mu T^{\mu\nu} &= -\frac{1}{4\kappa^2} [2(\partial_\lambda\phi)\nabla^\nu\nabla^\lambda\phi - 2(\partial_\mu\phi)\nabla^\mu\nabla^\nu\phi - 2(\partial^\nu\phi)\square\phi] + \nabla_\mu [u^\mu u^\nu(\rho_m + p) + p g^{\mu\nu}] \\
 &\quad -\mathcal{T} \left[\frac{\partial X}{\partial F_{\mu\lambda}} \nabla^\nu F_{\mu\lambda} + \frac{\partial X}{\partial\phi} \partial^\nu\phi \right] - F^\nu{}_\lambda \nabla_\mu G^{\mu\lambda} - G^{\lambda\mu} \nabla_\mu F_{\lambda}{}^\nu \\
 &= -g^{\nu\sigma} G^{\mu\lambda} \left(\frac{1}{2} \nabla_\sigma F_{\mu\lambda} + \frac{1}{2} \nabla_\mu F_{\lambda\sigma} + \frac{1}{2} \nabla_\lambda F_{\sigma\mu} \right) - F^\nu{}_\lambda J^\lambda \\
 &\quad + \nabla_\mu [u^\mu u^\nu(\rho_m + p) + p g^{\mu\nu}] \\
 &= -F^\nu{}_\lambda J^\lambda + \nabla_\mu [u^\mu u^\nu(\rho_m + p) + p g^{\mu\nu}] = 0,
 \end{aligned} \tag{5.63}$$

in which the fluid 4-velocity is $u_\mu = \delta_\mu^t \sqrt{-g_{tt}}$, and the right-hand-side has been simplified using the other field equations.

To solve these we adopt the following *ansätze* for the Maxwell field,

$$G^{tr} = \frac{D(r)}{L^2 \sqrt{-g_{tt}g_{rr}}}, \tag{5.64}$$

and the metric,

$$ds^2 = -e^{2a(r)} dt^2 + \frac{L^2 dr^2}{1 + r^2 - \kappa^2 m(r)/4\pi Lr} + L^2 r^2 d\Omega^2. \tag{5.65}$$

The equations for the unknown functions $D(r)$, $a(r)$, $m(r)$, $\rho_m(r)$, $\rho_c(r)$, $p(r)$ and $\phi(r)$ then simplify to a set of coupled ordinary differential equations. The Maxwell equation becomes

$$D' + \frac{2D}{r} - \frac{L^3 \rho_c}{\sqrt{1 + r^2 - \kappa^2 m/4\pi r L}} = 0, \tag{5.66}$$

and the dilaton equation is

$$\left(1 + r^2 - \frac{\kappa^2 m}{4\pi Lr}\right) \left(\phi' a' + \frac{2\phi'}{r} + \phi''\right) + \phi' \left(r - \frac{\kappa^2 m'}{8\pi Lr} + \frac{\kappa^2 m}{8\pi Lr^2}\right) + \frac{\hat{\mathcal{T}}(X^2 - 1)}{X} = 0, \tag{5.67}$$

while the Einstein equations are

$$m' - 4\pi \rho_m L^3 r^2 - \frac{4\pi L \hat{\mathcal{T}}}{X} (1 - X) - L\pi \left(1 - \frac{\kappa^2 m}{4\pi Lr} + r^2\right) (\phi')^2 = 0 \tag{5.68}$$

$$\text{and } 2a' - \frac{r}{4} (\phi')^2 - \frac{\frac{\kappa^2 m}{4\pi L} - 2r^3 + r^3 \left(L^2 \kappa^2 p - \frac{\hat{\mathcal{T}}}{X} (1 - X)\right)}{2r^2 (1 + r^2 - \kappa^2 m/4\pi Lr)} = 0. \tag{5.69}$$

Finally, conservation of energy-momentum becomes

$$p' + (p + \rho_m) a' - \frac{\rho_c e^{\phi/2} \sqrt{1 - X^2}}{\kappa^2 L^2 \sqrt{(1 + r^2 - \kappa^2 m/4\pi Lr)}} = 0, \tag{5.70}$$

and the function X reduces to

$$X^{-2} = 1 + \frac{D^2 e^\phi}{\hat{\mathcal{T}}^2 L^4}. \quad (5.71)$$

These equations are to be integrated subject to a choice of equation of state, $p = p(\rho_c)$ and $\rho_m = \rho_m(\rho_c)$, and in practice we solve these numerically (see however [26] for a semi-analytic approach to a similar problem). Figure 5.8 plots a solution assuming an incompressible equation of state, with ρ_m and ρ_c constants. For pure gravity and asymptotically flat spacetimes the mass at which a star forms a black hole with this equation of state is the largest possible [27], and so for simplicity we use it here for all explicit numerical integrations in the hopes that it also provides the most massive possible stars in this more complicated theory. However we do not believe this plays a crucial role for the purposes of identifying how the solutions scale with changes to L .

The boundary conditions to be satisfied require all fields be regular at $r = 0$, and so $a'(0) = m'(0) = m(0) = \phi'(0) = D(0) = 0$. They must also be continuous across the stellar surface — which is defined as the radius, $r = r_s$, where $p(r_s) = 0$. For instance, for the Maxwell field the function $D(r)$ must be matched to the exterior solution, for which $D_{\text{ext}}(r) = Q/r^2$, and so $D(r_s) = Q/r_s^2$. The metric functions similarly continuously match to the exterior solutions described in the previous sections, and the stellar mass, M , is identified as the ADM mass for the asymptotic external geometry.

All told, for a given equation of state we have a three-parameter family of initial conditions, corresponding to our choice for the central values, $\phi(0)$ and $p(0)$, as well as the periodicity, β' , of the euclidean time direction at infinity. (There are four parameters if we also include the local charge-to-mass ratio, rather than thinking of $\rho_c(0)/\rho_m(0)$ as an equation of state.) Integrating the equations then allows all other parameters to be computed for $r > 0$. For AdS/CFT applications these three parameters are instead regarded as all being specified at infinity, by giving β , ϕ_0 and the stellar mass, and then integrating the solutions towards smaller r . (Q is the fourth parameter if $\rho_c(0)/\rho_m(0)$ is also regarded as to be specified.) Since we build the star from charged matter, it is physically clear that no stable solution should be possible unless the mass is large enough compared with the charge to allow gravitational attraction to overwhelm electrostatic repulsion.

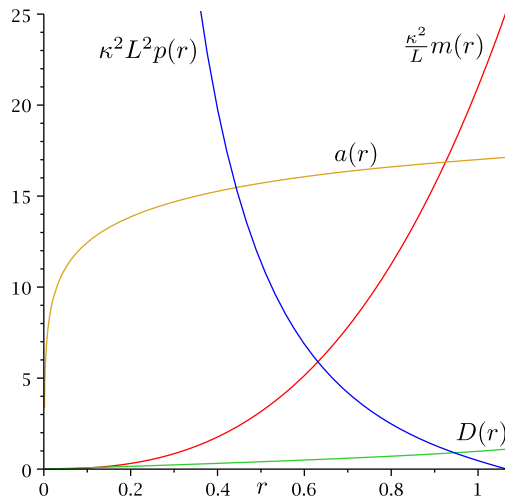


Figure 5.8. A plot of the properties of the interior of an incompressible star for $Q = 1.25$, $\hat{\mathcal{T}} = 1/1000$. The assumption of constant mass and charge density is used as an illustrative example, since we are not interested in the exact values of stellar masses or radii (colour online).

If we do scale the system size, $L \rightarrow \lambda L$, then dimensional analysis shows that the field equations remain invariant provided we also rescale, $\kappa^2 p \rightarrow \lambda^{-2} \kappa^2 p$, $\kappa^2 \rho_m \rightarrow \lambda^{-2} \kappa^2 \rho_m$, $\kappa^2 m \rightarrow \lambda \kappa^2 m$, and $\rho_c \rightarrow \lambda^{-3} \rho_c$. This implies that calculable quantities like the stellar size, r_s , and stellar mass, M , must obey scaling relations like

$$\kappa^2 M = L \mathcal{F} \left(L^2 \kappa^2 p(0), L^3 \rho_c(0), \hat{\mathcal{T}}, \phi_0 \right), \quad (5.72)$$

for some dimensionless function \mathcal{F} .

5.3.2 Energetics of the transition

In this section we work out the free energy of the black hole and stellar regimes and identify when thermodynamics prefers the crossover to be from one phase to the other.

Comparison of the free energies

The free energy in both phases is computed in appendix 5.B, leading to the following expressions

$$F_T(T) = \frac{4\pi L T \beta}{\kappa^2} \int_{r_h}^{r_\infty} dr e^{\xi(r)/2} r^2 \left[3 + \frac{\hat{\mathcal{T}}(X-1)}{X} \right] \quad (5.73)$$

$$F_S(T) = \frac{4\pi L T \beta'}{\kappa^2} \left\{ \int_0^{r_s} \frac{dr e^{a(r)/2} r^2}{\sqrt{1+r^2 - \kappa^2 m/4\pi L r}} \left[3 + \frac{\hat{\mathcal{T}}(X-1)}{X} + \frac{\kappa^2 L^2}{2} (p - \rho_m) \right] + \int_{r_s}^{r_\infty} dr e^{\xi(r)/2} r^2 \left[3 + \frac{\hat{\mathcal{T}}(X-1)}{X} \right] \right\}, \quad (5.74)$$

where F_T (or F_S) is the free energy computed with the black hole (or stellar) solution. β' is the periodicity of the time circumference for the stellar geometry, in the same way that β is for the black hole.

Both solutions are labeled by their total mass and charge, the asymptotic value, ϕ_0 , for the dilaton, and by the periodicity, β , of their time direction (in euclidean signature). As discussed earlier, $SL(2, R)$ invariance guarantees Q and ϕ_0 only appear through the combination $Q^2 e^{\phi_0}$, in principle leaving three independent parameters.

For the black-hole solution the total mass can be traded for the horizon radius, r_h , which should be regarded as a function of the other externally fixed variables. Regularity of the (euclidean signature) geometry at $r = r_h$ then also gives β as a function of these other quantities.

For a stellar solution, rather than specifying quantities like the central pressure deep within the star and integrating out to larger r , we instead regard the asymptotic mass, charge and dilaton field to be the quantities specified by the CFT parameters, and integrate in towards smaller values of r to find the properties interior to the star. In principle the total stellar mass can be traded for the

stellar radius, r_s , given a specific internal equation of state.

Since both r_s and r_h can be computed for a given set of asymptotically specified parameters, they can be compared with one another. Physically we expect $r_h < r_s$, since otherwise the metric function, g_{tt} , vanishes before the stellar surface is reached, making the solution a black hole. The left panel of figure 5.9 verifies this expectation in a comparison between r_s and r_h for shared external parameters, in the particular case where the geometry external to the star and black hole has the $z = 5$ attractor form given above. The calculation is much easier in this case because the quantity X is then a constant, and r_s for the stellar solution can be computed from the condition that $X(r = r_s) = X_h$, with r_h computed from $h(r_h) = 0$ in this geometry. For small r we do this by solving for r_h numerically using the implicit expression for $h(r)$ in (5.49).

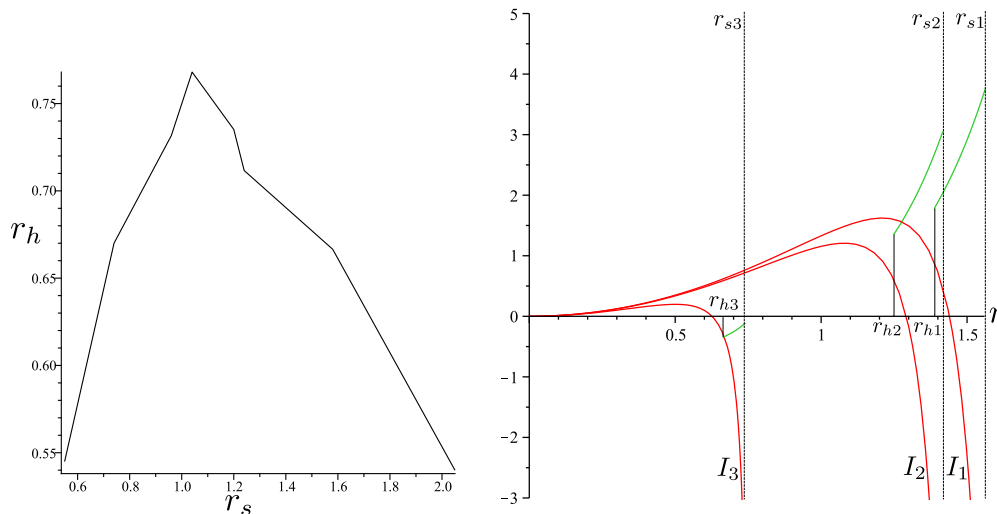


Figure 5.9. Left panel: A comparison of the black-hole horizon radius, r_h , and stellar size, r_s , for a shared choice of asymptotic boundary conditions in the special case that the external geometry just outside the star or black hole has the $z = 5$ asymptotic form (see text for discussion). Right panel: The integrands for the two terms in (5.75) for the free-energy difference between stellar and black-hole geometries. The red curves labeled I_1, I_2 , and I_3 give the contribution of the stellar interior, for the following values of central pressure: $\kappa^2 L^2 p(0) = 10^5, 10$, and 1 for which $r_s = 1.56, 1.42$, and 0.74 respectively. The remaining three (green) curves show the contribution from the exterior geometry. These curves rise sharply at r_h , which can be seen to occur at $r_h = 1.39, 1.25$, and 0.66 respectively. All curves stop at the value $r = r_s$ appropriate to the solution in question. The free energy difference evaluates to $\Delta F_1 = -.21$, $\Delta F_2 = -.01$, and $\Delta F_3 = .045$. Left panel uses $\hat{\mathcal{T}} = 10^{-5}$, and right panel uses $\hat{\mathcal{T}} = 10^2$ (colour online).

Because we specify the same quantities at large distances and integrate into the interior for both stellar and black hole solutions, both the black hole and stellar phase will share the same exterior geometry for $r > r_s$ at fixed $Q, \hat{\mathcal{T}}$ and ϕ_0 . Because of this $\beta' = \beta = 1/T$, although for the black-hole solution β is not regarded as being independent of the other quantities.

Given these observations, appendix 5.B shows that the free-energy difference, $\Delta F := F_T - F_S$,

takes the form

$$\Delta F = \frac{4\pi L}{\kappa^2} \left\{ - \int_0^{r_s} dr \frac{e^{a(r)/2} r^2}{\sqrt{1+r^2 - \kappa^2 m/4\pi L r}} \left[3 + \frac{\hat{T}(X-1)}{X} + \frac{\kappa^2 L^2}{2} (p - \rho_m) \right] + \int_{r_h}^{r_s} dr e^{\xi(r)/2} r^2 \left[3 + \frac{\hat{T}(X-1)}{X} \right] \right\}. \quad (5.75)$$

The right panel of figure 5.9 plots the integrands of this expression, with the red curves labeled I_1 , I_2 and I_3 giving the contribution of the stellar interior ($0 < r < r_s$) for successively smaller choices of central pressure. This shows that this integral contributes a negative contribution to ΔF for large central pressures (because of the explicit negative sign in front of the integral in (5.75)), which becomes less negative for smaller central pressures. The three smaller green curves plot the contribution of the external geometry ($r_h < r < r_s$) for the same external parameters, showing these contribute a decreasing (and eventually negative) amount to ΔF , that decreases with decreasing central pressure.

The figure shows that it is the black-hole phase that has the lower free energy (negative ΔF) for large enough central pressures, although the free-energy differential between the two solutions falls with falling stellar mass (and so also central pressure). Because the black-hole free energy has a minimum temperature and the stellar free energy does not, the free energy difference eventually changes sign, leading to an eventual crossover to the stellar phase (positive ΔF) at lower central pressures.

The physical picture that emerges is as follows. Imagine we fix the system size, L , and start the system at high temperatures with parameters chosen so that a $z = 5$ region exists for sufficiently small r . For sufficiently large temperatures only a black hole solution is possible, because the euclidean time direction at large r has a small enough circumference to ensure that integrating the field equations down to smaller r leads to a zero of g_{tt} for some r_h that is larger than the would-be size r_s of the star having the same mass and charge. Alternatively, large temperature means large r_h and for very large r_h no stellar solutions are possible because large r_h corresponds to a total mass above the Chandrashekar limit, for which there is no central pressure large enough to support a star.

As we bring down the temperature, the asymptotic circumference in the t direction increases, and so the value of r_h where g_{tt} vanishes decreases. Eventually we reach a point where r_h lies sufficiently below r_s to ensure that the total mass is below the Chandrashekar limit, in which case the stellar phase is permitted. Since the central pressure is high, the stellar phase at first has a higher free energy than the black-hole solution, and so the system remains in the black-hole phase. As T continues to fall, ΔF becomes less negative until eventually the stellar phase becomes preferable. Precisely where this occurs likely depends on the details of the stellar equation of state chosen (although we argue below that this is not important for the purposes of identifying how the transition temperature depends on system size). At sufficiently small temperatures no black hole solution exists at all as an

alternative to the stellar solution.

5.3.3 Shape of the transition curve

We now seek the shape of the transition curve, $T_s(L)$, that is defined by the condition $\Delta F = 0$. Notice that the free-energy expressions expose the variables on which ΔF depends,

$$\Delta F = \frac{4\pi L}{\kappa^2} \left[\mathcal{F}_T(r_h, Q e^{\phi_h/2}, \hat{\mathcal{T}}) - \mathcal{F}_S(r_h, Q e^{\phi_h/2}, \hat{\mathcal{T}}) \right]. \quad (5.76)$$

and we do not separately list r_s because, as we have seen, r_s and r_h are not independent of one another since they are both proxies for the total stellar (or black hole) mass.

If, however, the geometry of the region $r_h < r < r_s$ lies within the $z = 5$ attractor regime, as is required for successful description of quantum Hall temperature scaling, even fewer parameters turn out to be independent. This is because $X = X(Q e^{\phi/2}, \hat{\mathcal{T}})$ evaluates to an r -independent constant in this regime, whose value $X(r) = X(r_h) := X_h$ is completely determined by $\hat{\mathcal{T}}$. X is kept constant in this near-horizon regime because the dilaton adjusts itself as Q is varied to keep $Q e^{\phi/2}$ fixed at any given r , allowing any dependence on $Q e^{\phi_h/2}$ to be traded for a dependence on r_h and $\hat{\mathcal{T}}$, and so

$$\Delta F = \frac{4\pi L}{\kappa^2} \left[\mathcal{F}_T(r_h, \hat{\mathcal{T}}) - \mathcal{F}_S(r_h, \hat{\mathcal{T}}) \right]. \quad (5.77)$$

Finally, we know that $\hat{\mathcal{T}}$ drops out of the field equations and the integrand of the free energy when it is either very large or small. So long as this is true, we are effectively left with the free energy difference

$$\Delta F = \frac{4\pi L}{\kappa^2} \left[\mathcal{F}_T(r_h) - \mathcal{F}_S(r_h) \right]. \quad (5.78)$$

This shows that the condition $\Delta F = 0$ may be regarded as a condition that r_h takes on a fixed value (as anticipated in earlier sections).

Now the discussion follows the discussion below eq. (5.47), which tells us we may trade a dependence on r_h for a dependence on LT and r_c as shown in 5.2.2, with r_c depending differently on L depending on whether or not $\hat{\mathcal{T}}$ is large or small, so the free energy difference becomes

$$\Delta F = \frac{4\pi L}{\kappa^2} \left[\hat{\mathcal{F}}_T(LT r_c^4) - \hat{\mathcal{F}}_S(LT r_c^4) \right]. \quad (5.79)$$

Recalling equations (5.48), if there exists a T_s for which $\Delta F(LT_s r_c^4) = 0$, then clearly $T_s \propto 1/L^5$ for $\hat{\mathcal{T}} \ll 1$ and $T_s \propto 1/L^{n+1}$ for $\hat{\mathcal{T}} \gg 1$.

Notice that this argument is fairly robust, since it rests on only a small number of assumptions. The first is that the near-horizon geometry is well-described by the $z = 5$ attractor geometry, since then the attractor mechanism guarantees the value of X is independent of the boundary value of ϕ_0 and Q . This assumption is always satisfied for the parameter regime describing quantum Hall

systems, since it is this regime that ensures the success of the prediction $p = 2/z$ for the scaling exponent.

The second, more model-dependent, assumption is that the dimensionless tension, $\hat{\mathcal{T}} = \kappa^2 L^2 \mathcal{T}$ is either very large or very small. (If $\hat{\mathcal{T}}$ is large, then the discussion below eq. (5.51) shows that we must also require that $Q^2 e^{\phi_h} X_h / \hat{\mathcal{T}} \ll 1$.) The robustness of these choices shows that it should be generic that $T_s \propto L^{-1-n}$ for large dimensionless tension and $T_s \propto L^{-5}$ occurs when the dimensionless tension is very small. Finally, it should also be possible to choose special values $\hat{\mathcal{T}} \sim 1$ for which these behaviours fail.

These choices fall within the domain of validity of the calculation, which was defined by two separate conditions. The first is for small $\hat{\mathcal{T}}$, in which $Q^2 e^{\phi_h}$ is fixed by the attractor to a number independent of $\hat{\mathcal{T}}$, and the free energy has a transition that is only dependent on the quantity LT . The second is for large $\hat{\mathcal{T}}$, for which $Q^2 e^{\phi_h}$ is again fixed by the attractor, although this time proportional to $\hat{\mathcal{T}}$ because of (5.44). In both these cases Q can be large if e^{ϕ_h} is small enough since $SL(2, R)$ ensures they always appear together.

Conductivity in the low-temperature regime

It is one thing to have a new low-temperature regime, but does it have the right properties to describe real quantum Hall systems? Answering this is a research project in itself, but we suffice here to argue that conductivities become independent of temperature in this regime, as they must to agree with observations.

To see this, consider the formula for the Ohmic conductivity given in appendix 5.A,

$$\sigma_{\theta\theta}^2 \simeq \sin^2 \theta e^{-2\bar{\phi}} \mathcal{T}^2 \ell^8 + \frac{e^{-\bar{\phi}_0} Q^2 \ell^4}{L^4 r_h^4}. \quad (5.80)$$

For the black-hole solution quantities like r_h can be traded for temperature, because the nonsingularity of the horizon geometry relates the periodicity, β , to other geometrical quantities. The important observation is that this is no longer true for the stellar solutions, because there is no horizon on which to be singular. As a result, none of the variables appearing above depend on temperature, and so both Hall and Ohmic conductivities should be temperature-independent.

Thermodynamic signature

A noteworthy feature of the above description is that the AdS/CFT picture predicts that derivatives of F are discontinuous across the transition to a temperature-independent regime. This makes this a first-order phase transition, with definite implications for the thermodynamic properties of the quantum Hall fluid.

This discontinuity is seen in figure (5.10), which plots the temperature derivative

$$\begin{aligned} \frac{dF_T(T)}{dT} &= \frac{dF_T(T)}{dr_h} \frac{dr_h}{dT} \\ &= -\frac{4\pi L^2}{\kappa^2} \frac{e^{\xi(r_h)/2} r_h^2}{(e^{\xi(r_h)/2} h_1(r_h))'} \left[3 + \hat{\mathcal{T}} \frac{X_h - 1}{X_h} \right], \end{aligned} \tag{5.81}$$

obtained by implicitly differentiating the black-hole expression, eq. (5.91). The second line of this equation uses eqs. (5.54) and (5.91). Here primes denote derivatives with respect to r_h . Notice in particular the kink as we approach the minimum temperature, caused by the vanishing of dT/dr_h at $T = T_*$. There is no similar near-divergence in the stellar-phase free-energy derivative, indicating that it is the black hole free energy that dominates the discontinuity of dF/dT near the transition (see, *e.g.* figure 5.9).

Although it might seem odd to have a discontinuous transition in a finite-sized system, such as this, the discontinuity is a consequence of the large- N limit that is implicit on the CFT side of the AdS/CFT correspondence when working at the classical level on the gravity side.

5.4 Conclusions

We present here a method for modeling finite-size effects within the AdS/CFT description proposed for quantum Hall systems in ref. [7]. We do so following standard tools [19], but adapted to CFTs with nonzero chemical potential. We do so in order to see whether the very successful AdS/CFT description [15], $p = 2/z = 0.4$, of a scaling exponent for how a critical Hall resistance scales with temperature, is consistent with the existence — in the same experiments that measure p — of a crossover to a low-temperature regime for which the Hall resistance is temperature independent. The transition temperature, T_s , between these regimes is measured to depend on system size, L , according to $T_s \propto 1/L$, and we ask whether this is consistent with the holographic identification of $z = 5$ as a dynamical scaling exponent (which would naively predict $T_s \propto 1/L^5$).

We find the holographic AdS/QHE picture is consistent with a transition to a T -independent Hall conductivity at very low temperatures in finite-volume systems. We find that the transition temperature generically depends on system size, L , in a way that depends on how

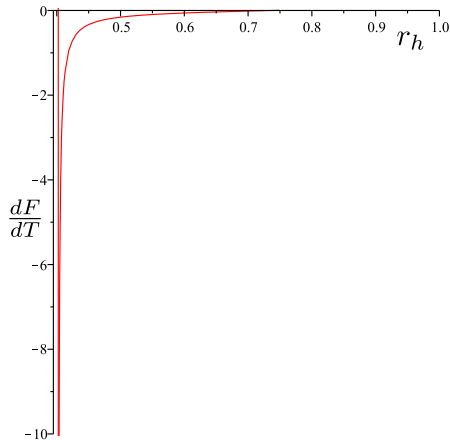


Figure 5.10. Derivative of the free energy in the black hole phase as a function of horizon position (in units of $4\pi L/\kappa^2$). Notice its singular behaviour as the temperature approaches the minimum of the black hole phase.

the brane tension, \mathcal{T} scales as L is varied. Remarkably, the transition is described on the gravity side by the Chandrashekar-like transition from an asymptotically AdS charged star to a black hole, extending similar treatments of stellar objects in AdS/CFT to finite-size systems [22, 21].

Furthermore, we find that the phenomenology of the transition to finite-size effects — and in particular the size-dependence of the transition temperature, $T_s \propto 1/L$ — *can be* consistent with the prediction $p = 2/z$ and the use of $z = 5$, if the dimensionless brane tension, $\hat{\mathcal{T}} = \kappa^2 L^2 \mathcal{T}$, appearing on the AdS side is sufficiently large, and if the brane tension itself scales as $\mathcal{T} \propto L^2$ (so $\hat{\mathcal{T}} \propto L^4$). More generally, when this tension is negligible then naive scaling prevails and the transition temperature satisfies $T_s \propto 1/L^5$. Large \mathcal{T} makes a difference because its presence alters naive scaling relations, and it does so in a way that depends on how \mathcal{T} itself varies as L is varied. If $\mathcal{T} \propto L^{2-n}$ then we find $T_s \propto 1/L^{n+1}$. The case $n = 4$ is scale-invariant in the sense that $\hat{\mathcal{T}} = \kappa^2 \mathcal{T} L^2$ is fixed, and again gives $T_s \propto 1/L^5$.

Tension changes the scaling relations by modifying the L -dependence of the radius, r_c , that defines the crossover between the $z = 5$ near-horizon geometry (relevant to the IR limit) to the asymptotic $z = 1$ geometry that obtains at large r (and is relevant in the UV). Recalling that the existence of different UV and IR scalings relies on the black hole being charged, it is no surprise that r_c grows with black-hole charge: $r_c^4 \propto Q^2 = (\rho_{CFT} L^2)^2$, which implies *in the absence of other scales* that $r_c \propto L$ when the CFT charge density ρ_{CFT} is held fixed. A sizable tension instead changes this relation to a different L -dependent result: $r_c^4 \propto Q^2 / \hat{\mathcal{T}} = L^2 \rho_{CFT}^2 / \kappa^2 \mathcal{T}$.

The L -dependence of r_c makes a difference because within the near-horizon $z = 5$ geometry the relation between the temperature and horizon radius, r_h , is $T \propto 1/(r_c^4 L)$ for fixed r_h . This predicts $T \propto 1/L^5$ in the naive scaling limit, or conformal case, where $r_c \propto L$. But it instead predicts $T \propto 1/L$ in the particular case r_c is L -independent, corresponding to $n = 0$ or $\mathcal{T} \propto L^2$.

Notice that because r_c does not depend on T none of these considerations about r_c modify the Hall conductivity's temperature dependence, which traces its roots to the relation $\sigma_{xy} \propto 1/r_h^2$ and $T \propto r_h^5$. It *does* modify how temperature scales with L , however, for any quantity (like the transition temperature between low- and high-temperature phases) that is defined by a fixed value for r_h .

In the AdS/QHE description the transition is predicted to be a first-order phase transition, for which derivatives like dF/dT are discontinuous.¹⁰ This has implications for the thermodynamics of the quantum Hall fluid at the transition regime, whose presence tests the entire framework. Although such effects would be experimentally challenging to find, their detection would be worth the effort.

Likewise, since both $T_s \propto 1/L$ and $T_s \sim L^{-5}$ are possible, depending on the size of $\hat{\mathcal{T}}$ and our particular UV completion, it would be worth better understanding what the parameter \mathcal{T} captures on the CFT side, in order to suggest how to obtain samples for which T scales differently than $1/L$. Our difficulty in doing so at present is a limitation of our phenomenological approach within which the AdS field equations and brane properties are assumed without reference to a UV completion

¹⁰Discontinuities are allowed at finite volume in holographic descriptions due to the large- N limit that is implicit, on the CFT side, when using semiclassical reasoning (as we do) on the AdS side.

(which would entail a full embedding into string theory).

This is one aspect of an important missing step in the AdS/CFT description of quantum Hall systems: a precise enunciation of its bounds of validity. If this were known we would also know what conditions were sufficient for the inter-plateaux behaviour to be universal and not sample-dependent. Ref. [15] sheds some experimental light on this issue, since it also shows how scaling changes as the samples are doped. Whenever scaling with T is robust — *i.e.* scaling lasts over two decades of temperature — its power is given by the universal value 0.42 ± 0.01 . But such robust scaling is only found for a relatively small range of doping; a range for which scattering from the doped atoms is likely to dominate the conductivity [15, 16]. For other dopings the temperature-dependence of the conductivity is more sample-dependent. It is important to understand from a microscopic point of view what it is about the quantity of dopant that promotes a universal description.

But the larger point is that the holographic AdS/QHE model presented in [7] still has the possibility to be able to agree well with more observations than those that are guaranteed by construction through its incorporation of emergent duality symmetries. We believe that the experimental success of these predictions for p and $T_s(L)$ provide strong evidence that holographic models provide the natural theoretical language for describing quantum Hall systems. As such, quantum Hall systems are also likely to be a rich environment for testing AdS/CFT methods.

Many steps in the AdS/QHE program remain incomplete. Perhaps most important is a robust treatment of disorder in holography, since this plays a central role in producing DC conductivity. Our present tools for exploring holographic conductors remain strongly hampered by an inability to incorporate disorder in a simple way. Work on all these issues proceeds apace.

Acknowledgements

We thank Gabor Csáthy, Brian Dolan, E. Fradkin, Michael Hilke, Janet Hung, S. Kivelson, Sung-Sik Lee, Rob Myers and Yanwen Shang for useful conversations. This research has been supported in part by funds from the Natural Sciences and Engineering Research Council (NSERC) of Canada. Research at the Perimeter Institute is supported in part by the Government of Canada through NSERC and by the Province of Ontario through the Ministry of Research and Information (MRI).

5.A Conductivity for finite size

Since fixed- r surfaces in the finite-size case are spheres rather than planes, linear-response theory is trickier since it is not possible to turn on a constant perturbing electric field. This section discusses how we think about performing this calculation.

To calculate the conductivity at finite size we make two simplifying assumptions.

- We use the $z = 5$ attractor solution of ref. [7], which involves two separate choices. The first

choice is that r_h is large, so that the black-brane solution is a good approximation to the black-hole solution. The second is to use the numerical value $z = 5$, that ref. [7] shows is the near-horizon solution for dilaton-gravity coupled to the DBI action for a non-probe brane. (We do so for the motivations given in the main text).

- The second assumption is to focus the conductivity calculation on a small patch of the sphere in the region of the equator. We do this to avoid any singularities (*e.g.* near the poles) that inevitably arise if a global electric field is applied everywhere on a sphere.

We assume the finite size background to be

$$ds^2 = -h_0 \frac{r^{10}}{r_c^8} \left(1 - \frac{r_h^7}{r^7}\right) dt^2 + \frac{L^2 dr^2}{h_0 r^2 \left(1 - \frac{r_h^7}{r^7}\right)} + r^2 L^2 (d\theta^2 + \sin^2 \theta d\varphi^2), \quad (5.82)$$

which has the temperature

$$4\pi T = \frac{7h_0 r_h^5}{r_c^4 L}. \quad (5.83)$$

Again, this solution is valid when $r_h \gg 1$ and $r_h^4 \ll \frac{Q^2 e^{\phi_0}}{\mathcal{T}^2}$ (which is not the same dilaton in what follows, since we use the probe brane approximation by taking a stack of branes to generate the background, and a separate brane to probe the geometry), that is away from the minimum temperature (and finite size phase transition.)

To get the conductivity, we place a flux through the surface of the sphere from pole to pole. That is, along the θ direction. Corresponding to

$$\begin{aligned} J^\theta &= \sqrt{-g} G^{r\theta} \\ E_\theta(\theta) &= F_{t\theta} \\ Q &= \sqrt{-g} G^{rt}, \end{aligned} \quad (5.84)$$

where $E_\theta(\theta)$ has some angular dependence that satisfies its Maxwell equation. Proceeding with the identical arguments of [7] we get the conductivity

$$\begin{aligned} \sigma_{\theta\theta}^2 &= \left[\mathcal{T}^2 \ell^8 e^{-2\tilde{\phi}} \frac{g_{\varphi\varphi}}{g_{\theta\theta}} + \frac{e^{-\tilde{\phi}} Q^2 \ell^4}{g_{\theta\theta}^2} \right]_{r=r_h} \\ &= \sin^2 \theta e^{-2\tilde{\phi}_0} \mathcal{T}^2 \ell^8 + \frac{e^{-\tilde{\phi}_0} Q^2 \ell^4}{L^4 r_h^4}. \end{aligned} \quad (5.85)$$

For low enough temperatures the second term is dominant, provided

$$\begin{aligned}
 e^{-2\tilde{\phi}_0} \mathcal{T}^2 \ell^8 &\ll \frac{e^{-\tilde{\phi}_0} Q^2 \ell^4}{L^4 r_h^4} \\
 \text{or, equivalently } e^{-2\phi_0} \mathcal{T}^2 \kappa^8 &\ll \frac{e^{-\phi_0} Q^2 \kappa^4}{L^4 r_h^4} \\
 \text{and so } r_h^4 &\ll \frac{Q^2 e^{\phi_0}}{\mathcal{T}^2},
 \end{aligned} \tag{5.86}$$

where the second line uses $\tilde{\phi} = \phi + 4 \log(\ell/\kappa)$ and we set $\sin \theta = 1$ since we are calculating the conductivity near the equator. This is the exact same condition as to be in the $z = 5$ region from (5.39). Expressed as a function of temperature (for the black hole geometry) the conductivity in the finite size case using (5.47), is then

$$\sigma_{\theta\theta} = \kappa^2 \rho_{CFT} e^{-\phi_0/2} \times \begin{cases} \left[\frac{\kappa^4 \mathcal{T}^2}{(7h_0) 4\pi L T \rho_{CFT}^2 e^{\phi_0}} \right]^{2/5} & \text{if } \hat{\mathcal{T}} \gg 1, \\ \left[\frac{119}{(7h_0) 100\pi L^5 T \rho_{CFT}^2 e^{\phi_0}} \right]^{2/5} & \text{if } \hat{\mathcal{T}} \ll 1. \end{cases} \tag{5.87}$$

Here we learn that the scaling of the conductivity with system size is very different in both the large and small tension cases. As we can see, in both cases the conductivity has the same temperature scaling. This can be understood from the fact that the changes in finite-size scaling enter entirely through the quantity r_c , which is independent of temperature.

5.B Free-energy calculations

According to the rules of the AdS/CFT correspondence, to calculate the free energy of the phase corresponding to the CFT we must evaluate the gravity action on shell; *i.e.* at the appropriate solutions to the field equations.

The stellar phase

Taking the trace of the Einstein equations

$$\frac{1}{2\kappa^2} \left[R + \frac{1}{2}(\partial\phi)^2 - \frac{12}{L^2} \right] = -\frac{\mathcal{T}}{X}(X-1)^2 + \frac{1}{2}(3p - \rho_m), \tag{5.88}$$

and using the fact (see ref. [21]) that $\mathcal{L}_{\text{on-shell}}^f = p$, the free energy for the system described by a star evaluates to

$$\begin{aligned}
 F_s(T) &= -TS_{\text{on-shell}} \\
 &= T \int d^4x \sqrt{-g} \left[\frac{3}{L^2 \kappa^2} + \frac{\mathcal{T}(X-1)}{X} - \frac{1}{2}(\rho_m - p) \right] \\
 &= \frac{4\pi L T \beta'}{\kappa^2} \left\{ \int_0^{r_s} \frac{dr e^{a(r)/2} r^2}{\sqrt{1+r^2 - \kappa^2 m/4\pi L r}} \left[3 + \frac{\hat{\mathcal{T}}(X-1)}{X} + \frac{\kappa^2 L^2}{2}(p - \rho_m) \right] \right. \\
 &\quad \left. + \int_{r_s}^{r_\infty} dr e^{\xi(r)/2} r^2 \left[3 + \frac{\hat{\mathcal{T}}(X-1)}{X} \right] \right\}.
 \end{aligned} \tag{5.89}$$

To evaluate the free energy, we numerically solve the field equations and then integrate these functions to some asymptotically large cutoff, r_∞ . Since there is no horizon in this free energy to relate to a temperature, one would naively expect that this free energy is independent of temperature (since the temperature in the definition of free energy will cancel the temperature from integrating the time circle.) While this is true at low temperatures, the free energy is only meaningful when comparing to an alternative (in this case black hole) phase and appropriately normalizing the circumference of the \mathbf{S}^1 's at infinity as in §5.2.1. Doing so causes the free energy of the stellar phase to behave as $\sim T^3$ in a similar way to pure AdS space at large T .

The black-hole phase

To obtain the free energy of the black hole phase we again trace the field equations, but this time without the presence of matter, to give

$$R + \frac{1}{2}(\partial\phi)^2 = \frac{12}{L^2} - \frac{2\kappa^2 \mathcal{T}}{X}(X-1)^2, \tag{5.90}$$

and plugging this into the action gives the free energy

$$\begin{aligned}
 F_T(T) &= -TS_{\text{on-shell}} \\
 &= T \int d^4x \sqrt{-g} \left[\frac{3}{L^2 \kappa^2} + \frac{\mathcal{T}(X-1)}{X} \right] \\
 &= \frac{4\pi L}{\kappa^2} \int_{r_h}^{r_\infty} dr e^{\xi(r)/2} r^2 \left[3 + \frac{\hat{\mathcal{T}}(X-1)}{X} \right].
 \end{aligned} \tag{5.91}$$

We use these expressions to compute the free energy difference between the two phases in §5.3.2.

Bibliography

- [1] J. M. Maldacena, “The large N limit of superconformal field theories and supergravity,” *Adv. Theor. Math. Phys.* **2** (1998) 231 [*Int. J. Theor. Phys.* **38** (1999) 1113] [hep-th/9711200];
S. S. Gubser, I. R. Klebanov and A. M. Polyakov, “Gauge theory correlators from non-critical string theory,” *Phys. Lett. B* **428** (1998) 105 [hep-th/9802109];
E. Witten, “Anti-de Sitter space and holography,” *Adv. Theor. Math. Phys.* **2** (1998) 253 [hep-th/9802150].
- [2] G. T. Horowitz and J. Polchinski, “Gauge / gravity duality: An introduction for nonspecialists,” [gr-qc/0602037];
- [3] O. Aharony, S. S. Gubser, J. M. Maldacena, H. Ooguri and Y. Oz, “Large N field theories, string theory and gravity,” *Phys. Rept.* **323** (2000) 183 [hep-th/9905111];
I. R. Klebanov, “TASI lectures: Introduction to the AdS/CFT correspondence,” [hep-th/0009139].
- [4] S. A. Hartnoll, “Lectures on holographic methods for condensed matter physics,” *Class. Quant. Grav.* **26** (2009) 224002 [arXiv:0903.3246 [hep-th]];
C. P. Herzog, “Lectures on Holographic Superfluidity and Superconductivity,” *J. Phys. A* **42** (2009) 343001 [arXiv:0904.1975 [hep-th]];
J. McGreevy, “Holographic duality with a view toward many-body physics,” arXiv:0909.0518 [hep-th];
S. Sachdev, “Condensed matter and AdS/CFT,” arXiv:1002.2947 [hep-th].
- [5] For a good (but fairly old) introductory review see S.M. Girvin, cond-mat/9907002;
For a more general and more modern review see B. Spivak, S. V. Kravchenko, S. A. Kivelson, X. P. A. Gao, “Transport in strongly correlated two dimensional electron fluids,” *Rev. Mod. Phys.* **82**, 1743 (2010) arXiv:0905.0414 [cond-mat].
- [6] S. A. Hartnoll and P. Kovtun, “Hall conductivity from dyonic black holes,” *Phys. Rev. D* **76** (2007) 066001 [arXiv:0704.1160 [hep-th]];

- J. L. Davis, P. Kraus and A. Shah, “Gravity Dual of a Quantum Hall Plateau Transition,” JHEP **0811** (2008) 020 [arXiv:0809.1876 [hep-th]];
- O. Bergman, N. Jokela, G. Lifschytz and M. Lippert, “Quantum Hall Effect in a Holographic Model,” arXiv:1003.4965 [hep-th];
- F. Aprile, S. Franco, D. Rodriguez-Gomez and J. G. Russo, “Phenomenological Models of Holographic Superconductors and Hall currents,” JHEP **1005** (2010) 102 [arXiv:1003.4487 [hep-th]];
- T. Albash and C. V. Johnson, “Landau Levels, Magnetic Fields and Holographic Fermi Liquids,” J. Phys. A **43** (2010) 345404 [arXiv:1001.3700 [hep-th]];
- J. Tarrío, “Holographic operator mixing - the Hall experiment,” arXiv:0911.4976 [hep-th];
- J. Alanen, E. Keski-Vakkuri, P. Kraus and V. Suur-Uski, “AC Transport at Holographic Quantum Hall Transitions,” JHEP **0911** (2009) 014 [arXiv:0905.4538 [hep-th]].
- Y. Hikida, W. Li and T. Takayanagi, “ABJM with Flavors and FQHE,” JHEP **0907**, 065 (2009) [arXiv:0903.2194 [hep-th]].
- M. Fujita, W. Li, S. Ryu and T. Takayanagi, “Fractional Quantum Hall Effect via Holography: Chern-Simons, Edge States, and Hierarchy,” JHEP **0906**, 066 (2009) [arXiv:0901.0924 [hep-th]].
- [7] A. Bayntun, C. P. Burgess, B. P. Dolan and S. S. Lee, “AdS/QHE: Towards a Holographic Description of Quantum Hall Experiments,” New J. Phys. **13**, 035012 (2011) [arXiv:1008.1917 [hep-th]].
- [8] For a small selection, see
- H.L. Stormer, Physica B177 (1992) 401;
- M. Hilke *et.al.*, Europhysics Letters, 46 (1999) 775-779; [cond-mat/9810217];
- M. Hilke *et.al.*, Nature, **395** (1998) 675-677; [cond-mat/9810172];
- K. Yang *et.al.*, Journal of Physics: Condensed Matter, **12** (2000) 5343-5360; [cond-mat/9805341];
- D. Shahar *et.al.*, Science 274 (1995) 589, [cond-mat/9510113];
- D. Shahar *et.al.*, Solid State Comm. 107 (1998) 19-23, [cond-mat/9706045];
- P.T. Coleridge, Phys. Rev. B60, 4493 (1999);
- P.T. Coleridge, Solid State Comm. 112, 241 (1999);
- Wanli Li *et.al.*, Phys. Rev. Lett. **94** 206807 (2005);
- C.F. Huang *et al.*, “An experimental study on $\Gamma(2)$ modular symmetry on the quantum Hall system with a small spin-splitting,” Journal of Physics: Condensed Matter **19** (2007) 026205; [cond-mat/0609310].

- [9] H.P. Wei *et.al.*, *Phys. Rev. Lett.* **61** (1988) 1294.
- [10] C.A. Lütken, *J. Phys.* **A26** L811 (1993); *Nuc. Phys.* **B396** 670 (1993);
C.P. Burgess and C.A. Lutken, “One-dimensional flows in quantum Hall systems,” *Nuc. Phys.* **500** (1997) 367, [cond-mat/9611118];
“On the Implications of Discrete Symmetries for the β -function of quantum Hall Systems,”
C.P. Burgess and C.A. Lutken, *Phys. Lett.* **B451** 365 (1999), [cond-mat/9812396];
B.P. Dolan, *J. Phys.* **A32** L243 (1999), [cond-mat/9805171];
C.P. Burgess, Rim Dib and B.P. Dolan, “Derivation of the Semi-circle Law from the Law of Corresponding States,” *Phys. Rev.* **B62** 15359 (2000), [cond-mat/9911476];
C. P. Burgess and B. P. Dolan, “The Quantum Hall Effect in Graphene: Emergent Modular Symmetry and the Semi-circle Law,” *Phys. Rev. B* **76** (2007) 113406 [cond-mat/0612269];
C. P. Burgess and B. P. Dolan, “Duality, the Semi-Circle Law and Quantum Hall Bilayers,” *Phys. Rev. B* **76** (2007) 155310 [cond-mat/0701535];
C. A. Lutken and G. G. Ross, “Geometric scaling in the quantum Hall system,” *Phys. Lett. B* **653** (2007) 363;
B. P. Dolan, “Holomorphic and anti-holomorphic conductivity flows in the quantum Hall effect,” *J. Phys. AA* **44** (2011) 175001 [arXiv:1011.6641 [cond-mat.str-el]];
C. A. Lutken and G. G. Ross, “Experimental probes of emergent symmetries in the quantum Hall system,” *Nucl. Phys. B* **850** (2011) 321.
- [11] J. L. Cardy and E. Rabinovici, “Phase Structure Of Z(P) Models In The Presence Of A Theta Parameter,” *Nucl. Phys. B* **205** (1982) 1;
D.E. Khmel'nitskii, *Pis'ma Zh. Eksp. Teor. Fiz.* **38** (1983) 454 [*JETP Lett.* **38** (1984) 552];
C.A. Lütken and G.G. Ross, *Phys. Rev.* **B45**, 11837 (1992); *Phys. Rev.* **B48**, 2500 (1993);
D-H. Lee, S. Kivelson and S-C. Zhang, *Phys. Lett.* **68**, 2386 (1992);
S. Kivelson, D-H. Lee and S-C. Zhang, *Phys. Rev.* **B46**, 2223 (1992).
- [12] M.P.A. Fisher and D.H. Lee, *Physical Review* **B39**, 2756 (1989);
A. Shapere and F. Wilczek, *Nuc. Phys.* **B320** 669 (1989);
S. J. Rey and A. Zee, “Selfduality of Three-Dimensional Chern-Simons Theory,” *Nucl. Phys. B* **352** (1991) 897;
C.P. Burgess and B.P. Dolan, “Particle-Vortex Duality and the Modular Group: Applications to the quantum Hall Effect and Other 2-D Systems,” *Phys. Rev.* **B63** 155309 (2001), [hep-th/0010246];

- E. Witten, “SL(2,Z) Action On Three-Dimensional Conformal Field Theories With Abelian Symmetry,” in Shifman, M. (ed.) et al.: *From fields to strings*, vol. 2, 1173-1200, [hep-th/0307041];
- [13] C. P. Herzog, P. Kovtun, S. Sachdev and D. T. Son, “Quantum critical transport, duality, and M-theory,” *Phys. Rev. D* **75** (2007) 085020 [hep-th/0701036];
- S. A. Hartnoll and C. P. Herzog, “Ohm’s Law at strong coupling: S duality and the cyclotron resonance,” *Phys. Rev. D* **76** (2007) 106012 [arXiv:0706.3228 [hep-th]];
- D. Bak and S. J. Rey, “Composite Fermion Metals from Dyon Black Holes and S-Duality,” arXiv:0912.0939 [hep-th].
- [14] K. Goldstein, S. Kachru, S. Prakash and S. P. Trivedi, “Holography of Charged Dilaton Black Holes,” *JHEP* **1008**, 078 (2010) [arXiv:0911.3586 [hep-th]];
- K. Goldstein, N. Iizuka, S. Kachru, S. Prakash, S. P. Trivedi and A. Westphal, “Holography of Dyonic Dilaton Black Branes,” arXiv:1007.2490 [hep-th].
- [15] Li, W., Vicente, C. L., Xia, J. S., Pan, W., Tsui, D. C., Pfeiffer, L. N., & West, K. W., *Physical Review Letters*, 102 (2009) 216801
- [16] Li, W., Csáthy, G.A., Tsui, D.C., Pfeiffer, L.N., and West, K.W., *Applied Physics Letters* 83 (2003) 2832.
- [17] L. W. Engel, D. Shahar, C. Kurdak, and D. C. Tsui, “Microwave frequency dependence of integer quantum Hall effect: Evidence for finite-frequency scaling,” *Phys. Rev. Lett.* **71**, 2638 (1993).
- [18] B. Huckestein, *Reviews of Modern Physics* **67** (1995) 357-396; [cond-mat/9501106].
- [19] E. Witten, “Anti-de Sitter space, thermal phase transition, and confinement in gauge theories,” *Adv. Theor. Math. Phys.* **2**, 505 (1998) [arXiv:hep-th/9803131].
- [20] A. Karch and E. Katz, “Adding flavor to AdS / CFT,” *JHEP* **0206**, 043 (2002) [hep-th/0205236];
- A. Karch and L. Randall, “Open and closed string interpretation of SUSY CFT’s on branes with boundaries,” *JHEP* **0106**, 063 (2001) [hep-th/0105132].
- [21] S. A. Hartnoll and A. Tavanfar, “Electron stars for holographic metallic criticality,” *Phys. Rev. D* **83**, 046003 (2011) [arXiv:1008.2828 [hep-th]].
- [22] X. Arsiwalla, J. de Boer, K. Papadodimas and E. Verlinde, “Degenerate Stars and Gravitational Collapse in AdS/CFT,” *JHEP* **1101**, 144 (2011) [arXiv:1010.5784 [hep-th]].
- [23] G. W. Gibbons and D. A. Rasheed, “SL(2,R) Invariance of Non-Linear Electrodynamics Coupled to An Axion and a Dilaton,” *Phys. Lett. B* **365** (1996) 46 [hep-th/9509141].

- [24] S. A. Hartnoll, J. Polchinski, E. Silverstein and D. Tong, “Towards strange metallic holography,” JHEP **1004**, 120 (2010) [arXiv:0912.1061 [hep-th]].
- [25] S. A. Hartnoll and C. P. Herzog, “Impure AdS/CFT correspondence,” Phys. Rev. D **77** (2008) 106009 [arXiv:0801.1693 [hep-th]].
M. Fujita, Y. Hikida, S. Ryu and T. Takayanagi, “Disordered Systems and the Replica Method in AdS/CFT,” JHEP **0812** (2008) 065 [arXiv:0810.5394 [hep-th]];
L. -Y. Hung and Y. Shang, “On 1-loop diagrams in AdS space,” Phys. Rev. D **83** (2011) 024029 [arXiv:1007.2653 [hep-th]];
S. Ryu, T. Takayanagi and T. Ugajin, “Holographic Conductivity in Disordered Systems,” JHEP **1104** (2011) 115 [arXiv:1103.6068 [hep-th]].
- [26] M. W. Horbatsch and C. P. Burgess, “Semi-Analytic Stellar Structure in Scalar-Tensor Gravity,” JCAP **1108** (2011) 027 [arXiv:1006.4411 [gr-qc]].
- [27] H. A. Buchdahl, Phys. Rev. **116** (1959) 1027.
- [28] B. McInnes, “A Universal Lower Bound on the Specific Temperatures of AdS-Reissner-Nordstrom Black Holes with Flat Event Horizons,” Nucl. Phys. B **848**, 474 (2011) [arXiv:1012.4056 [hep-th]].

Chapter 6

Conclusion

From the outset, the purpose of this thesis is to demonstrate both the power of phenomenological methods and thus effective theories, as well as to lend particular credence to stringy methods and models. String models have in general provided a large array of theories and frameworks that were not originally considered viable years ago. For instance, extra dimensional models and Kaluza-Klein compactification was originally disposed of due to the instability of the size of the extra dimensions, and the fact that there was no observation of a group of massive particles that were proportional to their (integer) charge. Another instance of a revived model is the case of the Born-Infeld action, which is now a required feature of any theory with open strings coupled to a gauge field.

Most important is the fact that extra dimensional models, when coupled with the existence of branes, are now a viable option in theory space because of string theory. We have seen that this allows for some very rich physics, whether these ideas and techniques are applied to cosmological scenarios or strongly coupled gauge theories. Finally, when we couple these powerful constructs with ideas learned about effective theories from decades of understanding quantum field theory, we can build models without having to rely on explicit string constructs. This allows us to focus on the physics resulting from these models without being buried in the details of the particular embedding in string theory. Of course, the trade-off is that one loses one of the main advantages of string theory, in that these phenomenological models end up having more free parameters than string theory itself has.

We now give a brief overview and outlook on the upshot of the papers present in this thesis.

6.1 Codimension-2 branes: Epilogue

While the codimension-2 back-reaction study essentially fleshed out the framework in treating brane back-reaction onto the full geometry of a theory, this was an important step towards developing cosmological models. In particular, the inclusion of a Maxwell field in this back-reaction framework

has allowed for a stabilization mechanism of the extra dimensions due to flux constraints [23]. Further studies have produced the realization that the effective on-brane cosmological constant is related to the dilaton and Maxwell field in the bulk and explored in [11]. This led to the observation that in this particular set of models, it is possible to have a technically natural small cosmological constant, at the expense of a large brane flux. However, the overarching theme of this study is the better understanding of effective theories in brane-world models. The general feature that the effective potential vanishes on the brane when one considers back-reaction onto the bulk is a striking feature that goes against the intuition that the brane tension should contribute to the effective potential. This allows for the creation of a broad class of cosmological models with the potential feature of a vanishing cosmological constant from back-reaction calculations. It is clear from this study that both string methods and the effective theory approach has led to a large potential of extremely rich physics.

6.2 Quantum Hall-ography: An Outlook

The holographic quantum Hall proposal has a number of extremely promising features. From a theoretical standpoint, it has furthered our understanding of AdS/CFT in application to condensed matter systems. A striking feature of this proposal (and other similar proposals) is that the symmetries of the bulk gauge fields map to the symmetries of the conductivities of the boundary CFTs. This is a rather remarkable feature that is entirely dependent on how the bulk gauge fields relate to the boundary operators by the AdS/CFT dictionary. From this symmetry correspondence alone, many potential models in condensed matter can be built by simply considering their CFT symmetries.

On a more specific point, even if it turns out that this particular model for the quantum Hall effect is inaccurate at describing experiments, there are still other possibilities of finding other models that also incorporate the $SL(2, Z)$. The important aspect of this whole program is that we now have a reliable method of constructing/vetting models of the quantum Hall system in AdS/CFT. This applies equally well to a string-embedded (top-down) or phenomenological (bottom-up) approach as one simply needs to check that one has the correct symmetries. Of course, the calculation of exponents and other conductivity measurements becomes the quantity which truly separates these models and determines the ones which should be taken seriously.

The other major development in this AdS/CMT paradigm is the quantification of finite size effects. We have clearly shown that in the case where one considers a black hole solution, as opposed to a black brane, the AdS radius can be interpreted as following the size of the system. While this observation seems fairly innocuous at first, when it is realized that at low enough temperatures, these black hole solutions are no longer able to describe the system, it is clear that an alternate phase is required to describe lower temperatures. This is an entirely welcome feature as typically condensed matter systems undergo some form of transition when the system size no longer can be neglected from

physical quantities. The purpose of alternate ‘stellar’ solutions are simply a means of quantifying the transition. However, based on recent studies by [26] there are additional interpretations of these stellar solutions in the CFT and further studies of this low temperature phase could produce more quantifiable predictions.

While there have been numerous other studies on finite size effects [27, 28] in Ads/CMT, these typically introduce domain walls and other additional objects into the model. The advantage of our approach is that by not introducing these additional objects, the calculations do not get too much more complicated, while we preserve the very powerful scaling arguments when only dealing with metric quantities.

Finally, with respect to the specifics of our model, we have been successful in reproducing some quantum Hall experiments, while others still remain a theoretical challenge. From simply the symmetry principles of $SL(2, Z)$, we have managed to reproduce the semi-circle features in the conductivity plane. In our particular model, we have seen that our model predicts the scaling exponent $p = 0.4$, with the dynamical exponent $z = 5$ when we allow our model to source the geometry in addition to probing it. Furthermore, microwave experiments that measure $z = 1$ in the UV are further confirmation that we’re on the right track. At present, the clear incompatibility lies in the fact that finite size experiments measure $T \propto 1/L$ while generically the quantum Hall-ography model sees $T \propto 1/L^{n+1}$. One resolution comes from our lack of understanding of the tension on the CFT side of the system, or the potential UV completion to our theory, which may provide a mechanism to allow for $T \propto 1/L$, or $n = 0$.

A potential solution to the disagreement between experiment and our result for $T_s \propto 1/L^{n+1}$ lies in the understanding of the critical exponents measured. In [25], at the transition between the high and low (temperature-independent) temperature phase, there are only two relevant length scales in the problem, the correlation length, $\xi \propto T^{-1/z}$, and localization length, $\zeta = |B - B_c|^{-\nu}$. If we write the conductivity as a function of these variables, the conductivity must take the form

$$\sigma \equiv \sigma(\xi/\zeta) = \sigma\left(\frac{|B - B_c|}{T^{1/\nu z}}\right). \quad (6.1)$$

This form is different from (4.86) in that the additional exponent ν now is present, with the case $\nu = 1/2$ agreeing with (4.86). The authors in [25] interpret measuring $z = 1$ and $1/z\nu = 0.4$ as the condition that $\nu \neq 1/2$. This suggests the localization length has an anomalous dimension associated with it, and it is this anomalous dimension which simultaneously allows the measurement of $p = 0.4$ and $z = 1$. However, it is understood in condensed matter that the presence of an anomalous dimension introduces a new length scale in the problem. Without the additional length scale, all scaling behaviour would be entirely determined by dimensional considerations, or the mean-field result¹.

In our AdS/QHE system we see similar effect happens in the case of the tension. This additional

¹For a particularly good exposition on this idea, see chapter 7 of [29]

scale changes naive scaling arguments, to allow for different dependence of the temperature on the system size. We mention this apparent similarity between the experiment and our model not as a suggestion that tension may model the localization length, but that the fact that we get an unconventional scaling (that isn't coming from the UV or IR region) may come from a similar mechanism in which the localization length plays a role. These questions can be resolved through either the introduction of localization in our model, or a better understanding of the tension on the CFT side.

There are still potential research directions associated with this model. The most pressing is to move away from the probe brane approximation since at this point we must distinguish between the charge carriers and branes that source the geometry, and the charge carriers and probe brane in which we calculate the boundary observables from. This is particularly awkward since it would be much more preferable to have one sector of the action which sources the geometry and further produce the CFT observables we're interested in. This may be particularly helpful from a top-down standpoint, since at some point it would be useful to embed our model in some string theory. Moreover, doing this will help identify the degrees of freedom on the CFT, while providing more insight into the behaviour of the electrons in these strongly correlated systems. Further directions include calculating the Hall viscosity [30] from this model, investigating potential non-abelian anyonic statistics in producing the even integer states, and potentially the states of graphene, which are known to be quantum Hall [31].

At the end of the day, we have shown that while string theory may still be directly unreachable by traditional collider methods (although this statement is becoming debatable), it has produced numerous powerful tools in the theoretical community which are now allowing us to make contact with experiment and observations. When string theory was originally being developed, it was famously slated as "21st century mathematics in a 20th century world". While this statement was likely originally intended to give awe to the layperson on how far away in energy we are from string scales, it is now entering the realm of truth. It is now the 21st century, and these string theories are making predictions on how we see the world around us.

Bibliography

- [1] C. Burgess & G. Moore, *The Standard Model: a Primer*. Cambridge University Press, 2007.
- [2] S. Weinberg, *Gravitation and Cosmology: principles and applications of the general theory of relativity*, John Wiley & Sons (New York) 1972.
- [3] P. W. Anderson. More is different. *Science*, 177(4047):393–396, 1972.
- [4] B. R. Greene, D. R. Morrison and J. Polchinski, “String theory,” Proc. Nat. Acad. Sci. **95**, 11039 (1998).
- [5] J. H. Schwarz, “Recent progress in superstring theory,” hep-th/0007130.
- [6] M. Blau and S. Theisen, “String theory as a theory of quantum gravity: A status report,” Gen. Rel. Grav. **41**, 743 (2009).
- [7] J. Polchinski, “String theory. Vol. 1: An introduction to the bosonic string,” Cambridge, UK: Univ. Pr. (1998) 402 p
- [8] J. A. Shapiro, “Reminiscence on the birth of string theory,” arXiv:0711.3448 [hep-th].
- [9] C. P. Burgess, D. Hoover, C. de Rham and G. Tasinato, “Effective Field Theories and Matching for Codimension-2 Branes,” JHEP **0903** (2009) 124 [arXiv:0812.3820 [hep-th]].
- [10] L. van Nierop and C. P. Burgess, “Sculpting the Extra Dimensions: Inflation from Codimension-2 Brane Back-reaction,” JCAP **1204**, 037 (2012) [arXiv:1108.2553 [hep-th]].
- [11] C. P. Burgess and L. van Nierop, “Technically Natural Cosmological Constant From Supersymmetric 6D Brane Backreaction,” arXiv:1108.0345 [hep-th].
- [12] G. T. Horowitz and J. Polchinski, “Gauge / gravity duality,” [gr-qc/0602037];
- [13] O. Aharony, S. S. Gubser, J. M. Maldacena, H. Ooguri and Y. Oz, “Large N field theories, string theory and gravity,” Phys. Rept. **323** (2000) 183 [hep-th/9905111];
I. R. Klebanov, “TASI lectures: Introduction to the AdS/CFT correspondence,” [hep-th/0009139].

- [14] S. A. Hartnoll, “Lectures on holographic methods for condensed matter physics,” *Class. Quant. Grav.* **26** (2009) 224002 [arXiv:0903.3246 [hep-th]];
C. P. Herzog, “Lectures on Holographic Superfluidity and Superconductivity,” *J. Phys. A* **42** (2009) 343001 [arXiv:0904.1975 [hep-th]];
J. McGreevy, “Holographic duality with a view toward many-body physics,” arXiv:0909.0518 [hep-th];
S. Sachdev, “Condensed matter and AdS/CFT,” arXiv:1002.2947 [hep-th].
- [15] J. M. Maldacena, “The Large N limit of superconformal field theories and supergravity,” *Adv. Theor. Math. Phys.* **2**, 231 (1998) [hep-th/9711200].
- [16] E. Witten, “Anti-de Sitter space and holography,” *Adv. Theor. Math. Phys.* **2**, 253 (1998) [hep-th/9802150].
- [17] E. Witten, “Anti-de Sitter space, thermal phase transition, and confinement in gauge theories,” *Adv. Theor. Math. Phys.* **2**, 505 (1998) [hep-th/9803131].
- [18] S. R. Wadia, “Gauge/Gravity Duality and Some Applications,” *Mod. Phys. Lett. A* **25**, 2859 (2010) [arXiv:1009.0212 [hep-th]].
- [19] P. Majumdar, “Black hole entropy and quantum gravity,” gr-qc/9807045.
- [20] K. v. Klitzing, G. Dorda, and M. Pepper. New method for high-accuracy determination of the fine-structure constant based on quantized hall resistance. *Phys. Rev. Lett.*, 45:494–497, Aug 1980.
- [21] R. B. Laughlin. Quantized hall conductivity in two dimensions. *Phys. Rev. B*, 23:5632–5633, May 1981.
- [22] D. C. Tsui, H. L. Stormer, and A. C. Gossard. Two-dimensional magnetotransport in the extreme quantum limit. *Phys. Rev. Lett.*, 48:1559–1562, May 1982.
- [23] C. P. Burgess and L. van Nierop, *JHEP* **1102**, 094 (2011) [arXiv:1012.2638 [hep-th]].
- [24] L. W. Engel, D. Shahar, C. Kurdak, and D. C. Tsui, “Microwave frequency dependence of integer quantum Hall effect: Evidence for finite-frequency scaling,” *Phys. Rev. Lett.* **71**, 2638 (1993).
- [25] Li, W., Vicente, C. L., Xia, J. S., Pan, W., Tsui, D. C., Pfeiffer, L. N., & West, K. W., *Physical Review Letters*, 102 (2009) 216801
- [26] S. A. Hartnoll and A. Tavanfar, “Electron stars for holographic metallic criticality,” *Phys. Rev. D* **83**, 046003 (2011) [arXiv:1008.2828 [hep-th]].

- [27] Z. Bajnok and L. Palla, “Boundary finite size corrections for multiparticle states and planar AdS/CFT,” *JHEP* **1101**, 011 (2011) [arXiv:1010.5617 [hep-th]].
- [28] A. M. Garcia-Garcia, J. E. Santos and B. Way, “Holographic Description of Finite Size Effects in Strongly Coupled Superconductors,” arXiv:1204.4189 [hep-th].
- [29] Nigel Goldenfeld. *Lectures on phase transitions and the renormalization group*, volume 85 of *Frontiers in Physics*, chapter 10. Addison-Wesley, Reading, MA, USA, 1992.
- [30] N. Read. Non-abelian adiabatic statistics and hall viscosity in quantum hall states and p_x+ip_y paired superfluids. *Physical Review B*, 79(4):045308, January 2009.
- [31] A. H. Castro Neto, F. Guinea, N. M. R. Peres, K. S. Novoselov, and A. K. Geim. The electronic properties of graphene. *Reviews of Modern Physics*, 81:109–162, January 2009.